Examining the neuroprotective and neuro-restorative efficacy of heat-treated human platelet pellet lysate in traumatic brain injury models

Ouada Nebie

Co-tutelle /Dual degree

Université de Lille
Ecole Doctorale Biologie-Santé (ED446)
et
Taipei Medical University
College of Biomedical Engineering

THÈSE
Présentée par

NEBIE Ouada

Pour l'obtention du grade de

DOCTEUR DE L'UNIVERSITÉ DE LILLE

Spécialités : Neurosciences et Ingénierie tissulaire

Examining the neuroprotective and neurorestorative efficacy of heat-treated human platelet pellet lysate in traumatic brain injury models

Soutenue publiquement le 11 Janvier 2021 devant le jury composé de :

Monsieur le Dr. Luc BUEE	**Président du jury**
Monsieur le Dr Emmanuel BROUILLET	**Rapporteur**
Madame le Dr. Sandrine HUMBERT	**Rapporteur**
Monsieur le Pr Chaur-Jong HU	**Examinateur**
Madame le Dr. Luisa LOPES	**Examinateur**
Madame le Dr Szu-Yi CHOU	**Examinateur**
Monsieur le Pr Chih-Wei PENG	**Invité**
Monsieur le Pr. David DEVOS	**Invité**
Messieurs le Pr. Thierry BURNOUF / Dr. David BLUM	**Directeurs de thèse**

Publications integrated in this thesis

Nebie O. Barro L., Wu Y.W., Knutson F., Buée L., Devos D., Peng C W., Blum D, and Burnouf. T. Heat-treated human platelet pellet lysate modulates microglia activation, favors wound healing, and promotes neuronal differentiation in vitro. Platelets. 1369-1635 (2020) doi: https://doi.org/10.1080/09537104.2020.1732324

Nebie O., Devos D., Vingtdeux V., Barro L., Devedjian J.C., Jonneaux A., Chou M. L., Bordet R., Buée L., Knutson F., *Blum D., and Burnouf T.* The neuroprotective activity of heat-treated human platelet lysate biomaterials manufactured from outdated pathogen-reduced (amotosalen/UVA) platelet concentrates. Journal of Biomedical Science 26, 89 (2019) doi: 10.1186/s12929-019-0579-9.

ACKNOWLEDGEMENTS

This work was carried out under a joint supervision agreement concluded between Lille University (INSERM UMR- S1172, "Alzheimer et Tauopathies") and Taipei Medical University (TMU, Graduate Institute of Biomedical Materials and Tissue Engineering) under Prof. Thierry Burnouf (TMU) and Dr. David Blum (University of Lille) supervision.

At this stage, I would like, firstly, to express my profound gratitude to Prof. Thierry Burnouf and Dr. David Blum for their support, for their patience, motivation, and immense knowledge. It has been an excellent opportunity to learn about things I never expected I would get to explore. You mainly and successfully created "the link between blood transfusion and neuroscience." Thank you again for your understanding throughout my ups and downs moments. You inspired me, guide me, and encourage me when needed. I am here today because you found the right words to convince me after my master to continue these studies, and I am forever grateful.

To all the committee members, thank you very much for accepting to examine this work.

My sincere thanks to Dr. Luc Buee, President of Lille Neuroscience & Cognition. You gave me a tremendous and fantastic privilege to pursue my studies in your Centre. Moreover, I particularly appreciate your kindness, and I do not have enough words to express my gratitude. Thank you for all.

To Dr. Emmanuel Brouillet, you have been associated with this work since the early stage. Great thanks for all your advice, suggestions, and efforts. I am grateful for your help and support during these three years.

To Pr David Devos, I would like to express my sincere thanks to you and your lab members Aurelie J., Dr. Devedjian J.C, Marie, and Flore G. You have also been involved in this work, and you allowed me to perform some of the experiments in your lab. Thank you very much.

To Dr. Sandrine Humbert, Dr. Luisa Lopes, Dr. Szu-Yi Chou, thank you for having agreed to examine my work. Thank you all for your suggestions and comment.

To Pr Chih-Wei Peng, Pr Chaur-Jong Hu, thank you very much for your advice and suggestions.

To my colleagues and lab members, past and present, thank you for continue support and for being there when I needed it the most. Thank you for sharing your stories and any insightful hour of discussions.

To Dr. Tsung-Hsun Sean Hsieh and Yen Hua Chen (Swallow) from the Graduate Institute of Neural Regenerative Medicine, college of Medical Science and Technology, Taipei Medical University, who allowed me to have the equipment, and the necessary knowledge in animal experiments, I would like to express my sincere thanks.

To Dr. Emilie F., Dr. Kevin, C. Victoria G., Hamza, I am grateful for your support, suggestions, and advice. You had ears to listen to all my requests. I bothered you a lot with my "one hundred" questions, but you did your best to help me. Thank you. Thank you very much.

To Dr. Didier Vieau, Dr. Marie, and all the "Alzeheimer and Tuaupathies" team in Lille, I am grateful to have shared six amazing months with you during this torturous journey, and I wish you all the best. Thank you for sharing your ideas and experiences with every student in other lab groups I have come across.

To Dr. Celine Brand, secretary General of Lille Neuroscience & Cognition, I would like to thank you for the great help in handling all the administrative documents. Your efficiency, promptitude, and availability help me a lot. Thank you again for everything.

Thank you for your support over these years to the rest of the TMU and external to TMU. To anyone who has supported or encouraged me over the years, I thank you too. I appreciate every kind of help. Thank you, all.

To my friends from Burkina Faso, thank you for your understanding and support. We shared memorable moments. May we continue to enjoy the remaining of our life together.

Finally, to my Family, I am wordless; thank you for your unconditional support, your sacrifice despite not knowing what I do. Your sincere love and encouragement allowed me to develop and explore my curiosity for the unknown. Thank you for teaching me since my younger age, the sense of courage, dedication, and hard work. I hope my decision to be involved in this Ph.D. will make you proud.

Peace and Love

Ouada

TABLE OF CONTENT

Table of content

List of figures

List of tables

List of abbreviations

AD: Alzheimer disease

ADP: Adenosine diphosphate

ALS: amyotrophic lateral sclerosis

ATP: Adenosine triphosphate

mARN: messenger RN

BBB: Blood brain barrier

BCA: Bicinchoninic acid assay

BDNF: brain-derived neurotrophic factor

BSA: Bovine serum albumin

Beta III-tub : bata III tubulin

CAD: compound adsorption device

CaCl2: Calcium chloride

CBS : Cortical brain scratch

C1q : complement component 1q

C3, 4,5 : Complement proteins 3, 4,5

CAD: compound adsorption device

cAMP: cyclic 3',5'-adenosine monophosphate

CCI: Controlled cortical impact

CCK-8: Cell counting kit-8

CCL2,3, 4,5: C-C Motif Chemokine Ligand 2,3, 4, 5

COX-2: anti-cyclooxygenase

CXCL4: C-X-C chemokine ligand 4

CNS: Central nervous system

CSF: Cerebrospinal fluid

CT: Computed tomography

DAA: Disease-associated astrocytes

DAM: Disease-associated microglia

DMEM: Dulbecco’s modified Eagle’s medium

DNA: Deoxyribonucleic acid

DPI: Day post-injury

EGF: epidermal growth factor

ELISA: enzyme-linked immunosorbent assay

EPO: Erythropoietin

FBS: fetal bovine serum

FPI: fluid percussion injury

GPX-4: Glutathione peroxidase 4

GFAP: Glial fibrillary acidic protein

HBV: Hepatitis B virus

HD: Huntington's disease

HCV: Hepatitis C virus

HO-1: Heme oxygenase-1

HPPL: heat-treated platelet pellet lysate

ICP; intracranial pressure

Iba-1: Ionized calcium binding adaptor molecule 1

I-HPPL: heat-treated intercept platelet pellet lysate

IGF-1: Insulin-like growth factor 1

IL1,6,8: Interleukin 1, 6, 8

LCM-MS: Liquid chromatography–mass spectrometry

LDH: Lactate dehydrogenase

LPS: lipopolysaccharide

LUHMES: Lund Human Mesencephalic neurons

MBP: Myelin basic protein

MMP1,2,9: Matrix metallopeptidase1, 2, 9

MCP1,2: monocyte chemoattractant protein-1

MnSOD: manganese superoxide dismutase

MRI: Magnetic resonance imaging

NGF: Nerve growth factor

NFH: Neurofilament heavy chain

NFL: Neurofilament light

NFM: Neurofilaments medium

NOR: Novel object recognition

NRF2: Nuclear factor erythroid 2-related factor 2

NSCs: Neural stem cells

NSE: Neuron-specific enolase

NQO1 : (NAD(P)H Quinone Dehydrogenase 1

OF: Open field

OCT: Optimal cutting temperature

PAS: platelet additive solution

PCs: platelet concentrates

PD: Parkinson's disease

PDGF: platelet-derived growth factor

PF4: like platelet factor 4

PFA: Paraformaldehyde

PI: Primary injury

PSD-95: Post-synaptic density 95

qPCR: Quantitative polymerase chain reaction

ROI: Region of interest

ROS: Reactive oxygen species

RBC; Red blood cells

RNA: Ribonucleic acid

SDF-1: The stromal cell-derived factor 1

SEM: Scanning electron microscope

S100b: S100 calcium-binding protein B

SOD: Superoxide dismutase

Syp: Synaptophysin

SNAP25: Synaptosomal-Associated Protein

TBI: traumatic brain injury

TH: Tyrosine Hydroxylase

TGFb: Transforming growth factor beta

TNF: tumor necrosis factor

TLR2,4: Toll-like receptors-2, 4

TREM2: Triggering receptor expressed on myeloid cells 2

UCHL-1: Ubiquitin carboxy-terminal hydrolase L1

VEGF: vascular endothelial growth factor

WHO: World Health Organization

WBC: White blood cells

ABSTRACT

Graphical abstract

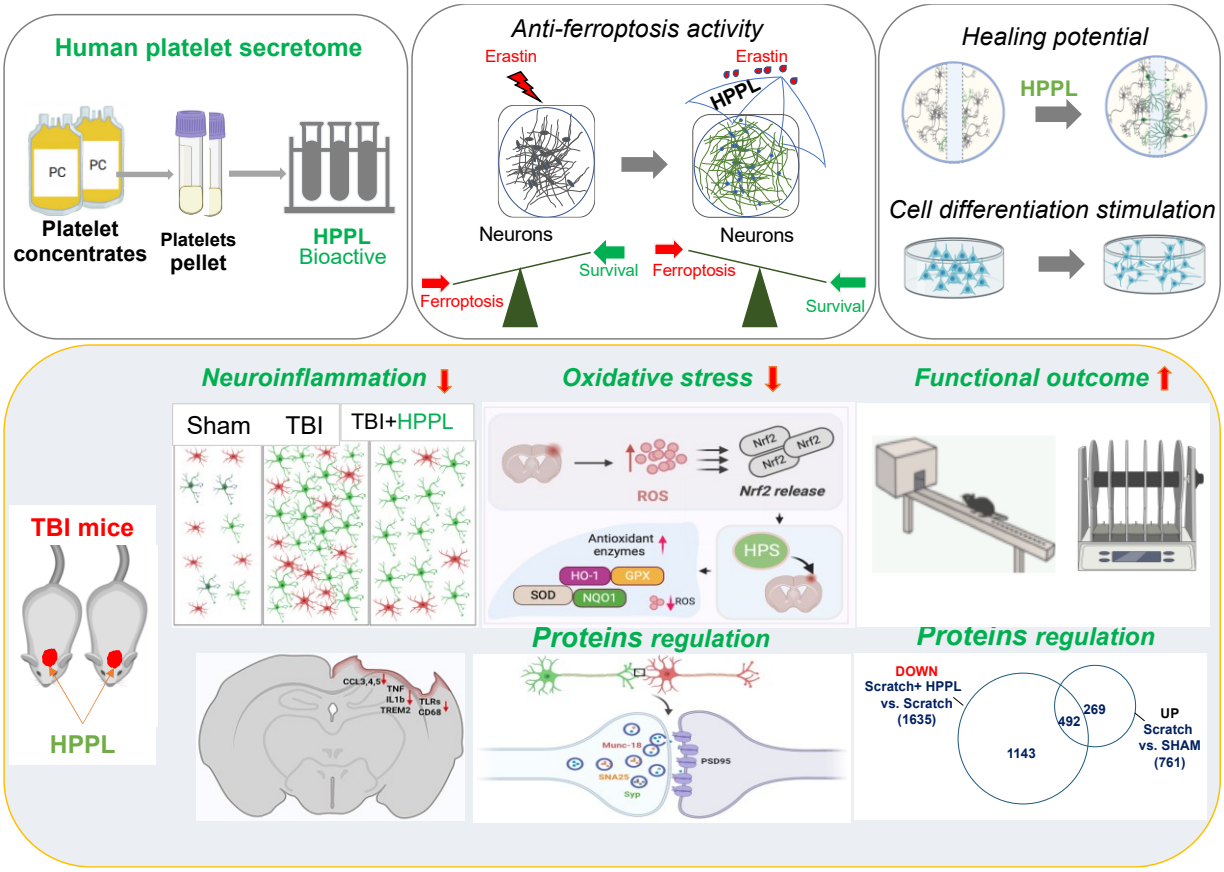

Résumé en Français

Les lésions cérébrales traumatiques (LCT) restent un défi de santé publique de nos jours car celles-ci touchent plus de cinquante millions de personnes dans le monde par an. Leur prise en charge nécessite généralement des soins de longue durée et ceci engendre malheureusement des dépenses financières importantes estimées à plus de 400 millions de dollars US par an. Les LCT font partie des plus complexes traumatismes affectant le cerveau humain. Dans les cas chroniques par exemple, l'une des complications des LCT est la persistance de la neuroinflammation qui conduit inévitablement à une dégénérescence neuronale et à un déficit cognitif. Malheureusement, les stratégies d'intervention se heurtent encore à plusieurs obstacles malgré les progrès technologiques actuels. Des efforts sont faits pour arrêter ce « tueur silencieux », mais jusqu'à nos jours, aucune stratégie ne s'est avérée efficace contre les perturbations physiologiques à long terme des LCT.

De nos jours, il apparaît de plus en plus clairement que le lysat plaquettaire contient une pléthore de molécules actives pouvant exercer des activités neuroprotectrices. Ce produit neuroprotecteur naturel pourrait donc être bénéfique dans le traitement des maladies neurodégénératives comme l'ont montré des études antérieures avec des modèles expérimentaux d'accidents vasculaires cérébraux, de sclérose latérale amyotrophique et de la maladie de Parkinson.

Nous avons émis l'hypothèse que l'injection de ce lysat plaquettaire dans une zone lésée du cerveau favoriserait la cicatrisation et réduirait la mort neuronale.

Notre projet avait donc pour but de développer une approche innovante pour le traitement de la lésion traumatique cérébrale. Nous visions à donner la preuve du concept de l'intérêt d'utiliser le lysat chauffé de plaquettes humaines (HPPL) comme agent neuroprotecteur.

Du HPPL a été préparé à partir de concentrés plaquettaires non viro-inactivés et viro-inactivés selon une procédure préalablement établie. L'impact sur la viabilité des cellules, l'absence d'activité pro-inflammatoire, le potentiel de stimuler la cicatrisation du HPPL ont été évalué à l'aide de modèles cellulaires pertinents. L'activité d'inhibition de la ferroptose par le HPPL a été aussi investiguée en utilisant des cellules de LUHMES et des cultures primaires de neurones.

En fin, des modèles de LCT de souris ont été utilisés pour évaluer le potentiel « neuro-restaurateur » du HPPL. Nous avons ciblé ici son impact sur la fonction motrice, la neuroinflammation, le stress oxydatif et la perte synaptique. Des tests de comportement, d'expression de gènes, d'histologie, d'ELISA, de Western blot et d'analyse protéomique ont été utilisés au cours de cette étude.

L'étude *in vitro* a révélé que les HPPL contiennent une pléthore de molécules bioactives qui sont non-toxiques pour les cellules, ni n'induisent de stress aux cellules traitées. Bien plus, les HPPL n'ont pas exercé d'impact négatif sur l'expression des protéines synaptiques et neuronales, et ont conservé leur potentiel « anti-ferroptose ». L'administration du HPPL à des souris ayant des LCT, a amélioré leur fonction motrice, atténué l'inflammation et le stress oxydatif et réduit la perte synaptique.

En résume, le HPPL/I-HPPL possède une activité neuroprotectrice révélée à travers les essais in vitro. In vivo, il a réussi à inverser le déficit moteur, moduler l'activation des cellules gliales et le stress oxydatif provoqués par la LCT induite aux souris.

Résumé substantiel en Français

La lésion cérébrale traumatique est définie comme une altération physique du tissu cérébral conduisant à une perturbation de la fonction cérébrale. Les traumatismes crâniens touchent des millions de personnes dans le monde. À titre d'exemple, il est indiqué que les accidents de la voie publique représentent en France la première cause de traumatisme crânien (60% des hospitalisations pour trauma crânien, et 70% des décès par trauma crânien), avec un pic de fréquence entre 15 et 30 ans (Campus de Neurochirurgie, 2006). Ces données bien qu'anciennes dépeignent un peu l'ampleur de ce fléau. Bien plus, selon l'organisation mondiale de la santé, les traumatismes crâniens constituent un problème de santé publique ayant un impact économique et social considérable méritant une attention particulière. La prise en charge des patients victimes de trauma crâniens chroniques se fait sur de longues durées et malheureusement le traitement reste encore un grand défi au niveau mondial malgré tous les progrès réalisés en matière sanitaire. Les méthodes de traitements actuels à savoir la neurochirurgie, l'oxygénation et la réduction de la pression intracrânienne peuvent être assimilées aux traitements d'urgence puisque les complications à long terme, en particulier les problèmes cognitifs, la mort cellulaire Etc. demeurent non résolus. Jusqu'à nos jours, sur le plan clinique, les stratégies thérapeutiques, notamment neuroprotectrices bien qu'ayant fournies des résultats probants chez l'animal, la plupart d'entre elles sont restées inefficaces chez l'humain. Par conséquent, le développement de nouvelles méthodes pouvant faire face à la mort neuronale, au déficit cognitif et à l'inflammation à long terme sont encore d'actualité.

Objectifs de notre projet

L'application des résultats de recherche sur le trauma crânien sur le plan clinique s'est traduite pour la plupart jusqu'à présent par des échecs et l'horizon semble sombre. Aucun traitement efficace et approprié n'a pu être validé pour pallier les séquelles à long-terme des lésions cérébrales traumatiques. Il apparaît donc urgent de développer de nouveaux modèles, de nouvelles techniques bien caractérisées et de nouvelles approches thérapeutiques. Sur la base des travaux de recherche menés sur les lysats plaquettaires humains, nous découvrons que ces produits contiennent une pléthore de molécules bioactives. Ces travaux ont aussi révélé le potentiel neuroprotecteur de ces

lysats dérivés des plaquettes suggérant du même coup qu'ils pourraient constituer un bon candidat parmi les agents thérapeutiques naturels pour les traumas crâniens ou les LCT.

L'objectif global de ce travail a été d'évaluer l'effet bénéfique d'un type précis de lysats de plaquettes humaines (HPPL) en tant qu'une approche thérapeutique innovante pour le traitement de la lésion cérébrale traumatique. Avec cet objectif à l'esprit, nous avons également développé et caractérisé un nouveau modèle murin de lésion corticale basé sur un modèle *in vitro* déjà validé.

Nous avons insisté, dans cette étude sur la qualité du lysat plaquettaire. Ensuite, nous avons investigué son effet neuroprotecteur à travers les phénomènes comme la ferroptose, le stress oxydant et l'inflammation qui, généralement se mettent en place au début d'une lésion cérébrale traumatique. Nous nous sommes intéressés aussi au potentiel de notre produit à exercer une action neurorégénérative à travers une stimulation de la cicatrisation et la maturation des cellules neuronales. Enfin, nous avons regardé le potentiel du lysat de plaquettes à contribuer à l'amélioration des fonctions neurologiques chez des souris auxquelles nous avons induit un traumatisme crânien par deux méthodes différentes, en utilisant des tests comportementaux moteurs, cognitifs et des tests biochimiques.

Plan de notre travail

Pour atteindre les objectifs ci-dessus cités, les travaux de notre thèse ont été subdivisés comme suit :

- ✓ Accumuler des preuves préliminaires sur la qualité, la composition et les effets neuroprotecteur et « neurorestauratif » du HPPL sur des modèles cellulaires *in vitro*.
- ✓ Évaluer l'impact de la méthode d'inactivation virale INTERCEPT appliquée aux concentrés plaquettaires sur l'activité fonctionnelle du lysat dérivant de ces concentrés plaquettaires.
- ✓ Développer et caractériser un nouveau modèle animal de lésion corticale chez la souris
- ✓ Évaluer l'activité neuroprotectrice du HPPL sur deux modèles expérimentaux de trauma crânien.

Résultats et discussion

Préparation du HPPL/I-HPPL

Les lysats de plaquettes utilisés dans cette étude ont été préparés à partir de deux types de concentrés plaquettaires. L'un viro-inactivé grâce à une technique appelée INTERCEPT et l'autre

provenant de concentrés plaquettaires communément utilisés, c'est-à-dire sans viro-inactivation. La méthode de préparation adoptée a été choisie sur la base de nos travaux antérieurs. Les concentrés plaquettaires sont d'abord centrifugés à 3 000 x g pendant 30 minutes et le culot constitué uniquement de plaquettes est repris dans 1/10ème du volume initial de concentré plaquettaire avec du tampon phosphate salin. Puis, la mixture est soumise à trois cycles de congélation -décongélation (-80℃ - 37℃-) dans le but de lyser les cellules et favoriser le relargage de leur contenu. Après une deuxième centrifugation, le surnageant est récupéré et chauffé dans un bain marie à 56℃ pendant 30 minutes. Une dernière centrifugation a 15 000 x g, pendant 15 minutes est faite et le surnageant collecté et congelé jusqu'à utilisation. Ce surnageant a été nommé HPPL s'il provient d'un concentré plaquettaire standard sans aucun traitement d'inactivation des agents pathogènes et I-HPPL s'il a été produit à partir de concentrés de plaquettes soumis à une filtration pour éliminer les globules blancs et une inactivation des agents pathogènes par le biais du traitement INTERCEPT.

Composition du lysat plaquettaire

Certains facteurs trophiques ont été sélectionnés et dosés par ELISA. HPPL et I-HPPL contiennent tous une concentration raisonnable de ces facteurs de croissance à savoir BDNF, PDGF-AB, EGF, VEGF et CCL5. Ces facteurs ont été sélectionnés à cause de leur rôles connus spécifiquement dans le fonctionnement du cerveau.

L'analyse du contenu du HPPL a été également effectuée en utilisant une méthode plus poussée, la spectrométrie de masse. Une liste de 1210 protéines a été générée et cette liste couvre une gamme très variée de molécules en termes d'implications dans les évènements biologiques. Elle couvre entre autres des facteurs de croissance, cytokines, antioxydants, enzymes, molécules immunitaires Etc. Le regroupement de ces protéines a révélé la présence de protéines membranaires, de signalisation, du cytosquelette, vésiculaires, mitochondrial Etc.

Qualité du HPPL utilisé

Effet du HPPL et I-HPPL sur la viabilité des cellules

Un autre objectif dans la caractérisation du produit était d'évaluer sa toxicité. Pour cela, nous avons testé son effet sur la viabilité cellulaire en utilisant plusieurs modèles de cultures cellulaires. C'est ainsi que des lignées cellulaires SH-SY5Y, LUHMES, BV-2, endothéliales EA-hy926 et des

cultures de neurones primaires de souris ont été traitées avec du HPPL et du I-HPPL à 5% (volume a volume).

Les tests de viabilité réalisés après un et deux jours dans certains cas ont tous démontré que les lysats plaquettaires utilisés à cette concentration n'étaient pas toxiques. Nous avons approfondi l'examen de l'effet toxique en regardant l'impact que ces produits pourraient avoir sur l'expression protéique chez des cellules comme les LUHMES et les neurones primaires. Sans surprises le HPPL et l'I-HPPL n'affectent pas l'expression des protéines synaptiques des neurones primaires et aussi les protéines neuronales des cellules dopaminergiques (LUHMES).

HPPL et I-HPPL sont-ils pro-inflammatoires ?

Le dernier point que nous avons voulu aborder dans ce volet sur la qualité du HPPL/I-HPPL était de vérifier qu'il n'induit pas d'activité pro-inflammatoire, ni de stress oxydatif. À cet effet, les cellules BV-2 ont été traitées d'une part avec les lysats de plaquettes sanguines et d'autre part avec des lipopolysaccharides (LPS) provenant de E. coli comme contrôle positif. Après une période de 24 heures, nous avons dosé la concentration de facteurs pro-inflammatoires, l'un dans le surnageant (TNFα) et l'autre (COX-2) dans les lysats de cellules de BV-2 traitées avec du HPPL ou du I-HPPL. Les résultats ont clairement montré que le HPPL et l'I-HPPL n'étaient pas capables d'activer les cellules microgliales en comparaison avec les cellules traitées au LPS et les cellules gardées dans les conditions normales. Mieux, lorsque les cellules ont été prétraitées au LPS, suivie des lysats plaquettaires une heure après, les niveaux d'expression des facteurs pro-inflammatoires dosés ont significativement diminué comparativement au témoin positif. Ce dernier résultat suggère donc que le HPPL et l'I-HPPL ont la capacité de moduler la production de ces facteurs par les cellules.

Lysats plaquettaires et stress oxydant

Pour ce qui concerne le stress oxydant lipidique les cellules de LUHMES ont été traitées avec les lysats et le niveau de peroxydation lipidique a été évalué en utilisant un capteur de peroxydation lipidique dénommé C11 BODIPY couramment utilisé dans ce type d'expérimentation. Après que les cellules aient été exposées au HPPL et I-HPPL, nous avons utilisé la méthode de cytométrie de flux pour détecter le marqueur précédemment utilisé.

Les résultats indiquent que les cellules traitées ne produisaient pas de peroxydation lipidique contrairement au contrôle positif qui était constitué de cellules traitées avec la neurotoxine, erastine.
Ces résultats constituent donc une preuve supplémentaire que les HPPL ne sont pas toxiques et ne sont pas non plus pro-inflammatoires.

Évaluation des effets bénéfiques du HPPL et du I-HPPL in vitro

Nous nous sommes intéressés dans cette section d'abord à la capacité réparatrice des lysats plaquettaires à savoir le HPPL et l'I-HPPL. Nous avons alors imité une lésion cérébrale *in vitro* en réalisant un test de « scratch » pour comprendre la capacité du HPPL / I-HPPL à stimuler la migration, la prolifération et le développement des cellules. Les cellules SH-SY5Y non-différenciées et des cellules endothéliales EA-hy926 ont été cultivées jusqu'à l'obtention d'une monocouche, puis elles ont été « scratchées » et traitées avec du HPPL et I-HPPL. Dans les 24 heures suivant le traitement, le HPPL et l'I-HPPL ont stimulé la prolifération des cellules et la migration mieux que les cellules non traitées.
Des résultats similaires ont été trouvés lors de la réalisation du même test en utilisant cette fois des cellules SH-SY5Y différenciées comme cellules neuronales. Après avoir induit leur différenciation avec de l'acide rétinoïque, la monocouche de cellules a été grattée, suivie d'une stimulation par les lysats de plaquettes sanguines. Au bout de 4 jours, nous avons constaté que les lysats ont stimulé efficacement la croissance des cellules dans la zone lésée.

Capacité des lysats à stimuler la différenciation des cellules

Nous avons examiné dans cette expérience le potentiel du HPPL et du I-HPPL à stimuler la différenciation des cellules neuronales. Nous avons utilisé des cellules SH-SY5Y non différenciées en l'absence d'acide rétinoïque. Les cellules ont été d'abord ensemencées dans des plaques à 06 puits en présence de FBS pendant 24 heures pour faciliter leur adhésion à la surface des plaques. Le milieu de culture a été ensuite renouvelé le jour suivant sans FBS suivi d'un traitement à 2% HPPL, ou 2% I-HPPL (volume /volume) ou encore 10 µM d'acide rétinoïque (témoin positif). Les cellules cultivées dans un tampon contenant 10% de FBS ont été utilisées comme contrôle négatif. Après sept jours d'incubation, des images ont été acquises, puis les cellules ont été colorées avec deux marqueurs protéiques considérées comme des marqueurs de différenciation : tubuline bêta

III et neurofilament. Les résultats obtenus suggèrent que le HPPL et l'I-HPPL ont été capable de stimuler la différenciation des cellules SH-SY5Y comme témoigne l'élongation des dendrites et l'intensité de la fluorescence obtenue avec le marqueur Tubuline beta 3.
Globalement, ces données ont mis en évidence la capacité des lysats plaquettaires standard et des lysats viro-inactivés à promouvoir la différenciation des cellules SH-SY5Y.

Potentiel d'inhibition de la ferroptose des lysats plaquettaires

Plusieurs études ont indiqué qu'il existe une forme de mort cellulaire, la ferroptose différente de l'apoptose et de la nécrose car n'induisant pas de modifications de la morphologie des noyaux des cellules et que ce type de mort peut être induit par l'erastine. Il est indiqué que la ferroptose pouvait être inhibée par des antioxydants. Les maladies comme celle de Parkinson, d'Alzheimer et le traumatisme crânien sont capables d'activer plusieurs voies de mort cellulaire, y compris la ferroptose.
Dans le but d'évaluer le pouvoir d'inhibition de la ferroptose par le HPPL et l'I-HPPL *in vitro*, nous avons utilisé deux modèles de cultures cellulaires : les cellules de LUHMES et les cultures primaires de neurones. Ces cellules ont été maintenues jusqu'à maturité puis ont été traitées avec de l'érastine comme inducteur de la ferroptose. Les cellules LUHMES différenciées ont été stimulées pendant une heure avec 5% HPPL ou I-HPPL avant le traitement à l'érastine à une concentration finale de 1,25 µM. Les cellules LUHMES sont vulnérables à l'érastine et, comme prévu, l'ajout de la toxine a entraîné une mort cellulaire significative et une augmentation de la peroxydation lipidique. Par contre, le HPPL et l'I-HPPL ont inhibé avec succès cette mort cellulaire et ont également réduit le niveau de peroxydation lipidique induite par l'érastine.
D'autre part, l'activité « anti-ferroptose » du HPPL et du I-HPPL a été évaluée à travers des cultures neuronales primaires obtenues de souris embryonnaires (E16) C57. Ces cellules ont été maintenues jusqu'au 21^{e} jour afin d'avoir des cellules neuronales matures. Et, comme pour les LUHMES, les neurones primaires ont d'abord été traités avec du HPPL ou du I-HPPL pendant une heure, puis stimulés avec de l'érastine. Ensuite, le relargage de l'enzyme, lactate déshydrogénase a été mesurée. Une fois de plus, les lysats ont prouvé leur pouvoir d'inhibition de la ferroptose. Ces résultats suggèrent donc que HPPL et I-HPPL sont capables d'atténuer l'effet de la neurotoxine et que la procédure d'inactivation virale ne modifie pas non plus les propriétés neuroprotectrices de HPPL.

L'activité neuroprotectrice du HPPL sur des modèles animaux expérimentaux de trauma crânien.

Sur la base de l'analyse *in vitro* et de la disponibilité du lysat plaquettaire, nous avons décidé d'évaluer *in vivo* le potentiel neuroprotecteur du HPPL préparé à partir de concentrés plaquettaires n'ayant pas subi de traitement d'inactivation de pathogènes.

Comme indiqué plus haut un de nos objectifs était aussi de décrire et de caractériser notre nouveau modèle animal de lésion corticale chez la souris. Cette caractérisation du modèle a été donc réalisée avant le traitement des souris au HPPL.

Caractérisation du modèle animal de lésion corticale

Procédure de réalisation de la lésion corticale chez la souris

Notre nouveau modèle de lésion corticale a été donc initié chez la souris tout en se basant sur le modèle de lésion par scratch *in vitro* et la lésion mécanique localisée en *in vivo*. La procédure consiste à réaliser deux lésions parallèles à l'image de rayures dans une monocouche de cellules, mais cette fois dans le cortex. C'est un modèle simple à réaliser et qui pourrait être utilisé pour cribler de façon rapide des produits. En bref, pour le réaliser, l'animal est d'abord anesthésié puis sa tête est fixée dans le cadre stéréotaxique. La peau au niveau du crâne est donc incisée en suivant la médiane pour laisser apparaitre l'os du crâne. Un cercle de 4 mm de diamètre au-dessus de l'hémisphère droit entre le lambda et le bregma est créé en coupant l'os du crane pour exposer le cerveau. Deux lésions parallèles à une profondeur d'approximativement 0,6 mm sont induites à l'aide d'une aiguille de calibre 18 G préalablement fixée sur le cadre stéréotaxique. Une fois le saignement arrêté, la plaie a été suturée et l'animal est retourné dans une nouvelle cage propre.

Pour comprendre le développement physiopathologique de notre nouveau modèle de lésion cérébrale, plusieurs approches ont été utilisées telles que l'imagerie, les tests comportementaux et les investigations moléculaires, biochimiques et histologiques. L'évolution du modèle a été comparée à un modèle déjà validé dénommé, l'impact cortical contrôlé (CCI).

La procédure du modèle CCI est similaire à celui de la lésion corticale sauf qu'au lieu d'induire une lésion dans le cortex à l'aide d'une aiguille, nous avons utilisé un appareil dédié à percuter le cortex avec une vitesse précise de 3m/s. Ce modèle est à mesure d'induire une mort cellulaire dans d'autres régions du cerveau autre que le cortex. Son impact est donc plus propagé.

Les résultats obtenus laissent entrevoir que le modèle, à l'instar des autres, déclenchait une neuroinflammation, altérait la fonction motrice, et induisait une perte synaptique mais à un degré plus important que le CCI utilisé dans notre étude.

Lésion corticale et inflammation

Pour comprendre les événements physiologiques survenant après la lésion dans le nouveau modèle, nous avons étudié l'expression d'une gamme de gènes pro-inflammatoires par qPCR dans le cortex sept jours après la lésion et comparée aux animaux CCI et Sham (témoin). Nous nous sommes focalisés sur l'évaluation de l'expression relative de l'ARNm des cytokines et chimiokines pro-inflammatoires telles que TNFα, IL1ß, CCL3, CCL4, CCL5. Il est intéressant de noter que ces marqueurs étaient significativement régulés à la hausse dans le cortex des souris avec la lésion corticale par rapport aux deux autres groupes d'animaux. Lors d'une deuxième tentative, nous avons examiné les niveaux d'expressions de certains gènes gliaux. De même, la lésion corticale a déclenché une régulation à la hausse de ces marqueurs de la microglie tels que : TLR2, TLR4, CD68, C1q et TREM2 ainsi que les marqueurs astrocytaires comme GFAP, vimentine par rapport au groupe Sham. Les tests d'histologie ont aussi confirmé l'activation des cellules gliales dans la zone lésée.

Lésion corticale et stress oxydatif

Outre l'inflammation, nous avons également mesuré le niveau des radicaux libres ou espèces réactives de l'oxygène (ERO) dans des tissus frais de cortex de souris soumises à une lésion corticale et des souris témoins c'est-à-dire sans lésion cérébrale apparente. Comme prévu, nous avons observé un niveau significativement plus élevé de production de radicaux libres dans le cortex lésé des souris par rapport aux souris contrôles une semaine après l'induction de la lésion. Les résultats ont indiqué que l'ajout de NADPH, a induit une augmentation du niveau de ROS dans le cortex des souris expérimentales plus de trois fois supérieur au niveau observé chez les souris Sham.

Impact de la lésion corticale sur l'expression des marqueurs synaptiques

Pour ce qui concerne les marqueurs synaptiques, nos analyses pour les protéines sélectionnées ont montré une réduction de l'expression de certaines protéines de synapses comme PSD95, SNAP25, synaptophysin et Munc-18.

Tests de comportement

Les tests réalisés ici sont essentiellement des tests visant à évaluer la fonction motrice et la capacité de reconnaissance des objets, encore appelé en anglais le « Novel Object recognition test ». Ces tests ont été réalisés en deux temps : trois et six jours après la chirurgie. Les animaux ont été maintenus en vie pendant une semaine avant d'être sacrifiés.

Les résultats des tests de comportements réalisés ont aussi révélé une perte de la fonction locomotrice significative chez les souris avec lésion cérébrale en comparaison au modèle CCI. Cependant pour le test de reconnaissance aucune différence significative n'a été observée.

Pour résumer cette partie sur la caractérisation du modèle de lésion corticale, nous dirons que le nouveau modèle de lésion cérébrale a conduit à une réaction neuro-inflammatoire massive, déclenché un stress oxydatif, perturbé le fonctionnement de certaines synapses et induit un déficit moteur. Le deuxième constat est que les effets observés s'avèrent plus importants dans ce modèle que celui du CCI.

Effets neuroprotecteurs de HPPL dans des modèles de lésions traumatiques cérébrales

Méthode d'administration du HPPL aux souris

Dans la présente étude, nous avons examiné pour la première fois l'efficacité du HPPL dans des modèles de lésions cérébrales. Nous avons utilisé le modèle de lésion corticale décrite ci-dessus et celui du CCI déjà décrit dans la littérature. Le HPPL a été administré par voie intracrânienne et intranasale. De façon précise, environ trente minutes après l'induction de la lésion cérébrale, ou l'impact cortical, soixante microlitres de HPPL ont été délicatement déposé goutte à goutte dans la zone lésée avant que la peau ne soit suturée. On s'est assuré au cours du processus que tout le HPPL déposé diffuse dans la plaie avant de la refermer. À partir du jour 1 jusqu'au jour 6 post-lésion, la même quantité de HPPL a été administrée par voie intranasale. Chaque souris non anesthésiée a été soigneusement maintenue par ses oreilles, immobilisée, puis positionnée sur le dos avec sa tête en position verticale. En utilisant une pipette de 20 µL, le produit est administré

par voie intranasale en alternant les narines. Un intervalle de cinq minutes a été observé entre chaque administration, pour un total de trois administrations. Cette procédure a été répétée six jours consécutifs. Pour les souris témoins, une solution saline de même volume, c'est à dire soixante microlitres, a été administré de la même façon. Les souris ont été toutes sacrifiées une semaine après la chirurgie.

Tests comportementaux

Les tests ont été réalisés après trois et six jours post-lésion. La fonction locomotrice et tests de reconnaissance d'objets ont été réalisés avec les souris traitées ou non. Les données obtenues ont montré une nette amélioration de la fonction motrice des souris traitées au HPPL comparativement aux souris ayant reçu uniquement la solution saline. Par ailleurs aucun impact sur la mémoire n'a été observé au jour sept. Cependant, deux semaines après la surgie, nous avons constaté un déficit de la mémoire chez les souris non traitées comparativement aux témoins. Le traitement au HPPL, a heureusement amélioré significativement le déficit cognitif dans le modèle de lésion corticale.

Les effets anti-inflammatoires des lysats plaquettaires

La capacité du HPPL administré par voie intracrânienne et intranasale à moduler l'inflammation déclenchée dans la lésion corticale et le CCI a été examinée en comparant l'expression différentielle des gènes entre les groupes. Les cytokines et chimiokines, TNFα, IL1β, CCL3, CCL4 et CCL5 ainsi que les marqueurs astrocytaires (GFAP, vimentine) et microglie (CD68, TREM2, C1qa) et TLR2, TLR4 étaient significativement plus élevés dans le cortex des souris traitées uniquement avec la solution saline. Par contre, avec l'administration du HPPL, des changements ont été observés. Il y a eu une régulation à la baisse significative d'IL-1β, CCL3, CCL4 et CCL5, TLR4, CD68 et TREM2, GFAP, et Vimentine chez les souris CCI traitées avec HPPL par rapport au groupe traité avec une solution saline. Dans le groupe de la lésion corticale, l'administration du HPPL a conduit à une diminution des changements transcriptionels de TNFα, IL1β, CCL3, TLR4, CD68, TREM2 et GFAP par rapport au groupe non traité. Ceci indique le potentiel du HPPL à moduler un tant soit peu l'inflammation initiée par la lésion que ce soit dans le CCI ou dans le cas de la lésion corticale.

Le stress oxydatif est connu pour son facteur aggravateur des dommages neuronaux après la lésion cérébrale. Nous avons donc analysé si l'administration d'HPPL pourrait atténuer le stress oxydatif.

Les résultats ont fourni des preuves indiquant que l'administration intracrânienne et intranasale de HPPL dans les deux modèles de lésion a significativement réduit le niveau de (ERO) par rapport aux animaux traités avec une solution saline. Nous avons analysé l'expression de gènes sélectionnés connus pour leur association dans la régulation du stress oxydatif tels que GPX-1, SOD1, HO-1, NQO-1, and MnSOD. Les résultats indiquent clairement qu'après le traitement au HPPL, les niveaux d'expression de ces antioxydants ont augmenté considérablement suggérant le déclenchement du processus d'inhibition du stress.

HPPL a amélioré l'expression des protéines synaptiques dans le cortex des souris

Comme observé dans la caractérisation du nouveau modèle de lésion cérébrale, nous avons évalué de nouveau l'expression des protéines synaptiques pour comprendre l'impact du traitement au HPPL. Ainsi, nous avons étudié l'expression de marqueurs pré-et post-synaptiques et neuronaux dans le cortex par ELISA et Western blot. Nous avons trouvé une réduction significative de synaptophysine, SNAP-25, Munc-18, PSD95 et NSE dans le groupe des animaux à lésion corticale et CCI n'ayant pas reçu de HPPL. Nos analyses ont montré une expression relativement plus élevée de la synaptophysine et de la PSD-95 dans le cortex des animaux traités par le HPPL par rapport aux souris traitées avec la solution saline dans le modèle CCI et, SNAP-25, synaptophysine, PSD95 et Munc-18 dans le groupe de la lésion corticale. Ceci laisse entrevoir que le HPPL pourrait contribuer à réduire les pertes synaptiques et neuronale, plus spécifiquement dans le cortex.

Évaluation des effets du HPPL à travers la spectrométrie de masse

L'analyse protéomique a apporté une preuve additionnelle de la capacité du HPPL à exercer un effet protecteur. Les résultats indiquent qu'il y a eu une régulation à la hausse des protéines inflammatoires, un dysfonctionnement de la myéline et une génération de stress oxydatif après le traumatisme cérébral. Environ 500 protéines ont été régulées à la hausse dans le modèle CCI, tandis que dans le modèle de la lésion corticale nous avons observé jusqu'à 700 protéines. Ces résultats viennent en appui aux précédentes analyses et confirment que le nouveau modèle a un impact potentiellement plus élevé que celui du CCI.

En ce qui concerne l'efficacité du HPPL en tant que produit naturel, nous avons constaté que la régulation à la hausse de la plupart des protéines régulées à la hausse déclenchée par le traumatisme cérébral était inversée par le traitement avec le HPPL.

Ce fort potentiel protecteur du HPPL a été confirmé avec l'analyse approfondie d'une catégorie spécifique de la microglie dénommée les (DAM) et les DAA (astrocytes associés à la maladie). Cette analyse particulière a révélé le potentiel du HPPL à moduler la réponse gliale.
Les améliorations fonctionnelles apportées par le sécrétome plaquettaire sont donc concordantes avec celles observées avec le sécrétome des cellules souches rapportées dans la littérature. Des études précédentes avaient aussi montré que le lysat plaquettaire était capable de stimuler la neurogenèse et l'angiogenèse dans un modèle d'AVC ischémique et améliorer également les fonctions motrices.

En conclusion, nous avons montré que dans les deux modèles de lésion cérébrale traumatique *in vivo*, un traitement séquentiel avec du HPPL par dépôt topique sur la zone du cortex lésée d'abord, suivi d'une administration intranasale de six jours a fourni des effets fonctionnels intéressants. Nous avons observé une régulation à la baisse de plusieurs marqueurs pro-inflammatoires dans le cortex. La réponse gliale a également diminué lors du traitement par HPPL. En plus, l'effet neuroprotecteur et neuro-réparateur du traitement au HPPL a été confirmé par une amélioration de l'expression des marqueurs pré- et post-synaptiques analysés et par l'augmentation significative du niveau d'antioxydants tels que NQO-1, HO-1, MnSOD. Les tests de comportement animal ont révélé que le traitement HPPL a conduit à une amélioration significative de la fonction motrice.

Perspectives

D'une façon générale, nos travaux montrent la possibilité d'exploiter le HPPL comme un produit naturel riche en molécules bioactives. Le HPPL, débarrassé des protéines plasmatiques, n'est pas toxique aux concentrations utilisées et contient une quantité raisonnable de protéines totales. Les molécules présentes dans le HPPL ont un potentiel neuroprotecteur et sont capables de moduler la neuroinflammation et le stress oxydant dans des cas de lésions cérébrales traumatiques.
Les résultats obtenus au cours de cette thèse sont encourageants et ouvrent un certain nombre de perspectives pour des travaux futurs avant une évaluation clinique du HPPL :

- L'évaluation du HPPL en utilisant un modèle animal plus proche de l'homme comme les primates

- La d détermination de la dose minimale effective et la dose maximale tolérée du HPPL. Nous n'avons pas pu aborder entièrement les questions de doses du HPPL et ces effets à long terme et donc, une étude plus approfondie de ces questions s'avère nécessaire.

- La détermination, dans le futur, de la voie d'administration la plus appropriée et qui pourrait être utilisée en clinique. C'est un autre facteur important à considérer, car nous avons utilisé une approche visant à maximiser les effets du HPPL en combinant la voie intracrânienne et celle intranasale. Cependant, il sera intéressant de déterminer si une seule voie d'administration du HPPL ne serait pas suffisante.

ENGLISH ABSTRACT

Traumatic brain injury (TBI) remains a global health challenge nowadays, impacting over 50 million people per year globally. This situation is partly linked to the fact that TBI is among the central nervous system disorders whose management mostly requires long-term care. It incurs a substantial economic burden to health systems and costing the global economy more than $400 million. In either high, middle, or low-income countries, TBI is associated with significant economic and societal changes that deserve attention. The disease is described as one of the most complexes, inducing some disproportionate effects between the countries. Unfortunately, the intervention strategies are still facing several limitations at the global level despite all the health sciences' progress. These obstacles are the surge of neuroinflammation, leading to progressive neuronal degeneration and cognitive deficit. Efforts are made to stop this "silent killer", but there is a failure to manage the long-term burden of TBI efficiently until now.

Nowadays, there is growing evidence that platelet lysates are full of bioactive compounds, and they could constitute a powerful natural neuroprotective agent. Few studies have already shown their therapeutic potential in stroke, amyotrophic lateral sclerosis, and Parkinson's disease. Thus, we hypothesized that the delivery of human platelet lysate at an injured area in the brain could provide a suitable environment for recovery.

The current project is intending to develop an innovative approach for the treatment of TBI. We aim to give the proof-of-concept of the interest of using heat-treated human platelet pellet lysate (HPPL) as a neuroprotective agent in TBI using experimental models.

We used cells and animal models of TBI to achieve our goal. We first prepared HPPL from non-pathogen-reduced platelet concentrates (PCs) and pathogen-inactivated PCs (I-HPPL) according to a previously established procedure. We evaluated their safety and functionality using cell models relevant to TBI, including viability assays, wound healing, anti-inflammatory activity, protein expressions, and anti-ferroptosis effect. The safety assessment of the platelet biomaterial was done using neuronal and endothelial cells and its neuroprotective potential with primary neurons, dopaminergic cells line and, a ferroptosis inducer.

Mouse TBI models were used to assess the therapeutic potential of HPPL. We targeted it impact on motor function, neuroinflammation, oxidative stress, and synaptic loss. Behavior tests, gene expression, fluorescent staining, ELISA, Western blot, and proteomics have been used during the investigation.

The *in vitro* experiment performed to investigate the platelet lysate's safety demonstrated clearly that HPPL/I-HPPL contain bioactive molecules and did not affect cell's viability or induced stress. Moreover, HPPL and I-HPPL did not affect synaptic and neuronal protein expression and revealed anti-ferroptosis potential. This finding leads to further investigation of HPPL's beneficial effect *in vivo*. HPPL administration to TBI mice improved their motor function, mitigated the inflammation and oxidative stress. HPPL also decreased the synaptic proteins lost.

HPPL is safe and exerted neuroprotective activity *in vitro*. It successfully reversed the motor deficit, inflammation, and stress triggered by brain injury in mice.

CHAPTER I: General introduction

INTRODUCTION

1.1 Traumatic brain injury

Traumatic brain injury, commonly called TBI in short, is one of the traumatic diseases affecting the central nervous system (CNS). TBI is a major concern in all the groups of populations worldwide without distinction of race and is one of the diseases described since ancient times. The pioneer of medicine, Hippocrates (460–377 BC), was the first who provided a description of brain trauma[1]. His awe-inspiring work, summarized in the treatise titled “On Wounds in the Head," is one of the first manuscripts addressing head trauma[1,2]. Surprisingly, Hippocrates was able to describe and classify the skull fractures as followed: “fissured,” “contused,’’ ‘’depressed,’’ ‘’dented’’ or ‘’scratched’’ (hedra), and ‘’contrecoup’’[2]. Furthermore, for treating the patient with a head injury he used the trepanation method well known in clinic nowadays. Following Hippocrates' work, several years later, two other Greeks, Celsus, and Galen contributed substantially to head injury management. In brief, Celsus precisely described the symptoms occurring after an injury to the brain, and he associated the loss of consciousness to bony injury and the damage into meninges[3]. On the other hand, Galen was able to describe in detail the ventricles. These scientists gave great value to the management of cranial injury.

With the development of new technologies, advanced knowledge of the disease physiopathology has been acquired, leading to an improvement in Hippocrates’ description of head injury. Currently, the definition of TBI still varies according to the circumstances and medical specialties. Nevertheless, traumatic brain injury is frequently presented as a non-degenerative, non-congenital brain insult that occurs after a physical impact on the skull with a short-term or permanent cognitive deficit, physical, and psychosocial functions alteration [4,5]. However, TBI is described in some cases with the broader term “head injury,” which could be misleading since head injury might not involve neurological dysfunction[4,6]. Despite the significant attention our ancient had on TBI, it remains a social concern nowadays.

1.2. Causes and epidemiology of traumatic brain injury

1.2.1 Causes

An insult to the brain can be an important cause of disability and mortality. Labeled a ‘’silent epidemic’’[7], TBI constitutes a multidimensional and complicated issue with significant social

impact. TBI is predominantly caused by road traffic accidents, falls, sport, and war[8-12]. However, recently, in high-income countries, there is a growing number of TBI cases among the elderly[13], and falls are becoming its leading cause in several countries[8]. Furthermore, the world is faced with a high proportion of major civil wars. In countries such as Afghanistan, Iraq, Nigeria, Pakistan, Somalia, Sudan, Syria, Ukraine, and Yemen, the war contributed to rising TBI cases[14,15].

12.2 Incidence

The incidence of a disease is the proportion of new cases in a determined period divided by the total population from which they are derived. The World Health Organization (WHO) in 2014 has indicated that the mortality rate due to tuberculosis, human immunodeficiency viruses, and malaria combined were lower than that of trauma-related deaths[16]. Therefore, the WHO considered that TBI could become the third leading cause of death in the world by 2030[17]. The epidemiological pattern changes partly in different directions in high-, middle-, and low-income countries. Globally, TBI incidence is estimated at 939 cases per 100,000 people[18]. According to meta-analysis, TBI incidence per 100,000 persons was estimated in North America to 1299 cases (95% CI 650–1947). In Europe, 1012 /100 000 cases, 801 cases have been recorded in African countries, and 897/100 000 cases in Eastern Mediterranean[18]. In India, Maas *et al*. (2017) has indicated that every 3 minutes, there is one case of TBI[8]. In the Middle East countries such as Israel, Qatar, and Iran, the incidence rate was between 38.5–367 per 100,000 population[15]. There is variation between the data recorded because of the difference in the terms used to define TBI during the data collection.

1.2.3 Prevalence

Some data indicate how common TBI is within a given population at a particular time. TBI's prevalence has been shown globally and estimated at 69.0 million cases each year[18,19]. According to the Global Burden of Diseases Study (GBD) published in 2013, around 973 million individuals had an injury and sought medication and approximately 4.8 million died[20]. Unfortunately, brain injury cases constituted the most severe cases among them. Europe has recorded 2.5 million TBI cases annually[8], and the Center for Disease Control and Prevention (CDC) in the United States of America, 3.5 million people each year[8,21].

1.3 TBI burden on patients, their family, and the community

As it can be seen through the incidence worldwide, TBI is devastating the lives of millions of people. For example, the severe TBI mortality rate is estimated to 30-40%[22]. The disease burden affects life conditions at the individual, family, and community levels. Patients who survived the injury could experience physical disability, psychiatric, cognitive, and emotional impairments. The long-term impact includes memory loss, decreasing abilities in managing stress, and temper. These situations affect the patient's relationships and, finally, their life in society.

TBI patients' management requires meticulous care and is everlasting. Clinicians and patients' families are always at the front line in this battle. Unfortunately, this uncomfortable situation also required the participation of the community. According to previously published data, approximately $400 billion is spent annually worldwide for TBI patients' management[8]. This colossal amount highlights the urgency and the implication of researchers, policymakers, therapeutists, and patient families at all levels in order to offer better living conditions to TBI patients.

1.4 Traumatic brain injury classes

The brain injury's heterogeneity and complexity led to TBI stratification according to the clinical severity, the injury mechanism, and pathophysiology.

1.4.1 Traditional classification method of head injuries

The traditional classification of TBI is based on the type of injury and its severity, and four categories have been defined as described by Pushkarna *et al*., (2010)[23]:

- **Open injuries***:* this category of injury commonly happens in combat.
- **Closed injuries***:* are predominantly seen in civilian and military operations.
- **Scalp injuries***:* this type of injury can be closed or open.
- **Skull fractures***:* a group of cases with a skull fracture.

In addition to the traditional classification, another standard scale is used during the clinical management of brain injury, the Glasgow Coma Scale (GCS). Three categories of TBI is defined based on this scale: mild (scores ≥ 13), moderate (scores 9–12), and severe (scores 3–8) and some

physicians determine TBI outcomes with the GCS outcome scale, which estimates the neurobehavioral ranges of recovery such as: dead; vegetative state; severe or moderate impairment; and well recovery[24,25] (see **Table 1**).

Table 1: the GCS (adapted from Hemphill *et al*., 2016)

Parameters	**Score**	Interpretation
Ability to open eye		
Sudden eye opening	4	
Reaction to a verbal command	3	
Reaction to pain feeling	2	
Inability to open eye	1	
Communication ability		o Score interval: 3 to15; (3= worst; 15=best)
Clear response	5	o Mild brain injury: score of 13
Uncomprehensive reaction	4	o Moderate injury: score: 9 to 12
Wrong wording	3	o Severe brain injury: score < 8
Lower sound	2	
Enable to speak	1	
Motor reaction		
Obeys to specific command	6	
Localized reaction to pain	5	
Withdraw action due to pain	4	
Flexion movement to due pain	3	
Extension movement due to pain	2	
No reaction	1	

Nevertheless, these two categorizations of TBI are limited by their inability to assess TBI's long-term effect. Therefore, new diagnostic tools have been associated with a better classification of TBI.

1.4.2 Classification using neuroimaging scales

Imaging instruments such as computer tomography (CT) and magnetic resonance imaging (MRI), developed for TBI diagnosis and management, can locate, or identify a skull fracture, intracranial hemorrhage, epidural and subdural hematoma, subarachnoid hemorrhage, intra-parenchymal

hemorrhage, intraventricular hemorrhage, focal and diffuse patterns of axonal injury with cerebral edema, and cerebral contusion[26]. The use of these imaging systems allowed us to define the Marshall and the Rotterdam scales. The Marshall scale uses CT imaging to define six types of injuries, as summarized in **Table 2**. In order to pave the limitations of the Marshall scale, the Rotterdam scale was proposed. However, this promising tool must undergo further validation steps.

Table 2:Brain injury categories according to Marshall and Rotterdam scales. (adapted from Adelson et al., 2003, Maas et al., 2005)[26].

MARSHALL SCALE		
TYPES		Significance
MULTIFOCAL INJURIES (MFI) I		No apparent pathology in the cranial
MFI II		midline shift of 0-5 mm with or without lesions densities; the presence or not of lesion >25^3 cm could associate bone fragments and external bodies
MFI III		absence midline shift 0-5 mm; absence of density lesion >25 cm^3
MFI IV (SHIFT)		Absence of obvious and mixed density lesion >25 cm^3
EVACUATED MASS LESION V		all lesion evacuated by surgical intervention
NON-EVACUATED MASS LESION VI		important density lesion >25 cm^3; no surgical evacuation
ROTTERDAM SCALE		
PREDICATORS		**Score**
NORMAL	Basal cisterns	0
COMPRESSED		1
ABSENT		2
ABSENCE OF SHIFT	Midline shift	0
SHIFT >5 MM		1
ABSENT	Epidural mass lesion	0
PRESENT		1
NO	Blood in the ventricle	0
YES	presence of hemorrhage	1

1.5 Physiopathology of TBI-related brain injury

Either mild, moderate, or severe, TBI is characterized by two main events: an initial injury (or primary insult) and the second event (or secondary injury) (**Fig.2**).

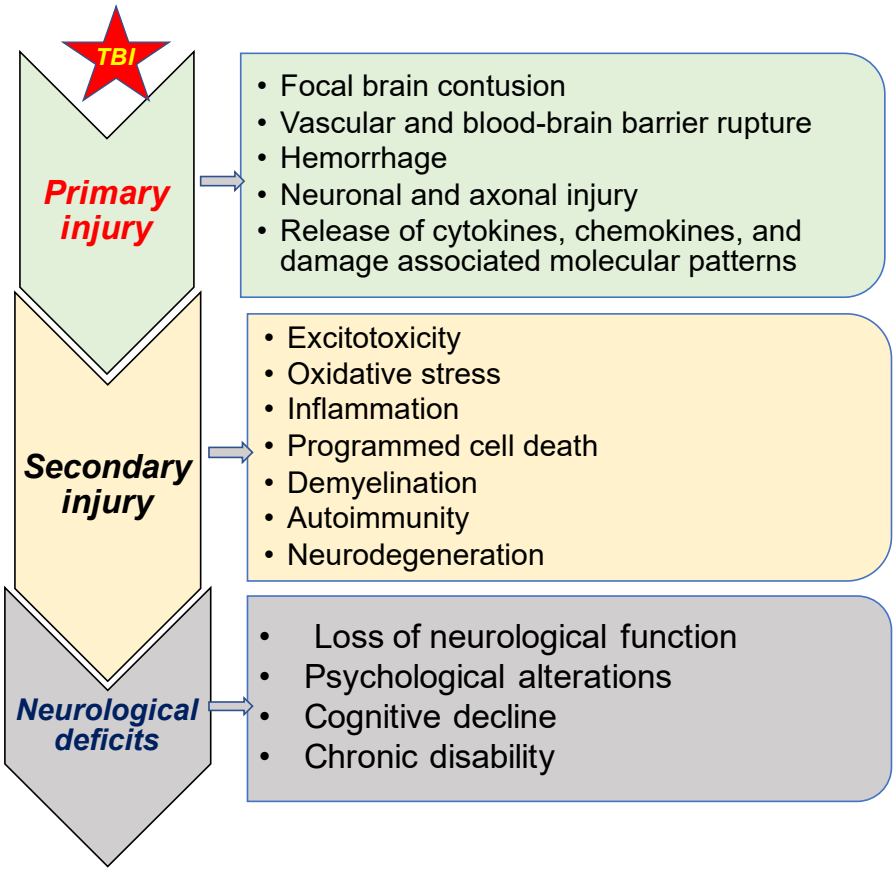

Figure 1: Summary of the events occurring following traumatic brain injury. *Immediately after the physical impact, there will be the development of the primary injury. This event will further trigger the secondary injury, and in chronic cases, there will be the development of neurological deficit*[27].

1.5.1 *Primary injury (PI)*

When the skull is impacted, the brain can be directly injured. This initial insult can traumatize the parenchyma or induce diffuse axonal damage and neuron tearing and shearing[28]. The severity of the primary trauma is directly proportional to the intensity of the physical insult. Therefore, there is heterogeneity in the event occurring at the time of the impact. Different types of injury were defined based on the mechanical insult: the penetrating injury, rotational acceleration, compression, and distension. At the cellular level, the PI can potentially damage the blood vessels, the neurons, and glial cells at the injured site or more, when the velocity can surpass the stretching

limit of the non-injured brain. One of the reasons for hemorrhage occurring after TBI is the vessel injury in the blood-brain barrier[29]. Finally, these changes are accompanied by an alteration in some genes' expressions and the occurrence of important events in TBI pathophysiology, such as the massive release of glutamate. The glutamate is the first brain transmitter, and its extended-release increases the activation of glutamate receptors with all the downstream detrimental effects on brain cells such as neuronal damage and cell death[29,30]. The typical glutamate receptors involved in this phenomenon are the N-methyl-d-aspartate (NMDA), alpha-amino-3-hydroxy-5-methylisoxazole-4-propionic acid (AMPA), and kainite, described as the ionotropic receptors[29]. Another critical event triggered by the PI is the increase of the intracellular calcium, which is known to be involved in mitochondrial function alteration and finally leads to reactive oxygen species (ROS) production[28]. This ROS production decreases mitochondrial respiration, favors lipids' peroxidation, induces protein function alteration and the oxidation of enzyme[31]. These molecular events could contribute to neuronal damage. Moreover, recently, studies have also highlighted the accumulation of iron in the brain of TBI patients who encountered intracranial hemorrhage[30]**.** The disruption of mitochondria function, the deposition of iron, and ROS generation are defined as ferroptosis characteristics[30]. Cell death due to ferroptosis is different from the other types of cell death, including apoptosis and necrosis. The main factors leading to ferroptosis are the inhibition of glutathione peroxidase 4 (Gpx4)[32] and glutathione disruption due to iron deposition.

1.5.2 Secondary injury

TBI pathophysiology is constituted by a cascade of initiated events following the physical impact **(Fig.3).** The PI generally triggers a cascade of molecular mechanisms described as a secondary injury and is caused precisely by the association of an over-activation of neurotransmitters, the neuronal and vascular damage, proteolytic pathways, the ROS, the caspases mediated-cell death, the neuro-inflammatory processes, Etc. In many cases, TBI patients show no clinical symptoms predicting the potential development of a secondary burden, but during the following hours, weeks, or even years, they develop serious complications deteriorating their health condition[33]. As TBI causes are heterogeneous, there is also a diversity in the secondary events[34].

As mentioned above, during the second phase, there is a surge of neuroinflammation characterized by the activation of microglia, astrocytes, oligodendrocytes, and leukocytes recruitment and infiltration into the brain[35,36], the over-release of mediators including cytokines, chemokines, and

complement proteins by glial, and neuronal cells[37]. The activation of glial cells is determined by the nature and the intensity of the stimulus. They usually pass through several states of activation and release a broader type of factors that promote the recovery (restoration) or contribute to the exacerbation of brain injury[38]. Among the inflammatory mediators investigated in the literature, the most common are glial-fibrillary acidic protein (GFAP), nestin, vimentin[39], ionized calcium-binding adaptor molecule 1 (IBA1), allowing to estimate the reactive gliosis. Moreover, cytokines such as interleukin-1 (IL-1), interleukin-6 (IL-6), interferon-γ, and tumor necrosis factor-a (TNF-α), Interleukin-8 (IL-8), transforming growth factor-β (TGF-β)[37,40], as well as chemokines (C-C motif) ligands 3, 4, 5 (CCL3, CCL4, and CCL5), the monocyte chemoattractant protein MCP-1 (CCL2), MIP-1α, MIP-2 are commonly produced during the inflammation process.

Additionally, the increase of inflammatory reactions of chemicals and molecules, including hemoglobin and iron accumulation, brain metabolism, and cerebral blood flow alteration, worsens the inflammatory events, oxidative stress, glutamatergic excitotoxicity, and mitochondrial dysfunction, leading to further brain damage[41].

The biomechanical insult stimulates the complement system's activation, which has a homeostatic function in physiological conditions and contributes significantly to the secondary injury process. This activation depends on three pathways, the standard and alternative complement signaling pathways, the mannose-binding lectin pathway[42], and the complement components involved in the activation cascade are C1q, C4, C3, and C5[43].

Besides the pathogenic effect of the secondary injury, other protective and restorative processes are also unleashed. These beneficial processes include the initiation of neurogenesis and synaptogenesis, the release of trophic factors such as brain-derived neurotrophic factor (BDNF), and nerve growth factor (NGF) as well as anti-inflammatory cytokines such as interleukin-4 (IL-4), interleukin-5 (IL-5), interleukin-10, or interleukin-33[44]. These factors are released in order to accelerate the repair process.

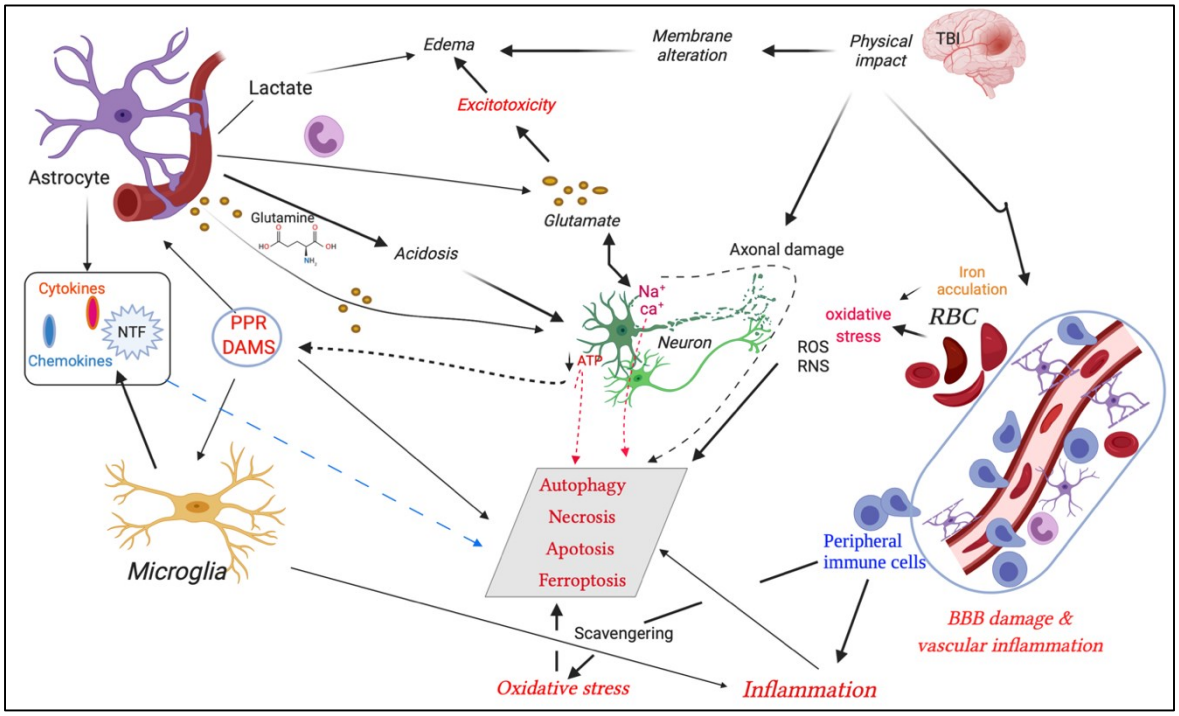

Figure 2: Traumatic brain injury pathophysiology. Illustration of the events occurring post-TBI. There is, in brief, acute, and chronic brain vasculature damage and activation of immune cells. The minutes following an impact, there is luckily an occurrence of neurovascular alteration and colossal production of damage-associated molecular patterns (DAMPs) leading to gliosis and infiltration of the peripheral immune cells. The first role of the cell infiltration is "clean" the injury site and limit the injury's propagation. Unfortunately, an upregulation of their activation increases the inflammation, the progression of the injury**.** Abbreviations: PRR: Pattern recognition receptors; ROS: Reactive oxygen species; RNS: Reactive nitrogen species; RBC: Red blood cells; Na+: Sodium-ion; Ca2+: Calcium ion; ATP: Adenosine triphosphate (adapted from Jarrahi A. et al., 2020)[27]

1.6 TBI diagnosis tools

The complexity of the human brain and the heterogeneity of TBI pathology led to the development of several diagnostic tools. The combination of these tools is useful for the diagnostic and clinical management of TBI. The use of biomarkers to reveal the pathology's severity and even predict the outcome are more than useful.

Traumatic brain injury biomarkers

The biomarkers with high specificity are good indicators of the disease state, and they can be measured from body fluids or tissues. There are essential changes in the metabolites' status after an insult to the brain. Thus, some proteins have been identified and evaluated as brain injury biomarkers using imaging and mass spectrometry techniques. Here, we listed the most investigated proteins and described in the literature[45]:

- Calcium-binding protein B **(**S100B)
- GFAP, Neuron Specific Enolase (NSE)
- Myelin Basic Protein (MBP)
- Ubiquitin C-terminal Hydrolase L1 (UCHL1)
- tau protein, and alpha II spectrin

1.6.1 Biomarkers of blood-brain barrier dysfunction

(a) S100 Calcium-binding protein B (S100B)

S100B (21 kDa), discovered in the 1960s, is a calcium-binding protein expressed in glia and Schwann cells. It participates in regulating the intracellular calcium levels[45]. S100B is one of the earliest markers evaluated in mild TBI[46,47] and considered as a promising biomarker due to the correlation between its level in serum and the severity of the injury or the outcome of patients[48-50]. The level of the protein rises quickly during the acute phase and decreases again rapidly[51]. Nevertheless, there is a possible occurrence of a second peak during the secondary injury[48]. Investigators confirmed the use of S100B as a TBI biomarker; however, some controversies still exist regarding its efficacy as a diagnostic tool[45]. For example, the levels of S100B increase in conditions such as muscle injury, but S100B is not specific in patients with hemorrhagic shock or circulatory arrest[52,53].

(b) CSF/serum albumin ratio.

The cerebrospinal fluid (CSF) and serum albumin ratio (AR) was used to assess blood-brain barrier (BBB) alteration in people with severe brain trauma and is still the common biomarker for BBB integrity[54,55]. The protein increased level suggests that the blood albumin has moved into the CSF due to the BBB alteration. However, these changes have not been observed in concussion and mild

TBI. Therefore, we can estimate that the AR may not be so precise to evaluate the disruption of the BBB.

(c) Tight junction proteins.

The occludin, one of the tight junction proteins, has been investigated as a possible biomarker of mild TBI[56]. However, the low-specificity of occluding limits its use as a biomarker.

1.6.2 Biomarkers of neuronal and axonal damage

(a) Glial Fibrillary Acidic Protein (GFAP)

GFAP (54 kDa) is a protein present in the cytoskeleton of astrocytes. Following brain injury, the astrocytes are activated, and therefore, it occurs a change in the level of GFAP, which increases. In previous studies, the protein concentration has been shown to increase in the serum in patients with brain injury[57]. GFAP is a promising biomarker of astrocyte damage and BBB damage and, therefore, specific to TBI. Compared to S100B, GFAP detection is more accurate in differentiating mild TBI from normal patients[58]. On the other hand, the variation in this protein concentration does not correlate well with the long-term outcome prediction and the GCS outcome score.

(b)Neuron Specific Enolase (NSE)

NSE (47 kDa) is an enzyme significantly released following neuronal damage. The concentrations of the enzyme identified in the serum of patients with moderate or severe TBI correlate with the CGS outcome scale according to previous studies[59,60]. Furthermore, other clinical studies have shown an elevated NSE level in the serum of patients who did not survive than the survivors and those in intensive care units[61]. Therefore, these findings highlighted the possible correlation between the increased level of NSE in the serum and the deterioration of the patient's health condition. In other words, NSE is an indicator of poor outcome in clinical investigation.

(c) Myelin Basic Protein (MBP)

An insult to the brain may affect either neurons, astrocytes, microglia, or oligodendrocytes. One of the TBI indicators, MBP (18-31 kDa), is the less studied brain cells constituent, oligodendrocytes[62]. Axonal injury potentially generates between one and three days after the injury

the release of a high amount of the protein into the blood. Compared to NSE, the myelin basic protein seems to be more specific for TBI and is also associated with bad outcomes, according to the literature[63,64]. MBP level remains elevated in serum several days post-injury, suggesting its suitability as an outcome predictor, specifically for children[65]. However, the specificity of MBP decreases in severe injury cases due to its presence in the peripheral nerves, which is generally affected in severe TBI.

(d) Ubiquitin C-terminal Hydrolase L1 (UCHL1)

In human TBI, one of the relevant biomarkers tested in the clinic is Ubiquitin C-terminal Hydrolase L1 (UCHL1). UCHL-1 is usually tested in association with GFAP for better categorization of TBI and its outcome prediction[66]. This enzyme of 25 kDa is present abundantly in almost all neurons and can provide vital information on these cells in a degenerative state. UCHL-1 likely contributes to adding or removing ubiquitin from proteins undergoing metabolization and therefore constitutes an essential protein in physiological and pathological situations[45]. In TBI cases, many investigators have found a significantly increased level of UCHL1, which was also found to correlate with CGS severity score[67,68] but not TBI outcome.

(e) Tau protein

Investigators have proposed the use of Tau protein as a biomarker of axon degeneration[69]. Tau, known as a microtubule-associated protein, is more involved in tauopathies than TBI, where its phosphorylation and aggregation are detrimental. However, TBI can lead to disturbance of axonal microtubules function and therefore affect Tau proteins activity. Examples showing increased C or T-Tau in the CSF of severe TBI cases are described recently in the literature[70,71]. These results suggest the use of Tau protein and other indicators to predict TBI severity or outcome.

(f) Neurofilaments

The neurons intermediate filaments, called neurofilaments (NF), are found abundantly in axons. Three subunits of these proteins have been discovered and described based on their size: the NF light (NF-L), 68-70 kD, the NF medium (NF-M), 145-160 kDa, and NF heavy (NF-H) with high molecular weight[72]. Following brain injury, the intermediate filaments can be disrupted and

released in the serum due to axonal damage. It was therefore suggested as a serum biomarker for TBI[73].

In addition to the above list of biomarkers, several other indicators of inflammation, including cytokines TNF, interleukins 1β, 6, and 10, Etc., and the chemokines C-C motif ligand 2, 5 (CCL5), and fractalkine[74,75], Etc., are used to diagnose further and predict TBI outcome.

1.7 Experimental models of TBI

The complexity of the human brain and the heterogeneity of trauma induced injury led to the development of several cellular and animal's models. The main goal is to:

(i) better understand the pathophysiology of TBI

(ii) evaluate potential therapeutic agents.

Neurons, glia, and brain endothelial cells are primary constituents of the brain parenchyma, and together, they form complex cellular and multicellular structures[76]. Moreover, they provide the required environment for neuronal function and protection against injury and diseases. Unfortunately, each cell type's specificity, the structure of every region of the brain, and the nature of the trauma limit the usage of one specific cell type or *in vivo* model over time to evaluate the consequences or screen the potential therapeutic agents[77].

1.7.1 In vitro strategies to modulate traumatic brain injury

1.7.1.1 The static mechanical injury models

(a) Transection models

Used to investigate mainly axonal injury and penetrating injuries following TBI, the transection models have been widely used in the research field[78]. In these models, the cells are damaged by scratching the monolayer using a plastic stylet, rotating scribe, or blades[79-81]. As *in vivo*, the surroundings of the scratched cells are also affected.

(b) Compression

The compression models are used to induce focal injuries. These models can be used both *in vivo* or *in vitro* and are generally valuable for investigating the secondary pathways of the trauma[82].

(c) Hydrostatic Pressure (Barotrauma)

In this model, the injury is generated by applying hydrostatic pressure of either transient or static pressure to cultures[83]. The model allows to mimic the close head injury and can be used to reproduce an injury and a gradient-induced deformation.

1.7.1.2 The dynamic mechanical injury models

(a) Acceleration/deceleration models

The acceleration or deceleration forces constitute a considerable factor allowing to mimic diffuse axonal injury, which leads to neuronal death[84]. The forces can be adjusted in this model accordingly to induce a clinical meaningful post-injury effect. However, it seems difficult to estimate the level of deformation resulting from the acceleration/deceleration forces.

(b) Hydrodynamic

Compared to the acceleration/deceleration model, the hydrodynamic model of TBI is more relevant in clinics. According to LaPlaca *et al*., the designed device in an *in vitro* cell shearing stress allows inducing some precise rotating speeds on cells grown on plates[85]. The hydrodynamic force generated depends mainly on the rotating speed selected and the position between the plate containing the cells and a second plate dedicated to producing the shear or the cells' stretch. Interestingly, with this model, direct visualization using a confocal microscope and measuring cell morphology[85] is possible. One of this model's limitations is the inconsistency in modeling the injury when 30/second of strain rate was reached[86].

(c) Fluid Shear Stress

This model is used in many cell types, and a precise deformation can be obtained by well controlling the design[87]. Like the hydrodynamic model, the fluid shear stress model is utilized to observe the cells' response under stress situations in a real-time manner. The use of these models was guided by the desire to describe the physiopathology of TBI better. Compressed gas, vacuum pulse to a thin deformable substrate, is used to mimic TBI *in vitro*[88].

1.7.1.3 The Chemical injury models

(a) Glutamate treatment

In addition to the mechanical injury models, some investigators have introduced chemical injury models of TBI. One of the chemical compounds tested is glutamate, known as a neurotransmitter. When neuronal cells are exposed to glutamate, there is a decrease in their viability accompanied by mitochondrial dysfunction[89]. A High concentration of glutamate-induced excitotoxicity and apoptosis[90] are also described as important events following brain injury.

(b) Peroxide treatment

The development of the second phase of brain injury is partly due to the generation of free radicals. Therefore, researchers have developed *in vitro* free-radical injury models to induce oxidative stress to cells and evaluate the potential of antioxidants[91].

1.7.1.4 Others models

Brain on chips systems

New *in vitro* strategies to mimic TBI are still needed. The brain on chips systems are newly developed methods to model the disease accurately. The pioneers of these systems wish to associate the electronic technologies to the biology. They allow creating a mini-environment of the disease in a microfluidic system using 3-D cell cultures[92]. This strategy successfully modeled axonal injury, BBB modeled with microfluidic[93], Etc. These systems' main goal is to provide a deep understanding of the TBI physiopathology by generating a more complex "*in vitro* model of human brain"[92]. However, the brain on-chip systems are under development, and challenges such as the verification of the fidelity between the microscopic representation and physiological state remain.

1.7.2 Animal Models of TBI

Researchers propose a diversity of animal models simulating TBI to understand the disease's pathophysiology and evaluate therapeutics. These models include:

- ✓ head acceleration,
- ✓ weight drop model,
- ✓ blast wave,
- ✓ fluid-percussion,

- ✓ controlled cortical impact (CCI),
- ✓ repetitive mild TBI/chronic traumatic encephalopathy.

Some of the experimental models used by the researchers are presented in **Fig.4.** The figure summarizes the diversity of the existing models, with the primary goal to address the complexity and the heterogeneity of human TBI. Each model has its advantages and disadvantages. There is no complete model that can fully mimic the physiopathological patterns developed following brain trauma.

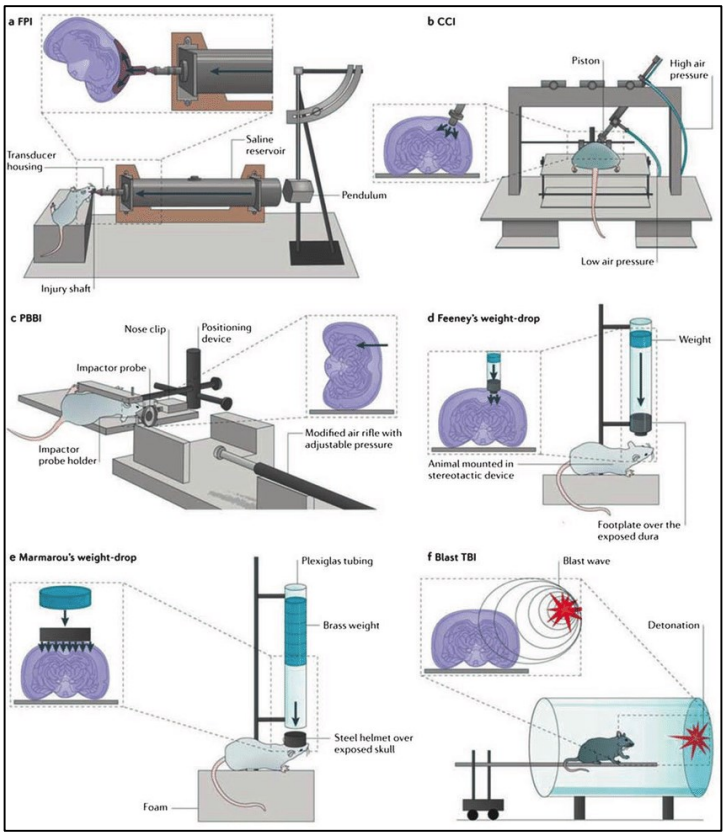

Figure 3: Animals of traumatic brain injury. *(a) The fluid percussion injury model (FPI): the device is designed to injection quickly a fluid pulse into the epidural space. (b) The controlled cortical impact (CCI) model utilizes air or electromagnetic driven piston to impact the brain with precise parameters. (c) The penetrating ballistic-like brain injury (PBBI) uses the transmission of projectiles with a metal rod's high energy or expansion of the probe's elastic balloon. (d) weight-drop model, an object with known weight is dropped onto the exposed dura. (e) Marmarou weight-drop model uses metal disk instead to protect from a bone fracture. (f) The blast injury model. (Reprinted in its entirety from Xiong et al. (2013) with permission from Nature Publications)94*

1.7.2.1 Weight drop model

Many authors consider it as the "original TBI model[95]. The weight drop injury is generated by dropping a mass with a known weight on the exposed skull using a tube guide. This impact typically produces contusion. Different types of injury severity are obtained by adjusting the weight and the height from which the mass falls. In some cases, the skull is subjected to a craniotomy before the impact. The simplicity of the model constitutes its advantage but is limited by the high mortality rate.

1.7.2.2 Fluid percussion injury model

Here, fluid pressure is applied to the brain in order to produce a closed head injury. After a craniotomy between the bregma and lambda, or at the desired location, a container filled with saline is disposed of on the craniotomy site using a pendulum. Depending on the height, a defined injury type can be obtained. Lindgren and Rinder developed this model in 1969 before being adapted as the fluid percussion injury (FPI), one the most common focal injury model among investigators[96,97]. Using this technique, the users simulate a contusion without inducing a fracture on the skull.

1.7.2.3 Controlled cortical impact model (CCI)

The CCI is widely used, and the parameters, including impact duration, velocity, and depth, can be controlled, and adjusted according to research interest. Specific impactor devices equipped with compressed air-driven metallic piston and tips can produce impacts on the brain tissue[98]. Mild, moderate to severe injury can be produced, leading to the generation of contusions, hematoma, high intracranial pressure, axonal injury, and even coma[99]. Compared to the weight drop and FPI, the CCI has low mortality but does not lead to brain stem deformation.

1.7.2.4 Blast tubes

The model has been developed for large animals in the 1950'ies by Clemedson and Criborn, 1955[100,101] but was finally modified and adapted to rodents[102]. A detonation charge produces waves with a short duration. A primary injury is simulated by the blast tube, and the secondary effect could derive from the emitted smoke.

1.7.2.5 Shock tubes

In this method, a tube with two chambers is created using a diaphragm (membrane). One of the chambers contains compressed air or gas, and the second contains the animal. Waves derived from the compressed air or gas are next propagated after a membrane's rupture, and several models exist[103-105].

1.8 Current interventions

The diversity of brain injury patterns required different diagnosis methods and treatment strategies. Depending on the injury type, severity, and location, a specific treatment approach will be defined. The treatment might be ranging from taking a simple rest to admission in intensive care units. In severe cases, rapid intervention is needed in order to keep the patient out of fatal conditions.
In the clinic, guidelines exist to help the physicians, and several strategies have been developed.

1.8.1 Non-invasive non-operative interventions

These techniques do not require any tissue damage, nor a surgical intervention

(a) Management of hyperosmolar and blood pressure

This strategy is mainly recommended to facilitate the venous drainage, reduce the blood inside the cranial compartment, and thereby reduce the intracranial pressure (ICP). The technique consists of adjusting the patient head's position at 30 degrees, creating hyperventilation, and providing agents known to decrease the ICP[106].

(b) Reduction of cerebral metabolic rate

Another treatment adopted in controlling the head injury is decreasing the blood flow in the brain, ICP, and tissue oxygen demand by using anesthetics and hypothermia that have the potential to reduce the cerebral metabolic rate of oxygen[107-109.]

1.8.2 Invasive non-operative interventions

These intervention strategies are recommended for treating moderate to severe TBI patients. The techniques use ICP, brain tissue monitors, and microdialysis catheters to help reach a better outcome and reduce hospital stay[110].

1.8.3 Surgical interventions

In severe TBI cases, the use of surgery is sometimes inevitable, specifically when there are skull fractures, severe edema, epidural hematomas, subdural hematomas, large vessel injuries, and intra-parenchymal contusions. In these cases, the surgical interventions are intended to limit the mortality rate, and increase outcome[111,112]. However, care should be taken and the guidelines regarding the method of surgery have been described.

1.9 TBI and blood transfusions

Blood transfusion is recommended in specific cases, multi-trauma patients, patients with hemorrhagic shock, or uncontrolled bleeding. Even in many investigations, when severe injured patients suffer from anemia, red blood cells' transfusion does not reverse the patients' conditions[113-115]. Likewise, the transfusion of platelets to TBI patients did not provide a better outcome. The dysfunction of platelets reported in these patients was not corrected, nor bleeding, stops after platelets transfusion[116].

The blood product potentially having some beneficial effect is plasma, which has been described to improve patient conditions when transfused before patient admission in the hospital. However, some controversies on the interest of plasma transfusion still exist[116,117].

So far, the limited number of studies done to assess the clinical outcome of blood and blood product transfusion in TBI patients failed to provide sufficient proof of their ability to reverse the coagulopathy induced by the trauma.

1.10 Pharmacological drugs for TBI

TBI is characterized by a surge of neuroinflammation and an excessive release of pro-inflammatory factors, worsening patients' conditions. Thus, several anti-inflammatory compounds have been intensively screened, and some underwent clinical trials. Molecules, such as erythropoietin (EPO)[118], minocycline, statins, N-acetylcysteine (NAC), rosuvastatin, pioglitazone, and rosiglitazone, dexamethasone, and melatonin as examples[119] have been intensively evaluated for their ability to modulate neuroinflammation. In *vitro* and animal models of TBI, these drugs exhibited beneficial effect[120]. However, in clinical trials, none of these pharmaceutical drugs was able to improve patients' outcomes[118]. All failed either at phase 1 or phase 2 in clinical trials[121].

1.11 Therapeutic strategies for neuronal recovery and neurobehavioral improvement

Several pharmaceutical drugs have been screened for their ability to manage the recovery of neuronal injury and subsequently improve the patients' behavioral deficit. A long list of tested compounds, cAMP, inhibitors such as rolipram, dipyridamole, BC11-38, fluoxetine, Etc., has been evaluated[119].

1.12 Neuropsychological Rehabilitation (NR) and Neurotherapy

TBI can induce an impairment of the motor function and patient cognition depending on the injury type. Generally, the disturbance of neurotransmitters' function and the disruption of neuron networks are the leading causes of memory loss and behavior changes. Therefore, the neuropsychological interventions aimed to improve the cognitive function and social behavior of TBI patients. These interventions provide support where modern medicine failed to provide efficient solution[122]. They focus on using training programs designed to ameliorate the cognition, the mnemonic, and patients' behavior[123,124].

1.13 New therapeutic strategies

Considering the limitations of the above therapeutic strategies, new approaches such as the use of biological products is under investigation. These approaches include gene therapy, eRNA, DNA, microRNA, antagomirs, peptide therapy, stem cells, exogenous growth factors, and peptides[125].

The use of biogenic compounds constitutes a promising and innovative strategy nowadays. Recent investigations have highlighted the neuro-restorative and neuro-regenerative ability of neural stem cells[126]. Additionally, evaluating the neuroprotective activity of natural neurotrophins is emerging with promising outcomes.

On the other hand, gene therapy and the delivery systems using viral and non-viral provide information in managing neuronal damage. The possibility of incorporating some genetic material into nanoparticles and their delivery via the intranasal route opens new windows regarding TBI treatment[127-129].

Despite the development of neuroprotective, neuro-restorative, and anti-inflammatory approaches, there is still disappointment regarding TBI's long-term effects. Thus, clinicians and researchers are still looking for new models, therapeutics, diagnosis tools, and biomarkers to bridge the gap. The need to look inside the brain for subtitle changes or alterations deeply is still necessary.

2. Platelet, platelet lysates and their role in neuro-regeneration

2.1 Platelet production, structure, and physiology

Human blood cells are red blood cells (RBC), white blood cells (WBC), and platelets or thrombocytes. The thrombocytes are the smallest cells, with an approximate diameter of 2 to 5 micrometers and a thickness of 0.5 micrometers. They have been recognized for the first time by Max Schultze in 1865 and finally described in a comprehensive way by Bizzozero in 1882[130]. Platelets are originating from the megakaryocytes, the large bone marrow pluripotent cells. An estimated 10^{11} platelets are released by the megakaryocytes daily through a process called thrombopoiesis, and their number per microliter of blood in a healthy adult is ranging between 150 to 350 x 10^3 [131,132]. Upon producing, the second most abundant blood cells spend, according to previous reports, between eight to ten days, followed by their degradation n the spleen.

Under physiological conditions, the thrombocytes circulate as discs shaped with precise structure. The platelets are enucleated and carry internal structure elements such as granules, cellular organelles, and mitochondria. The granules resemble to vesicles, and three types have been characterized in platelets:

***Alpha granules*:** an average of fifty to eighty alpha-granules can be found per platelet, making them the most abundant vesicles in these cells. When checked by SEM, the α-granules derived from human platelets in a resting state exhibit an ovoid morphology ultrastructure. These platelet vesicles constitute an important reservoir of proteins. They possess surface proteins as well as other soluble materials. As an example, a proteomics analysis of α-granules proteome revealed more than 200 proteins[121]. This result gives an idea of how large is the protein content of platelet granules.

Delta or dense granule are smaller than the α-granules, and each platelet contains three to eight delta granules. Contrary to other types, the dense granules contain mainly molecules such as calcium and magnesium ions, adenosine diphosphate (ADP), adenosine triphosphate (ATP), histamine, polyphosphate, and serotonin, which are not proteins but may be potentially involved in the activation process of platelets.

Lysosomal granules: they are less abundant and carry essentially proteases and hydrolases [132-134.]

T-granules: they constitute the newly discovered platelet granules and may contain toll-like receptors. T-granules present a tubular morphology[135].

In terms of platelet proteome, studies have reported more than 5000 proteins in platelets using LC-MS-MS analysis[133]. However, this abundance of proteins is highly dependent on the state of platelet activation during the analysis (activated or resting cells). Factors such as the donor's age and health condition and the platelets' storage conditions can induce changes in their proteomes[136-138].

2.2 Platelets function

Platelets are involved in several biological processes.

2.2.1 Platelet function in hemostasis

The hemostasis is the first role of platelet described in the literature since their discovery in 1885 by Bizzozero. Due to their small size, the thrombocytes are circulating next to the vessel's wall. In these areas, they contribute to preventing bleeding when a blood vessel is injured. During the process, the platelets first adhere to the injured blood vessels through their specific GPIbα-IX-V receptors with the von Willebrand factor. In brief, the exposed collagen from the injured vessel activates platelet collagen receptors and subsequently initiates, in the same manner, the activation of the fibrinogen receptor. Through their adhesion receptors, the von Willebrand factor receptor (required for platelet localization at the injury site), and the fibrinogen receptor, the platelets translocate and adhere to the endothelium of the injured vessel.

The other receptors' contribution strengthens the adhesion, the activation, and the aggregation of platelets at the wounded area[139]. Several activation cycles involving other adhesion receptors of platelets are usually required to empower platelets' response to bleeding[127]. Platelets have the potential to adhere to a damaged site, and once they are activated, they release their content and participate in healing processes.

Besides their homeostasis role, platelets are involved in biological processes, including inflammation, atherogenesis, antimicrobial effect, tumor growth etc[140].

2.2.2 Platelet function beyond haemostasias

The complexity of platelet morphology and their plethora of bioactive compounds released upon activation facilitate their implication in other functions beyond the homeostasis.

(a) The function of platelets in wound healing

Platelets are not only participating in halting the bleeding following a vascular injury but are also associated with the healing process. During their activation and aggregation, the platelets also secrete cytokines that mediate the injured vessel repair. By releasing the trophic factors including platelet-derived growth factor (PDGF), transforming growth factor (TGF) and vascular endothelial growth factor (VEGF), epidermal growth factor (EGF), angiopoietin, SDF-1 (CXCL12), MMP-1, MMP-2, and MMP-9 Etc. the thrombocytes stimulate cells growth, and differentiation, and therefore favor wound healing and angiogenesis[141-143].

(b) Role of platelet in inflammation:

Platelets have been recognized to contribute substantially to the inflammation process. According to many authors, the platelets communicate with immune cells to facilitate several biological events. Due to the presence in the alpha granules of some active substances, platelets can modulate the vascular permeability, interact (leucocytes) and recruit immune cells, interact with endothelial cells, and release important quantity of pro-inflammatory factors at the injury site [144,145]. The implication of platelets in inflammation is summarized in **Fig.4.**

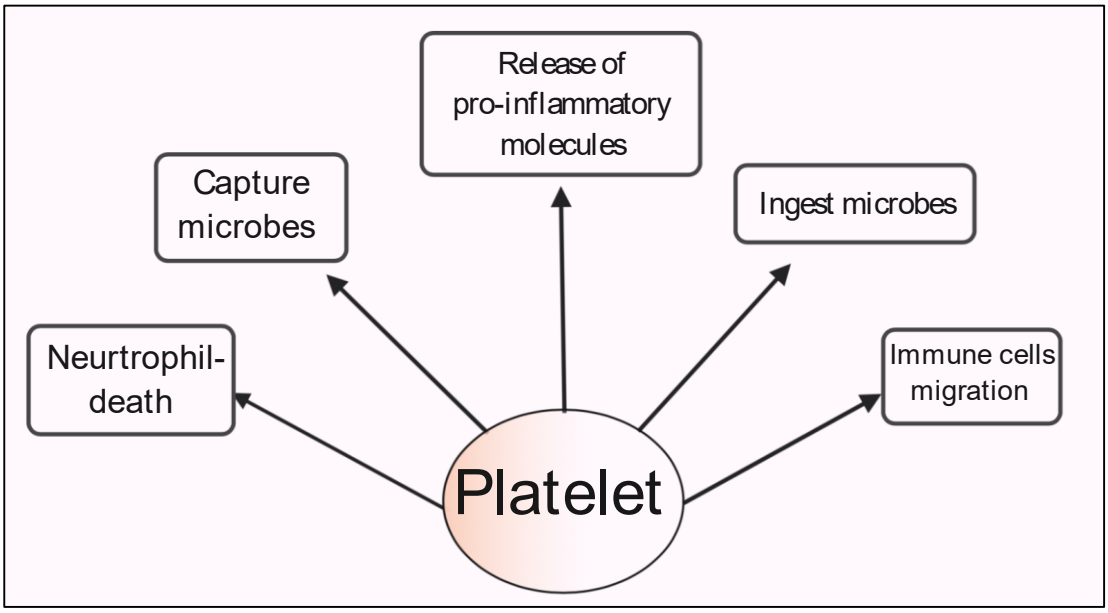

Figure 4:Platelets and inflammation. *Illustration of potential platelet participation in inflammation (adapted from Ame et al., 2015)[144].*

(c) The sentinel role of platelets

In addition to their ability to interact with leukocytes, the platelets have the potential to monitor the environment and defend it against pathogens thanks to its detectors such as the toll-like receptors. These receptors can trigger an immune response after recognizing the pathogen-associated molecular patterns[145,146].

2.3 Platelet concentrates

2.3.1 Preparation procedures

A therapeutic platelet concentrate (PC) is a blood-derived product produced in blood transfusion facilities from either whole blood donations or apheresis and utilized to treatment of bleeding disorders caused by platelet depletion or dysfunctions. A PC bag can be derived from either one or up to 5 or 6 donors, depending upon the collection mode.

Practically, the PCs can be prepared from whole blood donations with a total blood volume of 200-500 mL including the volume of anticoagulant/preservative solution. Since the whole blood contains red blood cells and plasma, a specific centrifugation step is done to produce the platelet concentrates. To reach the required number of platelets needed for transfusion in adult patients, 4 to 6 of the fractions containing the platelets and white blood cells (buffy coat) are pooled[147]. When the PCs are produced by apheresis, an automated device is used to collect around 150-300 mL of platelets concentrated four to five-fold compared to the average concentration in blood. The PC donation obtained by apheresis does not require a pooling step as the volume collected is sufficient for one adult dose.

Another critical factor in the preparation of platelet concentrates is the platelet storage buffer. The solution in which the platelets are suspended impacts their shelf life, which is generally between 5 to 7 days at 22 ± 2°C. For now, the platelets are maintained either in plasma or in plasma mixed with platelet additive solution (PAS) at a determined proportion (30-40% plasma and 60-70% PAS). The Council of Europe ‘‘Guide to the preparation, use and quality assurance of blood components’’ suggests at least 2 x 10^{11} platelets and less than 1x 10^{6} residual leukocytes in each PC unit[148]. Additionally, the PC should be free of pathogens. Therefore, various safety measures to ensure optimal quality control of PC used as sources of materials to produce human platelet lysate are in place. In blood establishments, the donors are firstly screened to select the healthy blood donor candidates, and the fresh PCs are next assessed for the presence of known viruses

such as human immunodeficiency virus (HIV), hepatitis B virus (HBV), and hepatitis C virus (HCV). Finally, to further warranty the PCs' safety, they are treated with licensed pathogen-reduction methods.

2.3.2 *Safety of platelet concentrates*

Two main approaches using Ultraviolet-Activated photosensitizers that target the nucleic acids have been developed regarding infectious organisms' elimination or reduction. These new strategies were required since the solvent-detergent treatment used in inactivating pathogens in plasma is not applicable to platelets and red blood cells. The solvent-detergent acts in destroying the virus' envelopes and this mode of action can also alter the blood cells.

- ✓ ***The Mirasol PRT system***

Terumo BCT has been developed this system for pathogen reduction of platelets and plasma. It intends to reduce the window period for known diseases and protect against the unknown and emerging pathogens[149]. The Mirasol system uses riboflavin as a photosensitizer and UV light (280–400 nm) treatment[148]. The properties of riboflavin described in the literature, such as its ability to interact with nucleic acids and to undergo a chemical change with those nucleic acids under light exposure[150], led to its selection in pathogen reduction strategy. In this approach, the platelets are collected into their storage bag and then transferred under sterile conditions into an illumination/storage bag. Next, the riboflavin solution (around 50 molars) is added and the mixture, illuminated using a particular device, the MirasolTM Illuminator. The UV light (280 to 400 nm) energy dose and the duration of illumination are calculated based on the size of the mixture[149] (see **Fig.5**). Furthermore, during the treatment process, the platelet bag is maintained under constant mixing by back-and-forth motion at a speed of 120 cycles per minute[149]. At the end of the illumination, the platelet concentrate is removed from the illuminator and stored without removing the riboflavin, and according to the regulations for platelet storage.

Mirasol PRT system method has been validated and licensed for its efficiency to inactivate pathogens. However, a general activation of the treated platelets was also observed[151].

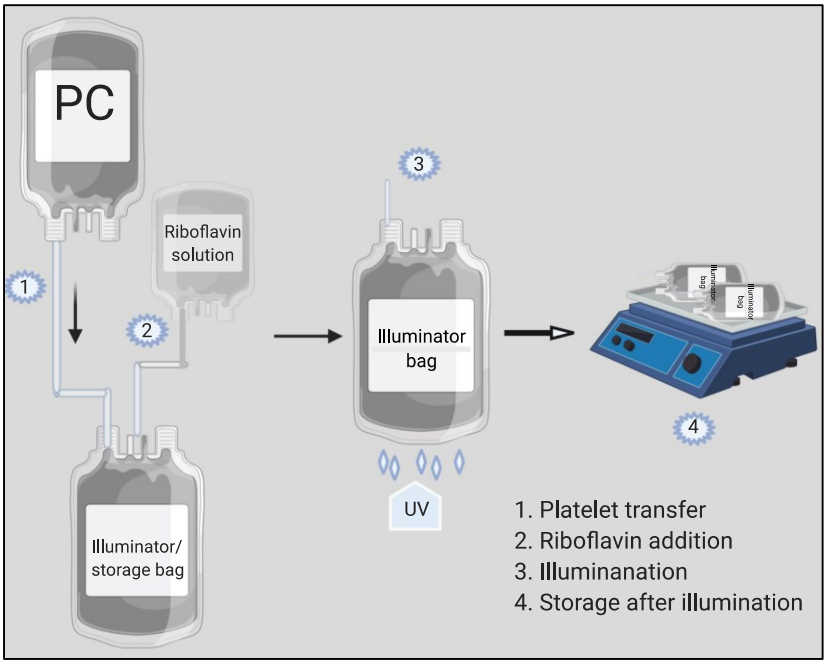

Figure 5:Mirasol treatment method. *A Strategy used to inactivate pathogens in platelet concentrates. Abbreviations: platelet concentrates (PC), ultraviolet violet (UV)*

- ✓ ***The INTERCEPT blood system for platelets***

The INTERCEPT Blood System is one of the pathogen reduction technologies developed by Cerus. The system targets the *ex vivo* preparation of platelet with a willingness to decrease the potential risk of pathogens infection[152]. INTERCEPT blood system uses ultraviolet A (UVA) light, amotosalen (S-59) as a photosensitizer, compound adsorption device (CAD) for the removal of residual of amotosalen, and metabolites[152]. The combination between the photosensitizer amotosalen and UV light (320–400 nm) allows the formation of an irreversible link that blocks pathogen replication[148,153]. The blockage of pathogen replication is possible because amotosalen can penetrate cells and intercalate in-between DNA and RNA nucleic acid bases.

The INTERCEPT blood system for platelets has four main steps (**Fig.6**). Upon collection, the platelet concentrate is first mixed with the photosensitizer. The mixture is then illuminated by UVA light using INTERCEPT illuminator, which delivers 3 Joules/cm2 (J/cm2) UVA within 3 to 4 minutes. When the illumination is completed, the PC is transferred to a bag containing the CAD and agitated for 6 to 24 hours at 22°C ±- 2°C for platelet suspended in 100% plasma and 6 to 16

hours for platelets in PAS[154]. The last step consists of transferring the platelets into a storage bag and stored at 20-24°C with continuous agitation until use.

An important range of pathogens, including enveloped viruses, bacteria, protozoa, and residual leukocytes, can be inactivated. Even if the final product is suitable for transfusion purposes, nevertheless, recent studies have indicated that the "INTERCEPT" treatment leads to biomolecular alterations[155]and the technique is also limited by its variable effect on non-enveloped viruses and the activation of platelets post-treatment[156,157].

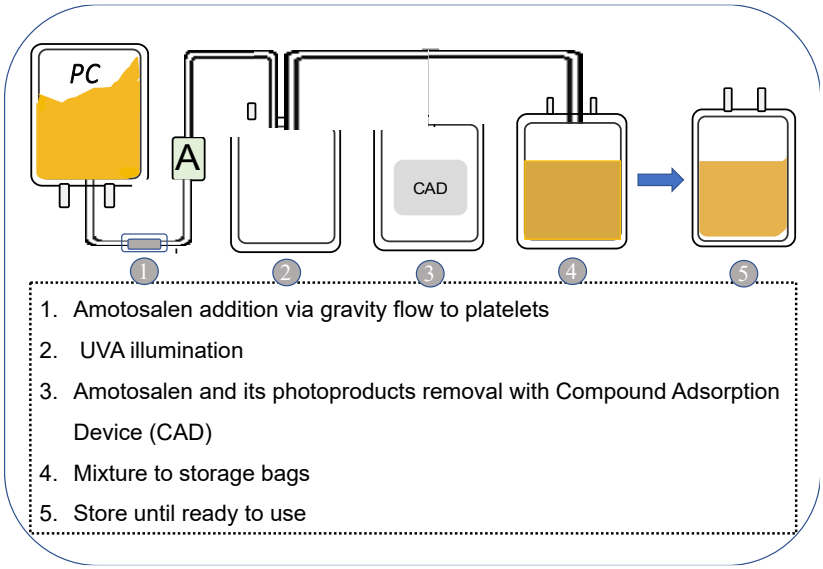

Figure 6:Process of INTERCEPT treatment for platelet concentrates

The shelf-life of a PC is 5 to 7 days at 22 ± 2°C depending upon legislation. Unfortunately, the short shelf-life of platelet concentrates due to bacterial growth risk leads to the loss of 10-20% of PC produced. These PCs, after their expiration date, are disqualified for transfusion and have to be discarded[147]. There is an increasing interest in using these expired-PCs as raw materials to prepare lysates for regenerative medicine.

2.4 Human platelet lysates

Platelet lysates are prepared from platelets isolated from whole blood donations or collected by plateletpheresis[158]. The lysis can be induced by physical disruption or activation by platelet agonists, resulting in a complex protein mixture rich in bioactive molecules and trophic factors[159].

PCs derived from either one or several donors are generally used to prepare platelet lysate biomaterials for regenerative medicine applications. The need to make pools of PCs is to reduce the individual variations between the donors since it is clear nowadays that the sex, age, weight, and genetic background can potentially introduce variations between PCs' batches. A typical platelet lysate is a combination of plasma and platelet proteins. Platelets in PC for transfusion are suspended in plasma or a plasma/PAS' mixture. However, for some applications, a platelet pellet is first obtained by centrifugation steps before being lysed.

2.4.1 HPL Preparation strategies

Platelets contain numerous components that can be released under specific conditions. Various methods to induce the release of these components have been developed and described in the literature. The standard procedures used and reported are the freeze-thaw method, platelet activation using thrombin or other activators, sonication, and solvent/detergent (S/D) treatment[160]. Therefore, the lysate content is likely dependent on the method used to activate or break the cell membrane. Moreover, the use of PAS during PC preparation has an impact on the total protein content.

(a) Freeze-thaw protocol

A straightforward method, namely repeated freeze, and thaw, does not require specific chemicals, possibly explaining its frequent use. The PC is centrifuged to pelletize the cells. The platelet pellet is then subjected to freezing and thawing cycles to trigger the secretion or the release of platelet factors. This procedure breaks the cell membranes and facilitates the release of platelet content. Three cycles of freezing (-80°C) and thawing (37°C) have been reported in the literature to achieve a complete release of platelet content[161]. Compared to the other procedures, the freeze-thaw approach leads to a sufficient release of factors.

(b) Thrombin activation

Here, the platelets are directly activated by adding of calcium chloride ($CaCl_2$) in the presence of glass beads to generate endogenous thrombin or by exogeneous thrombin[162,163].

(c) Sonication

Some researchers are using sonication at the frequency of 20 kHz for 30 min to achieve an efficient release of platelet content[164,165]. However, this method is less common, and it is sometimes combined with the freeze/thaw process to break the cell membranes further.

(d) Solvent/detergent (S/D) treatment

This method is intended to stimulate the release of the platelet content as well as virus inactivation[166,167]. When the treatment is completed, the mixture is centrifuged to remove cell debris and fibrin clots. The use of the platelet releasate after SD treatment may require the use of an anticoagulant to avoid coagulation during the use of the lysate.

2.4.2 Safety of platelet lysates

There is a risk of pathogen transmission through human platelet lysate since they are derived from PCs. Precautions should be taken, and recently, some strategies are emerging to improve the products' safety margin further. The strategies target the platelet concentrates as they constitute the source of materials for platelet lysate preparation, or the lysates are directly subjected to pathogen reduction treatment. As such, Solvent/detergent (S/D) treatment, Gamma irradiation, or platelet lysate screening using nucleic acid amplification tests[147] are evaluated.

2.4.3 HPL bioactive molecules

Platelets contain a plethora of bioactive proteins. As recognizing their involvement in many biological processes is emerging, identify the molecules they carry and understanding their function become crucial. Thus, researchers have tried to identify human platelets' content by LC-MS-MS. In many investigations, more than one thousand proteins were identified[168,169]. The long list covers cytokines, growth factors, neurotrophins, enzymes, Etc. Some variations have been recorded, and they may be associated with factors like donor age, sex, health condition, and technical specificities of the analysis.

Depending on the tissue microenvironment, platelet secretions play different roles. For example, more than 300 trophic factors are involved in the wound repair capability of platelets[142]. The function of some of the bioactive substances is summarized in **Table 3.**

Table 3: Platelet-derived molecules and their potential functions

Category	**Molecules**	**Functions**
Mediators	Histamine	Actions on CNS; promotes coagulation and T cell activation
	Serotonin (also known as 5-HT)	Promotes inflammation and coagulation
	Thromboxane A2	Promotes inflammation
	PAF	Promotes wound healing
Pro-inflammatory and anti-inflammatory cytokines and chemokiness	TGFβ	Growth inhibition; immunosuppression
	CXCL7 (NAP2)	Chemokine
	CXCL4 (PF4)	Chemokine
	CXCL1 (GROα)	Chemokine
	CXCL5 (ENA78)	Chemokine
	CCL5 (RANTES)	Chemokine
	CCL3 (MIP1α)	Inflammatory gene regulation
	CCL7 (MCP3)	Inflammatory gene regulation
	HMGB1	T cell activation; multiple effects
	IL-1β (and IL-1 precursor protein)	Chemokine
	CCL2	Chemokine
	MCP1,-3	Chemotactic protein
	IL-8	Cytokine
Receptors-ligands	Thrombocidins 1 and 2	Antibacterial peptides
	CD40	Co-stimulation; endothelial interactions
	CD154	Co-stimulation; endothelial interactions
Patern recognition receptors	TLR1, TLR2, TLR3, TL4, TLR5, TLR6, TLR7, T	Pathogen detection
	TREM1 ligand	
Trophic factors	PDGF	Neurons survival, differentiation, synaptic plasticity and outgrowth
	VCAM1	
	BDNF	
	EGF	
	VEGF	
	FGF	
	IGF-1	
	HGF	
Enzymes	Catalase	Antioxidants
	Glutathione peroxidase,	
	Superoxidase dismutase	
	Glutathione S-transferase	

3. Human platelet lysate, a novel and smart thoroughfare for the treatment of CNS disorders?

In the past decades, the prominent known role of platelets was their involvement in homeostasis. As indicated above, their diverse roles are increasingly described in the literature in recent years. In addition to this previous thought, it is now clear that the platelets are a major contributor to

wound healing and several other biological processes. Their ability to sense, communicate with other cells such as immune cells, and release broader ranges of active molecules justify their diverse functions. In recent publications, the investigators have described and highlighted the possible link between these blood cells and the brain, as well as their instrumental roles in CNS disorders[170,171]. Platelets must be activated to achieve a specific function at a specific time. The specificity of their role depends on the stimulus that triggered their activation. The cells' shape and their interactions with other cell types are highly dependent on the environmental conditions as described previously[172,173]. This specific behavior of platelets led to the investigation of their potential role in regulating brain function.

3.1 Platelet and brain function

3.1.1 *Platelets involvement in neurodegenerative diseases*

Platelets play diverse roles, and their dysfunction is also associated with several neurological disorders such as Huntington's disease (HD), Parkinson's disease (PD), and multiple sclerosis[174-176]. According to some researchers, platelets are active contributors to innate and adaptive immunity. By expressing immune molecule CD154, platelets can be a link between the innate and adaptive immune systems and, therefore, help to stimulate $CD8^+$ T cells[177]. The platelets also express Toll-like receptors known to stimulate the release of tumor necrosis factor-α (TNFα) by the leucocytes[178]. Additionally, they can interact with leukocytes and endothelial cells through their P-selectin and trigger many inflammatory events such as leukocyte recruitment, migration, activation to injured tissue, and release of cytokine[179,180]. In AD, platelet in the patient brain is described as detrimental since the cells carry naturally amyloid-ß and can be secreted after their activation[181]. This production of amyloid-ß could therefore, favor the aggregation of the protein in the cerebral vessels[182].

Despite the detrimental effect of platelets observed in some neurological diseases, the platelets are also involved in many other beneficial and repair processes.

3.1.2 Platelets are also implicated in regulating brain function

Evoking platelets' implication in brain function could be unreasonable or unusual since there is no obvious or apparent connection between these cells and the brain. However, as indicated previously, platelets perform diverse functions in human body and CNS is not free from their

action. They release signaling molecules that contribute potentially in the growth and survival of immature brain cells. This contribution to regulating brain function has been highlighted, for example, through the evaluation of factors such as TGF-β[183], β-2 microglobulin[184], and gelsolin[185]. Platelets constitute an important source of trophic factors that are also keys factors in brain function[142,167,186]. They participate in regenerative processes through their interaction with CNS stem cells[187]. Neurogenesis is an important phenomenon in brain plasticity, and it occurs mainly for adults, in the sub-granular zone of the hippocampal dentate gyrus and the subventricular zone (SVZ) of the lateral ventricles[188-192]. Even if the BBB controlled the exchanges tightly in the brain, there are still exceptions, such as interactions between the blood and the brain. These events have been shown recently through the comparison between young versus adult mice's blood on neurogenesis promotion. The young mice blood could promote neurogenesis in the adult brain[193-195], but this was not achieved with adult mice's blood. Moreover, the platelets are also able to affect significantly the function of synapses after TBI according to several authors[196,197]. They can stimulate the activity of neurons and therefore increase the survival of neurons surrounding the injury site. Growth factors such as platelet-derived serotonin can induce upregulation of cFos, Arc, and Egr1, and PSD95 genes and subsequently increased early the synaptic plasticity. Moreover, platelet-derived FGF-2 is able to exert neuroprotective activity[198,199], and stromal cell-derived factor 1-α (SDF-1-α)[200,201] contributes to recruiting progenitor cells as well as neural tissue repair stimulation[201]. Even if other cell types can secrete the same factors, the platelets could still contribute to higher the level of these factors when needed. The proteomics analysis of platelet proteome has revealed the presence of immune molecules, neurotrophins, growth factors, cytokines, chemokines, enzymes, etc[202], and therefore supported these findings.

On the other hand, the discovery of the immune molecules in platelets proteome has led to the investigation of their immune actions by some researchers[203]. These studies have highlighted using an experimental model of inflammation, the ability of platelets to activate glial cells in the cortex, as well as the modification of proteins adhesion in the brain microvasculature[204]. Other studies have also shown the pro-inflammatory role of platelet CD40L[205] and the release of complements C3 and C5 during their activation that could explain their immune actions[206]. Regulating macrophage recruitment and their activity is considered as an important factor during CNS myelin repair[207]. Thus, platelets' specific ability of might be beneficial since inflammation is not mainly an aggravating factor but is also crucial for CNS repair, as shown recently[207-209].

Platelets-derived extracellular vesicles contribution to platelet roles

The thrombocytes communicate through exosomes or microparticles, and 60 to 90% of blood extracellular vesicles are derived from platelets, according to several authors[210,211]. When activated, the platelets release an important number of particles, and their molecular cargo depends on the activation initiator[173,212,213]. Exosomes seem to be involved in the communication between adult stem cells or neural stem cells. They are also useful in the regulation of neural precursor cells in the neurogenic niches[214]. Moreover, either exosomes or microparticles, the evaluation of their functional activity revealed that they contain bioactive molecules that to promote neurogenesis. Platelets seem to be involved in brain function; however, a question remains to be addressed. Could the mixture of platelet molecular cargo alone represent a possible therapeutic approach to treating the treatment of CNS disorders?

3.2 Role of human platelet lysate in the modulation of neural stem cells (NSCs) proliferation, survival, and differentiation

Platelet lysates are prepared through several methods with the primary goal to lysis the cells and recover their content. These preparations are commonly called platelet lysate or human platelet lysate for human-derived platelets. They constitute a natural product. Investigations regarding platelet lysate as a novel therapeutic approach for CNS disorders treatment is emerging nowadays. Pieces of evidences are being collected both by researchers and clinicians regarding the platelet lysate potential in regenerative medicine. Trophic factors were described several years ago as crucial signaling molecules involved in several biological events. Some of these factors, named the neurotrophins, are playing specific functions in essential phenomena related to the central nervous system such as neuronal cell differentiation, development, metabolism, repair, the axons, and dendrites outgrowth[215,216]. They are also controlling the formation of synapses[217]. Their roles optimized the brain function and were also investigated as possible therapeutics for neurodegenerative diseases. As indicated in Table 3, some of these growth-promoting molecules are found in platelet lysates in a considerable amount.

The neurotrophic factors such as VEGF, EGF, FGF-2, PDGF, BDNF, PF-4, TGF-ß, IGF-1, connective tissue growth factor, and BMP-2, -4, and -6, Etc. are all involved in neurogenesis and

neuro-epithelial cells proliferation, differentiation, migration, and survival[187,218]. Several studies have confirmed their ability to control these vital events of brain development[219].

3.3 Current investigation of the neuroprotective roles of human platelet lysate in CNS injury

Most brain insults lead to the generation of neuro-inflammatory, oxidative stress, apoptosis, vascular disruption, neuronal death, Etc., which could compromise the brain neuroplasticity seen in CNS disorders. The proper function of the CNS relies on several molecular systems, including neurotrophic factors. The growth, maturation, migration, synapses formation, and transformation are principally regulated by neurotrophic factors, particularly by neurotrophins, typically produced by brain cells (microglia cells, oligodendrocytes, astrocytes, and neurons). Recently, the use of neurotrophins as therapeutics has gained the attention of researchers. Studies have been performed to evaluate their protective activity in diseases such as stroke[220,221,] Parkinson's disease[222], traumatic brain injury[221,223], Amyotrophic lateral sclerosis (ALS)[224,225], and nerve injury[226]. It led to the evaluation *in vitro* and *in vivo* of recombinant neurotrophic factors or proteins as potential therapeutic agents.

The agents were administered via the parenteral route, intra-cerebroventricular route, or via the intranasal cavity. The use of oral delivery was excluded due to the proteins' potential degradation before reaching the brain. Even though each delivery route has its advantages and disadvantages, as an illustration, the intranasal delivery may be safe and is less invasive. A drug can be administered without any surgery with a high possibility of reaching the injured area without being degraded along the delivery route and without negotiating BBB. It is a direct and rapid route for protein delivery[227]. However, the nasal route may require more time for large volume delivery with the probability of irritation in the nasal cavity during the process. Local intracranial delivery is precise but is invasive and is technically more challenging and demanding to the patients.

In many reports, successful delivery of peptides, trophic factors, or neurotrophins was achieved with promising findings. For examples, investigators have demonstrated:

- The neuroprotective activity of NGF following neonatal rat hypoxia-ischemia[227],
- An exogenous BDNF treatment after acute ischemic insult reduced infarct volume and significantly restored the behavioral function[228,229].
- An EGF infusion into the ventricle stimulated cell proliferation in the subventricular zone[230].

Clinical studies have also been initiated and reported in the literature, especially for TBI treatment; all the trials, unfortunately, failed up to date to provide good outcomes[231].

Face to this dilemma; researchers are investigating new strategies of intervention. Therefore, platelet lysates are therefore being involved in the list of natural therapeutics based of their known role in tissue repair. Several studies were performed to clarify their protective potential in neurodegenerative diseases. The treatment of neurodegenerative diseases such as ALS and PD has been evaluated experimentally *in vitro* and in animal models. For example, Gouel *et al.* have evaluated human platelet lysate's neuroprotective activity using *in vitro* models of PD and ALS[232]. The biomaterials were able to neuroprotect neural stem cells against the toxic effect of staurosporine, and menadione, or against erastin-induced cells death[232]. They demonstrated the platelet biomaterial's protective potential, and the Akt and MEK signaling pathways seems to be involved[232]. Chou *et al*. further investigated the neuroprotective activity of a specific type of human platelet lysate both in *in vitro* and *in vivo* using mouse model of PD. A specific preparation of the platelet lysate was done to deplete it from plasma proteins, and a strong protective effect was observed in the substantia nigra and striatum of the mice following an intranasal administration[233]. Other studies using different animal models have also shown the beneficial effect of human platelet lysate. In the stroke model, Hayon *et al*. have demonstrated the potential of human platelet lysate to stimulate the formation of new blood vessels, neurogenesis, as well as their neuroprotective activity[234]. Another investigator also highlighted the functional ability of platelet biomaterials using a mouse model of AD. The lysate has been administrated to rats, and they stimulated angiogenesis significantly, improved the motor function of the rats, and the proliferation of neural precursor cells[235]. In other animal model of a focal demyelinating lesion, the platelet lysate administration successfully reduced the number of apoptotic cells and promoted the proliferation and survival of neural precursor cells in the sub-ependymal zone, and the damaged area[218].

Moreover, the neuro-regenerative effect was observed in other models of CNS disease[236]. Encouraging results have been reported, and the lysate was shown to be able to modulate inflammation and stimulate cells growth and differentiation. Therefore, exploring the use of platelet lysate to address the other types of CNS injuries remains more than necessary.

4. Statement of aims

Research on TBI has not translated into clinical advances until now, and the horizon seems to be bleak. No efficient and appropriate TBI treatment has been validated in the clinic, and no treatment options are beyond supportive and rehabilitative care. There is, therefore, an urgent need for new models, well-characterized techniques, and new therapeutic approaches. Based on the growing evidences that human platelet lysates contain a plethora of bioactive agents and their powerful neuroprotective potential found in previous studies, including ours, they could constitute a promising candidate among the therapeutic agents administrated into the brain.

5. Aims

The overall aim of this work was to evaluate the beneficial effect of heat-treated human platelet pellet lysates (HPPL) as a new therapeutic approach for the treatment of TBI. With this goal in mind, we have also developed and characterized a new mouse model of cortical injury based on an *in vitro* scratch injury validated against the established controlled cortical impact model, and, with clinical applications in mind, verify whether an effective and safe heat-treated human platelet pellet lysate could be prepared from pathogen-reduced PC.

The specific aims were:

Aim 1: To accumulate preliminary evidence of the safety and neuroprotective and neurorestorative effect of HPPL in *in vitro* models of TBI.

Aim 2: To evaluate whether the INTERCEPT pathogen reduction technology applied to PC could impact the functional activity of heat-treated human platelet pellet lysate.

Aim 3: To develop and characterize a new *in vivo* mouse model of cortical injury.

Aim 4: To investigate the neuroprotective and neuro-restorative activity of HPPL using two *in vivo* models of traumatic brain injury.

Chapter II: Materials and Methods

A. Overall study design

This thesis combined *in vitro* and *in vivo* approaches to examine the neuroprotective and neuro-restorative activity of HPPL in TBI model. The overall design of our study is presented in **Fig.7.** We started this study by preparing and characterizing the platelet biomaterial, our tailor-made platelet pellet lysate. In a second step, we investigated the selected platelet lysate's safety of using several techniques, including colorimetric assays, protein expression, flow cytometry, and five cell types. The third step was to assess the functional activity of HPPL *in vitro*. Three types of experiments have been performed. The capacity of HPPL to stimulate scratch healing in an *in vitro* scratch healing test was investigated using human cell lines (SH-SY5Y and EA-hy926). Besides, the anti-inflammatory and neuroprotective activity of two different types of HPPL prepared from two sources of platelet concentrates, pathogen-reduced by INTERCEPT or not, were investigated. A cellular model of ferroptosis was used to investigate the neuroprotection potential of HPPL. Moreover, platelet biomaterial ability to stimulate neurites outgrowth *in vitro* was also assessed. The last and most essential step in this study was to establish and validate, against the CCI model, a new in vivo model of TBI and evaluate the neuro-restorative activity of HPPL in two mouse models mimicking TBI mild and intermediate severity.

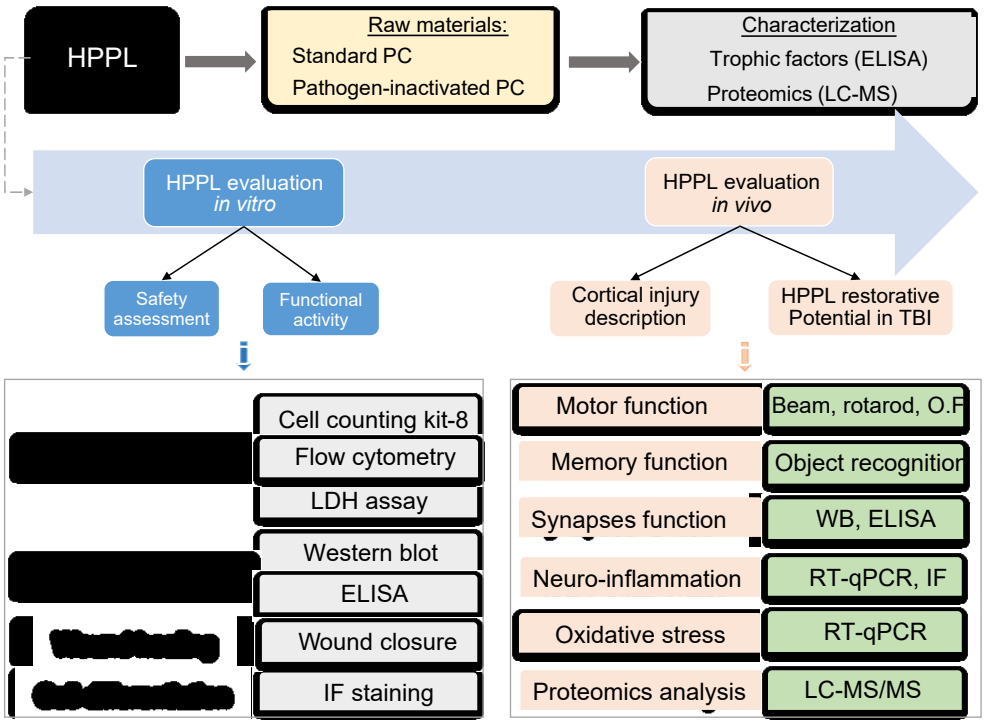

Figure 7: Experimental design. Heat-treated platelet pellet lysate (HPPL) was prepared from standard and pathogen-inactivated platelet concentrates (PCs). HPPL was characterized by determining some trophic factors and its proteome by Liquid chromatography-mass spectrometry (LC-MS/MS). The safety of our preparation and its functional potential were investigated using cell cultures and animal models of traumatic brain injury (TBI). Abbreviations: Lactate dehydrogenase (LDH), enzyme-linked immuno-assay (ELISA), immunofluorescence (I.F), open field (O.F), Western blot (WB), Reverse Transcription Quantitative Polymerase Chain Reaction (RT-qPCR),

B. *In vitro* investigation of human platelet pellet lysate bioactivity

1. Human platelet lysate used in this study

1.1 The platelet concentrates

The tailored-made human platelet lysate evaluated in the present study was prepared from therapeutic grade human PCs. The use of these PCs for research, was approved by the Institutional Review Board of Taipei Medical University (TMU-JIRB n° 201802052). Two categories of PCs were used in the overall study.

The first type of PCs obtained from healthy regular donors at the Taipei Blood Center using standardized, Taiwan FDA-licensed procedures, was not subjected to pathogen inactivation, or leukoreduction, and the platelets were suspended in 100% plasma.

The second category was leukoreduced PCs (n =8) suspended in 65% SSP+ PAS and 35% plasma. The pathogens were inactivated using the INTERCEPT technology for platelets (150 µM psoralen (amotosalen photosensitizer/3.9 J/cm2 of UVA light; Cerus Corporation, Concord, CA, USA)[237]. These PCs were obtained from the Uppsala University Hospital blood bank (Uppsala, Sweden). All the PCS were delivered to our laboratory for further processing. Furthermore, all the donations were non-reactive for blood-borne viruses' markers such as HIV, HBV, HCV.

1.2 Preparation of the Heat-treated Platelet Pellet Lysates (HPPL)

Upon receipt in our laboratory at Taipei Medical University, the standard PCs were processed as described previously[232,238], to obtain the HPPL. The PCs were first transferred in convenient centrifugation tubes (250 mL sterile containers) under a laminar flow hood to ensure sterility. Next, the platelets were pelletized at a speed of 3 000 x g for 30 min, and then the pellet surface was gently washed with around 5 to 6 mL of phosphate buffer saline to avoid plasma protein contamination and resuspended in 1/10 PBS of the initial volume of the PC. The platelet pellet was lysed to release the platelet content by three cycles of freezing at -80°C and thawing at 37°C. The mixture was centrifuged 4500 x g for 30 minutes at 22 ± 2°C to recover the supernatant, which was next heated at 56°C for 30 minutes. The supernatant was finally put-on ice to cool down. To ensure the removal of any cell debris and precipitate, the suspension was next spun at 10 000 x g for 15 minutes to obtain the HPPL supernatant. To avoid repeated freeze-thawing of the HPPL, we prepared aliquots and stored them at -80°C until use.

For the PCs received from Uppsala, a slight modification was introduced in the above preparation procedure of HPPL to obtain the heat-treated intercept platelet pellet lysate (I-HPPL). As done for

the standard PCs, the intercept treated PC bags were also centrifuged at 4 000 x g for 30 minutes, and the supernatant was discarded. The platelet pellet was frozen at −40°C and shipped to Taipei Medical University (TMU; Taipei, Taiwan). The pellets were next thawed, suspended in PBS. To keep the same number of freezing/thawing cycles, the suspension was again freeze-thaw two times before being centrifuge at 4500 x g for 30 minutes. The supernatant (I-PPL) was collected and after making four pools, one part of each pool was heated as done for HPPL[238]. I-PPLs and I-HPPLs were stored at −80°C until use. The preparation process of HPPL and I-HPPL is summarized in **Fig.8.**

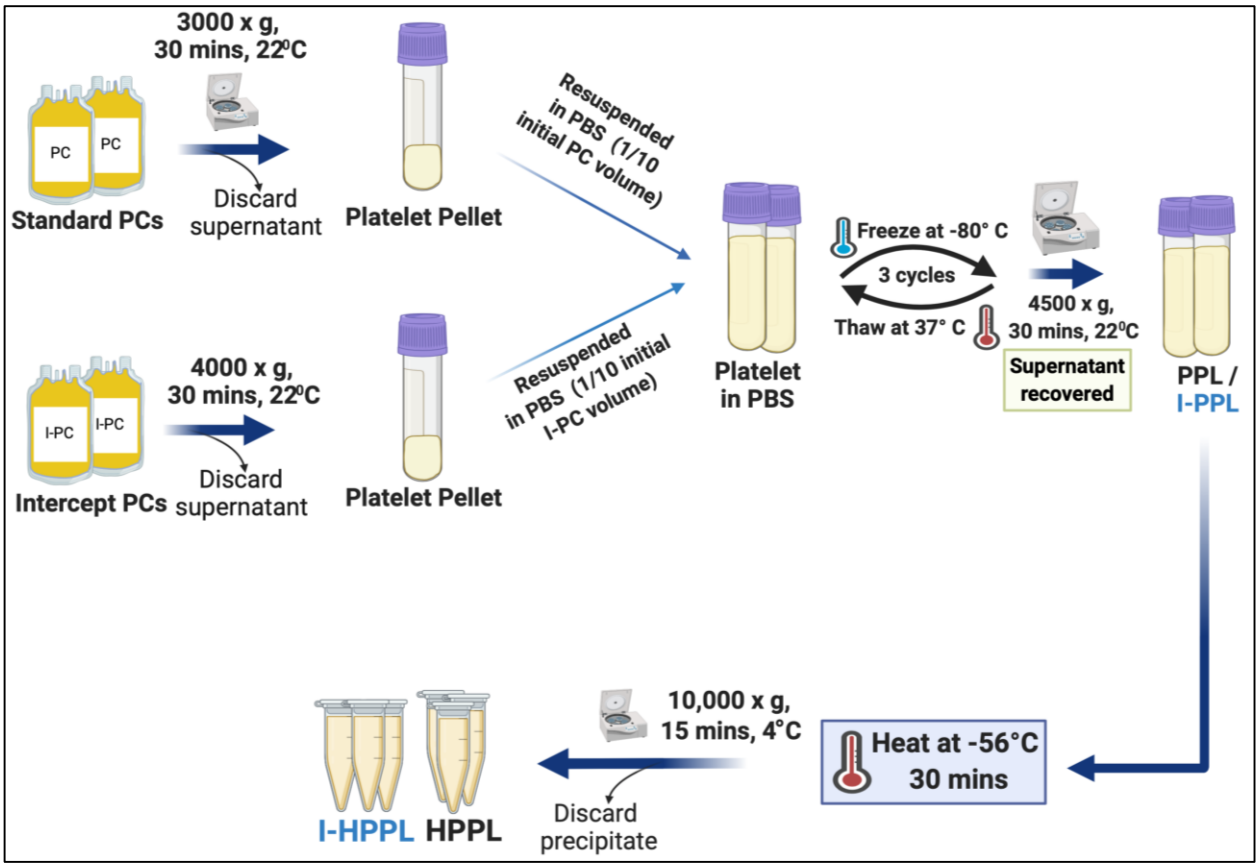

Figure 8: Heat-treated platelet pellet lysate preparation procedure. The lysates were prepared from two types of platelet concentrates. Abbreviations: Phosphate buffer saline (PBS), INTERCEPT-platelet pellet lysate (I-PPL), INTERCEPT heat-treated platelet pellet lysate (I-HPPL), Heat-treated platelet pellet lysate (HPPL), Platelet pellet lysate (PPL), INTERCEPT platelet pellet lysate (I-PPL).

1.3 Platelet lysate characterization

1.3.1. *Total protein and growth factors determination by ELISA*

The total protein content was quantified using a bicinchoninic acid protein assay kit (Pierce Biotechnology, Rockford, IL, USA). Selected trophic factors including, BDNF, EGF, PDGF-AB, and VEGF concentrations, were determined by a sandwich enzyme-linked immunosorbent assay (ELISA) technique (DuoSet ELISA; R&D Systems, Minneapolis, MN, USA) as described before[238] following the manufacturer's protocol. Platelet lysate samples were thawed at 37°C and centrifuged at 10 000 x g for 10 minutes to further remove cell debris. The lysates were then diluted 5 to 500 folds based on our previous experience in the laboratory. Standard reference curves were prepared using 0 -2,000 pg/mL recombinant human VEGF, 0-1,000 pg/mL for the recombinant human PDGF-AB, 0-250 pg/mL for EGF, and 0-1500 pg/mL BDNF. Prior to the testing day, 96-well plates were coated with 100 µL capture antibody diluted in PBS, covered with an adhesive strip, and incubated overnight at room temperature. On the test day, the plates were washed three times with 0.05% Tween 20 in PBS (wash buffer) and blocked by 300 µL of reagent diluent (RD, 1% BSA in PBS, w/v) for one hour. After the washing step, 100 µL of serial dilutions in reagent diluent of standard and samples were added and incubated for two hours at room temperature. Before adding the detection antibody (100 µL/well), the wells were rewashed and were incubated for another 2 hours. The ELISA plate was incubated with 100 µL of Streptavidin horse-radish peroxidase (HRP, from R&D system) for 20 minutes after washing three times. The plate was protected from direct light using a plate with aluminum foil. The plate rewashed, and then 100 µL of tetramethylbenzidine (TMB) substrate solution (solution A and solution B (1:1), v/v) was added to each well and incubated in the dark for 20 minutes. The reaction was stopped with 50 µL 2N H_2SO_4, and the absorbance was read at 450 nm (Infinity M200, Tecan). Based on the standard curves, the concentrations of growth factors were estimated.

1.3.2 Proteomics analysis of heat-treated platelet pellet lysate

Crude HPPL (n=3) was treated with acetone pre-cooled at -20°C and incubate overnight at -20° C. The ratio between the sample and the acetone was ¼, respectively. Following the incubation, the mixture was spun at 15 000 x g for 10 min at 4°C. The supernatant was then discarded, and the protein pellet was washed twice with cold acetone in water (1/4). The sample was spun at 13 000 x g for 10 minutes at 4 °C for each wash. Finally, the supernatant was discarded, and the pellet

was air-dried prior to being resuspended in 6M urea. A BCA protein assay kit was used to determine the total protein concentration, and 20 μg of protein was sent to the proteomics core at National Taiwan University (Taipei, Taiwan) for proteomics analysis.

The Liquid Chromatography-Mass Spectrometry (LC-MS/MS) analysis was performed on an Orbitrap Fusion Lumos Tribrid quadrupole-ion trap-Orbitrap mass spectrometer (Thermo Fisher Scientific, San Jose, CA). The peptides mixtures were separated on an Ultimate system 3000 nanoLC system (Thermo Fisher Scientific, Bremen, Germany) before being loaded onto a 75 μm ID, 25 cm length C18 Acclaim PepMap NanoLC column (Thermo Scientific, San Jose, CA, USA) packed with 2 μm particles with a pore of 100 Å. Two mobile phases were selected: a mobile phase A (0.1% formic acid in water) and mobile phase B composed of 100% acetonitrile with 0.1% formic acid. A segmented gradient in 90 min from 2% to 40% solvent B at a flow rate of 300 nL/min was used. The mass spectrometry analysis was performed in a data-dependent mode with Full-MS (externally calibrated to a mass accuracy of <5 ppm, and a resolution of 120,000 at *m/z*=200, AGC target 5e5, maximum injection time of 50 msec) followed by HCD-MS/MS of the most intense ions in 3 s.

For this running, a high-energy collision activated dissociation (HCD)-MS/MS (resolution of 15,000) was used to fragment multiply charged ions within a 1.4 Da isolation window at a normalized collision energy of 32. AGC target 5e4 was set for MS/MS analysis with previously selected ions dynamically excluded for 180 s, and a maximum injection time of 50 ms was selected.

At the end of the running, the raw MS/MS data were searched against the UniProt knowledgebase reviewed (Swiss-prot) human protein database (downloaded on August 2017) by using the Mascot search algorithm via the Proteome Discoverer (PD) package (version 2.2, Thermo Scientific). The following parameters regarding the database were considered during the searching procedure:

Enzyme: Trypsin

Missed cleavage: 2

MS tolerance: 10ppm

MS/MS tolerance: 0.02Da

Modification: Oxidation (M), Deamidation (NQ), Carbamidomethyl (C), Phospho (STY), Acetyl(K), Methyl(K)
FDR: <1%

The list of proteins generated was next classified based on the biological function using DAVID Bioinformatics Resources 6.8.

2. Cell cultures

2.1 LUHMES cell culture

The Lund Human Mesencephalic (LUHMES) cell line were provided by Pr David Devos (Department of Pharmacology and Neurology, School of Medicine, University of Lille, France). They were selected for our study to assess some neuroprotective functions of the HPPL and I-HPPL as they are commonly used as dopaminergic neurons in *in vitro* models of Parkinson's disease or ferroptosis[239-241] due to their sensibility to a neurotoxin such as erastin. Two million cells were seeded in ten milliliters proliferation buffer composed by Advanced DMEM/F12 (Invitrogen, UK), 1x N-2 supplement (Invitrogen, Grand Island, NY, USA), 2 mM L-glutamine (Gibco, Rockville, MD, USA), and 40 ng/mL recombinant basic FGF (R&D Systems, Minneapolis, USA) in Nunclon™ cell culture flasks (Nunc, Guangzhou, China). The proliferation medium reagents were combined as followed: Advanced DMEM/F1, 9.8mL, N2 (100x), 100µL; 200mM L-glutamine,100 µL; bFGF, 2.5 µL.
Prior to cells seeding, the flasks (75T flaks) were coated (7mL/flask) for 3 hours with 50 µg/mL (300 µL) Poly-L-ornithine (PLO, Sigma, St. Louis, USA) and 1 µg/mL fibronectin (7µL, Sigma), distilled water (6.7mL), then rinsed with sterile double distilled water (ddH2O), and left under the hood until they were completely dried. After seeding, cells were incubated at 37ºC in a humidified 95% air, 5% CO2 until confluence. Their differentiation into neurons was performed by seeding 2 x 10^6 into PLO coated 75T flasks in proliferation medium. The pre-differentiation was started the next day (d0) by renewing the medium with a buffer that stimulate cell differentiation: advanced DMEM/F12 (9.7mL), 1x N-2 supplement (100µL), 2 mM L-glutamine (100 µL), 1 mM cAMP (100 µL), Sigma Aldrich, St Quentin Fallavier, France), 1 µg/mL tetracycline (10µL, Sigma) and 2 ng/mL (1 µL) recombinant glial-derived neurotrophic factor (GDNF; R&D Systems). On day 2

of differentiation, the cells were transferred into 24-well plate at 0.25 x 10^6 cells per well or in 6-well plates at 1.1 x 10^6 cells per well for three additional days (**Fig.9**).

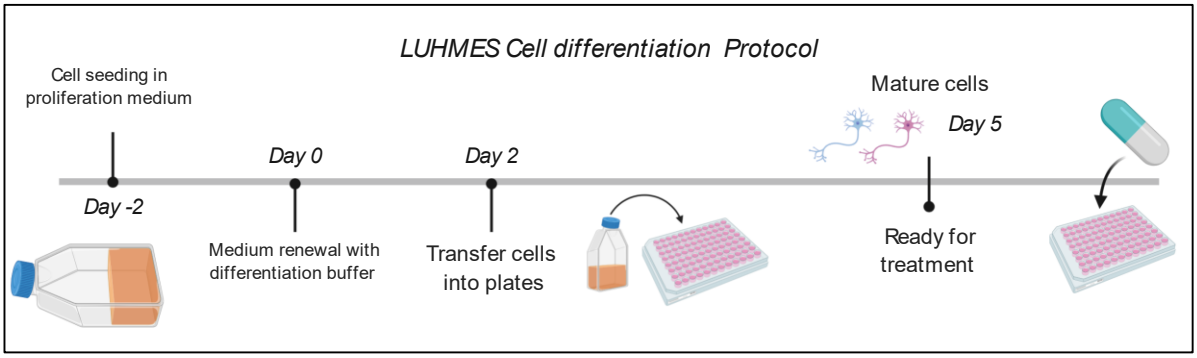

Figure 9: LUHMES cell culture procedure. *The cells were used after five days of differentiation*

2.2 SH-SY5Y cell maintenance

The neuroblastoma SH-SY5Y was provided by Professor David Devos and used as a neuronal cell model. They were maintained in DMEM supplemented with 10% fetal bovine serum (FBS, Gibco, Invitrogen Taipei, Taiwan), 1% non-essential amino acids (NEAA), 100 U/mL penicillin, and 100 U/mL streptomycin at 37°C in a saturated humid atmosphere with 5% CO2. 75T flasks were used for the cells seeding, and when they reached 80 - 90% confluence, the cells were gently washed with PBS before the addition of 4mL trypsin-EDTA. The flask was incubated for 2-3 min in the incubator to allow the cells to detach. According to the experiment type, they were next re-suspended in medium, counted, and seeded in 75 T-flask or plates at specific density. For some experiments, SH-SY5Y cells were differentiated using ten µM retinoic acid (RA) in a complete growth medium (Sigma Cat n° 302-79-4) for seven days by changing the medium every two days.

2.3 BV-2 microglia

The immortalized mouse microglial cells BV-2 was selected to evaluate platelet lysate safety and their ability to modulate microglia activation. They were a generous gift from Dr. Wan-Wan Lin (National Taiwan University, Taipei, Taiwan). BV-2 was cultured in DMEM supplemented with 10% FBS (4 mM L-glutamine, 100 U/mL penicillin, 100 µg/ml streptomycin, and 1% NEAA) and maintained in a T175 flask. Their incubation conditions were: 37°C ± 1°C and 5% CO2 humidified incubator. When reach 80-90% confluence, the flask's bottom was slightly taped to detach the cells. The cell number was determined by counting cells with a hemocytometer. 10 000 or 20 000

cells were then seeded per well in 24-wells plates and used in our experiments. The medium was supplemented with 100 ng/mL lipopolysaccharides (LPS) in DMEM and 10% FBS for their activation.

2.4 Human Endothelial Cell Line (EA-hy926)

The EA-hy926 cells were kindly obtained from Dr. Fabrice Cognasse (University Jean Monnet, Saint-Etienne, France) and expanded for our study. Several passages of these cells were therefore frozen before initiating any experiment. EA-hy926 cells were seeded in a 37°C ± 1°C and 5% CO_2 humidified incubator with DMEM/high glucose (Cyclone) containing 10% FBS, 4 mM L-glutamine, 100 U/ml penicillin, 100 µg/ml streptomycin and 1% NEAA. Two million of cells were grown in 75T flask first to confluence in Dulbecco's modified DMEM supplemented with 10% FBS, then seeded at a density of 2×10^5 cells /well onto 24 well plates. Once cells have been attached to plates completely, they were used for the toxicity tests and the scratch assay described below.

2.5 Primary cortical neuronal cultures

A pool of mouse cortex and hippocampus neurons was cultured with the support of Dr. Valerie Vingtdeux (INSERM, UMR-S1172, Lille, France) according to a previous protocol described in the literature[242]. The primary cultures derived from 18.5 days' mouse embryos (C57BL/6J) by taking the forebrains in cold Hanks' balanced salt buffer (Invitrogen, Carlsbad, CA, USA) with 0.5 % w/v D-glucose (Sigma) and 25 mM HEPES (Invitrogen) supplementation. The isolation procedure was performed in cold dissection solution in the presence of 0.01% w/v papain (Sigma), 0.1% w/v dispase (Sigma), and 0.01 % w/v DNase I (Roche, Rotkreuz, Switzerland), and by incubation at 37°C for 15 min twice. Then, the solution was centrifuged at 220 x g for 5 minutes at 4°C. The cell pellet was re-suspended in Neurobasal medium supplemented with 2% B-27, 1 mM NaPyr, 100 units'/mL penicillin, 100 µg/mL streptomycin, and 2 mM Glutamax (Invitrogen), and filtered through a 40-µm cell strainer. The total number of cells was evaluated and then plated on Poly-L-ornithine- and laminin-coated 12-well plates at a density of 5 $x10^5$ cells/well. The buffer was renewed with fresh culture media (1:3 of starting volume) every three days until the end of the culture period.

3. Safety and Functional assessment of HPPL

A battery of assays was first done to ensure the safety of the platelet lysates biomaterial used in this study. Next, the functional activity of HPPL was evaluated. All the experiments were completed at least 3 times and results were expressed as mean ± SD.

3.1 Safety assessment of HPPL and I-HPPL

3.1.1 Viability assays

The viability of the cells was assessed by the WST-8 (2-(2-methoxy-4-nitrophenyl)-3-(4-nitrophenyl)-5-(2,4-disulfophenyl)-2H-tetrazolium, monosodium salt) assay kit. WST-8 is reduced by dehydrogenases present in cells to produce a water-soluble formazan dye (orange in color). The relative amount of formazan dye in the cells has been estimated to be directly proportional to the number of living cells. The cells were seeded in 24 or 96 well plates and treated consequently depending on the experiment type. SH-SY5Y, EA-h926, and BV-2, 10^4 cells/mL cells were seeded in 96-well plates and incubated for 24 h to allow attachment. They were then treated with 5% (v/v) HPPL or 5% I-HPPL and incubated for an additional 24 h.

For LUHMES cells, 250 x 10^3 cells per well were seeded in 24-wells plates. The cells were stimulated at day 5 of differentiation with 5% (v/v) platelet lysates for either 24 or 48 hours. At the desire time points, the Cell Counting Kit-8 (CCK-8) reagent solution was added at a final ratio 1/10 and incubated for 4 h at 37˚C. Absorbance in each well was acquired at 450 nm using 96-wells microplate reader on a spectrophotometer (Infinity M200, Tecan, Männerdorf, Switzerland). The absorbance of untreated cells was considered as corresponding to 100% survival, and that of treated cells was taken as a percentage of viable cells relative to the control. A value higher than 100% was considered to indicate a metabolic activity higher than that obtained in the medium supplemented with 5% FBS. Wells containing medium and supplements were also incubated with the CCK-8 reagent and used as the background. The optical density values were normalized and the effect of the treatment on cell viability was presented for each concentration as the mean ± standard deviation (SD).

3.1.2 Flow cytometry

Flow-cytometry was also used to analyze the impact of the treatment on the cell viability. After exposure to HPPL for 24 or 48 hours, the cells were collected and spun at 1100 x g for 5 minutes. A propidium iodide, known by its capacity to bind to double stranded deoxyribonucleic acid (DNA) but excluded from cells with intact plasma membranes, was used to stain the cells. The cells were harvested and centrifuged at 1100 x g for 5 minutes. The pellet was next re-suspended in 400 µL PBS and 4 µL PI dye was added immediately before proceeding to cell counting. Following gentle vortex, the samples were analyzed using a flow cytometer (BD FACSCanto II, Becton Dickinson, Biosciences, Franklin Lakes, NJ, USA). The percentages of dead and live cells were quantified and presented as percent of our untreated. A total of ten thousand events were evaluated per sample.

Furthermore, we performed a lipid peroxidation assessment using C-11 Bodipy (1 µM, Life Technologies Saint Aubin, France) according to the manufacturer's instruction. The analysis was performed with a total of 10^4 cells per sample using a CANTO II flow cytometer.

3.1.3 Calcein-AM Cell Viability Assay

The Calcein-AM reagents were purchased from Sigma-Aldrich (St. Louis, MO, USA) and used to assess the cells' membrane integrity under platelet lysate stimulation. This experiment was performed according to the manufacturer's recommendation. The treated and controls cells were incubated with 10 µL, 2 µM calcein-AM for fifteen minutes at 37°C. The cells were examined under a fluorescence microscope and images were taken. The quantification of the fluorescent images was performed using National Institute of Health Image (NIH, Bethesda, MD, USA) 1.61 ImageJ software and the variations in the fluorescence intensity resulting from calcein-AM staining were quantified. The background was subtracted to normalize the density.

3.1.4 Lactate dehydrogenase assay

Lactate dehydrogenase (LDH) release assay was performed to measure the platelet lysate impact 'on viability of the primary neuron culture. The cytotoxicity was measured at fourteen days' *in vitro* (DIV21) using lactate dehydrogenase release as per indicated by manufacturer's instructions (CytoTox 96® non-radioactive cytotoxicity assay, Promega, Madison, WI, USA). LDH activity was detected separately in the supernatant and cell homogenate. For that, the medium was first

removed and the cells were lysed in PBS with 0.5% Triton X-100 for 20 minutes. 50 µL of each sample and CytoTox 96 reagent were distributed into wells. The plate was protected from light and incubated for 30 minutes at room temperature. 50µL of stop solution was next added to each well and the absorbance was read at 490 nm using a SpectraMax® i3 (Molecular Devices, Sunnyvale, CA 94089, USA), and the toxicity was calculated based on this formula: Percent cytotoxicity = 100 × (experimental LDH release (OD490)-blank (OD490))/ (LDH total (OD490)-blank (OD490)).

3.1.5 ELISA for Tumor necrosis factor (TNF-α)

For TNFα detection, the microglia BV-2 cells were grown in 24-wells plates at the ratio of 10 x 10^3 per well and incubated for one day. The cells were next treated with 5% platelet lysate or stimulated with 100 ng/ml LPS followed by treatment with 5% HPPL or 5% I-HPPL, and incubated for another 48 h. The supernatants were collected at each time point and assayed for TNFα content using DuoSet ELISA (R&D Systems) kit following the manufacturer's protocol. All treatments were completed at least three times and data were expressed as mean pg/mL ± SD.

3.1.6 Western Blot analysis for protein detection

This technique has been used to investigate proteins' expression in LUHMES and primary neuronal cells treated with our platelet biomaterials. The cells were lysed in radioimmunoprecipitation assay (RIPA) buffer (50 mM Tris-HCl pH7.2, 150 Mm NaCl,1% NP40, 0.1% SDS, 0.5% DOC, 1 mM PMSF, 25 mM MgCl2) (Sigma-Aldrich), spun for 10 minutes at 10^4 x g and 4ºC, and supernatants were collected. The total protein content was measured with a Pierce bicinchoninic acid Protein Assay Kit (Pierce Biotechnology, Rockford). 20 µg proteins from each sample were mixed with LDS 2X (LDS NuPAGE® Buffer) supplemented with reducing agents (Invitrogen), boiled for 10 min at 100 °C, and then separated on 4-12% Criterion XT Bis-Tris polyacrylamide gels (Bio-Rad, Paris, France) or 4-12% gradient GenScript's Bis-Tris precast gel (GenScript, Hong Kong, China). The proteins were transferred to nitrocellulose membranes, which were incubated in blocking buffer, 5% non-fat dry milk or 5% bovine serum albumin in TNT (Tris 15mM, pH 8, NaCl 140 mM, 0.05% Tween) and incubated at 4°C overnight with the primary antibodies: Anti-β-actin antibody (1/10,000 dilution, A5441, Sigma), anti-Neuron Specific Enolase/NSE (1/1000, NA12-47, BioMol) for LUHMES cells, anti-synaptophysin H-93 (1/1000, sc-9116, Santa Cruz), anti-

Munc-18 (1/1000, M2694, Sigma), anti-SNAP25 (1/1000, Sc-376713, Santa Cruz), anti- Tyrosine hydroxylase/TH (1/1000, AB152, Millipore), and anti-GluA2/3/4 (1/1000, 2460S, Cell Signaling) for primary neuronal cells. The membranes were washed three times with 1x TNT, and probed with a secondary antibody (horseradish peroxidase (HRP)-conjugated anti-rabbit immunoglobulin G (1/5000, GeneTex) for 45 minutes and washed again. The protein bands were detected using the chemiluminescence (ECL) kit (GE Healthcare, Chicago, NY, USA) and visualized with the UVP system (Analytic Jena, Upland, CA, USA). Image J software (1,52k, Wayne Rasband, NIH) was used for the quantification of the intensity of the protein bands.

3.2 Protective activity of HPPL/I-HPPL in a cell model of ferroptosis

For the potential neuroprotective assessment, LUHMES cells (passage 16-19) were seeded in 24-well plate at the density of 2.5×10^5 cells per well. 5 days' post-differentiation, the cells were pre-treated first with 5% platelet lysates followed by erastin addition (Sigma-Aldrich) at a 1.25 µM final concentration in the culture medium and incubated for 24 or 48 hours. At the indicated time point, cells were collected and analyzed by FCM using PI (Sigma-Aldrich) staining, and cell counting kit-8 (CCK-8) assay. The proteins expression was also assessed by Western blot, as described above. Furthermore, the lipid peroxidation was measured by FCM using a C-11 BODIPY sensor.

The primary neuronal cell culture was maintained until 21 days of culture (DVI21) to ensure complete maturation, then subjected to 0.5% (v/v) platelet lysates stimulation and 1.25 µM erastin treatment one hour later. They were next incubated for additional two days. The cytotoxicity was measured at DIV23 using LDH release assay, as described above. We investigated the potential ability of platelet lysates to protect the cells from erastin cytotoxicity.

3.3 In vitro scratch healing assay

An *in vitro* scratch *healing* assay was performed using cell cultures to evaluate platelet lysate's capacity to exert a beneficial effect on wound healing. The SH-SY5Y (passages 22-28) and EA-hy926 (passage 3-13) cells were used, and the scratch performed as previously described[243]. Cells were seeded in 24-well plates until forming a confluent monolayer. A wound was then created in the cell monolayer by scraping a straight line using a p200 pipette tip. A new medium specific for each cell line was added. Cells were incubated with or without 5% (v/v) platelet lysate. In the

conditions with platelet lysates supplementation no FBS was added. Wound closure was captured 24 h for non-mature SH-SY5Y and EA-hy926 or four days' post-treatment for differentiated SH-SY5Y with a fluorescence microscope (Leica DMi8 microscope, Wetzlar, Germany). The data are presented as a wound-healing index, which was calculated as follows: Wound area (initial) – Wound area (final) / Wound area (initial) for non-differentiated SH-SY5Y and EA-hy926.
For differentiated SH-SY5Y cells all the total neurites length in the scratched area were measured using Image J software. The cells were further stained with synaptophysin to confirm their viability.

3.4 Neurites outgrowth assay

We used a neurites outgrowth assay as described before[244] to investigate the ability of HPPL and I-HPPL to stimulate neurite extension. SH-SY5Y (passages 22 to 28) cells were grown in 6-wells plates at the ratio 10 x 10^4 cells/well. Twenty-four hours after seeding, the medium was refreshed. 10µM of retinoic acid (RA; positive control) or 2% HPPL/I-HPPL (v/v) was also added to the culture buffer. The buffer was changed every three days. Pictures were taken on day 7 (**Fig.10**). The effects of HPPL and I-HPPL on SH-SY5Y cell differentiation were then investigated by fluorescent staining of two neuronal markers: neuro-filament medium and beta III tubulin (abcam cat. Ab18207; 55kDa). At day seven, the medium was removed and the cells were washed with PBS, followed by fixation in 2% paraformaldehyde for 30 minutes. The cells were next permeabilized by incubation with 0.25% PBS-triton X-100 for 20 minutes at room temperature and blocked by 1% BSA in PBS for 1h. The cells were incubated overnight at 4 °C with primary antibodies (all from Abcam, Cambridge, UK) anti- neuro-filament (ab64300-100, 160kDa; 1:500 dilution), and anti-beta III tubulin (ab18207; 54kDa 1:500 dilution). Cells were incubated with Alexa Fluor-488-conjugated goat anti-rabbit IgG antibody (abcam) for 2 h followed by DAPI staining to label the nucleus. A fluorescence microscope (Leica DMi8 microscope, Sage Vision, West Chester, PA, USA) was used to visualize immunofluorescence. For this experiment, three images were taken per treatment at random and for 3 independent experiments and the cells processes extension were then analyzed using the National Institute of Health Image (NIH) 1.61 software ImageJ plugin Simple Neurite Tracer. The length of each extension was measured individually under bright field captured images and the total outgrowth estimated. The mean of the neurites' length, and percent of differentiated cells determined by counting 100 cells in each

condition were calculated. Any cell with a neurite length greater than 10 µm was considered as differentiated. On the other hand, the increase in beta III tubulin was estimated by the integrated density of fluorescence.

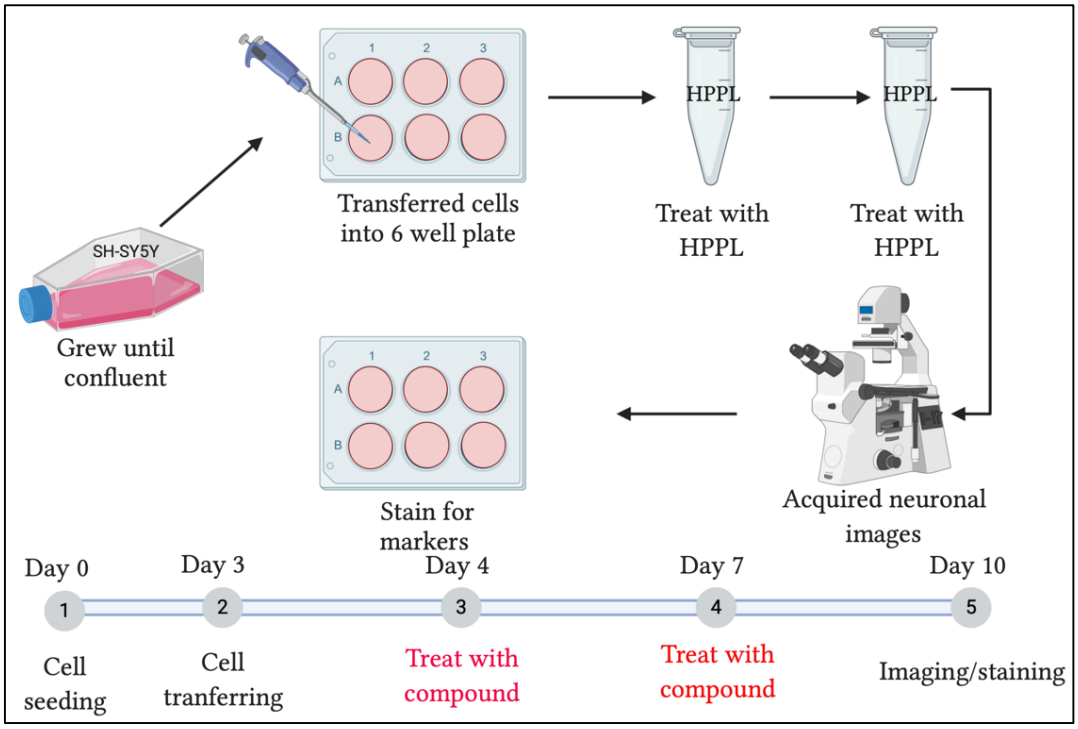

Figure 10: Workflow illustrating our simplified process for analyzing neurite outgrowth. *Non-differentiated SH-SY5Y cells were seed until confluence in a 75T flask then transferred into 6 well plates. The medium was supplemented with 10% FBS. 24 hours after the cells being seeded in the plate, the medium was renewed without FBS, but with 2% HPPL or I-HPPL, or retinoic acid (positive control). The negative control wells were kept in FBS only. The treatment was done twice and one week following the first treatment, bright field images were acquired for neurites length quantification. The cells were further stained with beta3 tubulin and neurofilament medium.*

C. *In vivo* study

1. Study approval and animal experiment design

In this study, all the animal experiments were executed in compliance with the guidelines for animal welfare and the approval of animal use protocol from TMU (application n° 2017-0410). Adult male C57/BL6 mice (aged 8-12 weeks, weighting 20–30g) were purchased from Taiwan national laboratory animal Center and housed in TMU animals' facility (Taipei, Taiwan) and housed in a reversed light-dark cycle. One hundred seventy-seven (177) mice in total have been used in this study. The animals were separated into batches to ensure efficient handling during the experiments. The design of the *in vivo* experiments is presented in **Fig.11**.

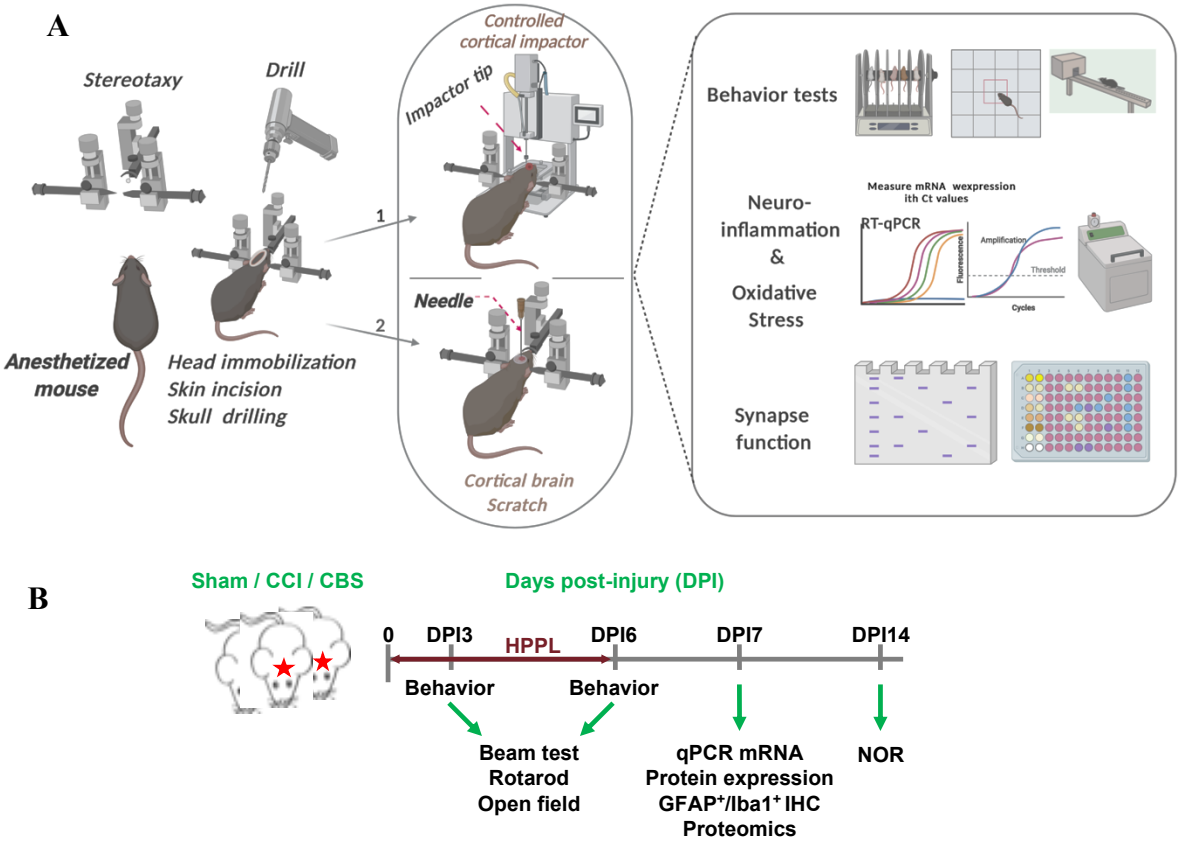

Figure 11: In vivo study design. *Drawing illustrating the models of mouse TBI and the assays used to assess the beneficial effect of HPPL (A). HPPL was delivered by intracranial and intranasal routes followed by behavior, genes, and biochemical analyses. The timeline of the behavior tests, HPPL administration, and samples collection (B).*

2. Traumatic brain injury models and HPPL administration

2.1 Anesthesia and surgical preparation

In this study, the solution for anesthesia was prepared prior to the surgery procedure by combining Zoletil 50 and xylazine. The animals were then anesthetized by intraperitoneal injection of 10 µL/g body weight. The surgical site was shaved, and the animal was placed in a stereotaxic device. Its head was maintained immobile with ear bars. The cotton tips were soaked in betadine and ethanol before being used to clean the surgical site. The materials used in the surgical procedure are listed in table 4.

Table 4: list of surgical materials

Name	Usage
Iodine 10%	Surgical scrub
Cotton tipped applicators	Remove blood and debris
Scissor	Surgery
Forceps	Surgery
Hemostat	Surgery
Micro Drill	Combine with Burrs for generating the bone window
Burrs for Micro Drill	skull drill
Suture monofilament	Suture
70% ethanol	clean off the iodine
H_2O_2	Remove membrane
Stereotaxic frame (mice)	Head fixation
Needles 16 G	Scratch brain
Hair clipper	Shave hair
Tissue paper	Cleaning
Weight machine	Weight animals
Syringe 5cc	Injection
Warm pad	Maintain the temperature
Bio-punch (4-mm)	Tissue sampling
Iodine solution	Cleaning

2.2 Cortical brain scratch assay model

The *in vivo* cortical scratch injury (CBS) was initiated as a translation of the *in vitro* scratch injury model described in the literature[245], where a localized mechanical injury was induced by drawing parallel scratches in the cells monolayer. Using the same approach, we developed an *in vivo* scratch injury as a cheap and straightforward drug screening model and addressing the multifaceted TBI. To perform the CBS, the animal was first anesthetized using a combination of Zoletil (10 mg/kg) and xylazine (10 mg/kg). The anesthetized mouse head was next fixed in the stereotaxic frame (Stoelting, Wood Dale, IL) using the ear bars, shaved, and cleaned with 10% iodine and 75% ethanol. A midline incision using scissors is made to expose the skull. A 4-mm diameter circle was drawn between lambda and bregma on the right skull, and a drill was used to cut along the marked circle to expose the brain. Two parallel lines at a depth of 0.6mm were drawn using an 18-gauge needle fixed on the stereotaxic frame **(see Fig.12).** Once the bleeding stopped, the wound was sutured with a non-absorbable suture (nylon, 4-0, NC124), and antibiotic ointment was applied before the animal returned to a new clean cage for recovery. The Sham mice were subjected to a hole drill as before without scratching the brain.

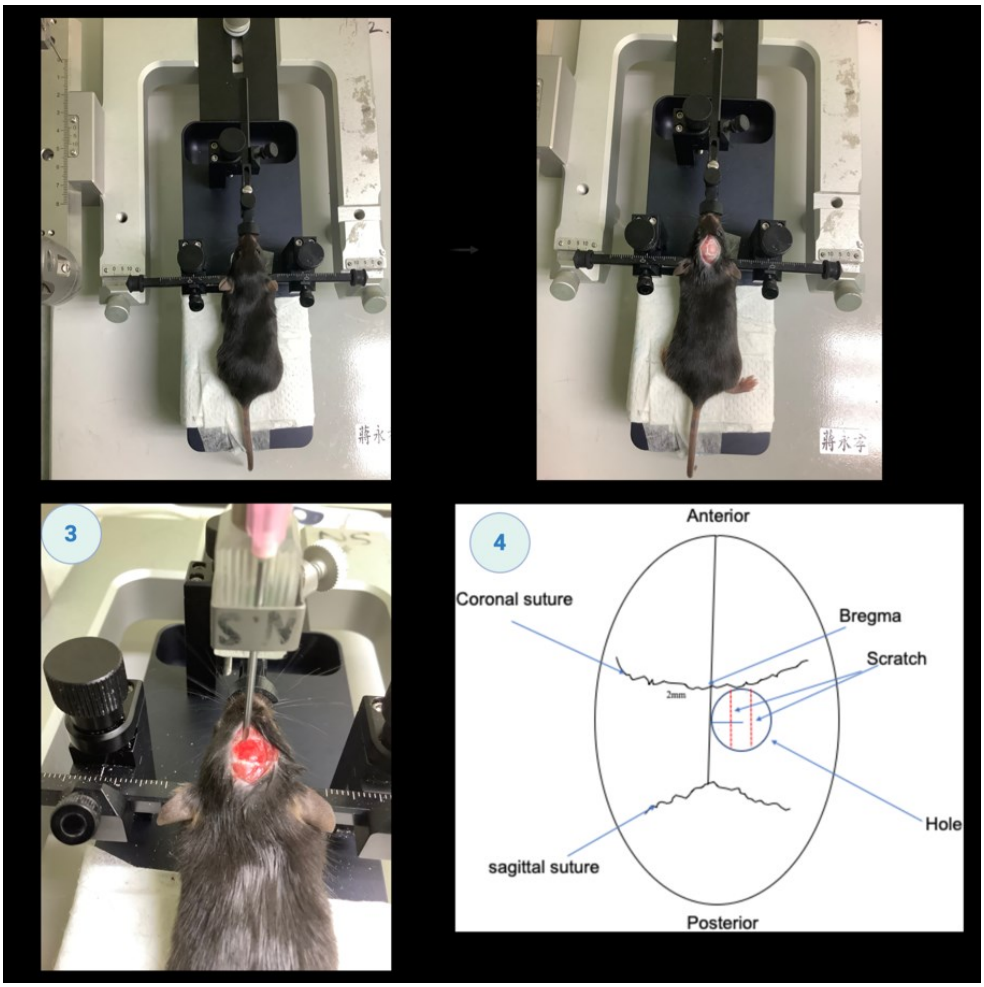

Figure 12: Cortical brain scratch injury procedure. *(1) Fixation of the animal head in the stereotaxic frame, (2) exposure of the skull, (3) fixation of the needle and brain scratching; (4) drawing showing the location of the hole*

2.3 Mild traumatic brain injury model using the controlled cortical impact device

In the CBS's validation process, a well-characterized model, CCI, was used for qualitative comparison reasons. The same strain of mice as the cortical brain scratch was used. The mice were subjected to a mild traumatic impact with a CCI machine (eCCI-6.3, Custom Design & Fabrication, Inc, Sandston, USA) after zoletil/xylazine-induced anesthesia as follows. Briefly, the animal head is fixed in a stereotaxic frame using the ear bars. A midline incision using scissors was made at the right side to expose the skull. 4mm circle in the center of lambda and bregma with 0.5 mm away from the midline is drawn and drilled along the marked circle. The injury was then induced using the CCI device after setting the following impact parameters: velocity of the actuator, 3 m/sec; deformation depth, 0.2 mm; and dwell time, 250 milliseconds. The skin was

next closed, and after applying an antibiotic ointment on the suture to prevent bacterial infection, the mouse was moved to a heated cage to recover (**see Fig.13**). As indicated in the study design, the mice were allowed to live one or two weeks based on our experiment.

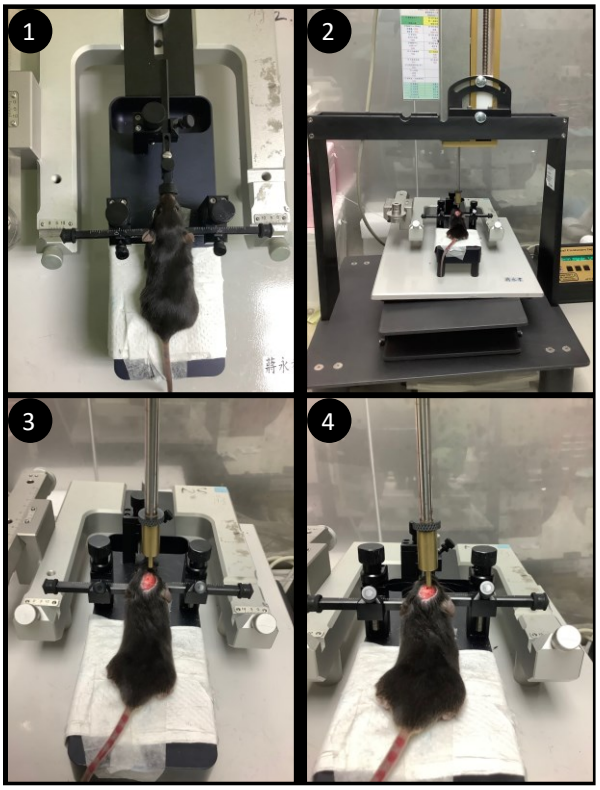

Figure 13: Controlled cortical impact procedure. *(1) Fixation of the mouse head in the stereotaxic frame, (2) exposure of the skull and fixation on the impactor device, (3) adjustment of the impactor tip, (4) impact at the desired location.*

2.4 Treatment administration procedure

The bioactive compound, prepared from three PCs bags, was delivered by intracranial and intranasal routes to address the acute phase of the injury, and optimize the effect of HPPL. Approximatively thirty minutes after the scratch or the cortical impact, sixty microliters of HPPL were slowly applied drop by drop into the wounded area before the skin being sutured. Starting from DPI1 to DPI6, the same amount of HPPL was delivered by intranasal according to a modified protocol[246,247]. Briefly, each non-anesthetized mouse was held carefully by his ears, immobilized, and then positioned on his back with his head upright. Using a pipette, 20µL HPPL was administered intranasally in four drops by alternating the nostrils. Five minutes' interval was observed between each administration, for a total of three times. This procedure was repeated six

consecutive days **(Fig.14)**. For Sham-treated mice or TBI-saline groups, the same volume of saline was delivered following the same route.

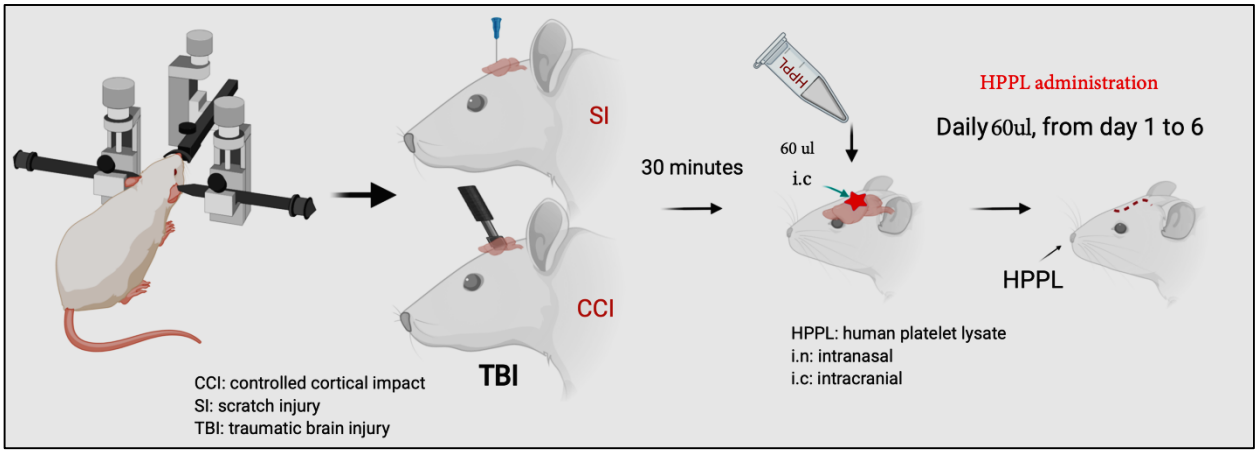

Figure 14: Treatment administration procedure. HPPL or saline was delivered by intracranial route 30 minutes post-injury and intranasally from day 1 to 6.

3. Animals behavior tests

The tests investigating the animals' behavior were performed between 11 am and 6 pm. During the experiment, the materials were carefully wiped with 75% ethanol before and after each experiment to prevent the olfactory distraction. A beam and rotarod tests were performed at 3- and 6-days' post-injury to evaluate the sensory-motor function. The locomotor activity and anxiety behavior were tested using an open-field (OF), and the short memory was investigated by the novel object recognition test (NOR) **(Fig.15)**

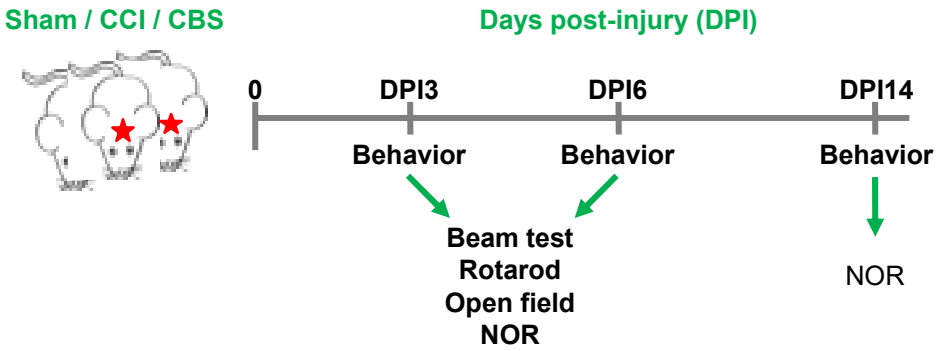

Figure 15: Behavior tests time line. The animals were trained for beam test and Rotarod five days prior to the injury induction. They were tested at 3- and 6-days' post-injury for beam, rotarod, open field, and novel object recognition test. At DPI14, only NOR was performed.

3.1 Beam test

Animals were trained for 5 days before the surgery on a one-meter flat beam placed on the top of a table. One box was placed at the end of the beam to attract the animal. We used a timer to record the time spent by each mouse to cross the beam. The mice's ability to cross the beam was recorded on days three and six post-injury or Sham procedures. Three trials per animal were performed, and an average was calculated and used as the animal's performance to cross the beam.

3.2 Rotarod test

During the last week before the experiment's beginning, a daily 30 min training trial was performed on a rotarod apparatus (Harvard apparatus, model LE8205, Panlab, s.l.u., Barcelona, Spain; RotaRod RR02, Orchid Scientifics, Maharashtra, India). The animals were placed on the rotating rod at a constant speed on day one, and an acceleration model was used during the remaining days of the training step. In case an animal falls off, it was immediately placed back on the rod. The task evaluated the ability of each mouse to walk forward on the rotating rod without falling off. The animals were randomized afterward into the different groups. The test phase consists of three trials separated by 5 minutes' inter-trial intervals, and an acceleration mode was set up from 4 to 40 rpm in an interval of time ranged from 30 to 300 seconds. The time each animal spent on the rod before falling off is recorded as its latency to fall[248]. An average of the three trials was calculated and recorded as the performance of the animal.

3.3 Open field test

We evaluated the mice's spontaneous activity in an open field box (60 x 60 cm) made by a black wooden box under a camera. The middle region of the box field was considered as a 15 cm × 15 cm virtual zone. Each mouse was allowed to explore the field for ten minutes, and the behavior was recorded. The total traveled distance and the time spent in the center of the box by each animal were analyzed using EthoVision XT 11 software (Noldus Information Technology, Wageningen, the Netherlands).

3.4 Novel object recognition (NOR) test.

To evaluate the experimental mice's ability to distinguish a new and familiar object, we performed the NOR test to address the recognition memory. This test was conducted for three days, as described below:

Day 1 (habituation phase): the mice were individually allowed to explore for ten minutes an open field box (60 x 60 cm) in the absence of objects before being transferred to their cages. Cleaning was done using 75% ethanol between the sessions.

Day 2 (familiarization phase): Each animal had 10 minutes to discover two identical objects;

On day 3 (testing day), the animals were again subjected to habituation and familiarization as on days 1 and 2. They were allowed to rest for one hour. These two-steps for each mouse were separated by 2 minutes. One of the objects was next replaced by a new one, which differs in shape and texture. Each animal behavior regarding the two items was recorded by an automated video tracking system during10 minutes. Between the sessions, the objects and surface were cleaned with 75% ethanol. According to this formula, the mice's memory performance was calculated and expressed as a discrimination index (DI). DI= (time spent at the novel object – time spent at the familiar object) / (time spent at the unknown object + time spent at the familiar object) *100.

4. Tissue collection and processing

The mice were sacrificed by cervical dislocation and their brains were quickly removed, and rinse in cold PBS. The region of interest, the ipsilateral cortex, was dissected and divided into two parts before freezing in liquid nitrogen. One part was lysed using a tissue ruptor in 200 µL lysis buffer, Tris buffer pH 7.4 containing 10% sucrose and protease inhibitors (Complete; Roche Diagnostics GmbH), and stored at -80°C until used either for western blot or ELISA. Before their use, the extracted protein from each sample was subjected to total protein concentration determination using BCA kit.

5. Oxidative stress (ROS) detection

Here, we used the lucigenin-enhanced chemiluminescence assay to determine NADPH oxidase-mediated superoxide radical (O2-) production. Briefly, at DPI7, the animals were anesthetized with zoletil 50 followed by their decapitation. For each one, the cortex was quickly dissected and kept in cold Krebs buffer (2.38 mM KCl, 1.2mM KH2PO4, 118mM NaCl, 25 mM NaHCO3,

11mM glucose, 1.2mM MgCl2, 1.2 mM MgSO4, and 2.5mM CaCl2, in de-ionized water pH 7.4) oxygenated (saturated with 95% O2 and 5% CO2) for 10 minutes. The fresh tissue was next placed in 150 µL of the buffer with 50 µL lucigenin (5 µmol/L). Using a single-tube luminometer, a baseline was first measured for 60 seconds. Finally, 50µL NADPH (100 µmol/L) was added to the test tube, and the chemiluminescence was then measured over 350 seconds and expressed in counts per second (cps) per Square centimeter. At the end of the measurement, all the samples were weighed and used to normalize the cps values.

6. Western Blot analysis for synaptic proteins determination

The samples collected at the regions of interest (cortex) from mice brain were subjected to protein extraction (see above) and the total protein content was measured with BCA Protein Assay Kit (Pierce Biotechnology, Rockford, IL, USA). 20 µg proteins from each sample were suspended with LDS 2X (LDS NuPAGE® Buffer) supplemented with reducing agents (Invitrogen), boiled for 10 min at 100 °C. The same protocol, as described in the *in vitro* section (paragraph ***3.1.6***), was used to run the samples. The following primary antibodies were used: Anti-β-actin antibody (1/10,000, A5441, Sigma), anti-Neuron Specific Enolase/NSE (1/1000, NA12-47, Biomol), anti-Synaptophysin H-93 (1/1000, sc-9116, Santa Cruz), anti-Munc-18 (1/1000, M2694, Sigma), anti-SNAP25 (1/1000, Sc-376713, Santa Cruz), anti-PSD-95 (1/1000, 2507S, Cell Signaling), anti-HSP60 loading control (1/10 000, ab45134, Abcam).

7. ELISA for synaptic proteins assessment

Three ELISA kits, Mouse DLG4 / PSD95 ELISA kit (#E-EL-M1303), Mouse SNAP25 ELISA Kit (#E-EL-M1106), and Mouse SYP/Synaptophysin ELISA kit (E-EL-M1105) from Elabscience were used to determine the levels of synaptic proteins in Sham, CCI, CCI-HPPL, scratch, scratch-HPPL samples according to the manufacturer protocols. The brain tissue homogenates were prepared, and their protein amount was evaluated using the BCA assay kit. The samples were diluted in samples diluent, 25-fold for DLG4 and SNAP25, and 10-fold for SYP detection. The synaptic proteins concentrations were expressed in ng/mg of total protein.

8. Genes expressions analysis by quantitative reverse transcription PCR (RT-qPCR)

8.1 RNA purification

According to the manufacturer's protocol, total RNA was purified from the collected tissue using the RNeasy Lipid Tissue Mini Kit (cat. 74084, Qiagen, genomics, Taiwan). 1000 µL of Qiazol was added to the frozen samples and homogenized using a tissue ruptor. After five minutes, 200 µL of chloroform was added and shaken vigorously. The sample was spun at 12,000 x g, 15 minutes at 4°C, then, the upper aqueous phase containing the RNA was transferred to a new tube, and an equal volume of 70% ethanol was added and vortexed. 700 µL of each sample was next assigned to a RNeasy Mini Spin column sitting on a 2-mL collection tube and centrifuged at 8000 x g for 15 seconds. The flow-through was discarded, and the spin column was put back on the tube. Then 700 µL of RW1was added to the spin column and spun at 8 000 x g for 15 seconds. Again, the flow-through was discarded, and 500 µL of RPE was added into the spin column. The column was spun at 8000 x g for 15 seconds. The flow-through was then discarded, and this step was repeated. Finally, the spin column was transferred to a new 1.5 mL Eppendorf tube, and the total RNA was eluted by adding 50 µL of RNase-free water by centrifugation at 8000 x g for one minute. NanoDrop2000 (Thermo Fisher Scientific, Waltham, MA, USA) was next quantified the total RNA concentration.

8.2 RT-qPCR for inflammatory markers and oxidative stress

One microgram of total RNA was used to synthesize a complementary DNA (cDNA) using the Applied Biosystems High-Capacity cDNA reverse transcription kit (ref 4368814). Afterward, the RT was run with the following program at a thermal cycler (Machine: Veriti™ 96-Well Thermal Cycle): 10 mins at 25°C, 60 mins, 37°C, 60 mins, 37°C, 85°C, 5 min, 5 min at 4°C. The obtained cDNA was stored at -20°C before using in qPCR. Validated primers were used to perform qPCR. Reactions were prepared using 5 µL of Power SYBR Green PCR Master Mix (cat.4367659, ThermoFisher Scientific, Watham, MA, USA), 0.1 µL of forward primer, 0.1 µL of reverse primer, 2 µL of cDNA pre-diluted 20 times, and 2.8 µL of RNase-free water for each sample. StepOne™ Real-Time PCR System (ThermoFisher Scientific, Watham, MA, USA) was used with an amplification profile of 50°C, 12 min, 95°C for 10 min, followed by 40 cycles of (95°C for 15 s, 60°C, 30 s, 95°C for 15 s), 60°C for one min and a step and hold melt curve analysis. Various

inflammatory markers were screened targeting astrocytic markers, microglial markers, cytokines and chemokines, and chemokines receptors, and antioxidants using the primers described in Table 5.

Table 5:list of oligomers used in the present study

Name	Forward primer	Reverse primer
C1qa (v2)	ggagcatccagtttgatcg	catccctgagaggtctccat
CD68	gacctacatcagagcccgagt	cgccatgaatgtccactg
CCL3	tgcccttgctgttcttctct	gtggaatcttccggctgtag
CCL4	gccctctctctcctcttgct	gagggtcagagcccattg
CCL5	ctcactgcagccgccctctg	ccgagccatatggtgaggcagg
Cyclophillin	agcatacaggtcctggcatc	ttcaccttcccaaagaccac
GFAP	cgcgaacaggaagagcgcca	gtggcgggccatctcctcct
IL1b	tgtaatgaaagacggcacacc	tcttctttgggtattgcttgg
TLR2	ggggcttcacttctctgctt	agcatcctctgcgatttgacg
TLR4	ggactctgatcatggcactg	ctgatccatgcattggtaggt
TNFa	tgcctatgtctcagcctcttc	gaggccatttgggaacttct
TREM2 (v2)	cgagaggctgaggtcctg	tctccagcatcttggtcatcta
Vimentine (v2)	ccaacctttttcttccctgaac	ttgagtgggtgtcaaccaga
GPX-1	tttcccgtgcaatcagttc	tcggacgtacttgagggaat
SOD-1	gtccatcagtatggggacaa	atgatggaatgctctcctga
MnSOD	tggacaaacctgagccctaa	gacccaaagtcacgcttgata
NQO1	ggtagcggctccatgtactc	catccttccaggatctgcat
HO-1	gtgaggacccactggaggag	cacagatggcgtcacttcgtc

9. Immunofluorescence for histological analysis

9.1 Animal perfusion and brain samples handling procedure

For this specific experiment, the mouse was deeply anesthetized by zoletil/xylazine intraperitoneal injection and placed on a grid associated with a collection container. The thorax was carefully opened, and the beating heart was exposed. The heart was held with forceps, and the perfusion cannula connected to a needle is inserted into the left ventricle and maintained in place during the whole perfusion period. The right atrium was cut to allow the solution to exit from the mouse circulatory system. A minimum of 30 mL cold phosphate buffer saline was required per animal.
Following the perfusion, the skull was delicately opened, the brain removed, and rinse in cold PBS. The brain was immediately dropped in a 15mL tube containing 8mL of 4% paraformaldehyde (PFA) in PBS for at least 48 hours at 4°C. Next, the brains were transferred into 30% sucrose in PBS and kept until they sink (24 to 48 hours). Then, the brains were next removed from the sucrose. The residual solution was removed using tissue papers and dropped in a beaker containing

isopropanol pre-cooled until - 40°C in dry ice for at least one minute. Finally, the samples were returned in labeled small plastic bags and stored at -80°C until cryo-section.

9.2 Tissue sectioning and staining procedure

Prior to brain sectioning, the samples were removed from -80 °C and allowed to equilibrate at -20°C for at least 30 minutes as the cryostat temperature. The tissues were then embedded in optimum cutting temperature medium (OCT) on tissue holders. 10 µm thick coronal sections were cut, mounted on commercial gelatin-coated slides (Platinum PRO, adhesive glass slides), and stored at - 80 ºC until needed. Before staining, the slides were allowed to thaw at room temperature for 30 minutes and fixed in ice-cold acetone for 5-10 minutes. They were washed in PBS three times (5 minutes each) and proceed to the staining procedure. Firstly, the slides were permeabilized in 0.2% Triton X-100 in PBS, washed as previously and incubated with M.O.M blocking buffer from Vector (Cat. No. PK-2200) for 1hr. Then, incubated overnight with the primary antibodies (rabbit anti-GFAP (Dako, ref Z0334); rabbit anti-Iba1 (Wako, ref 019-197441) diluted 1/250, and 1/200 respectively in M.OM diluent (Cat. No. PK-2200). After a new washing step, the slices were incubated with the indicated secondary antibody, anti-rabbit (Alexa fluor 647) and anti-mouse (Alexa fluor 488). The slides were again washing and counterstained with DAPI for 10 minutes. Finally, they were washed and coverslips mounted with Ever Brite mounting medium. The coverslips were fixed using nail polish solution and images were taken. The selected slices were, four slices anterior from the middle of the lesion and four slices posterior. The fluorescence images were acquired using TissueFAXS acquisition. For consistency, we kept the same camera and software parameters, including the brightness of the excitation light, the detector sensitivity (gain), or the camera exposure time across the samples or tissue sections. The intensity of immunostaining was analyzed by ImageJ (NIH) software.

10.Proteomics analysis of mice cortex samples

Eight mice ipsilateral cortex in each condition were subjected to protein extraction in tris-sucrose buffer and pooled. The protein samples were precipitated with a fourfold volume of 100% cold acetone and kept overnight at −20 °C. The samples were next spun at 15 000 X g for 10 min. The supernatants were discarded, and the pellets were washed twice in acetone/water (1/4). After drying, the pellets were dissolved in 150 µL of 6.5 M urea and assayed for their protein content.

An equal amount of protein was then sent to the proteomics core at National Taiwan University, Taipei, Taiwan, for further processing. The samples were analyzed as done with HPPL proteome and described in section A/1.2.3 above.

The raw data's protein identification was performed by Uniprot's reference database of mus musculus (release 03_2020). We performed a fold change using each sample's relative abundance to identify the significantly differential protein expressions among the groups. The ratios of Sham/CCI; Sham/CCI-HPPL; CCI/CCI-HPPL, Sham/Scratch; Sham/Scratch-HPPL, and Scratch/Scratch-HPPL were utilized to estimate the differential expression of proteins as down-regulated proteins with <0.5 folds. Upregulated proteins were conditions with a fold change > 2.

11. Bioinformatics analysis.

To better understand HPPL treatment's impact on molecular functions, physiological pathways in biological processes, DAVID (http://david.abcc.ncifcrf.gov/) (Database Annotation Visualization, and Integrated Discovery) database for functional analysis was used. Other software such as Venny (https://bioinfogp.cnb.csic.es/tools/venny/index.html) and Panther (http://www.pantherdb.org/) were also used to compare the lists of proteins between the groups and conditions.

12. Statistical Analysis

GraphPad Prism (Version 8.0, San Diego, CA) was used to perform all the analyses, and the data were expressed as mean ± standard deviation or error of the mean accordingly. Multi-comparisons using a one or two-way (ANOVA) followed by Fisher's Least Significant Difference (LSD) test to identify significance ($P< 0.05$) between the groups as explained in the legend. A t-test analysis followed by a two-tailed test was also used accordingly in this study. The details regarding the n independent values, the type of comparison, and the statistical significance are indicated in the figures' legends. For Western blot images and florescence images analysis, image J software (NHI, USA) was used.

Chapter III: Results

1. Heat-treated platelet pellet lysate is a biomaterial full of bioactive substances

We prepared, based on our previous work, a tailored-made platelet pellet lysate dedicated to brain administration. For this study, two types of heat-treated human platelet pellet lysate fractions have been prepared. The first one, HPPL derived from a standard platelet concentrate without any pathogen inactivation treatment, and the second (I-HPPL) has been produced from platelet concentrates subjected to filtration to remove the white blood cells and pathogen inactivation treatment by INTERCEPT blood system.

Some selected trophic factors were determined by ELISA in these platelet lysate fractions. Both HPPL and I-HPPL showed a reasonable amount of growth factors.

Each HPPL used, derived from a pool of three PCs bags and was found to contain 40.7 ±1 ng/mL for BDNF, 82.2± 5 ng/mL (PDGF-AB), 5.4 ± 0.01 ng/mL for (EGF), 2.8 ±0.003 ng/mL (VEGF), and 140.2 ng/mL (CCL5). Additionally, HPPL contains approximatively 6 mg/mL total protein.

To ensure the impact of the new pathogen inactivation system called the INTERCEPT blood system on the platelet lysate fractions, we prepared I-HPPL from eight outdated INTERCEPT treated-PCs initially dedicated to transfusion, using the same procedure as the standard HPPL. The total protein concentration determined by BCA was 10 mg/mL. The levels of growth factors were also determined and I-HPPL contained 62.5 ± 1 ng/mL (BDNF), 46.2 ± 0.8 ng/mL (PDGF-AB), 2± 0.05 ng/mL (EGF) and 0.09 ± 0.01 ng/mL (VEGF), 407.2 ± 4.9 ng/mL (CCL5). The data were presented in **Fig.16**.

Differences between HPPL and I-HPPL in terms of concentration in protein content have been found. In comparison to the standard HPPL (6 mg/mL), the total protein level in I-HPPL was significantly higher ($p < 0.01$). Moreover, the selected bioactive substances content analysis showed a lower EGF, PDGF, and VEGF concentrations, excepted for BDNF and CCL5, compared to HPPL.

The richness of HPPL was examined using mass spectrometry analysis as described in **Fig17.** A list of 1210 proteins was generated (**Annex1)** that certainly covers a large range of the HPPL proteome since the experimental conditions were like those described previously in the literature. Among these proteins, growth factors, cytokines, antioxidants, enzymes, immune molecules, Etc. are present in the list. We next grouped the proteins based on their cellular component and the

molecular functions to facilitate the identification of the potential roles of the identified proteins. The results are presented in **Fig.17.**

The analysis regarding the cellular components indicated that the proteins were associated with the intracellular region, plasma membrane, cell periphery, Etc. On the other hand, the molecular functions in which the identified proteins are involved are: transcription regulator activity, translation regulator activity, catalytic activity, and transporter activity Etc. Finally, gene ontology analysis using DAVID Bioinformatics Resources v6.8 revealed that the HPPL proteome was involved in many processes such as Wnt signaling pathway, myelin sheath, response to reactive oxygen species, complement activation Etc.

The groups and the distribution of proteins within HPPL proteome are mainly membrane proteins, signaling, cytoskeletal, vesicular, extracellular, mitochondrial, protein processing, metabolic enzymes.

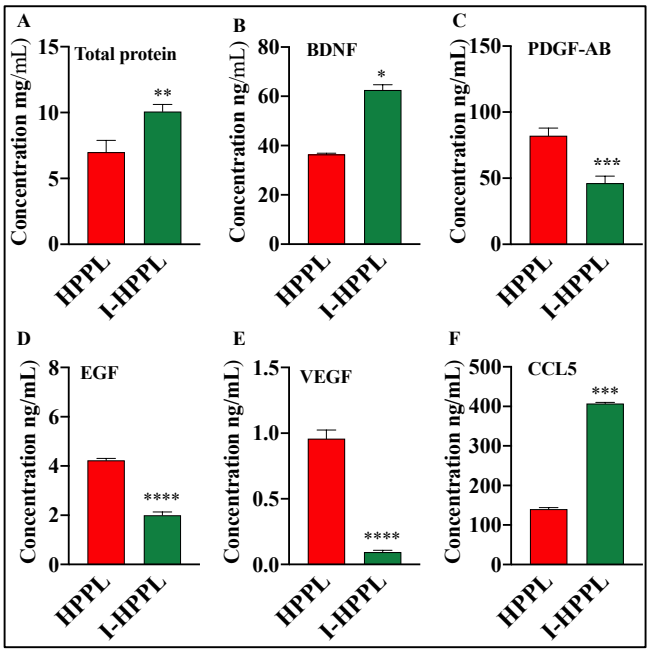

Figure 16: Total proteins and growth *factors in heat-treated human platelet pellet lysates. The protein concentration (mg/mL) (A). The trophic factors levels were expressed in ng/mL. (B) brain-derived neurotropic factor (BDNF), (C) platelet-derived growth factor (PDGF)-AB, (D) epidermal growth factor (EGF), and (E) vascular endothelial growth factor (VEGF), (F) Chemokine (C-C motif) ligand 5 (CCL5). The values are expressed as the mean ± SD. I-HPPL was compared to the standard HPPL. *P< 0.05, **P< 0.01, ***p < 0.001, ****p < 0.0001. t test analysis followed by two-tailed test (n=3).* ***Abbreviations****: heat- treated human platelet pellet lysate (HPPL), Intercept heat-treated human platelet pellet lysate (I-HPPL).*

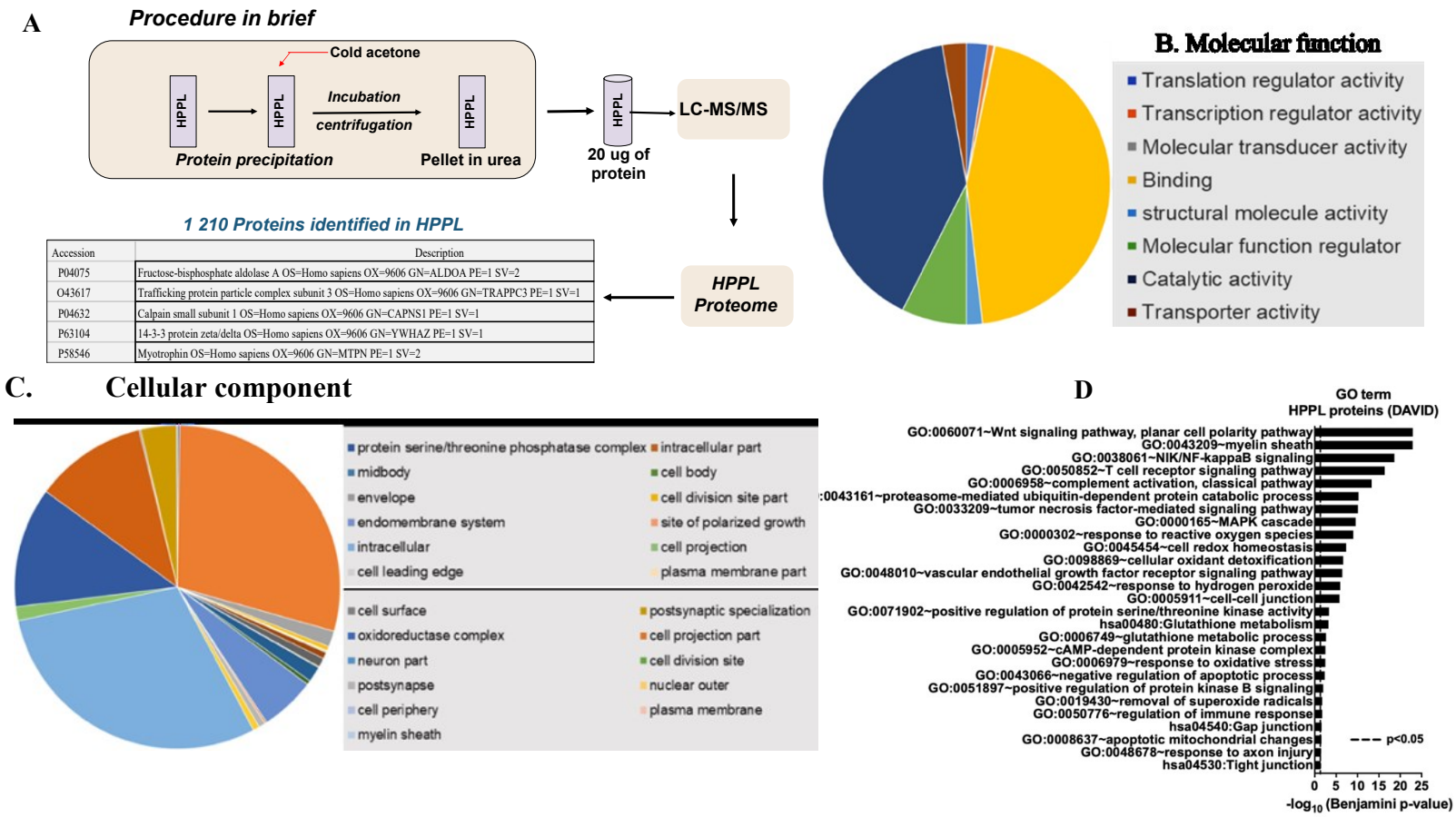

Figure 17: HPPL proteome analysis method. *The proteins from three batches were first precipitated using acetone and washed. The pellet was suspended in urea, and 20 µg of these proteins were analyzed by LC-MS/MS. Using Uniprot database, more than 1000 proteins were identified (A)HPPL protein precipitation procedure in brief. Bioinformatics analysis of HPPL proteomic results. (B) molecular function analysis, (C) cellular component of identified proteins. (D) Gene Ontology (GO) analysis summary showing the relevant biological aspects of HPPL* proteome.

.

2. Safety assessment of the heat-treated human platelet pellet lysate fractions

Before testing the beneficial effect of the platelet biomaterials, it was essential to examine their safety. *In vitro* experiments have been used to address this particular point.

2.1 Impact of heat-treated platelet pellet lysates on cell viability

To ensure that our biomaterials are safe and do not have toxic effects, we performed several analyses, including viability assays and protein expression determination. Four cell lines and one primary neuronal cell culture have been involved in this experiment.

The standard and INTERCEPT heat-treated platelet pellet lysate were not toxic to human neuroblastoma SH-SY5Y, EA-hy926, nor mouse BV-2 cells after 1 day of treatment. The cells were exposed to either 5% (v/v) of HPPL or I-HPPL. The controls were cells maintained in their normal conditions; culture buffer supplemented with 10% fetal bovine serum. The viability of the treated-cells was measured by CCK-8, a colorimetric assay, and estimated as the percent of cells maintained in normal conditions. The data presented in **Fig.18A-C** indicate that none of the fractions exerted a toxic effect after 24 hours' post-treatment ($p < 0.05$).

Besides the colorimetric test, the cytotoxicity evaluation was also done using flow cytometry analysis. For that, at one-day post-exposure, we examined the viability of the cells stimulated with 5% (v/v) HPPL or I-HPPL using propidium iodide staining. The propidium iodide was used as a viable dye, which is able to penetrate dead cells with an altered membrane, but not in live cells. For this test, only three cell lines were used, SH-SY5Y, LUHMES, and EA-hy926 cells.

As presented in **Fig.18,** HPPL and I-HPPL fractions did not exert any detrimental effect on cell viability after 24 hours of treatment. The viability of the treated cells was above 80% compared to control.

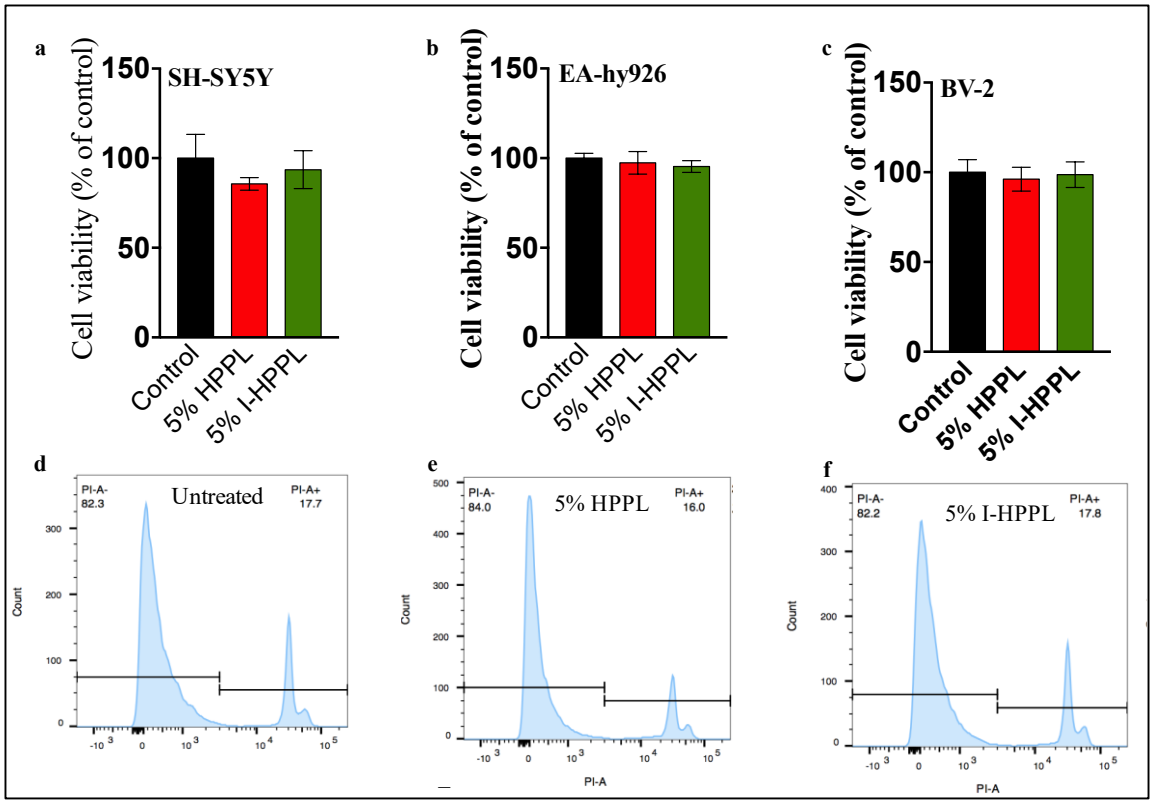

Figure 18: Safety assessment of platelet pellet lysate fractions. *The viability (at least n=3) of SH-SY5Y cells (a), endothelial cells, EA-hy926 (b) and BV-2 (c) treated by 5% HPPL or I-HPPL was analyzed by CCK-8 at 24 h post-treatment. (d-f) viability of SH-SY5Y analyzed by flow cytometry. None of the fractions showed a toxic effect.*

Furthermore, we examined the potential impact of HPPL and I-HPPL on differentiated LUHMES cells as well as on primary cell cultures. LUHMES cells were stimulated with 5% (v/v) platelet lysate for 1 or 2 days and the viability assayed using the CCK-8 test (**Fig.19 A, B**). For the primary cells culture, the effect of the lysate fractions was assessed on mature neurons (DIV21). The level of LDH release was determined and compared to the control (untreated). The cells were stimulated with 0.5% (v/v), and the results are presented in **Fig.19 C.** Again, no sign of toxicity was observed on LUHMES cells and mice primary cells.

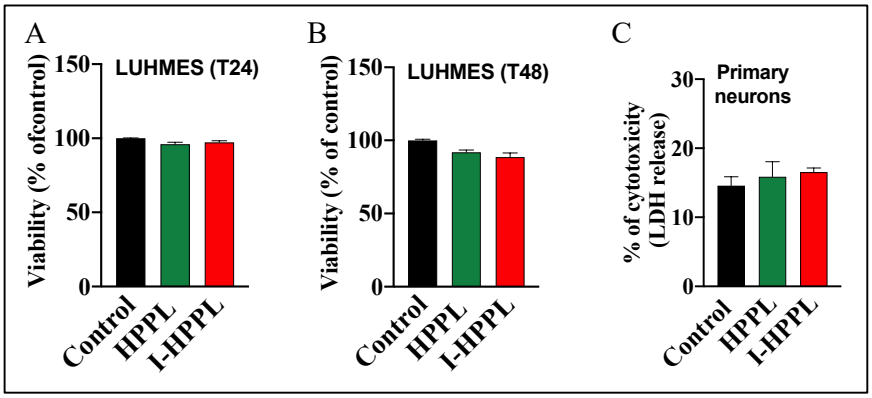

Figure 19: LUHMES and primary neurons viability. *LUHMES cells were grown at the ratio of 2.5 x 105 cells/well and differentiated before being treated with 5% I-HPPL, or HPPL (v/v) for 24 or 48 hours. The primary neurons were treated with 0.5% HPPL/I-HPPL after 21 days of cultures and incubated for 2 days.*

2.2 Impact of heat-treated platelet pellet lysates on SH-SY5Y cells membrane integrity

To further evaluate the safety of our biomaterials, we assessed also, the long-term (seven days) impact of HPPL and I-HPPL treatment using SH-SY5Y cells. The cells were stained with calcein-AM, a membrane-permeant cell indicator that is able to cross the viable cell membrane. The cells status was next analyzed. Clearly, the stimulated cells kept their membrane integrity **(Fig.20),** further confirming the non-toxic nature of human platelet lysates used.

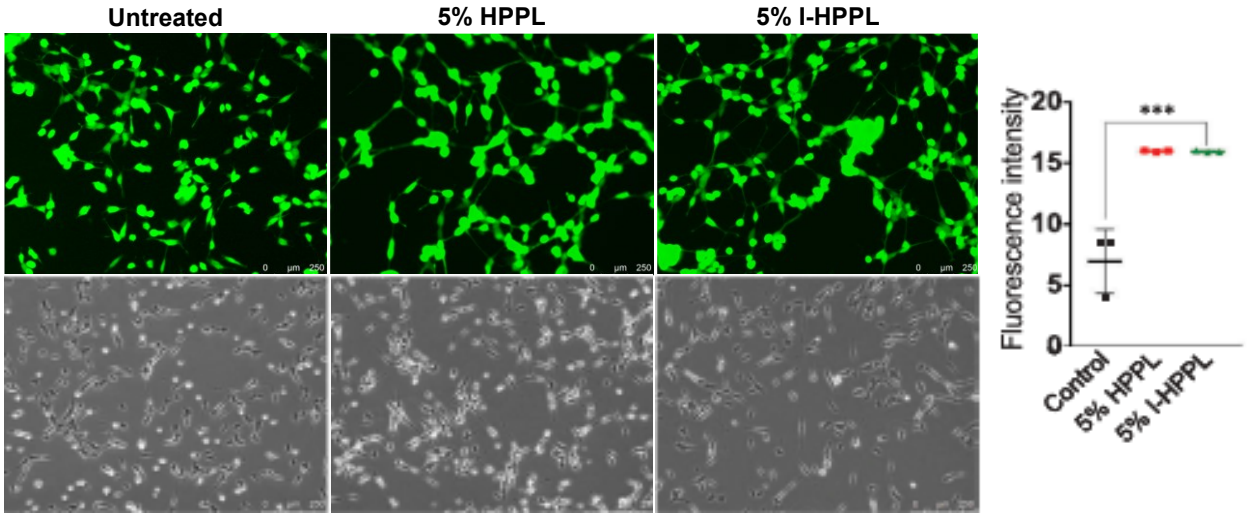

Figure 20: Cell viability assessment. *Cells images were acquired (bright-field images). After one week of exposure, the cells were labeled with calcein-am to investigate the integrity of their membrane. Representative images of n=3 experiments are shown in the upper panel, and the intensity of fluorescence was evaluated. The scale bar is 250 µm.*

2.3 Impact of heat-treated platelet pellet lysates on proteins expression

Intending to address the impact of HPPL and I-HPPL on the neuronal cell proteins expression, we investigated by western blot the level of selected neuronal and synaptic markers on LUHMES and primary neuronal cells, respectively. Interestingly, the Western blot analysis **(Fig.21A-C**) showed that the treatment of differentiated LUHMES cells with an HPPL and I-HPPL for 48 hours significantly improved Tyrosine Hydroxylase (TH) and Neuron-Specific-Enolase expressions (NSE) ($p < 0.05$). The expression was higher in I-HPPL compared to HPPL.

We next investigated the effects of the two fractions of platelet lysate on primary neurons synaptic proteins: SNAP25, Munc-18, Synaptophysin, and post-synaptic (GluR2/3/4) expression. The impact was investigated just before they exhibited a mature phenotype. Therefore, the stimulation with HPPL and I-HPPL has been initiated from DIV1 to DIV14. The cell growth medium was renewed with platelet lysates supplementation every 3 days. As described in **Fig.21D-H**, the repeated treatment with I-HPPL and HPPL did not significantly affect the expression of and the pre- and post-synaptic markers investigated compared to cells maintained without any additional treatment (controls).

In the present experiment, the non-heated fraction of I-HPPL, I-PPL was introduced as quality control of our heat-treated INTERCPET platelet pellet lysate fraction. When compared I-PPL to I-HPPL, we can clearly demonstrate that the heat-treatment constitutes an important step of purification of the platelet-biomaterial as the viability of the cells were significantly affected with the non-heated fraction.

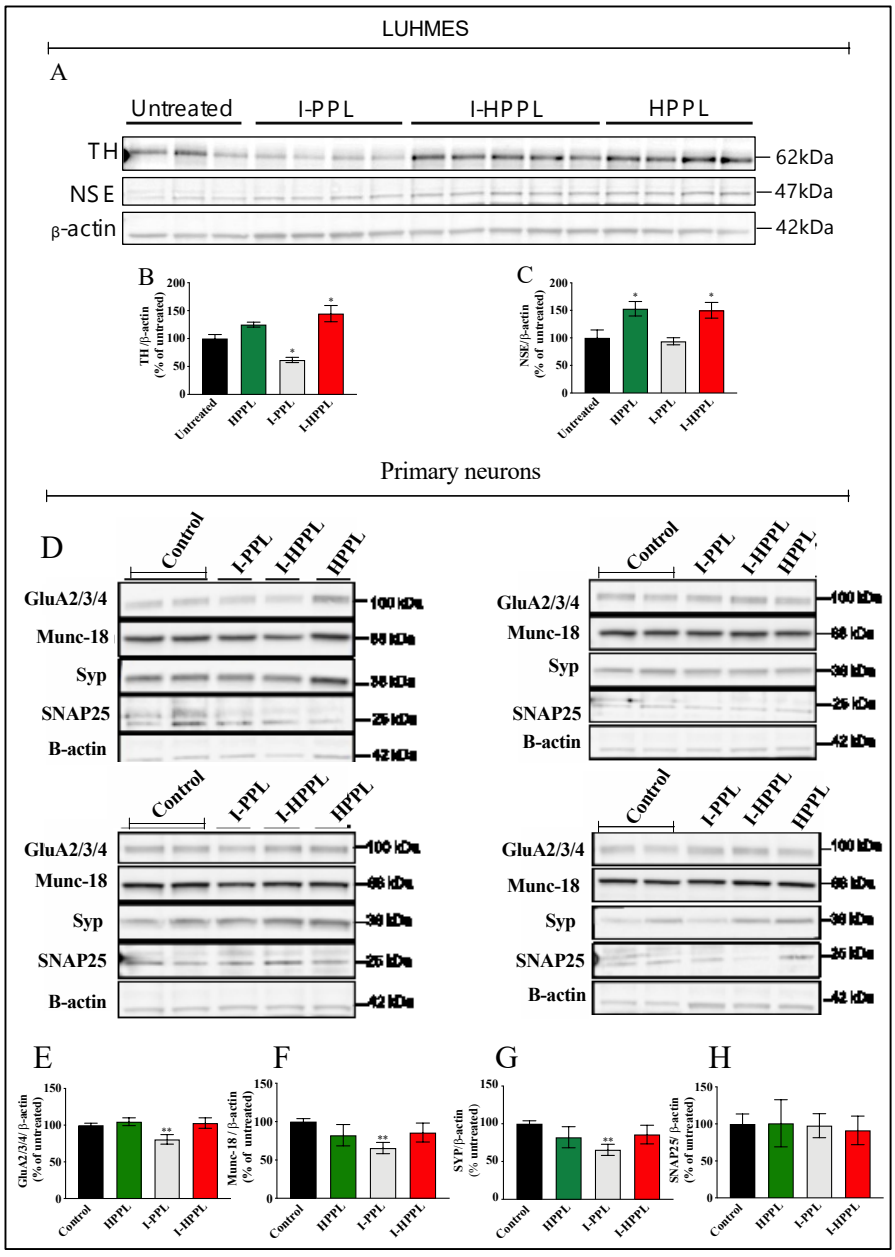

Figure 21: Proteins expression evaluation under HPPL/I-HPPL stimulation.

*Western blot analysis was done using the lysates of LUHMES and primary (A) Western blots images for Tyrosine hydroxylase (TH) and Neuron Specific Enolase (NSE) expression in LUHMES cells. (B) and (C), graphs of the western blot quantification; (D-H) Western blots images and quantification of synaptic proteins expression in primary neurons. Data (n=3) were expressed as the mean ± SD of controls. *p < 0.05, **p < 0.01 vs control using One-way analysis of variance (ANOVA) followed by Fisher's Least Significant Difference (LSD) test. Abbreviations: day 0 (d0*

.4 Impact of heat-treated human platelet pellet lysates on lipid peroxidation

One of our interest was to evaluate in addition to the above assays, the possible involvement of the platelet biomaterials in a new described form of cells death, the ferroptosis. Therefore, we measured the level of lipid peroxidation using (Bodipy) and detected by FCM in LUHMES cells as it is associated with the event. Interestingly, HPPL and I-HPPL did not favour lipid peroxidation after 1-day post-treatment compared to a negative control (cell culture in normal conditions). We also added a positive control, which was cells treated with the toxin erastin (**Fig.22**). In the positive control, there was a significant increase in lipid peroxidation as expected.

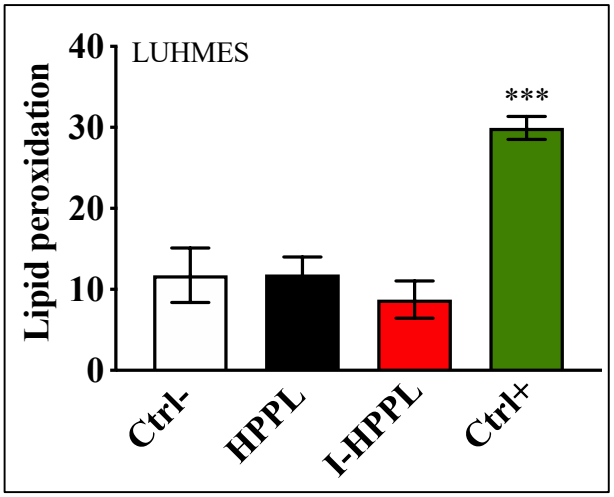

Figure 22: Effect of HPPL/I-HPPL on LUHMES viability. *The cells were stimulated with 5% HPPL or I-HPPL for 24 hours, and the control negative (Ctrl) were maintained in normal conditions. Cells treated with Erastin only were used as the positive control (Ctrl+) for cell death evaluations. The cells were stained by C11-Bodipy for lipid peroxidation measurement (n=3).*

2.5. HPPL and I-HPPL did not activate microglia BV-2 cells.

Our objective is to investigate the possible use of HPPL or I-HPPL as a neuro-protectant in brain injury conditions. We thought it was crucial to know whether the platelet biomaterial is able itself to activate inflammatory cells. We used BV-2 cells to provide at least a preliminary answer to our concern. The cells have been therefore challenged with 5% HPPL or I-HPPL. The negative control was cells without treatment, and the positive control was cells under LPS stimulation. We measured the inflammatory enzyme COX-2 and the pro-inflammatory cytokine TNFα. Both are released by microglia cells upon LPS activation. The results presented in (**Fig.23a-b)** suggest that in normal condition (no LPS), HPPL, and I-HPPL-treated cells did not impact significantly COX-

2 expression. All the lysates successfully reduced the increased COX-2 expression associated with LPS pre-treatment ($p< 0.001$). Similarly, a very low level of TNFα was detected by ELISA when the cells were exposed to 5% HPPL or I-HPPL for 1 day (<0.5 ng/mL) **(Fig.23c**) in comparison to control and LPS treatment. After a pre-treatment with LPS, BV2 released less TNFα in the presence of HPPL ($p<0.05$; 166 ± 23ng/mL) and I-HPPL ($p< 0.001$; 142 ± 20ng/mL) as compared to LPS alone (216 ±30ng/mL).

Additionally, the morphological changes were evident in LPS-treated BV-2 cells after one day (**Fig.23 d**). Stimulated with LPS, BV-2 cells developed an amoeboid large morphology typical of an activated state, whereas BV-2 cells treated with 5% of HPPL were morphologically similar to the control group. These findings suggest that either HPPL or I-HPPL are able to inhibit LPS-induced activation of BV2 cells.

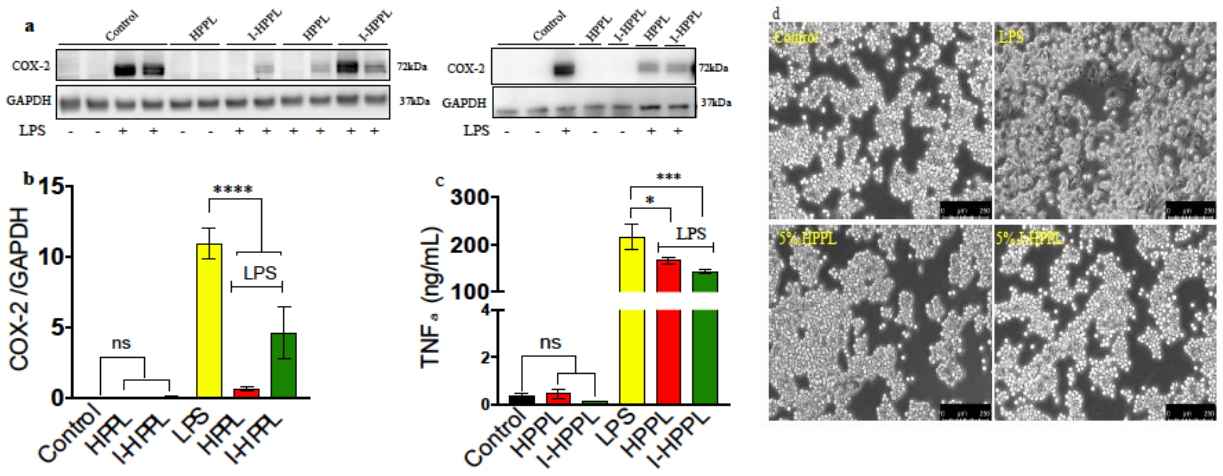

Figure 23: Safety and anti-inflammatory activity. *BV-2 was exposed to 5% HPPL or I-HPPL for 48h to assess the potential pro-inflammatory effect of HPPL and I-HPPL. LPS was used as the positive control. Additionally, for the ani-inflammation potential evaluation, the cells were exposed to LPS for an hour followed by HPPL or I-HPPL addition and incubated for two days. COX-2 expression was evaluated in cell lysate via Western blot, and levels of TNFα were quantified in the cell culture supernatant (n=3). (a, b) expression of COX-2:). TNFα release (c) in cells culture medium. Data were expressed as mean ± SEM (*P < 0.05; ***P < 0.001; ****P < 0.0001). (d) Morphology of BV-2 cells treated with HPPL or I-HPPL. The scale bar is 250 µm.*

3. Investigation of heat-treated platelet lysates activity *in vitro*

3.1 *Platelet lysates can enhance a wound healing*

To mimic brain injury *in vitro,* a scratch test was done to understand at the first step, the ability of HPPL/I-HPPL to stimulate the migration and proliferation of undifferentiated SH-SY5Y cells and EA-hy926 endothelial cells. SH-SY5Y and EA-hy926 were grown until a monolayer was observed, then they were wounded and treated with HPPL and I-HPPL. Within 24 h of treatment, the platelet materials stimulated cells proliferation and the migration better than untreated cells (control) (**Fig.24**). An average of the wound closure index (for SH-SY5Y cells) was calculated and found to be approximately 0.3 in the control condition, 0.79, and 0.8 for HPPL and I-HPPL, respectively ($p<0.0001$ vs. control). For EA-hy926 cells, the wound closure index was 0.4 for control. 0.9, and 0.89 for HPPL and I-HPPL, respectively.

Similar results were found when performing the same test using differentiated SH-SY5Y cells as neuronal cells. After inducing their differentiation by retinoic acid, the cells' monolayer was scratched, followed by platelet pellet lysates stimulation. The wound area was monitored over 4 days and captured. As shown in Fig.**24 (e-k)**, the bioactive agents supported efficiently the growth of the cells into the scratched area. When the cells were stained with synaptophysin, a synaptic marker to ensure that the cells expressing cell neurites, visible in bright field images, are still viable, we further evidenced our results.

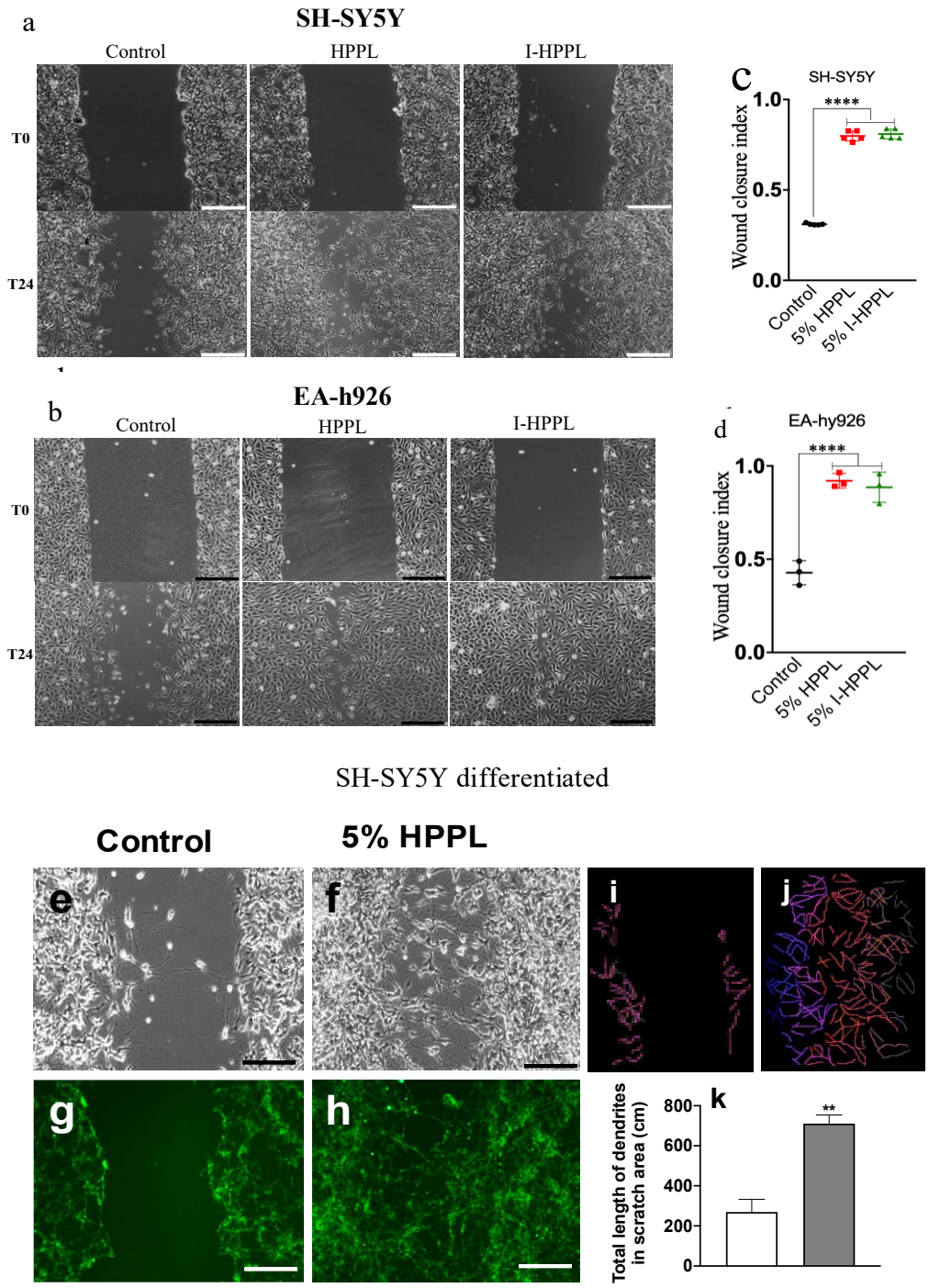

Figure 24: Scratch healing test. *All the cells were exposed to 5% HPPL or I-HPPL or not, and images were taken at the desired time points. Samples of images of the scratch test on non-differentiated SH-SY5Y (a) and EA-HY926 cells (b), differentiated SH-SY5Y cells (e, f) The scale bar is 100 µm. The closure index was calculated one-day post-treatment: (c) SH-SY5Y, (d) EA-hy926, (g, h) differentiated SH-SY5Y cells stained with synaptophysin, (i-k) total neurites length in the scratch area estimated at day 4 post-treatment (n=4).*

3.2 Heat-treated platelet lysate stimulated the differentiation of human neuroblastoma cells

We examined in this experiment, the potential of HPPL and I-HPPL to stimulate neuronal cells differentiation. Therefore, we used non-differentiated SH-SY5Y cells in the absence of retinoic acid, a differentiation agent commonly used. The cells were seeded in six-well plates in presence of DMEM supplemented with 10% FBS for 24 hours to help their attachment to the plates' surface. The buffer was renewed the next day with DMEM without FBS followed by 2% (v/v) HPPL, 2% I-HPPL or 10 µM retinoic acid (positive control) treatment. The cells cultured in buffer containing 10% FBS were used as negative control. After seven days of incubation, bright-field images were acquired before staining with two neuronal markers: beta III tubulin and neurofilament. These two proteins were considered as differentiation markers. When compared to the negative control, we could observe in the bright field images (**Fig.25)** a significant ($p < .01$) increase in the number of cells with neurites in RA-treated cells (80%) as well as in HPPL (76%) or I-HPPL (74%) treated-cells. By measuring the neurites length, we found in HPPL, and I-HPPL treated groups, an average neurite length of approximately 130 µm and 117 µm, respectively. Compared to retinoic acid treatment, the bright-field images did not reveal a significant difference with HPPL, and I-HPPL treated-cells.

Additionally, the fluorescence intensity, obtained from beta-III staining, was significantly higher in cells treated by either 2% (v/v) HPPL or 2% I-HPPL as compared to negative control. However, no difference was observed when they were compared to the positive control. NFLM staining allowed to visualize the morphological changes in terms of neurites growth under HPPL and I-HPPL stimulation but no marked difference in the fluorescence intensity **(Fig.26).**

Together, these data evidenced the ability of standard and pathogen-reduced platelet pellet lysates to promote the differentiation of SH-SY5Y cells.

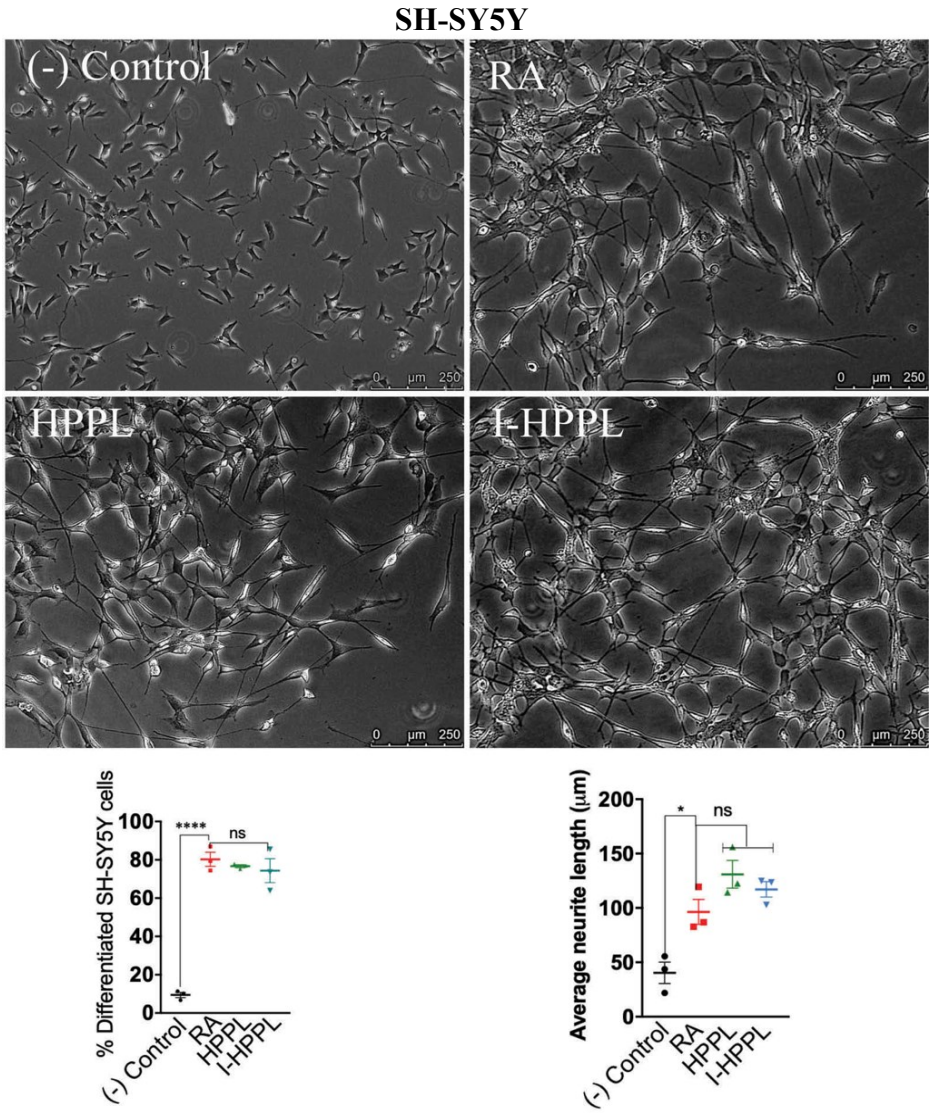

Figure 25: SH-SY5Y differentiation. *Bright-field images showing SH-SY5Y cells following HPPL/I-HPPL treatment (upper panel). The percentage of cells with neurites and the average neurites length were calculated in all the conditions (lower panel). Scale bar: 250µm*

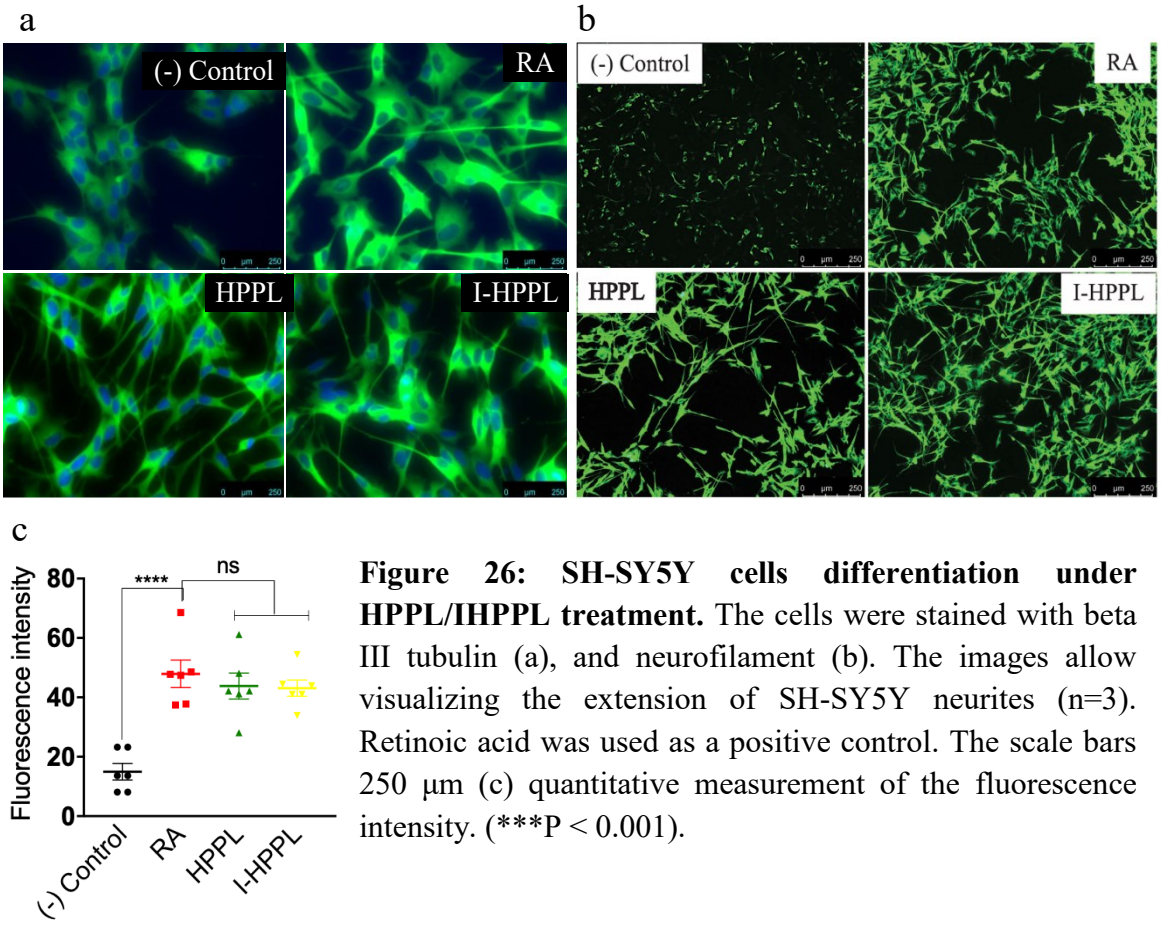

Figure 26: SH-SY5Y cells differentiation under HPPL/IHPPL treatment. The cells were stained with beta III tubulin (a), and neurofilament (b). The images allow visualizing the extension of SH-SY5Y neurites (n=3). Retinoic acid was used as a positive control. The scale bars 250 µm (c) quantitative measurement of the fluorescence intensity. (***P < 0.001).

3.3 Anti-ferroptosis potential of heat-treated platelet pellet lysate fractions

It is well described in the literature, AD, PD, and TBI trigger cell death pathways, including ferroptosis[249]. To investigate the neuroprotective activity of HPPL and I-HPPL *in vitro*, robust ferroptotic cell death models using LUHMES cells, primary neurons, and erastin as ferroptosis inducer were adopted.

Differentiated LUHMES cells were first prepared, then stimulated one hour with 5% HPPL or I-HPPL prior to erastin treatment at a final concentration of 1.25µM. LUHMES cells are vulnerable to erastin and as expected, the addition of the toxin has led to higher cell death **(Fig. 27A-B**) and an increase of lipid peroxidation (**Fig. 27C**). In addition, there was a strong loss of TH and NSE expressions **(Fig.27E-G**). When compared to erastin condition, HPPL and I-HPPL successfully protected the cells from erastin-induced LUHMES cell death. The viability of the cells was examined by CCK-8 test and propidium iodide staining, and the results are presented in **Fig.27H**.

Furthermore, lipid peroxidation level was also significantly ($p<0.05$) reduced following HPPL and I-HPPL treatment compared to erastin treated-cells only.

With the addition of erastin, TH and NSE levels were reduced; however, the situation was reversed in the presence of platelet lysate. The cells treated with HPPL or I-HPPL showed significantly high expression of TH and NSE in LUHMES cells (**Fig.27E-F**).

In other hand, the anti-ferroptosis activity of HPPL and I-HPPL was analyzed in mouse primary neuronal cultures, which were obtained from embryonic (E16) C57 mice. The cells were maintained until DIV21 in order to have mature neuronal cells. As for the LUHMES, the primary neurons were first treated with HPPL and I-HPPL for an hour and then stimulated with erastin for two days. Next, the release of lactate dehydrogenase was measured. As presented in **Fig.27D,** the toxicity of erastin was significantly reduced in the presence of platelet lysates. These results suggest that HPPL and I-HPPL are able to mitigate the effect of the neurotoxin, and the pathogen inactivation procedure does not alter the neuroprotective properties of HPPL.

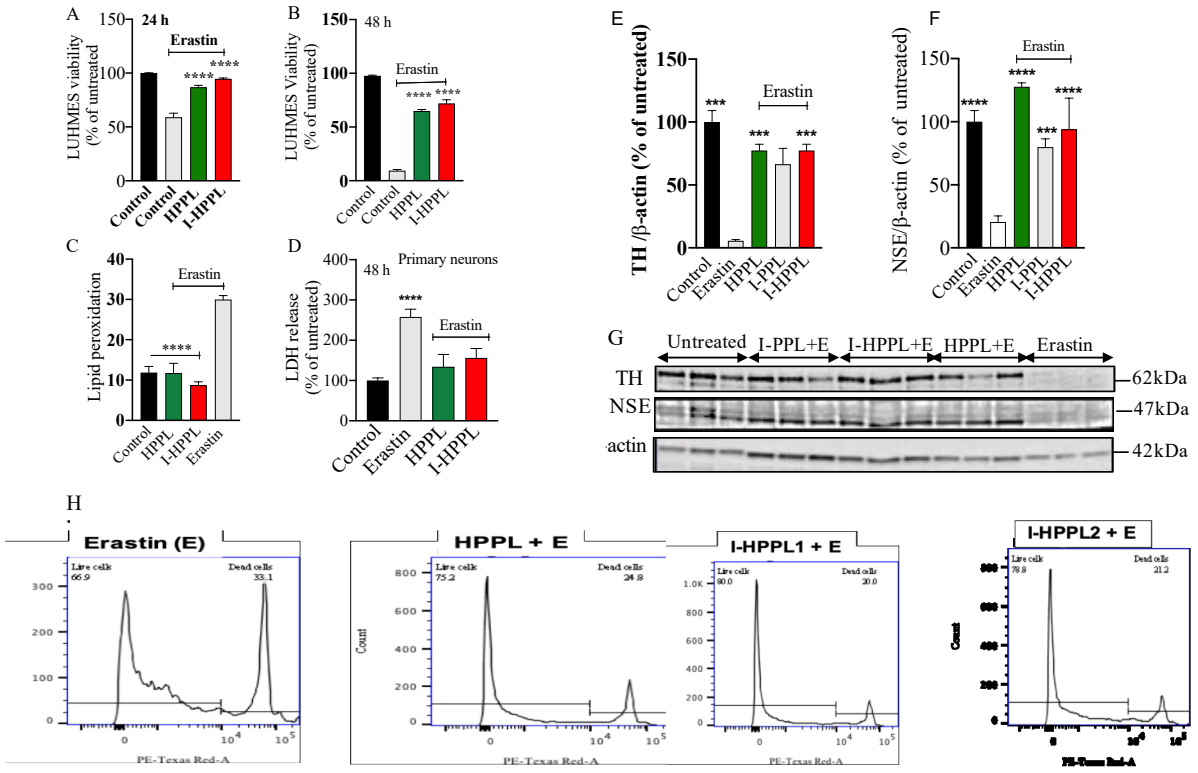

Figure 27: Ferroptosis inhibition evaluation. *LUHMES cells were pre-treated with 5% HPPL or I-HPPL for an hour before erastin stimulation. Our controls were cells under erastin stimulation or maintained in normal condition. One day, post-incubation, some cells were labeled with propidium iodide for cell viability analysis (A) or C11-Bodipy for lipid peroxidation quantification (C) by flow cytometry. After two days of incubation, the treated cells viability was estimated using CCK-8 (B). The inhibition of erastin toxicity was also investigated with primary cells culture. The mature neurons were treated with 0.5% I-HPPL and HPPL 1 hour prior to 1.25µM erastin addition. The effect of HPPL/I-HPPL was assessed by LDH assay (D). The expression TH and NSE was also quantified by western blot (E, G). (H) Samples of micrographs of flow cytometry. The data (at least n=3) were estimated were expressed as a mean ± SD of control. *p < 0.05, **p <0.01 ***p < 0.001 vs. control, ****p < 0.0001 vs erastin treatment.*

B. *In vivo* neuroprotective effect of heat-treated platelet pellet lysate

Base on the *in vitro* analysis and the availability of platelet lysate, we decided to evaluate *in vivo* the potential of the non-pathogen-inactivated HPPL. However, this experiment was performed after the description of the cortical brain scratch model.

1. Pathophysiological development of brain lesions in cortical brain scratch and CCI models.

We first characterized the pathophysiological development of our new mouse TBI model, the cortical brain scratch injury, intended to mimic the consequences of TBI leading to penetrating injury. The model's evolution was compared to a well-validated in vivo TBI model, the controlled cortical impact (CCI). Several approaches have been used, such as imaging, behavioral tests, and molecular/biochemical/histological investigations.

1.1 The brain scratch induced behavioral deficits in motor dependent tasks but not in novel object recognition at DPI7.

In the process of understanding the brain scratch's potential patterns, we performed some behavior tests, including beam, rotarod, open field, and novel object recognition tasks. At least nine animals per condition were used. We first checked the mice's motor function at DPI3 and DPI6 compared to Sham and CCI groups. The beam test revealed a significant increase ($p< 0.05$) in the time spent by the brain scratch injured mice to cross the elevated beam compared to Sham-treated animals at DPI3 and DPI6 (**Fig. 28A, B)**. The same trend was observed when comparing the CCI groups and the control at DPI3. However, only a slight difference between the CCI and Sham groups was observed at DPI6.

Besides the beam test, we also investigated the animals' ability to stay on a rotating rod at DPI3 and DPI6. The rotarod evaluation evidenced that the scratch injury mice spent significantly less time ($p<0. 05$) at DPI3 and DPI6 compared to Sham and CCI animals (**Fig.28C, D**).

The motor function tests were completed by observing the mice's behavior in an open field box over ten minutes. In the open field test, the mice could navigate freely, and their behavior was recorded. The total distance and time spent in the center of the field were not significantly different when comparing the scratch and Sham animals (**Fig.29A-B**). However, at DPI3 and DPI6, the CCI mice spend more time ($p<0.05$) in the center of the field compared to cortical scratch group and Sham animals (**Fig.29C-D**).

Impact on short memory investigated by the novel object recognition task evidenced that both CBS and CCI animals moved significantly less that the Sham mice. However, no statically difference was found among the groups for the discrimination index (**Fig. 29E-F).**

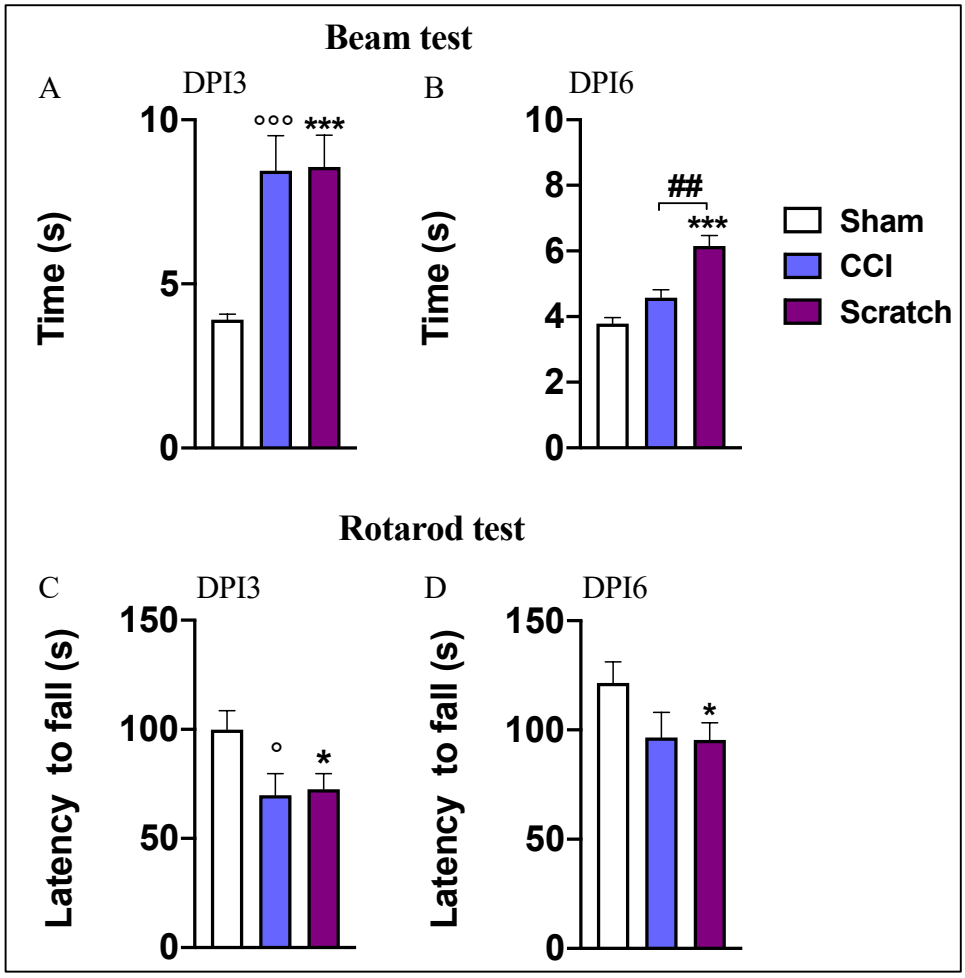

Figure 28: The effects of scratch on mice behaviors. *The beam test and rotarod were performed at DPI3 and DPI6. All mice were tested for (A, B) locomotor function (beam walking); (C, D) Rota rod test. Data were presented as means ± SEM (n = 14 in each group). *p < 0.05 or **p < 0.01 compared to scratch vs Sham; °p < 0.05 or °°p < 0.01, °°° p < 0.001 for CCI vs Sham, ##p < 0.01 CCI vs Scratch.*

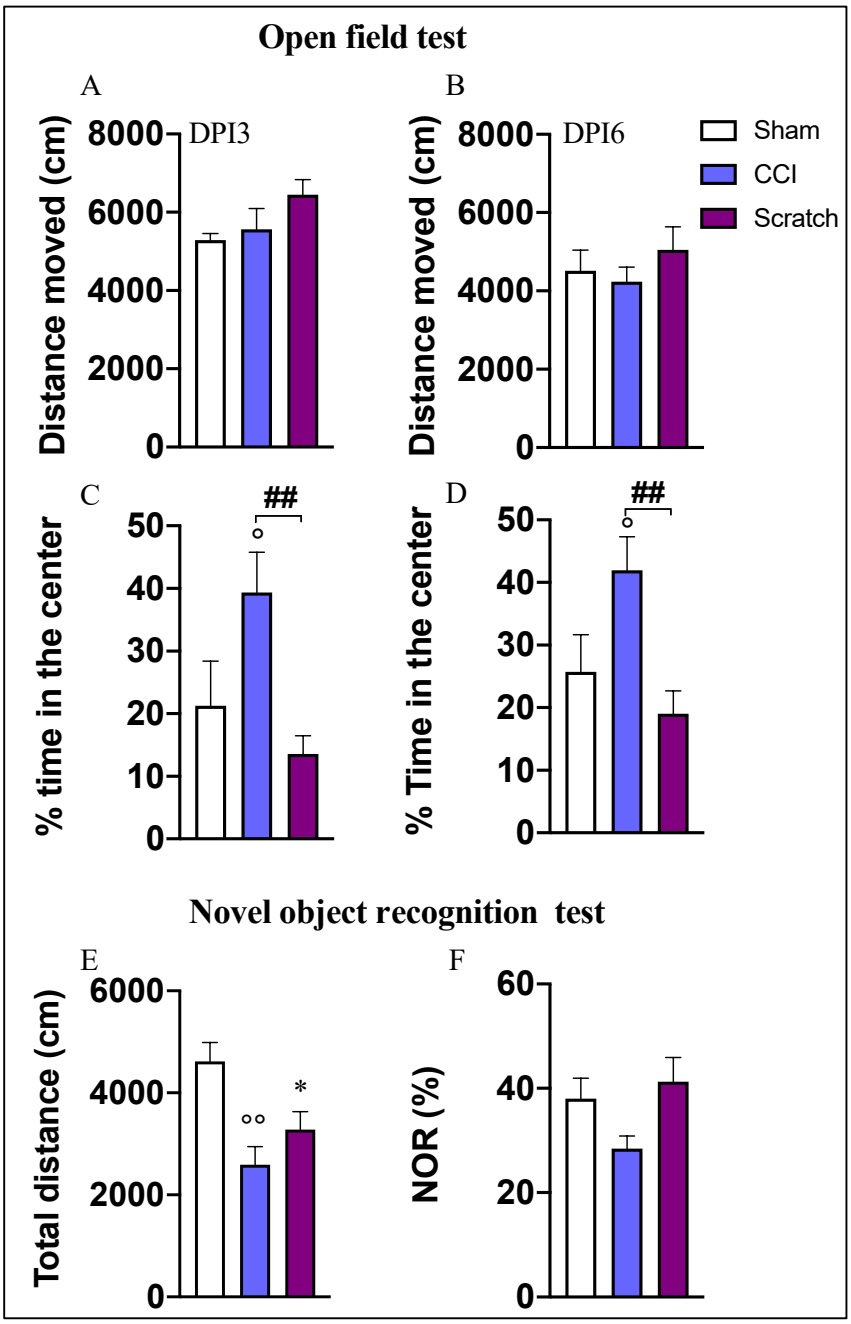

Figure 29: Impact of the scratch injury on mice behaviors. *For the open field, the animals were left in a box and allowed to explore freely for 10 minutes. For the NOR test, three days were required. Habituation, familiarization, and novel object recognition are the main phases of the test. All mice were tested for (A-D) locomotor function (open field); (E-F) novel object recognition. Data were presented as means ± SEM (n = 9 in each group). *p < 0.05 or **p < 0.01 compared to scratch vs Sham; °p < 0.05 or °°p < 0.01, °°° p < 0.001 for CCI vs Sham, ##p < 0.01 CCI vs Scratch.*

1.2 The brain scratch injury triggered cortical neuroinflammation

To understand the physiological events occurring after the Scratch model of TBI, we investigated the expression of a batch of neuro-inflammatory genes by RT-qPCR in the cortex seven days post-injury, using cyclophilin as internal control, and compared to CCI and Sham animals (**Fig.30**). We focused on assessing the relative mRNA expression of TNFα, IL1ß, CCL3, CCL4, CCL5 pro-inflammatory cytokines, and chemokines in the ipsilateral cortex as the first step. Interestingly, these markers were significantly upregulated (P <0.01) in the cortical injured mice cortex compared to Sham-treated animals. At a second attempt, we examined the levels of some glial genes. Similarly, the brain scratch triggered the upregulation of microglial markers such as toll-like receptors TLR2, TLR4, CD68, C1q, TREM2, and astroglia markers GFAP, vimentin as compared to the Sham group. Globally, our new model of TBI led to a significantly higher neuroinflammatory reaction as compared with CCI.

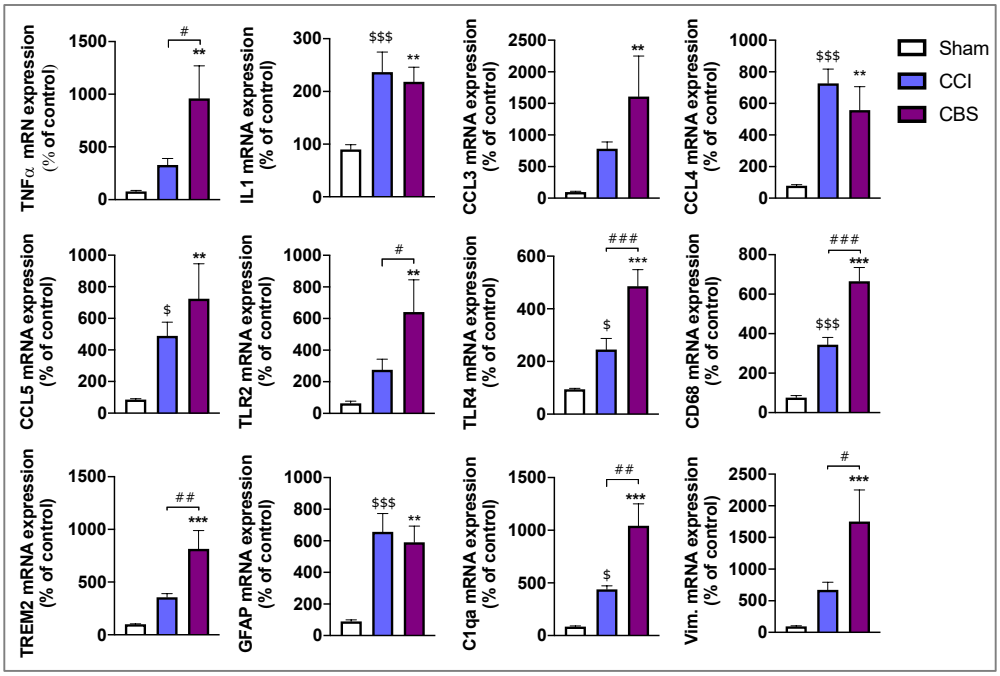

Figure 30: Changes in pro-inflammatory indicators expression. *Cytokines and chemokines, glial markers levels in the ipsilateral cortex at day 7 post-injury: (A) All the genes tested were significantly upregulated in the scratch mice compared to Sham. Pro-inflammatory cytokines (TNFα, IL1ß) and chemokines (CCL3, CCL4, CCL5) chemokines receptors (TLR2, TLR4, CD68, TREM2) and glial markers (GFAP, C1q, vimentin). Data (n=10) are reported as mean (SEM) percentages of the control (hole only without the scratch). *P <0.05, **P <0.01, ***P <0.001. $^{\#\#}p < 0.01$, $^{\#\#\#}p < 0.01$ CCI vs Scratch, $^{\$}P <0.05$, $^{\$\$}P <0.01$, $^{\$\$\$}P <0.001$ CCI vs Sham.*

We further investigated the activation of cells following cortical scratch injury using the immunostaining technique. For this experiment, we used two markers related to astrocyte activation (GFAP) and microglial marker Iba-1 (**Fig.31).** As found in the gene's analysis, both makers' fluorescence intensity was significantly ($p<0.05$) in the cortex ipsilateral of the mice subjected to brain scratch and cortical impact compared to Sham. Moreover, when compared the Scratch group to CCI animals, a significant difference was also observed. This result suggests that the astrocytes and microglia were activated. It confirmed the previous results again.

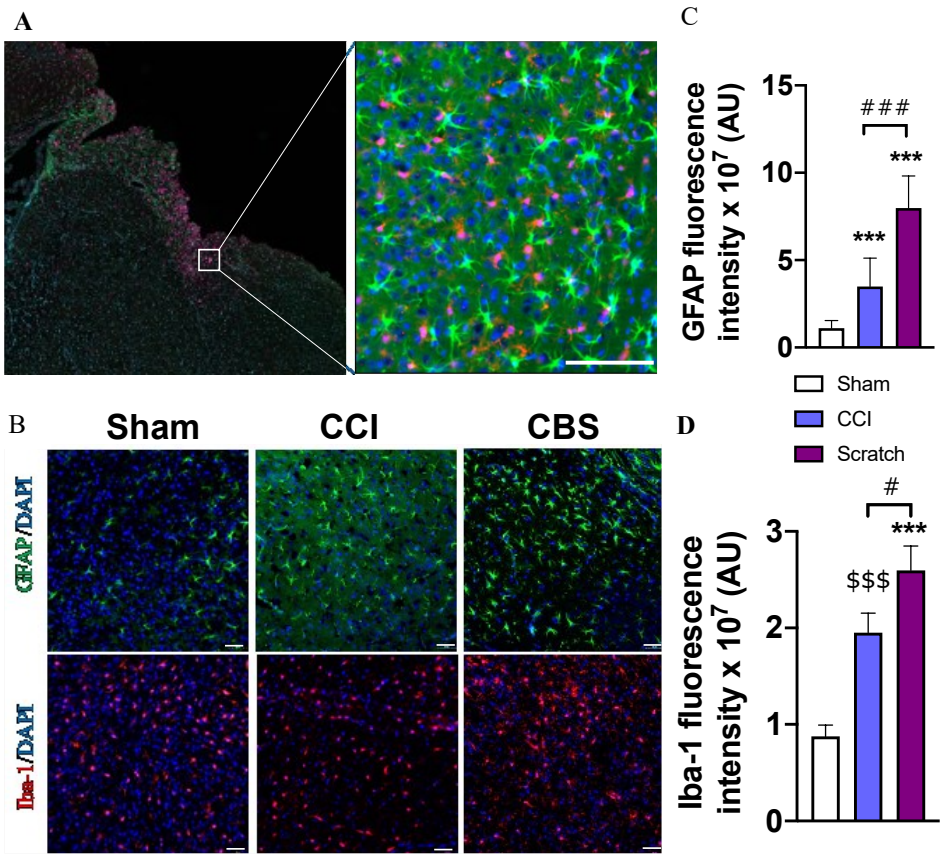

Figure 31: Immunofluorescence staining of brain sections *(cortex) for GFAP and Iba-1 as described in the method section. The sections were counterstained with DAPI. The staining was analyzed using Tissue Fax microscopy system. The glial cells activation was confirmed following the cortical brain scratch. The scratch induced microglia and astrocytes activation as indicated by the increase of the fluorescence intensity. (A) Illustration of the scratched site; (B) Illustration of the scratch cortex after GFAP and Iba-1 staining (merge image), (C, D) Fluorescence intensity quantification of GFAP and Iba-1 immunoreactivity using ImageJ (NIH, USA). Scale bar = 50 µm n = 4/group. *p < 0.05, **p < 0.01, ***p < 0.001 Scratch vs. Sham, $^{\#\#\#}$p < 0.001 vs CCI vs Scratch. $^{\$}$P <0.05, $^{\$\$}$P <0.01, $^{\$\$\$}$P <0.001 CCI vs Sham*

1.3 The scratch injury induced oxidative stress

Besides the inflammation, we also measured the level of ROS in fresh tissue. As expected, a significantly higher NADPH oxidase-dependent superoxide ion production was found in the ipsilateral cortex of the scratch injury mice compared to Sham. The results in **Fig 32** indicated that with NADPH's addition, the ROS level in CBS mice had enhanced three times higher in the cortex than the Sham.

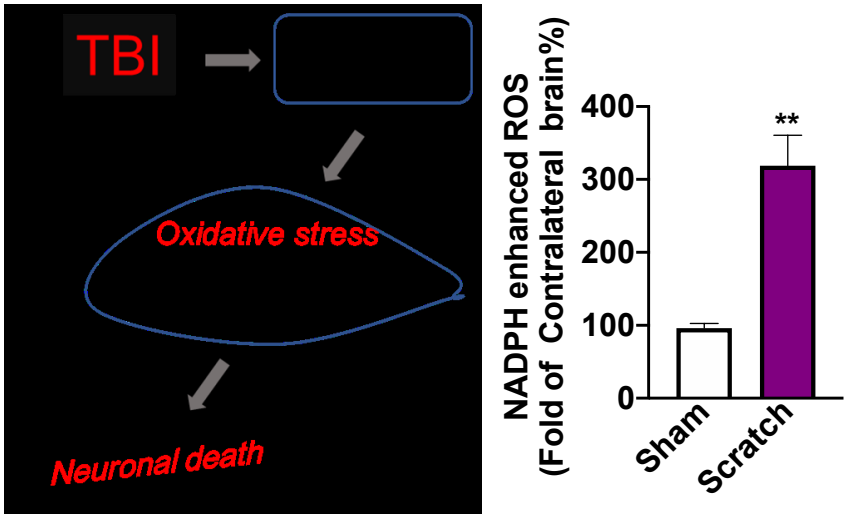

Figure 32: Reactive oxygen species level after the scratch at 7 days' post-scratch. *The cortex of each animal (n=4) was dissected at DPI7 and quickly dropped in an equilibration buffer (Krebs buffer for 10 minutes. Next, a baseline was measured prior to NADPH addition. The level of reactive oxygen species was determined over 350 seconds. Data are expressed as mean (SEM (SEM), **P <0.01.*

1.4 The impact of the cortical brain injury on synapses

We hypothesized that scratch induced to the brain could affect the level of synaptic proteins. Thus, we investigated pre-and postsynaptic markers in the cortex by ELISA and western blot. We found a significant reduction of Munc-18, SNAP-25, synaptophysin pre-synaptic, and the PSD95, postsynaptic proteins in scratch and CCI animals at DPI7 ($p < 0.05$). However, no significant difference was found when comparing CCI vs Scratch. The reduction of Synaptophysin, and PSD95 was confirmed by ELISA analysis. All the results are shown in **Fig.33**.

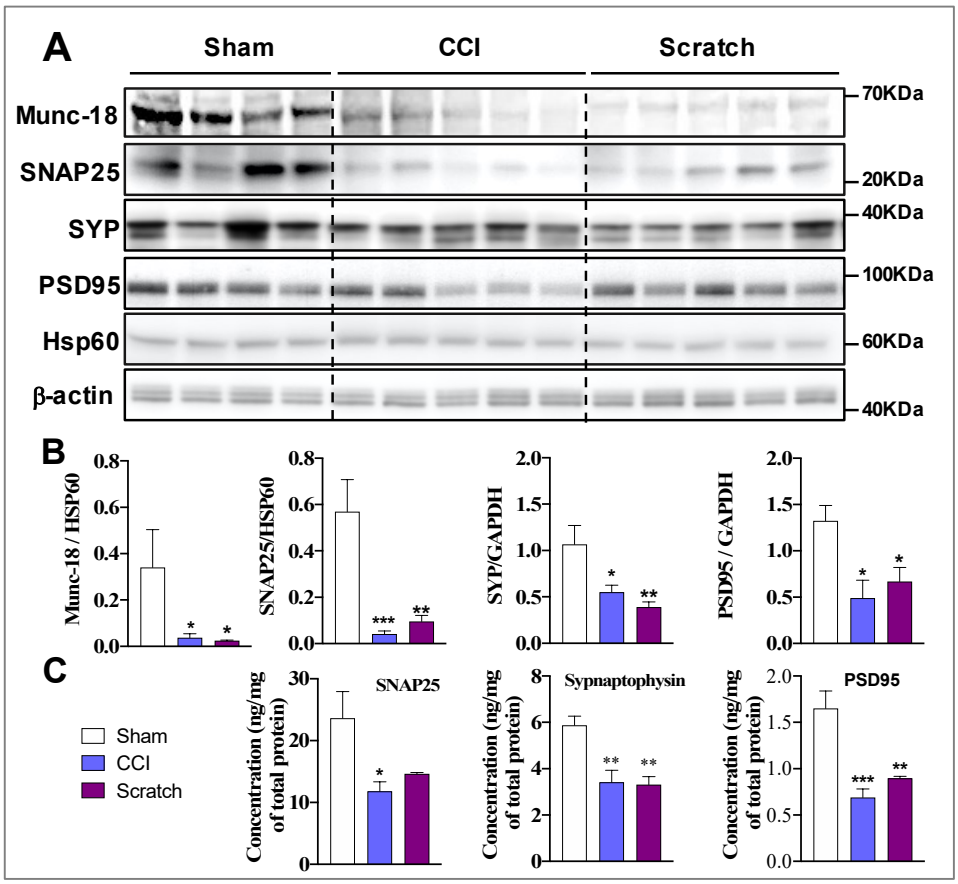

Figure 33: Impact of scratch injury on synaptic proteins expression. *Three pre-synaptic and one post- proteins were assessed by Western blot. (A) western blot images, (B) quantification of the blot bands. Three of the proteins were also assayed by ELISA (B). Data are expressed as a mean ± SEM (n = 9). CCI and scratch group were compared to Sham. *p < 0.05, **p < 0.01, ***p < 0.001 vs. Sham.*

2. The functional outcomes of HPPL administration in TBI-mice

2.1 HPPL administration improved motor and cognitive function of TBI mice.

Beam and rotarod tests, performed at DPI3 and 6 as described in the characterization of the Scratch model section, showed that the Scratch and CCI injuries induced a significant ($p < 0.001$) increase in the time the saline-treated animals spent to cross the beam and a significant decrease ($p < 0.05$) in the latency to fall off from the rotating rod as compared to Sham-treated mice at DPI3 (**Fig.34 A-D**). Interestingly, in the CCI model, HPPL-treated animals spent slightly less time at DPI3 crossing the beam than saline-treated mice (**Fig.34A)**. A significant improvement in the latency to fall in the rotarod test was also found at DPI3 **(Fig.34 B).** However, at DPI6, the CCI mice treated with HPPL did not show a significant difference compared to the saline group in the beam and rotarod test (**Fig 34 E, F**)

In the cortical brain scratch model, HPPL-treated mice spent significantly less time crossing the beam both at DPI3 and 6 (**Fig 34 C, G)**. Their latency to fall was improved significantly at DPI3 (**Fig 34 D)** but not significantly compared to saline treatment **(Fig 34 H).**

In addition, we also investigated the long-term effect of TBI on cognitive function at DPI14 using a novel object recognition test at DPI12 to 14. There was a significant effect of the discrimination index ($p < 0.001$) between saline-treated mice and Sham animals in both TBI models (**Fig. 34 I, J).** HPPL delivery successfully increased the discrimination index in the scratch injury model as shown in **Fig. 34 J**. The same trends were seen in the CCI -HPPL-treated animals, but no statistical difference was reached (**Fig. 34 I)**. Thus, HPPL-treatment helped animals to distinguish the old object from the new one with a specific preference for the later one.

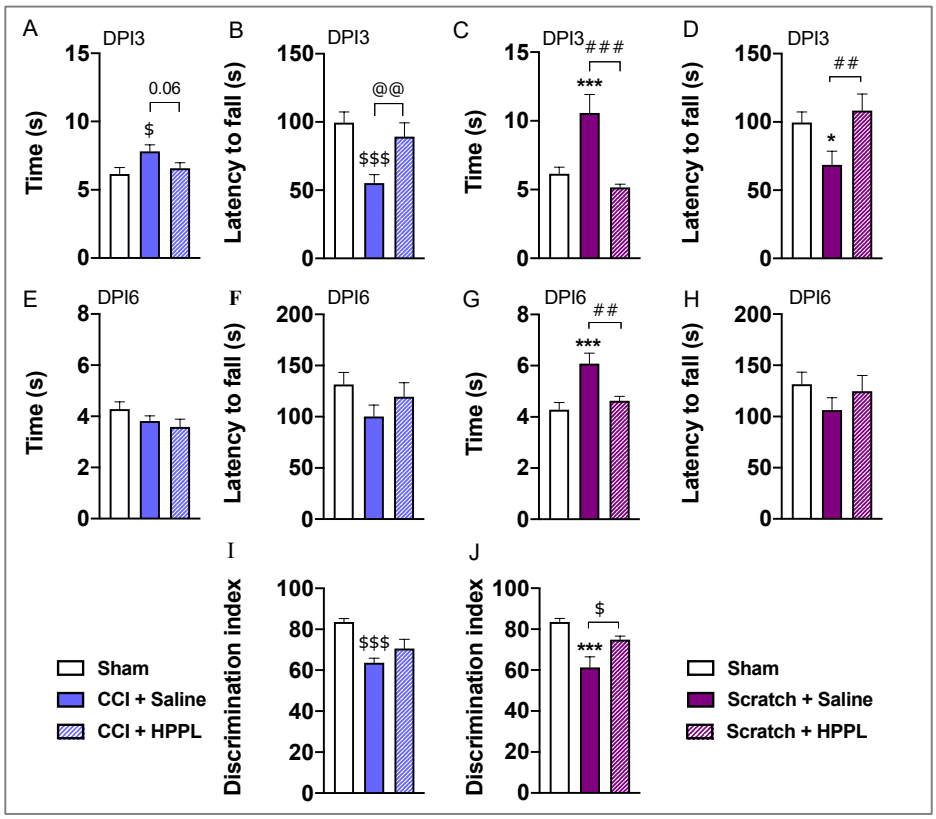

Figure 34: Beneficial effects of HPPL on mice behavior. *The beam test and rotarod were performed at DPI3 and DPI6. Mice were tested for (A-E, C, G) locomotor function (beam walking); (B, F, D, H) rotarod test. Data were presented as means ± SEM (n = 9 in each group).* ***CCI model****: $p < 0.05 or $$p < 0.01, $$$p < 0.001 for CCI- saline compared to Sham; @@p < 0.01 for CCI-saline vs CCI-HPPL.* ***Scratch model****: *p < 0.05 or **p < 0.01, ***p < 0.01 for Scratch-saline compared to the Sham; #p < 0.05 or ##p < 0.01, ###p < 0.001 for Scratch-saline vs Scratch-HPPL. n = 5 animals per group were tested for novel object recognition at day 14 post-scratch (I, J). Data were presented as means ± SEM*

2.2 Neuro-inflammatory markers modulation by HPPL *in vivo*.

The ability of intracranial and intranasal administration of HPPL to modulate the inflammation triggered in the scratch injury and CCI was examined by comparing the differential genes expression to vehicle treatment.

In the mild traumatic brain injury model induced using the controlled cortical impact device, we observed some changes in the expression of the pro-inflammatory genes. Regarding the cytokines and chemokines, we confirmed the upregulation of TNFα, IL1β, CCL3, CCL4, and CCL5

previously observed in the cortical brain scratch characterization model with the mice subjected to saline administration. The same trend was also found with the astrocytic (GFAP, vimentin) and microglia (CD68, TREM2, C1qa) markers, and the receptors TLR2, TLR4. These genes were significantly higher in the cortex of the saline-treated mice group, as expected compared to Sham. Following HPPL administration, the data presented in **Fig.35** indicated the downregulation of most of the tested genes. Only TNF and C1q were not significantly downregulated by the HPPL in the CCI model. All the others pro-inflammatory markers were modulated down significantly in CCI mice treated with HPPL.

Similarly, when we addressed the impact of HPPL administration using the cortical brain scratch model, we observed the ability of HPPL to modulate some inflammatory genes initially up following the brain scratch. There was a significant downregulation of TNFα, CCL3, CCL4, TLR4, CD68, TREM2, and GFAP mRNA ($P < 0.05$) in the mice treated with HPPL as compared to the saline-treated group (**Fig.35**) in cortical area at DPI7 for the scratch injury model.

These results provided additional evidence of the scratch injury's ability to triggered inflammation and activate astrocytes and microglia. Moreover, we were able to observe the anti-inflammatory effect of HPPL through this model.

We also performed an immuno-fluorescence staining to address the impact of HPPL treatment further. By GFAP and Iba-1stainings, we again highlighted that HPPL administration modulated the activation of glia cells. There was a decrease in the expression of these proteins compared to vehicle only (**Fig.36**)

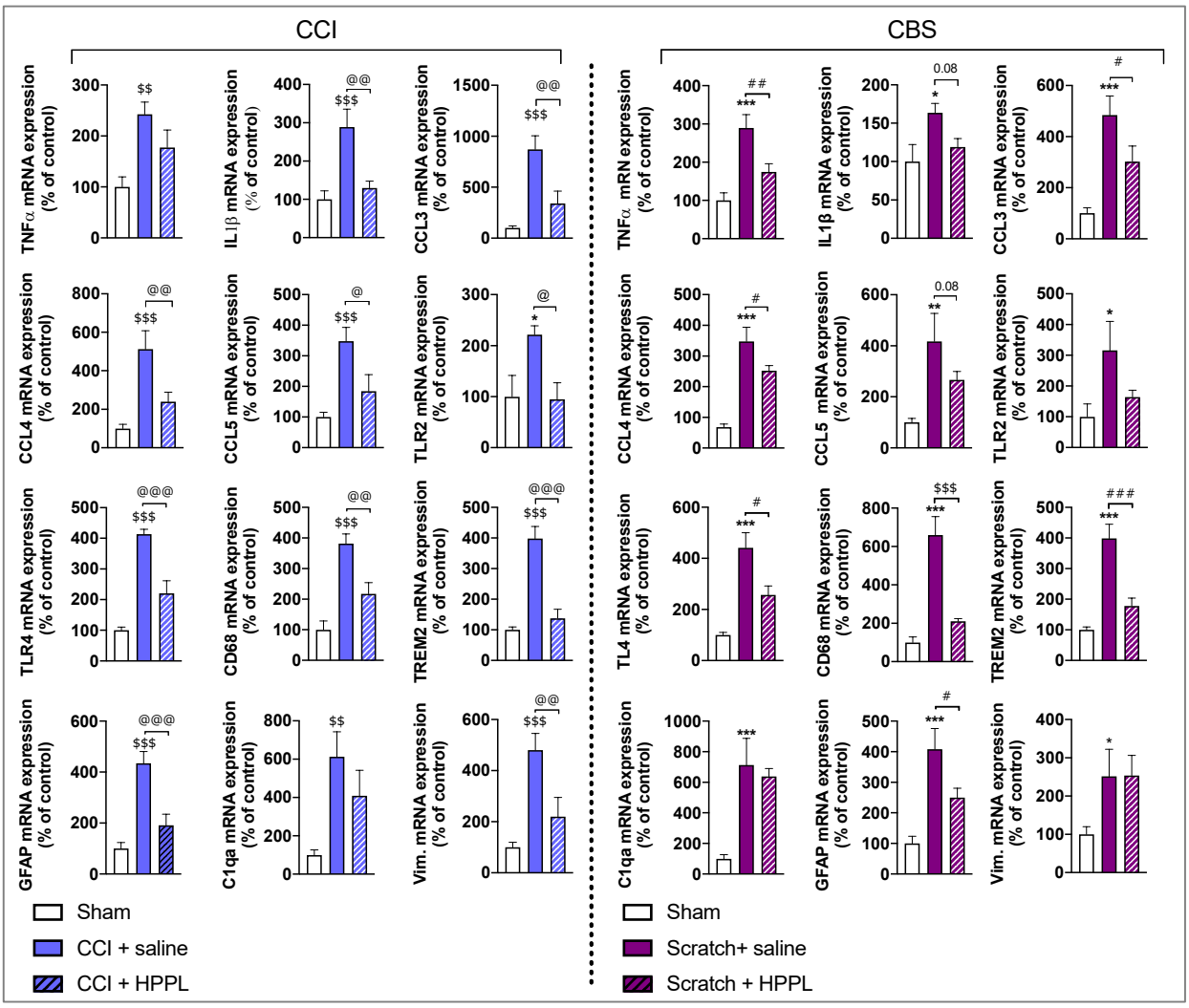

Figure 35: Effect of HPPL treatment on the expression of inflammatory markers. *Changes in cytokines, chemokines, and glial markers expression in the cortex at day 7 post-injury. Left panel summarized the data obtained from Controlled cortical impact model (CCI). Right panel, genes expression data in the cortical brain scratch model. Data were presented as means ± SEM (n = 9 in each group).* $^{@}p < 0.0\,5$; $^{@@}p < 0.01$; $^{@@@}p < 0.001$ *for CCI-saline vs CCI-HPPL,* $^{\$}p < 0.05$ *or* $^{\$\$}p < 0.01$, $^{\$\$\$}p < 0.001$ *for CCI-saline vs Sham; *p < 0.05 or **p < 0.01, ***p < 0.001 for Scratch-saline compared to Sham;* $^{\#}p < 0.05$ *or* $^{\#\#}p < 0.01$, $^{\#\#\#}p < 0.001$ *Scratch-saline vs Scratch-HPPL.* **Abbreviations:** controlled cortical impact (CCI), cortical brain scratch (CBS), heat-treated human platelet pellet lysate (HPPL)

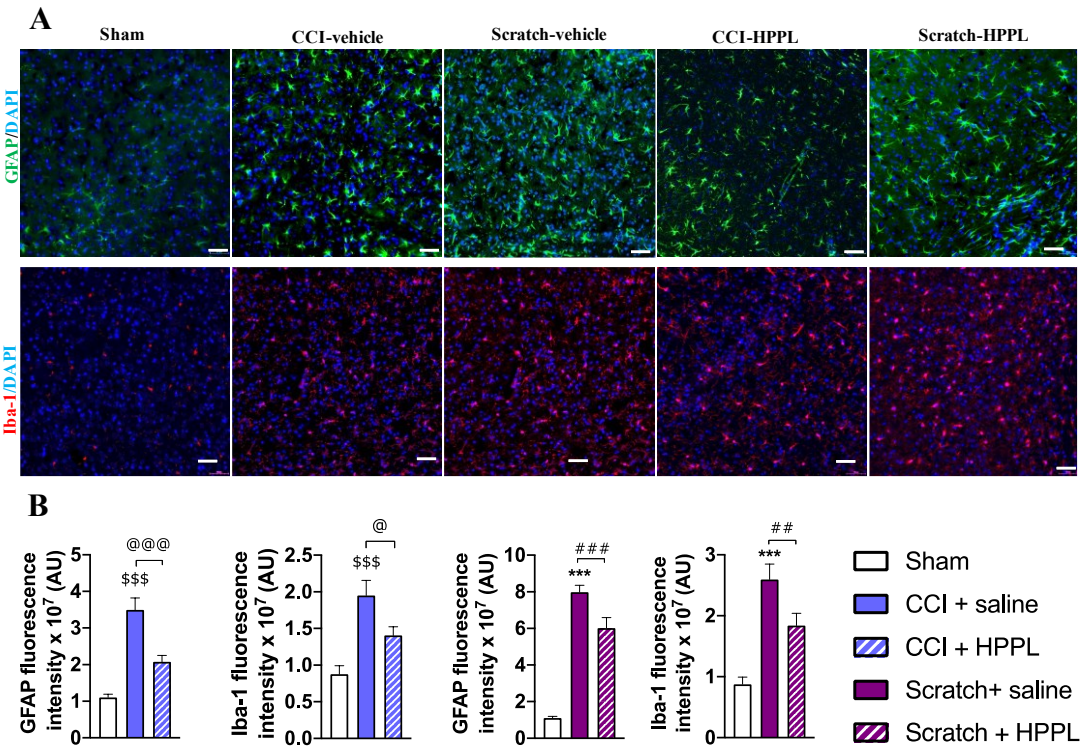

Figure 36: Immunofluorescence staining of brain sections. *(ipsilateral cortex) for GFAP and Iba-1 as described in the method section. The sections were counterstained with DAPI. The staining was analyzed using TissueFax microscopy. The HPPL treatment only decreased significantly the cells activation triggered by the brain injury as compared to vehicle group. (A) fluorescence images (GFAP and Iba-1), (B) Fluorescence intensity quantification of GFAP and Iba-1 immunoreactivity using ImageJ (NIH, USA). Scale bar = 50 µm n = 5/group.* $^{@}p < 0.0\,5$; $^{@@}p < 0.01$; $^{@@@}p < 0.001$ *for CCI-saline vs CCI-HPPL,* $^{\$}p < 0.05$ *or* $^{\$\$}p < 0.01$, $^{\$\$\$}p < 0.001$ *for CCI-saline vs Sham;* $^{*}p < 0.05$ *or* $^{**}p < 0.01$, $^{***}p < 0.001$ *for Scratch-saline compared to Sham;* $^{\#}p < 0.05$ *or* $^{\#\#}p < 0.01$, $^{\#\#\#}p < 0.001$ *Scratch-saline vs Scratch-HPPL.*

2.3 HPPL enhanced the expression of synaptic proteins in the cortex of mice

With the intention to address the impact of HPPL on the synaptic protein level following TBI procedures, we investigated by western blot and ELISA the expression of selected pre-and postsynaptic protein in Sham, CCI and scratch treated or not with HPPL. The analyses showed a downregulation of synaptic proteins following TBI. Munc-18, PSD95, SNAP25 and synaptophysin levels were lower in CCI/Scratch-saline compared to Sham. However, this phenomenon was partly reversed by the treatment with HPPL. A relatively higher expression of Munc-18, PSD-95 in the cortex of CCI- HPPL-treated animals (**Fig.37 A)**. Similarly, the level of

Munc-18 and SNAP25 increased in Scratch-HPPL compared to saline-treated mice (**Fig.37 B**). Following ELISA analysis (**Fig.37 C**), only synaptophysin concentration was significantly increased by HPPL compared to saline in CCI and Scratch. However, PSD95 and SNAP25 followed the same trends.

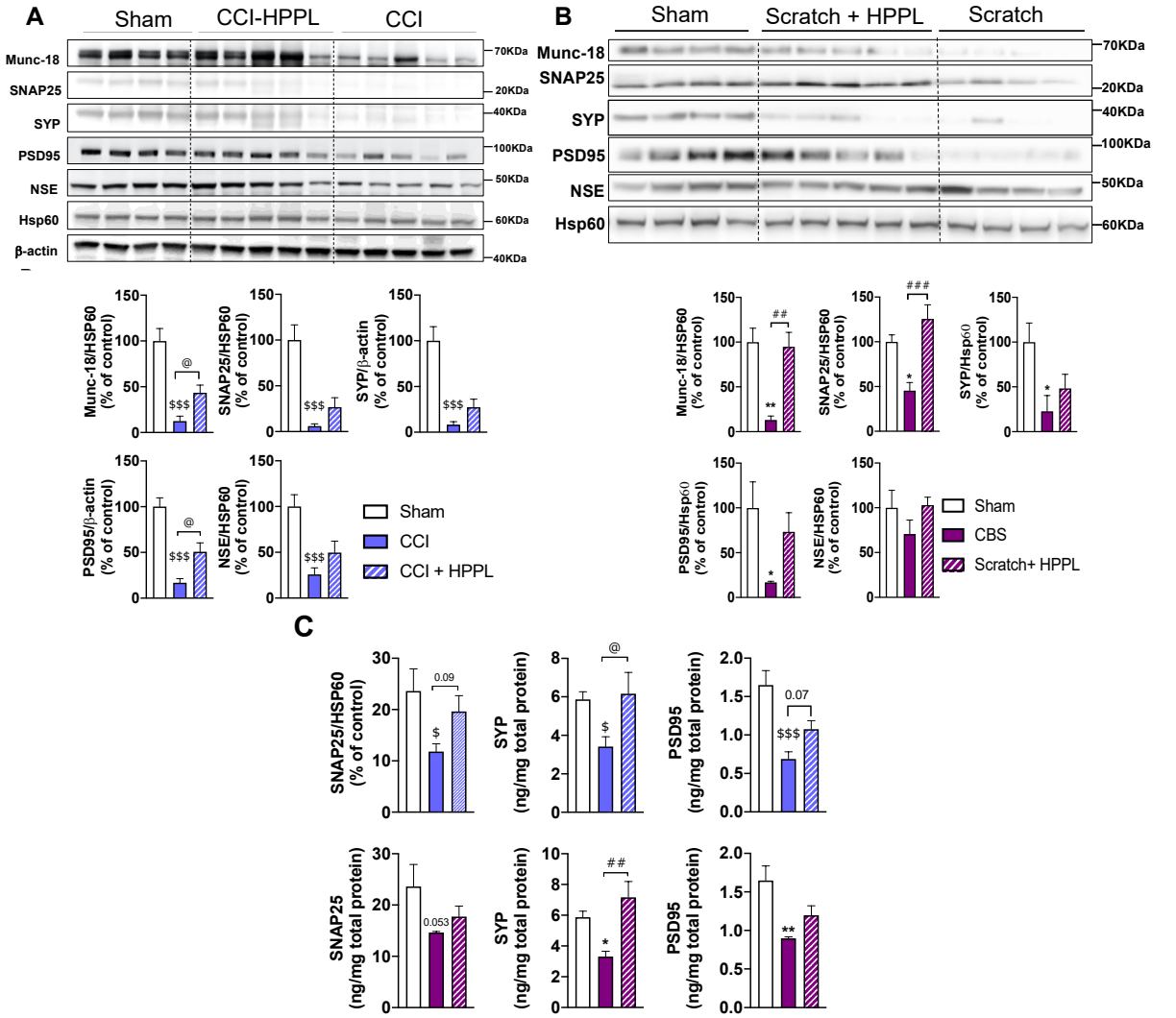

Figure 37: Expression of synaptic proteins following HPPL administration. *Western blot and ELISA quantification illustrating the expression of Munc-18, Synaptophysin, SNAP25, and PSD95 in the cortex at 7 days' post-scratch. (A) Western blot analysis in the CCI model. (A) Western blot analysis in the Scratch model, (C) ELISA quantification in the CCI mode (upper panel) and in the Scratch model (lower pane). Data are expressed as a mean ± SEM (n =4- 6).* $^{@}p < 0.0\,5$ *for CCI-saline vs CCI-HPPL,* $^{\$}p < 0.05$, $^{\$\$\$}p < 0.001$ *for CCI-saline vs Sham; *p < 0.05 or **p < 0.01, for Scratch compared to Sham;* $^{\#\#}p < 0.01$ *for Scratch-saline vs Scratch-HPPL.*

2.4 HPPL administration reduced a level of oxidative stress in the cortex of TBI mice.

Oxidative stress is known to aggravate neuronal damage after TBI. We, therefore, investigated whether HPPL administration could attenuate this phenomenon. The results showed that intracranial and intranasal administration of HPPL in the Scratch model of TBI significantly ($p<0.05$) reduced ROS level compared to saline-treated animals. We analyzed the expressions of selected genes known for their association in regulating oxidative stress, such as GPX1, SOD1, NQO-1, and MnSOD, and HO-1. These indicators were upregulated significantly ($p <0.05$) by HPPL administration excepted SOD-1 (in CCI group) (**Fig.38**) in both groups, suggesting the repair process's initiation.

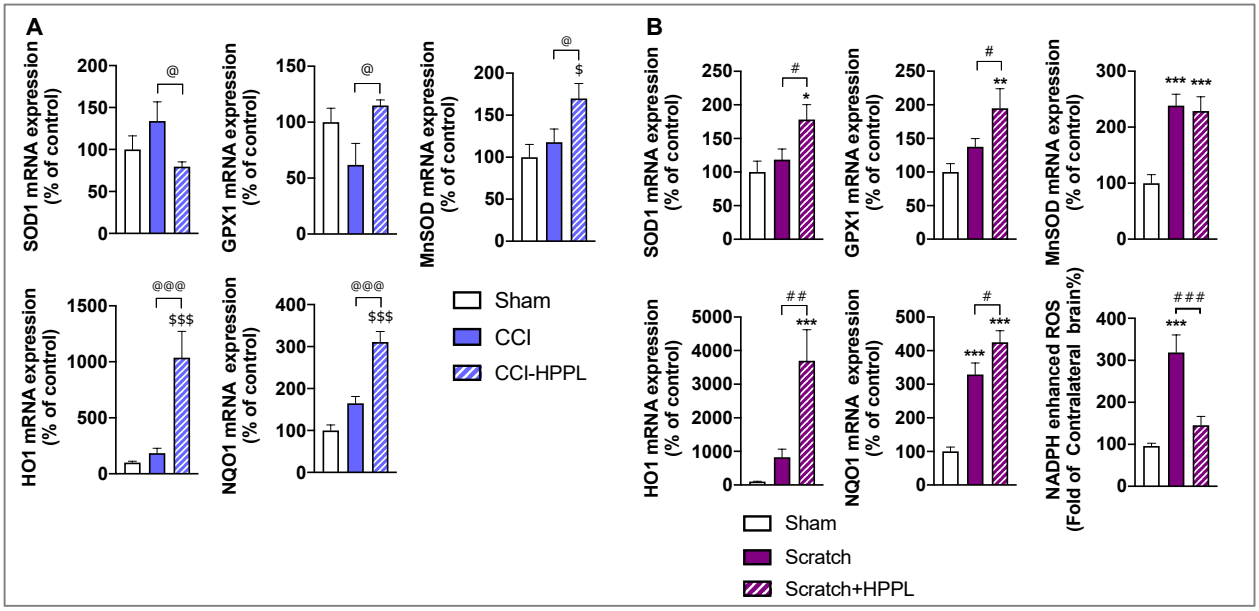

Figure 38; Analysis of ROS level and antioxidants genes involved in oxidative stress. *(A) Expression of genes following HPPL administration in the CCI-model. (**B**)Analysis of antioxidants gene and ROS level in the cortical brain scratch model. Data were presented as means ± SEM (n =5- 6 in each group). $^{\$}p < 0.05$, $^{\$\$\$}p < 0.001$compared to Sham; $^{@}p < 0.05$, $^{@@@}p < 0.001$ for CCI-saline vs CCI-HPPL. Scratch model: $^{*}p < 0.05$ or $^{**}p < 0.0$, $^{***}p < 0.001$ compared to the Sham; $^{\#}p < 0.05$, $^{\#\#\#}p < 0.001$ for Scratch-saline vs Scratch-HPPL.*

3. What proteomics analysis told us about HPPL potential in brain injury models?

We performed proteomics analysis to understand better the contribution of human platelet pellet lysate in treating TBI. Therefore, we focused first on investigating the pathological profile triggered by CCI and the brain scratch model compared to Sham animals used as control.

The main effect of the injury found (both in « CCI vs Sham », and « Scratch vs Sham ») is a considerable number of dysregulated proteins in the cortex of the animals. 634 dysregulated proteins were found in the CCI model (**Fig.39A**), while 817 proteins were changed in the cortical scratch animals **(Fig. 39B)**. The scratch led to more dysregulation compared to CCI and this further supported our previous results. In both models, several markers were found highly upregulated, such as CD44, Vimentin, GFAP suggestive of astrogliosis as well as microglial C1q proteins involved in the synaptic loss. To investigate in which biological process, we used the functional annotations tool, and it indicated that, overall, the present TBI procedures modulate several pathways related, for instance, to exosomes, mitochondria, cytoskeleton, myelin, or neurons, as compared to Sham (**Fig. 39 C**).

To summarize the impact of the CCI and the Scratch revealed by proteomics, we could say, both Scratch and CCI induced microglial and astrocytic activation and the loss of synaptic/neuronal markers.

Effect of HPPL on CCI and Scratch mice

The main biological effect of HPPL on TBI observed by proteomics analysis of mice cortex (both in « CCI-HPPL vs. CCI » and « Scratch-HPPL vs. Scratch ») is an increased number of downregulated proteins and a reduction of upregulated proteins.

Overall, the proteomic analysis supports that HPPL can, indeed, mitigate several of the TBI-related pathways (**Fig.39C**). Five hundred thirty-three proteins were found upregulated in the cortex of CCI animals compared to Sham (**Fig.39D).** Among these 503, 72 (17%) were found downregulated by HPPL (**Fig. 39D**). Among the 761 cortical proteins upregulated in the scratch model, 492 (64%) were found downregulated by HPPL (**Fig.39E).** These proteins belong to pathways related, for instance, to exosomes, transport, mitochondria, or synapse (**Fig.40A**). In addition, considering the link between both TBI models and neuroinflammatory processes, we compared our proteomics data with two recent transcriptomic signatures of disease-associated

microglia (DAM; Keren-Shaul et al., 2017) and astrocytes (DAA; Habib et al., 2020). Among the 471 upregulated DAM markers, signing pathological phenotype of microglia, 25 and 38 were found upregulated in the cortex of CCI and Scratch animals, respectively (**Fig.40B).** Among these, 2 and 23 were found downregulated in HPPL-treated animals. Moreover, among the 269 upregulated DAA markers, signing pathological phenotype of astrocytes, 44 and 38 were found upregulated in the cortex of CCI and Scratch animals, respectively (**Fig.40B**). Among them, 2 and 15 were found downregulated in HPPL-treated animals. HPPL strongly mitigates the effect triggered by brain damage by reducing the number of upregulated proteins. These data highlight the overall ability of HPPL to reduce neuroinflammatory load, notably in the most severe conditions. The number of proteins upregulated by TBI procedures exceeds the proteins downregulated, and HPPL exerted a limited action on the latter (**Fig.40C**). HPPL successfully reversed some pathological pathways triggered by TBI.

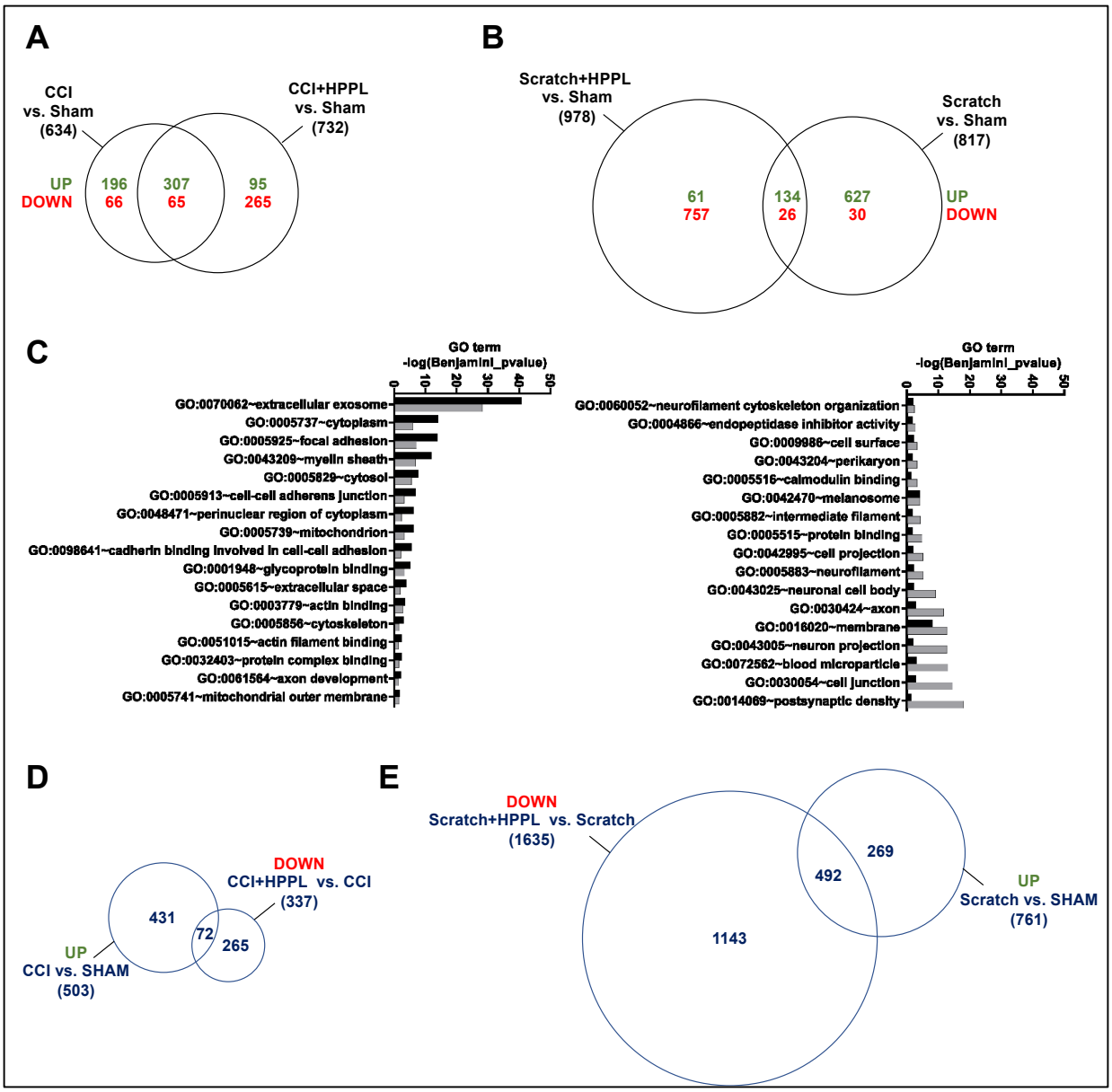

Figure 39: Bioinformatics analysis of proteomics results. *The samples were derived from mice cortex (n=8). (A) Venn diagram of the differential expressed proteins in CCI vs Sham and CCI-HPPL vs Sham and their interaction. (B) Venn diagram of the differential expressed proteins in Scratch vs Sham and Scratch-HPPL vs Sham and their interaction. (C) Gene Ontology (GO) enrichment analysis of differently expressed proteins and their statically significance. (D)diagram of protein initially up in CCI vs Sham and those down by HPPL treatment (CCI-HPPL vs CCI). (E)diagram of protein initially up in Scratch vs Sham and those down by HPPL administration (Scratch-HPPL vs Scratch)*

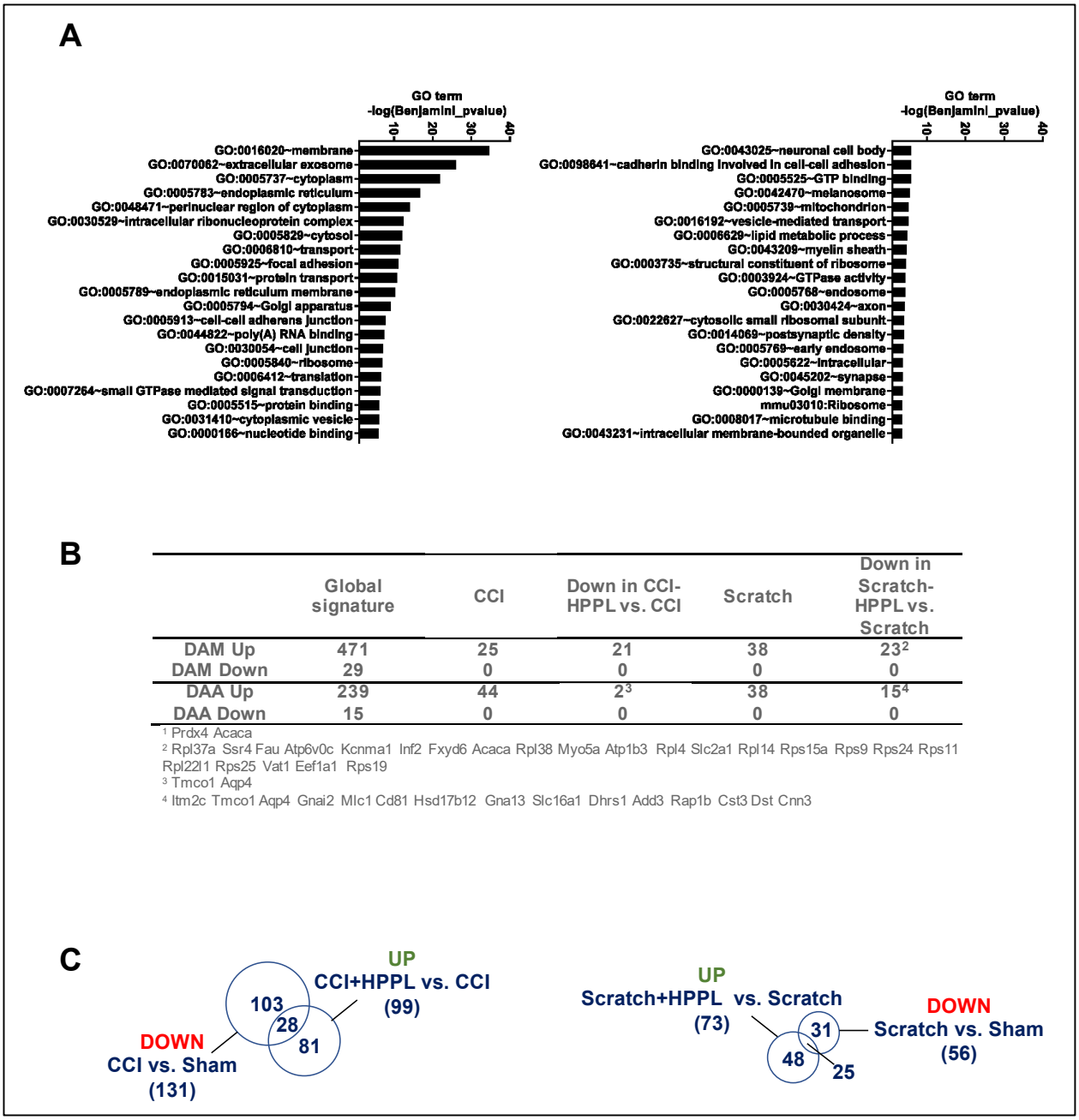

	Global signature	CCI	Down in CCI-HPPL vs. CCI	Scratch	Down in Scratch-HPPL vs. Scratch
DAM Up	471	25	21	38	23[2]
DAM Down	29	0	0	0	0
DAA Up	239	44	2[3]	38	15[4]
DAA Down	15	0	0	0	0

[1] Prdx4 Acaca
[2] Rpl37a Ssr4 Fau Atp6v0c Kcnma1 Inf2 Fxyd6 Acaca Rpl38 Myo5a Atp1b3 Rpl4 Slc2a1 Rpl14 Rps15a Rps9 Rps24 Rps11 Rpl22l1 Rps25 Vat1 Eef1a1 Rps19
[3] Tmco1 Aqp4
[4] Itm2c Tmco1 Aqp4 Gnai2 Mlc1 Cd81 Hsd17b12 Gna13 Slc16a1 Dhrs1 Add3 Rap1b Cst3 Dst Cnn3

Figure 40: Bioinformatics analysis of proteomics results. *(A) GO analysis of proteins downregulated by HPPL treatment. (B) comparison between our proteomics data with two recent transcriptomic signatures of disease-associated microglia (DAM) and astrocyte (DAA). (C) Venn diagrams showing the proteins initially down in CCI vs Sham and up in CCI-HPPL vs CCI (right) and Scratch vs Sham and up in Scratch-HPPL vs Scratch and their interactions.*

Chapter IV: Discussion

Overview

The therapeutic management of pathologies affecting the CNS remains exceptionally challenging. TBI affects 262 per 100,000 persons worldwide[250,251] with increasing incidence. Severe forms can lead to contusion, blood vessel damage, hemorrhage, and axonal shearing and stretching,[252]. These events will be followed by an increased release of neurotransmitters, ROS and finally leading to programmed cell death with devastating effects[253]. A secondary occurrence of neuro-inflammation propagates and increases brain cell death, worsen energy failure, and ultimately leads to brain atrophy[254-256]. So far, clinical research has been unable to develop an effective TBI therapy[121,257] . No pharmacological drugs are licensed, and the current clinical management does not efficiently eliminate the secondary injury burden. Therefore, TBI is seen as a "silent epidemic"[258] and one major cause of death worldwide. A need exists for a pluripotent therapeutic strategy ensuring immediate anti-inflammatory effect, neuroprotection, and neuro-restoration through enhanced angiogenesis and neurogenesis, remodeling of the neurovasculature, and stimulation of the neuronal cells network reconstruction[259]. Interestingly, thrombocytes and their content are keys contributors in tissue repair and regeneration[260]. In particular, platelet lysates are full of healing molecules and neurotrophic factors and have the potential to modulate inflammation, support angiogenesis, exert neuroprotection in pre-clinical models of PD,[233,261,262] ALS,[261] AD,[263] and ischemic stroke,[264] as well as spinal cord injury.[265] This prompted us to investigate their potential benefits in controlling TBI-associated pathological events.

Platelet lysate and their safety

We have evaluated here the neurorestorative activity of our tailor-made platelet pellet lysate, named heat-treated platelet pellet lysate for brain administration[233] made from PC, pathogen-reduced or not, using cell models of TBI. The types of lysate contained BDNF, PDGF-AB, VEGF, and EGF neurotrophins in a concentration comparable with our previous studies.[233,261] Differences in the initial PCs' preparation procedures (e.g., the expiry date of five versus seven days; use of PAS; pathogen-reduction; method of centrifugation), as well as individual donor variations may explain the moderate differences in PDGF-AB, VEGF, and EGF content in HPPL and I-HPPL. We went beyond the classical biochemical ELISA analysis to look in deep at the content of HPPL with the goal to be able to link any of its biological effects to their content.

Addressing their content using proteomics analysis, we further confirmed that our biomaterial, which derived from platelets is full of molecules as their cells of origin. It is well known nowadays that platelets, despite the absence of nucleus, their proteome contains more than 5000 [266]. Here we found that HPPL proteome comprised around 1210 proteins, 1/5 of approximately what is found in platelets, which is exciting and suggests that our preparation method does not heavily affect the number of proteins. The HPPL proteomics constitutes a powerful tool that can provide new insights into research questions. The list of proteins generated from HPPL highlighted the abundance of structural proteins, cytokines, chemokines, enzymes, and antioxidants Etc. Furthermore, it improves our knowledge about the fundamental and potential massive roles that this natural bioproduct could play when considered as therapeutics in CNS disorders treatment strategies.

Regarding the safety of the bioproduct used in this investigation, neither HPPL nor I-HPPL induced significant cell death at 5% for neuronal, microglial, and endothelial cells. This supports our previous findings with LUHMES cells used as PD model.[233,261] Even after seven days of stimulation with both HPPL and I-HPPL, the cells remain viable as shown by calcein-AM, fluorescent labeling. Further, BV2 cells exposed to HPPL and I-HPPL kept their normal state and did not stimulate the release of TNF-α and COX-2, pro-inflammatory molecules. This is an addition proof of the safety and, importantly, the lack of pro-inflammatory capacity, consistent with previous in vitro findings,[267] and *in vivo* following intranasal administration in mice PD[233,262] and AD models.[233] Moreover, treating pre-activated BV2 cells, to simulate the activation of microglia occurring after TBI, by HPPL/I-HPPL led to a reduction in TNF-α and COX-2 expression, indicating a potential to modulate neuro-inflammation and activation of microglia, one of the therapeutic target in the management of TBI[268]. The proteome of HPPL revealed the presence of antioxidants enzymes such as GPX-1 GPX-4, SOD Etc., and anti-inflammatory molecules (interleukins 4, 5, 33…) that have potentially contributed to obtaining this beneficial effect as expected.

The impact of the INTERCEPT pathogen-inactivation on HPPL content

Platelet lysates play increasingly crucial roles in cell therapy, tissue engineering, and regenerative medicine thanks to their human origin and remarkable ability to favor cell growth and tissue repair[269]. We evaluated for the first time the effect of a validated pathogen reduction technology

treatment (Amotosalen/UVA; Intercept) of PCs on the protective potential of platelet lysates. The investigations of the possible impact of the PCs subjected to intercept treatment previously have indicated the only slight impact of Intercept on the platelets hemostatic function[270-272]. To our knowledge, no data were available on the preservation of the neurotrophic factors' functions. Therefore, we prepared HPPL from eight INTERCEPT treated-PCs initially collected from healthy donors and used them to address this aspect.

As mentioned above, biochemical data indicated that the protein concentration in the platelet biomaterial derived from the pathogen reduced-PCs was not statistically different from the standard HPPL: 6 mg/mL were detected in HPPL, whereas in I-HPPL, the concentration was 8 mg/mL. Therefore, the level of total protein in I-HPPL is similar to those found in the HPPL prepared from the PCs non-pathogen reduced[233]. The concentrations of selected growth factors such as BDNF, PDGF-AB, VEGF, EGF, and CCL5, which have been recognized to favor neuronal survival[273-275] were also quantified. I-HPPL contained more BDNF and CCL5, less PDGF-AB, VEGF, and EGF than HPPL made from fresh PC non-pathogen inactivated. These differences could be related to (a) inevitable variations in platelet growth factors among blood donors[276,277] (b) probable effect of Intercept on platelet activation and release of some trophic factors in the (discarded) plasma compartment before the expiry date, or (c) to the expiry date of 7 days allowed for the pathogen-reduced PCs (which are less prone to bacterial contaminations) instead of 5 days for untreated PCs. This will deserve the most in-depth investigations in the future.

In vitro functional outcomes

With the idea that platelets and their content participate in regulating several functions in wound healing,[278,279], we next investigated the potential of HPPL and I-HPPL to favor *in vitro* the healing of brain cells. Therefore, we performed a commonly used technique, a scratch test as cell model of TBI[280,281] on both non-differentiated and differentiated SH-SY5Y and endothelial cells. The results clearly showed that the HPPL and I-HPPL could significantly increase the wound repair capabilities by enhancing wound closure. This is in line because multiple platelet trophic can promote cell proliferation, migration, and tsurvival[143,282]. As examples, PDGF is able to promote the proliferation of SH-SY5Y cells, but also their migration and invasion through an extracellular matrix barrier.[283] Other factors such as VEGF, (TGF)-β, EGF contribute to neuronal activity, function, cells migration, and survival, support angiogenesis, neurogenesis, and provide neuroprotection[284,285] Etc. As such, HPPL and I-HPPL could contribute to enhance NSCs

migration in an injured site following TBI. They have also shown protective potential by improving mature SH-SY5Y cells' survival against mechanical injury-induced-apoptotic cell death, proving their beneficial roles as a protective agent.

We wished also to assess whether HPPL or I-HPPL could promote neurite outgrowth, as it is an essential parameter in neuronal repair strategy. SH-SY5Y cells have been used to base on their capability to differentiate and resemble to dopaminergic neurons.[286,287] In addition, these cells are able under specific stimulus to become mature and express neuronal proteins including GAP43 and β3-tubulin[288] in a time-dependent manner. We observed, both with HPPL and I-HPPL, and retinoic acid, the growth of neurites in a consistent way. The lysate could, therefore, possess the capacity to stimulate the regeneration of axons and dendrites. The neurites length increased consistently over time, supporting previous findings that growth factors induce the differentiation of neuroblastoma cells line[289]. An increased expression of β3-tubulin accompanied the morphological changes supporting the differentiation of the cells. This is an essential point since the long-term effect of TBI occurring during secondary injury is the progressive death of neurons leading to a failure of axons and dendrites regeneration. Our results are suggesting a potential for HPPL to support the surviving neurons to reorganize their connections and build new synapses, promoting axonal plasticity and functional recovery after TBI[290].

Neuroprotective activity of platelet lysates

Our tailored-made platelet pellet lysate has been prepared from platelet concentrates pathogen-reduced or not. Platelets are known for carrying a plethora of molecules in their dense and alpha granules. Without any surprise, the platelet lysate carries these proteins as found with the proteomics analysis. To investigate the functional properties of HPPL and I-HPPL, a specific and newly described type of cell death, the ferroptosis was used. Ferroptosis characteristics are mitochondrial shrinkage and an increase of mitochondrial membrane density [291]. It is presented as one of the mechanisms involved in PD pathogenesis[292]. This form of cell death is usually aggravated by iron- accumulation and lipid peroxides. According to previous studies, the toxic lipid peroxides generated during ferroptosis can be reduced to nontoxic molecules by GPX4 when glutathione is present[293,294]. This antioxidant is able to eliminate the intracellular reactive oxygen species.

In this study, HPPL and I-HPL were evaluated through well described and commonly used, the LUHMES cells[295] and a ferroptosis inducer, erastin. Erastin promotes cell death by raising the level of iron and lipid peroxidation according to many researchers[291,296-298]. LUHMES were stimulated initially with 5% platelet lysates followed by erastin treatment, leading to a strong reduction in cell death associated with less generation of lipid peroxidation, similar to the standard HPPL described previously [233,299]. I-HPPL and HPPL protective activity was also assessed in mature primary cells, and as for LUHMES experiment, the platelet biomaterials attenuated the toxic effect of by decreasing the level of LDH. The platelet lysates exerted protective activity and provided objective evidence that the INTERCEPT process as well as the use of expired PCs had no potential impact on their potential to inhibit ferroptosis. As expected, the platelet lysates contain well known antioxidants such as SOD, GPX, Etc. These antioxidants have certainly mitigated the toxic effect of erastin. Moreover, in cell models of PD (LUHMES) and ALS (NSC-34), we had found the involvement of the Akt and MEK signalling pathways when cells were exposed to our standard HPPL[299]. Therefore, other platelet-derived molecules present in the platelet lysate could also be involved this physiological events[300].

Another important aspect drawn from these data is the possibility of using expired Intercept derived-PCs as raw material to produce functional HPPL. It is crucial since most of the blood facilities in the world are considering to use at least one technology of pathogen inactivation PCs preparation process [155]. Moreover, our results are in line with the recent studies that suggest the use of expired, and Intercept-treated PCs to prepare a specific type of lysate that support MSC expansion [301,302]. The possibility of using pathogen-reduced PCs to produce HPPL is also essential since the need to prepare a large pool of PCs for consistency and standardization[303-306] reason is in consideration. This step of pathogen inactivation will undoubtedly limit the risk of pathogen transmission through the platelet lysates. It increases virus safety concerns and makes dedicated virus/pathogen inactivation steps, such as Intercept, a useful tool. Other virus inactivation treatments of PC can be considered for HPPL for regenerative medicine, such as riboflavin/UV (Mirasol) [307] or short-wave UVC (Theraflex)[308]. However, as done for intercept derived HPPL, it is mandatory to investigate the impact of these pathogen reduction treatments on the neuroprotective activity of HPPL.

In vivo restorative potential of HPPL

TBI is a complex multifaceted progressive pathology, that potentially leads to chronic long-term cognitive defects[309,310] for which treatments are still lacking. Therefore, before investigating the potential of HPPL, we performed an experiment to describe and verify the biological events following our new TBI model, the cortical brain scratch in line with the common CCI model. The scratch injury model was performed by exposing the dura mater and precisely scratching the exposed brain with two parallel injuries of 0.6mm depth and a 4mm length using a 16-gauge needle.

Our results have indicated that the cortical brain scratch was able to induce the activation of brain cells such as microglia and astrocytes known to play keys roles in inflammatory processes. This was shown by the upregulation of the pro-inflammatory genes and the immunostaining of GFAP and Iba-1 proteins. The cortex samples' proteomics analysis confirmed the surge of inflammation in the cortex of mice subjected to brain scratch and the cortical impact. Our data supported what has been described in the literature regarding TBI and inflammation. Moreover, the proteomics results have shown in both models, several markers highly upregulated including CD44, Vimentin, and GFAP suggestive of astrogliosis as well as microglial C1q proteins, involved in synaptic loss. This result is in line of previous work in which the authors highlighted the potential association between the microglia activation and the synaptic loss[311,312]. The development of neuroinflammation following the Scratch and CCI could be associated with the loss of the synaptic proteins observed. We did not address the expression of neuronal markers in the present investigation. However, it is well known that TBI is responsible for neuronal death[313], which can potentially lead to the reduction of the synaptic proteins in the injured area.

On the other hand, our results have evidenced in addition to the neuroinflammation, the generation of reactive oxygen species following the cortical brain scratch. After one week, ROS's level was still significantly higher in the cortex compared to the Sham animals. These further supported the link between TBI, the ROS, and the reactive nitrogen species production indicated by many authors. They have shown that these factors are important contributors to TBI pathophysiology[314].

The scratch injury triggered important pathophysiological cortical changes including glial activation, oxidative stress, and synaptic impairments ultimately translated into major motor deficits. The overall detrimental pathophysiological and behavioral effects of scratch injury compared to Sham animals were obvious, and more pronounced than that resulting from CCI, as expected.

In this study, our main goal was to investigate the neuroprotective activity of HPPL. As we know, the promotion of neuro-regeneration and restoration of neurological functions in a traumatized brain is extremely challenging[315]. In the search of effective treatment, several recent lines of evidence now suggest that the platelet biomaterials may emerge as a potent novel biotherapy in the treatment of neurological disorders,[264,316] as a result of abundant content in neurotrophic, antioxidants and angiogenic factors, among other active biomolecules[317]. In the present study, we used two *in vivo* models of TBI based on different triggers and outcomes, in order to capture the potential benefit of HPPL in a context of unpredictable pathophysiological events associated with this complex pathology: the well-established CCI model was used to mimic mild TBI resulting from concussion,[98] whereas our novel *in vivo* scratch injury model of the cortex to capture the pathophysiological cascade of events associated with penetrating and local trauma. As it was targeted, both models provided well-identified quantitative biochemical and motor function read-outs to characterize the functional capacity of HPPL treatment to modulate TBI pathology. Thus, we examined for the first time the efficacy of HPPL delivered through intracranial and intranasal routes to exert neuroprotective and neuro-restorative actions following TBI in mice.

The HPPL used in this study has been characterized by proteomic analysis, which evidenced the presence of several trophic factors that are known to exert potent neuroprotective anti-oxidative and anti-inflammatory activity. Previous characterization of the HPPL by ELISA has established its high content in neurotrophic, angiogenic, anti-inflammatory growth factors such as PDGF, BDNF, b-FGF, VEGF, and TGF-β1[233,318-320]. This complex secretome can exert potent synergistic functional activities contributing to neuroprotection and neurorestoration[321]. As expected, in both *in vivo* TBI models, sequential treatment with HPPL by topical deposit on the injured cortex area, first, followed by six days' intranasal delivery provided potent functional effects evidenced by potent downregulation of multiple inflammatory markers in the cortex of CCI model. These findings suggest that the molecules found in HPPL maintained their activity and the samples

preparation strategy did not alter their function. And the anti-inflammatory molecules certainly contributed to modulate the inflammation initiated by the brain trauma. This was in line with the *in vitro* finding, where the addition of HPPL on activated BV-2 cells by LPS reduced the levels of the pro-inflammatory TNF and COX-2. The glial response was also decreased upon HPPL treatment in the ipsilateral cortex. The neuroprotective and neuro-restorative effect of HPPL treatment was demonstrated by enhanced expression of the pre-and postsynaptic markers studied in the cortex. Furthermore, an antioxidative effect of HPPL was found with the significant increase of the antioxidants level, such as NQO-1, HO-1, MnSOD. This was associated with significant improvement in motor function in both models. The ability of HPPL to mitigate the generation of oxidative stress is as expected due to its content in antioxidants as indicated above. Additionally, antioxidants therapy is one of the strategies under investigation in the management of traumatic brain injury[322].

Above all, the proteomics analysis clearly supported the ability of HPPL to exert a protective effect. Our data suggest an upregulation of inflammatory proteins, myelin dysfunction, and a generation of oxidative stress following brain trauma. This is not surprising since previous investigators have already indicated the occurrence of these events in TBI pathophysiology. Regarding the HPPL efficacy as a natural bioactive biomaterial, we found that most of the upregulated proteins triggered by the brain trauma were reversed upon HPPL treatment. This robust protective potential of HPPL was confirmed when analyzing the disease-associated-microglia (DAM) and DAA (Disease-associated-astrocyte) closely. This further confirmed the gene expression analysis. For example, inflammation markers (CD68, C1qa, Vim, GFAP) were investigated by qPCR and proteomics, which led to the same conclusion. This detailed analysis revealed the protective potential of HPPL on the glial response in the TBI model. Previous investigators have also shown that platelet lysate can reduce neuronal death and supported the proliferation of new neurons in a mouse model of AD[323].

The functional improvements provided by the platelet secretome are consistent with the physiological repair mechanisms of the injury microenvironment seen with MSC secretome, rich in trophic factors and leading to behavioral recovery subsequent to TBI.[324] Our data are also consistent with finding that intracranial injection of a human platelet lysate stimulated neurogenesis and angiogenesis in a rat model of ischemic stroke and could also enhance motor

functions.[264] Such beneficial effects could reflect a pro-survival and anti-apoptotic action exerted on endogenous neural progenitor cells.[325] HPPL that is rich in a range of neurotrophic factors may also have the capacity to promote neurogenesis by the differentiation of the neurogenic niche and thereby stimulate neurogenesis in the dentate gyrus of the hippocampus. HPPL in cellular models of ALS and PD protects from apoptosis and ferroptosis cell death through Akt and MEK signaling,[233,318,320] enhances the expressions of tyrosine hydroxylase and neuron-specific enolase in LUHMES cells,[320] is strongly neuroprotective of primary neurons exposed to erastin,[320] and decreases microglia inflammation after lipopolysaccharide stimulation and induce neuronal cell differentiation.[319] The observation that HPPL administration resulted in biochemical and behavioral improvements in both animal models suggests a broad therapeutic utility for mild and intermediate TBI. These results have been obtained through the treatment modality, including a single topical cranial administration followed by intranasal administration in penetrating injury characterized by a breach of the skull and dura as in our scratch injury model, and intranasal administration only in the case of closed-head injuries.

Perspectives

Overall, our work shows the possibility of exploiting HPPL as a natural product rich in bioactive molecules. HPPL free from plasma proteins is not toxic at the concentrations used and contains a reasonable amount of total protein. The molecules present in HPPL have neuroprotective potential and can modulate neuroinflammation and oxidative stress in traumatic brain injury cases. The results obtained during this thesis are encouraging and open some perspectives for future work before an eventual clinical evaluation:

o Assessment of HPPL protective activity using animal models closer to human such as primates

o We were unable to fully address the dose dependent effect of HPPL and its long-term effects. The minimum effective dose and the maximum tolerated dose of HPPL should be determined. Further investigations regarding this issue are therefore necessary.

o Another essential factor to consider is the route of administration of HPPL. We used an approach to maximize the effects of HPPL. A combination of the intracranial and intranasal route was

therefore used. However, it will be interesting to determine the most appropriate route of administration in the future and which could be used clinically.

CONCLUSION

The present thesis provided meaningful insights in HPPL neuroprotective and neurorestorative potential specially in traumatic brain injury treatment.

Firstly, we successfully prepared HPPL from both standard and pathogen-reduced platelet concentrates and demonstrated their non-toxicity at certain doses. We also demonstrated that HPPL exerted beneficial anti-inflammatory and neuro-restorative activities in cellular models of ferroptosis. The lack of detrimental effect of the pathogen reduction step on the functional activity of HPPL confirms our recent neuroprotective data using PD *in vitro* models. HPPL conserved their richness in proteins and neurotrophines and could be used at a desired dose to stimulate cells proliferation and maturation. This study supports the strong scientific rationale to evaluate the neuroprotective potential of HPPL/I-HPPL in *in vivo* models of TBI.

In vivo, HPPL exerted strong modulatory control of the detrimental inflammatory and oxidative effects associated with TBI, protected neuronal damages, and improved motor neuron behavior in two animal models. As such, HPPL can emerge as a pragmatic biotherapeutic approach to treat brain trauma and stroke and other neurological disorders, as suggested recently. Such clinical applications in neurology are supported by the fact that platelet concentrates for transfusion are used as raw materials for preparing HPPL, and they constitute an already licensed essential medicine with known quality and safety profile.

References

1. Ganz J. Hippocrates, Celsus and Galen: head injury, the brain, and the bone. History of Medicine 2015;**2**.
2. Panourias IG, Skiadas PK, Sakas DE, Marketos SG. Hippocrates: a pioneer in the treatment of head injuries. Neurosurgery 2005;**57**: 181-9.
3. Ganz JC. Head injuries in the 18th century: the management of the damaged brain. Neurosurgery 2013;**73**: 167-76.
4. Freire FR, Coelho F, Lacerda JR, da Silva MF, Gonçalves VT, Machado S, Velasques B, Ribeiro P, Basile LFH, Oliveira AMP. Cognitive rehabilitation following traumatic brain injury. Dementia & Neuropsychologia 2011;**5**: 17.
5. McKee AC, Daneshvar DH. The neuropathology of traumatic brain injury Handbook of clinical neurology: Elsevier, 2015:45-66.
6. Menon DK, Schwab K, Wright DW, Maas AI. Position statement: definition of traumatic brain injury. Archives of physical medicine and rehabilitation 2010;**91**: 1637-40.
7. Peters ME, Gardner RC. Traumatic brain injury in older adults: do we need a different approach?: Future Medicine, 2018.
8. Maas AI, Menon DK, Adelson PD, Andelic N, Bell MJ, Belli A, Bragge P, Brazinova A, Büki A, Chesnut RM. Traumatic brain injury: integrated approaches to improve prevention, clinical care, and research. The Lancet Neurology 2017;**16**: 987-1048.
9. Tagliaferri F, Compagnone C, Korsic M, Servadei F, Kraus J. A systematic review of brain injury epidemiology in Europe. Acta neurochirurgica 2006;**148**: 255-68.
10. Peeters W, van den Brande R, Polinder S, Brazinova A, Steyerberg EW, Lingsma HF, Maas AI. Epidemiology of traumatic brain injury in Europe. Acta neurochirurgica 2015;**157**: 1683-96.
11. Majdan M, Plancikova D, Brazinova A, Rusnak M, Nieboer D, Feigin V, Maas A. Epidemiology of traumatic brain injuries in Europe: a cross-sectional analysis. The Lancet Public Health 2016;**1**: e76-e83.
12. Brazinova A, Rehorcikova V, Taylor MS, Buckova V, Majdan M, Psota M, Peeters W, Feigin V, Theadom A, Holkovic L. Epidemiology of traumatic brain injury in Europe: a living systematic review. Journal of neurotrauma 2016.

13. Roozenbeek B, Maas AI, Menon DK. Changing patterns in the epidemiology of traumatic brain injury. Nature Reviews Neurology 2013;**9**: 231.
14. Fares Y, Fares J, Kurdi MM, Haidar MAB. Physician leadership and hospital ranking: Expanding the role of neurosurgeons. Surgical neurology international 2018;**9**.
15. El-Menyar A, Mekkodathil A, Al-Thani H, Consunji R, Latifi R. Incidence, demographics, and outcome of traumatic brain injury in the Middle East: a systematic review. World neurosurgery 2017;**107**: 6-21.
16. Organization WH. Injuries and violence: the facts: World Health Organization, 2010.
17. Mathers CD, Loncar D. Projections of global mortality and burden of disease from 2002 to 2030. PLoS medicine 2006;**3**: e442.
18. Dewan MC, Rattani A, Gupta S, Baticulon RE, Hung Y-C, Punchak M, Agrawal A, Adeleye AO, Shrime MG, Rubiano AM. Estimating the global incidence of traumatic brain injury. Journal of neurosurgery 2018;**130**: 1080-97.
19. Majdan M, Ingebrigtsen T, Tenovuo O. Epidemiological Aspects Management of Severe Traumatic Brain Injury: Springer, 2020:3-7.
20. Haagsma JA, Graetz N, Bolliger I, Naghavi M, Higashi H, Mullany EC, Abera SF, Abraham JP, Adofo K, Alsharif U. The global burden of injury: incidence, mortality, disability-adjusted life years and time trends from the Global Burden of Disease study 2013. Injury prevention 2016;**22**: 3-18.
21. Taylor CA, Bell JM, Breiding MJ, Xu L. Traumatic brain injury–related emergency department visits, hospitalizations, and deaths—United States, 2007 and 2013. MMWR Surveillance Summaries 2017;**66**: 1.
22. Rosenfeld JV, Maas AI, Bragge P, Morganti-Kossmann MC, Manley GT, Gruen RL. Early management of severe traumatic brain injury. The Lancet 2012;**380**: 1088-98.
23. Pushkarna A, Bhatoe H, Sudambrekar S. Head injuries. Medical Journal Armed Forces India 2010;**66**: 321-4.
24. Teasdale G, Jennett B. Assessment of coma and impaired consciousness: A practical scale. Lancet 1974; 2: 81–4. World Health Organization. Safe Surgery Saves Lives: The Second Global Patient Safety Challenge. www. who. int/patientsafety/challenge/safe. surgery/en/Jenner's legacy: Creating vaccines for the future Azad N and Rojanasakul Y. Vaccine delivery–current trends and future. Curr Drug Deliv 2006;**3**: 137-46.

25. Hemphill J, Phan N. Traumatic brain injury: epidemiology, classification, and pathophysiology. UpToDate. UpToDate 2016;**21**.
26. Maas AIR, Hukkelhoven CWPM, Marshall LF, Steyerberg EW. Prediction of Outcome in Traumatic Brain Injury with Computed Tomographic Characteristics: A Comparison between the Computed Tomographic Classification and Combinations of Computed Tomographic Predictors. Neurosurgery 2005;**57**: 1173-82.
27. Jarrahi A, Braun M, Ahluwalia M, Gupta RV, Wilson M, Munie S, Ahluwalia P, Vender JR, Vale FL, Dhandapani KM, Vaibhav K. Revisiting Traumatic Brain Injury: From Molecular Mechanisms to Therapeutic Interventions. Biomedicines 2020;**8**.
28. Sundstrøm PT, Grände P-O, Luoto T, Rosenlund C, Undén J, Wester KG. Management of Severe Traumatic Brain Injury.
29. Guerriero RM, Giza CC, Rotenberg A. Glutamate and GABA imbalance following traumatic brain injury. Current neurology and neuroscience reports 2015;**15**: 27.
30. Tang S, Gao P, Chen H, Zhou X, Ou Y, He Y. The Role of Iron, Its Metabolism and Ferroptosis in Traumatic Brain Injury. Frontiers in Cellular Neuroscience 2020;**14**.
31. Fischer TD, Hylin MJ, Zhao J, Moore AN, Waxham MN, Dash PK. Altered mitochondrial dynamics and TBI pathophysiology. Frontiers in systems neuroscience 2016;**10**: 29.
32. Angeli JPF, Schneider M, Proneth B, Tyurina YY, Tyurin VA, Hammond VJ, Herbach N, Aichler M, Walch A, Eggenhofer E. Inactivation of the ferroptosis regulator Gpx4 triggers acute renal failure in mice. Nature cell biology 2014;**16**: 1180-91.
33. Johnson VE, Stewart JE, Begbie FD, Trojanowski JQ, Smith DH, Stewart W. Inflammation and white matter degeneration persist for years after a single traumatic brain injury. Brain 2013;**136**: 28-42.
34. Lenzlinger PM, Morganti-Kossmann M-C, Laurer HL, McIntosh TK. The duality of the inflammatory response to traumatic brain injury. Molecular neurobiology 2001;**24**: 169-81.
35. Bye N, Habgood MD, Callaway JK, Malakooti N, Potter A, Kossmann T, Morganti-Kossmann MC. Transient neuroprotection by minocycline following traumatic brain injury is associated with attenuated microglial activation but no changes in cell apoptosis or neutrophil infiltration. Experimental neurology 2007;**204**: 220-33.

36. Kubes P, Ward PA. Leukocyte recruitment and the acute inflammatory response. Brain Pathology 2000;**10**: 127-35.
37. Morganti-Kossmann MC, Rancan M, Otto VI, Stahel PF, Kossmann T. Role of cerebral inflammation after traumatic brain injury: a revisited concept. Shock 2001;**16**: 165-77.
38. Donat CK, Scott G, Gentleman SM, Sastre M. Microglial activation in traumatic brain injury. Frontiers in aging neuroscience 2017;**9**: 208.
39. VandeVord PJ, Leung LY, Hardy W, Mason M, Yang KH, King AI. Up-regulation of reactivity and survival genes in astrocytes after exposure to short duration overpressure. Neuroscience letters 2008;**434**: 247-52.
40. Aungst SL, Kabadi SV, Thompson SM, Stoica BA, Faden AI. Repeated mild traumatic brain injury causes chronic neuroinflammation, changes in hippocampal synaptic plasticity, and associated cognitive deficits. Journal of Cerebral Blood Flow & Metabolism 2014;**34**: 1223-32.
41. Stocchetti N, Carbonara M, Citerio G, Ercole A, Skrifvars MB, Smielewski P, Zoerle T, Menon DK. Severe traumatic brain injury: targeted management in the intensive care unit. The Lancet Neurology 2017;**16**: 452-64.
42. Ricklin D, Hajishengallis G, Yang K, Lambris JD. Complement: a key system for immune surveillance and homeostasis. Nature immunology 2010;**11**: 785-97.
43. Hammad A, Westacott L, Zaben M. The role of the complement system in traumatic brain injury: a review. Journal of neuroinflammation 2018;**15**: 24.
44. Dugue R, Nath M, Dugue A, Barone F. Roles of pro-and anti-inflammatory cytokines in traumatic brain injury and acute ischemic stroke. Mechanisms of neuroinflammation. London: IntechOpen 2017: 211-61.
45. Mehta T, Fayyaz M, Giler GE, Kaur H, Raikwar SP, Kempuraj D, Selvakumar GP, Ahmed ME, Thangavel R, Zaheer S. Current trends in biomarkers for traumatic brain injury. Open access journal of neurology & neurosurgery 2020;**12**: 86.
46. Rothermundt M, Peters M, Prehn JH, Arolt V. S100B in brain damage and neurodegeneration. Microscopy research and technique 2003;**60**: 614-32.
47. Vos P, Jacobs B, Andriessen T, Lamers K, Borm G, Beems T, Edwards M, Rosmalen C, Vissers J. GFAP and S100B are biomarkers of traumatic brain injury: an observational cohort study. Neurology 2010;**75**: 1786-93.

48. Raabe A, Seifert V. Protein S-100B as a serum marker of brain damage in severe head injury: preliminary results. Neurosurgical review 2000;**23**: 136-8.
49. Rothoerl RD, Woertgen C, Brawanski A. S-100 serum levels and outcome after severe head injury Brain Edema XI: Springer, 2000:97-100.
50. Pleines UE, Morganti-Kossmann MC, Rancan M, Joller H, Trentz O, Kossmann T. S-100 β reflects the extent of injury and outcome, whereas neuronal specific enolase is a better indicator of neuroinflammation in patients with severe traumatic brain injury. Journal of neurotrauma 2001;**18**: 491-8.
51. Jackson RGM, Samra GS, Radcliffe J, Clark GH, Price CP. The early fall in levels of S-100 β in traumatic brain injury. Clinical Chemistry and Laboratory Medicine (CCLM) 2000;**38**: 1165-7.
52. Jönsson H, Johnsson P, Bäckström M, Alling C, Dautovic-Bergh C, Blomquist S. Controversial significance of early S100B levels after cardiac surgery. BMC neurology 2004;**4**: 24.
53. Routsi C, Stamataki E, Nanas S, Psachoulia C, Stathopoulos A, Koroneos A, Zervou M, Jullien G, Roussos C. Increased levels of serum S100B protein in critically ill patients without brain injury. Shock 2006;**26**: 20-4.
54. Blyth BJ, Farhavar A, Gee C, Hawthorn B, He H, Nayak A, Stöcklein V, Bazarian JJ. Validation of serum markers for blood-brain barrier disruption in traumatic brain injury. Journal of neurotrauma 2009;**26**: 1497-507.
55. Pisani V, Stefani A, Pierantozzi M, Natoli S, Stanzione P, Franciotta D, Pisani A. Increased blood-cerebrospinal fluid transfer of albumin in advanced Parkinson's disease. J Neuroinflammation 2012;**9**: 188.
56. Cummins PM. Occludin: one protein, many forms. Mol Cell Biol 2012;**32**: 242-50.
57. Okonkwo DO, Yue JK, Puccio AM, Panczykowski DM, Inoue T, McMahon PJ, Sorani MD, Yuh EL, Lingsma HF, Maas AIR, Valadka AB, Manley GT, Transforming R, Clinical Knowledge in Traumatic Brain Injury I. GFAP-BDP as an acute diagnostic marker in traumatic brain injury: results from the prospective transforming research and clinical knowledge in traumatic brain injury study. Journal of neurotrauma 2013;**30**: 1490-7.
58. Bogoslovsky T, Wilson D, Chen Y, Hanlon D, Gill J, Jeromin A, Song L, Moore C, Gong Y, Kenney K, Diaz-Arrastia R. Increases of Plasma Levels of Glial Fibrillary Acidic

Protein, Tau, and Amyloid β up to 90 Days after Traumatic Brain Injury. J Neurotrauma 2017;**34**: 66-73.

59. Berger RP, Beers SR, Richichi R, Wiesman D, Adelson PD. Serum biomarker concentrations and outcome after pediatric traumatic brain injury. Journal of neurotrauma 2007;**24**: 1793-801.
60. Ramont L, Thoannes H, Volondat A, Chastang F, Millet M-C, Maquart F-X. Effects of hemolysis and storage condition on neuron-specific enolase (NSE) in cerebrospinal fluid and serum: implications in clinical practice. Clinical Chemistry and Laboratory Medicine (CCLM) 2005;**43**: 1215-7.
61. Gradisek P, Osredkar J, Korsic M, Kremzar B. Multiple indicators model of long-term mortality in traumatic brain injury. Brain Injury 2012;**26**: 1472-81.
62. Richter-Landsberg C. The oligodendroglia cytoskeleton in health and disease. Journal of neuroscience research 2000;**59**: 11-8.
63. Thomas D, Palfreyman J, Ratcliffe J. Serum-myelin-basic-protein assay in diagnosis and prognosis of patients with head injury. The Lancet 1978;**311**: 113-5.
64. Levin S, Hoyle N, Brown J, Thomas D. Cerebrospinal fluid myelin basic protein immunoreactivity as an indicator of brain damage in children. Developmental Medicine & Child Neurology 1985;**27**: 807-13.
65. Berger RP, Bazaco MC, Wagner AK, Kochanek PM, Fabio A. Trajectory analysis of serum biomarker concentrations facilitates outcome prediction after pediatric traumatic and hypoxemic brain injury. Developmental neuroscience 2010;**32**: 396-405.
66. Mondello S, Papa L, Buki A, Bullock MR, Czeiter E, Tortella FC, Wang KK, Hayes RL. Neuronal and glial markers are differently associated with computed tomography findings and outcome in patients with severe traumatic brain injury: a case control study. Critical Care 2011;**15**: R156.
67. Papa L, Akinyi L, Liu MC, Pineda JA, Tepas III JJ, Oli MW, Zheng W, Robinson G, Robicsek SA, Gabrielli A. Ubiquitin C-terminal hydrolase is a novel biomarker in humans for severe traumatic brain injury. Critical care medicine 2010;**38**: 138.
68. Brophy GM, Mondello S, Papa L, Robicsek SA, Gabrielli A, Tepas III J, Buki A, Robertson C, Tortella FC, Hayes RL. Biokinetic analysis of ubiquitin C-terminal

hydrolase-L1 (UCH-L1) in severe traumatic brain injury patient biofluids. Journal of neurotrauma 2011;**28**: 861-70.

69. Hampel H, Blennow K, Shaw LM, Hoessler YC, Zetterberg H, Trojanowski JQ. Total and phosphorylated tau protein as biological markers of Alzheimer's disease. Experimental gerontology 2010;**45**: 30-40.
70. Marklund N, Blennow K, Zetterberg H, Ronne-Engström E, Enblad P, Hillered L. Monitoring of brain interstitial total tau and beta amyloid proteins by microdialysis in patients with traumatic brain injury. Journal of neurosurgery 2009;**110**: 1227-37.
71. Chatfield D, Zemlan F, Day D, Menon D. Discordant temporal patterns of S100 β and cleaved tau protein elevation after head injury: a pilot study. British journal of neurosurgery 2002;**16**: 471-6.
72. Ching GY, Liem R. Assembly of type IV neuronal intermediate filaments in nonneuronal cells in the absence of preexisting cytoplasmic intermediate filaments. The Journal of cell biology 1993;**122**: 1323-35.
73. Anderson KJ, Scheff SW, Miller KM, Roberts KN, Gilmer LK, Yang C, Shaw G. The phosphorylated axonal form of the neurofilament subunit NF-H (pNF-H) as a blood biomarker of traumatic brain injury. Journal of neurotrauma 2008;**25**: 1079-85.
74. Frugier T, Morganti-Kossmann MC, O'Reilly D, McLean CA. In situ detection of inflammatory mediators in post mortem human brain tissue after traumatic injury. Journal of neurotrauma 2010;**27**: 497-507.
75. Eddleston M, Mucke L. Molecular profile of reactive astrocytes—implications for their role in neurologic disease. Neuroscience 1993;**54**: 15-36.
76. Hemphill MA, Dauth S, Yu CJ, Dabiri BE, Parker KK. Traumatic brain injury and the neuronal microenvironment: a potential role for neuropathological mechanotransduction. Neuron 2015;**85**: 1177-92.
77. Lööv C, Shevchenko G, Nadadhur AG, Clausen F, Hillered L, Wetterhall M, Erlandsson A. Identification of injury specific proteins in a cell culture model of traumatic brain injury. PLoS One 2013;**8**: e55983.
78. Gatchalian CL, Schachner M, Sanes JR. Fibroblasts that proliferate near denervated synaptic sites in skeletal muscle synthesize the adhesive molecules tenascin (J1), N-CAM,

fibronectin, and a heparan sulfate proteoglycan. The Journal of cell biology 1989;**108**: 1873-90.

79. Tecoma ES, Monyer H, Goldberg MP, Choi DW. Traumatic neuronal injury in vitro is attenuated by NMDA antagonists. Neuron 1989;**2**: 1541-5.
80. Mukhin A, Ivanova S, Knoblach S, Faden A. New in vitro model of traumatic neuronal injury: evaluation of secondary injury and glutamate receptor-mediated neurotoxicity. Journal of neurotrauma 1997;**14**: 651-63.
81. Morrison III B, Elkin BS, Dollé J-P, Yarmush ML. In vitro models of traumatic brain injury. Annual review of biomedical engineering 2011;**13**: 91-126.
82. Church AJ, Andrew RD. Spreading depression expands traumatic injury in neocortical brain slices. Journal of neurotrauma 2005;**22**: 277-90.
83. MURPHY EJ, HORROCKS LA. A model for compression trauma: pressure-induced injury in cell cultures. Journal of neurotrauma 1993;**10**: 431-44.
84. Lucas JH, Wolf A. In vitro studies of multiple impact injury to mammalian CNS neurons: prevention of perikaryal damage and death by ketamine. Brain research 1991;**543**: 181-93.
85. LaPlaca MC, Thibault LE. Anin vitro traumatic injury model to examine the response of neurons to a hydrodynamically-induced deformation. Annals of biomedical engineering 1997;**25**: 665-77.
86. Kumaria A. In vitro models as a platform to investigate traumatic brain injury. Alternatives to Laboratory Animals 2017;**45**: 201-11.
87. Schnittler H-J, Franke RP, Akbay U, Mrowietz C, Drenckhahn D. Improved in vitro rheological system for studying the effect of fluid shear stress on cultured cells. American Journal of Physiology-Cell Physiology 1993;**265**: C289-C98.
88. LaPlaca MC, Thibault LE. Dynamic mechanical deformation of neurons triggers an acute calcium response and cell injury involving the N-methyl-D-aspartate glutamate receptor. Journal of Neuroscience Research 1998;**52**: 220-9.
89. Pereira CF, de Oliveira CR. Oxidative glutamate toxicity involves mitochondrial dysfunction and perturbation of intracellular Ca2+ homeostasis. Neuroscience research 2000;**37**: 227-36.
90. Mattson MP. Apoptosis in neurodegenerative disorders. Nature reviews Molecular cell biology 2000;**1**: 120-30.

91. Armogida M, Spalloni A, Amantea D, Nutini M, Petrelli F, Longone P, Bagetta G, Nisticò R, Mercuri NB. The protective role of catalase against cerebral ischemia in vitro and in vivo. International journal of immunopathology and pharmacology 2011;**24**: 735-47.
92. Pamies D, Hartung T, Hogberg HT. Biological and medical applications of a brain-on-a-chip. Experimental biology and medicine 2014;**239**: 1096-107.
93. Wevers NR, Kasi DG, Gray T, Wilschut KJ, Smith B, van Vught R, Shimizu F, Sano Y, Kanda T, Marsh G, Trietsch SJ, Vulto P, Lanz HL, Obermeier B. A perfused human blood–brain barrier on-a-chip for high-throughput assessment of barrier function and antibody transport. Fluids and Barriers of the CNS 2018;**15**: 23.
94. Xiong Y, Mahmood A, Chopp M. Animal models of traumatic brain injury. Nature reviews. Neuroscience 2013;**14**: 128-42.
95. Dail WG, Fenney DM, Murray HM, Linn RT, Boyeson MG. Responses to cortical injury: II. Widespread depression of the activity of an enzyme in cortex remote from a focal injury. Brain research 1981;**211**: 79-89.
96. Sullivan HG, Martinez J, Becker DP, Miller JD, Griffith R, Wist AO. Fluid-percussion model of mechanical brain injury in the cat. Journal of neurosurgery 1976;**45**: 520-34.
97. Dixon CE, Lyeth BG, Povlishock JT, Findling RL, Hamm RJ, Marmarou A, Young HF, Hayes RL. A fluid percussion model of experimental brain injury in the rat. Journal of neurosurgery 1987;**67**: 110-9.
98. Dixon CE, Clifton GL, Lighthall JW, Yaghmai AA, Hayes RL. A controlled cortical impact model of traumatic brain injury in the rat. Journal of neuroscience methods 1991;**39**: 253-62.
99. Romine J, Gao X, Chen J. Controlled cortical impact model for traumatic brain injury. JoVE (Journal of Visualized Experiments) 2014: e51781.
100. Clemedson C, Criborn C. A detonation chamber for physiological blast research. The Journal of aviation medicine 1955;**26**: 373.
101. Garman RH, Jenkins LW, Switzer III RC, Bauman RA, Tong LC, Swauger PV, Parks SA, Ritzel DV, Dixon CE, Clark RS. Blast exposure in rats with body shielding is characterized primarily by diffuse axonal injury. Journal of neurotrauma 2011;**28**: 947-59.
102. Risling M, Davidsson J. Experimental animal models for studies on the mechanisms of blast-induced neurotrauma. Frontiers in neurology 2012;**3**: 30.

103. Säljö A, Bao F, Haglid KG, Hansson H-A. Blast exposure causes redistribution of phosphorylated neurofilament subunits in neurons of the adult rat brain. Journal of neurotrauma 2000;**17**: 719-26.
104. Chavko M, Koller WA, Prusaczyk WK, McCarron RM. Measurement of blast wave by a miniature fiber optic pressure transducer in the rat brain. Journal of neuroscience methods 2007;**159**: 277-81.
105. Koliatsos VE, Cernak I, Xu L, Song Y, Savonenko A, Crain BJ, Eberhart CG, Frangakis CE, Melnikova T, Kim H. A mouse model of blast injury to brain: initial pathological, neuropathological, and behavioral characterization. Journal of Neuropathology & Experimental Neurology 2011;**70**: 399-416.
106. Abdelmalik PA, Draghic N, Ling GS. Management of moderate and severe traumatic brain injury. Transfusion 2019;**59**: 1529-38.
107. Eisenberg HM, Frankowski RF, Contant CF, Marshall LF, Walker MD. High-dose barbiturate control of elevated intracranial pressure in patients with severe head injury. Journal of neurosurgery 1988;**69**: 15-23.
108. Kelly DF, Goodale DB, Williams J, Herr DL, Chappell ET, Rosner MJ, Jacobson J, Levy ML, Croce MA, Maniker AH. Propofol in the treatment of moderate and severe head injury: a randomized, prospective double-blinded pilot trial. Journal of neurosurgery 1999;**90**: 1042-52.
109. Andrews PJ, Sinclair HL, Rodriguez A, Harris BA, Battison CG, Rhodes JK, Murray GD. Hypothermia for intracranial hypertension after traumatic brain injury. New England Journal of Medicine 2015;**373**: 2403-12.
110. Carney N, Totten AM, O'Reilly C, Ullman JS, Hawryluk GW, Bell MJ, Bratton SL, Chesnut R, Harris OA, Kissoon N. Guidelines for the management of severe traumatic brain injury. Neurosurgery 2017;**80**: 6-15.
111. Hutchinson PJ, Kolias AG, Timofeev IS, Corteen EA, Czosnyka M, Timothy J, Anderson I, Bulters DO, Belli A, Eynon CA. Trial of decompressive craniectomy for traumatic intracranial hypertension. N Engl J Med 2016;**375**: 1119-30.
112. Kolias AG, Kirkpatrick PJ, Hutchinson PJ. Decompressive craniectomy: past, present and future. Nature Reviews Neurology 2013;**9**: 405-15.

113. Sekhon MS, McLean N, Henderson WR, Chittock DR, Griesdale DE. Association of hemoglobin concentration and mortality in critically ill patients with severe traumatic brain injury. Critical care 2012;**16**: R128.
114. Oddo M, Levine JM, Kumar M, Iglesias K, Frangos S, Maloney-Wilensky E, Le Roux PD. Anemia and brain oxygen after severe traumatic brain injury. Intensive care medicine 2012;**38**: 1497-504.
115. Yang C-J, Hsiao K-Y, Su I-C, Chen I-C. The association between anemia and the mortality of severe traumatic brain injury in emergency department. Journal of Trauma and Acute Care Surgery 2011;**71**: E132-E5.
116. Anglin CO, Spence JS, Warner MA, Paliotta C, Harper C, Moore C, Sarode R, Madden C, Diaz-Arrastia R. Effects of platelet and plasma transfusion on outcome in traumatic brain injury patients with moderate bleeding diatheses. Journal of neurosurgery 2013;**118**: 676-86.
117. Zhang L-M, Li R, Zhao X-C, Zhang Q, Luo X-L. Increased transfusion of fresh frozen plasma is associated with mortality or worse functional outcomes after severe traumatic brain injury: a retrospective study. World Neurosurgery 2017;**104**: 381-9.
118. Robertson CS, Hannay HJ, Yamal J-M, Gopinath S, Goodman JC, Tilley BC, Baldwin A, Lara LR, Saucedo-Crespo H, Ahmed O. Effect of erythropoietin and transfusion threshold on neurological recovery after traumatic brain injury: a randomized clinical trial. Jama 2014;**312**: 36-47.
119. Crupi R, Cordaro M, Cuzzocrea S, Impellizzeri D. Management of Traumatic Brain Injury: From Present to Future. Antioxidants 2020;**9**: 297.
120. Peng W, Xing Z, Yang J, Wang Y, Wang W, Huang W. The efficacy of erythropoietin in treating experimental traumatic brain injury: a systematic review of controlled trials in animal models: A review. Journal of neurosurgery 2014;**121**: 653-64.
121. Stein DG. Embracing failure: What the Phase III progesterone studies can teach about TBI clinical trials. Brain injury 2015;**29**: 1259-72.
122. Chantsoulis M, Mirski A, Rasmus A, Kropotov Y, Pachalska M. Neuropsychological rehabilitation for traumatic brain injury patients 2015.
123. Wilson BA, Gracey F, Evans JJ, Bateman A. Neuropsychological rehabilitation: Theory, models, therapy and outcome: Cambridge University Press, 2009.

124. Bradley V, Kapur N. Neuropsychological assessment of memory disorders 2003.
125. Mouhieddine TH, Kobeissy FH, Itani M, Nokkari A, Wang KK. Stem cells in neuroinjury and neurodegenerative disorders: challenges and future neurotherapeutic prospects. Neural regeneration research 2014;**9**: 901.
126. Liao GP, Harting MT, Hetz RA, Walker PA, Shah SK, Corkins CJ, Hughes TG, Jimenez F, Kosmach SC, Day M-C. Autologous bone marrow mononuclear cells reduce therapeutic intensity for severe traumatic brain injury in children. Pediatric critical care medicine: a journal of the Society of Critical Care Medicine and the World Federation of Pediatric Intensive and Critical Care Societies 2015;**16**: 245.
127. Murlidharan G, Samulski RJ, Asokan A. Biology of adeno-associated viral vectors in the central nervous system. Frontiers in molecular neuroscience 2014;**7**: 76.
128. Das M, Wang C, Bedi R, Mohapatra SS, Mohapatra S. Magnetic micelles for DNA delivery to rat brains after mild traumatic brain injury. Nanomedicine: Nanotechnology, Biology and Medicine 2014;**10**: 1539-48.
129. Harmon B, Aly A, Padegimas L, Sesenoglu-Laird O, Cooper M, Waszczak B. Intranasal administration of plasmid DNA nanoparticles yields successful transfection and expression of a reporter protein in rat brain. Gene therapy 2014;**21**: 514-21.
130. Brewer DB. Max Schultze (1865), G. Bizzozero (1882) and the discovery of the platelet. British journal of haematology 2006;**133**: 251-8.
131. Deutsch VR, Tomer A. Megakaryocyte development and platelet production. British journal of haematology 2006;**134**: 453-66.
132. Twomey L, Wallace RG, Cummins PM, Degryse B, Sheridan S, Harrison M, Moyna N, Meade-Murphy G, Navasiolava N, Custaud M-A. Platelets: From Formation to Function Homeostasis-An Integrated Vision: IntechOpen, 2018.
133. Freson K. 8 - The Platelet Proteome. In: Michelson AD, ed. Platelets (Fourth Edition): Academic Press, 2019:155-67.
134. Heijnen H, Van der Sluijs P. Platelet secretory behaviour: as diverse as the granules… or not? Journal of thrombosis and haemostasis 2015;**13**: 2141-51.
135. Thon JN, Peters CG, Machlus KR, Aslam R, Rowley J, Macleod H, Devine MT, Fuchs TA, Weyrich AS, Semple JW. T granules in human platelets function in TLR9 organization and signaling. Journal of Cell Biology 2012;**198**: 561-74.

136. Cini C, Yip C, Attard C, Karlaftis V, Monagle P, Linden M, Ignjatovic V. Differences in the resting platelet proteome and platelet releasate between healthy children and adults. Journal of proteomics 2015;**123**: 78-88.
137. Schubert P, Culibrk B, Karwal S, Goodrich RP, Devine DV. Protein translation occurs in platelet concentrates despite riboflavin/UV light pathogen inactivation treatment. PROTEOMICS–Clinical Applications 2016;**10**: 839-50.
138. García Á. Platelet clinical proteomics: Facts, challenges, and future perspectives. PROTEOMICS–Clinical Applications 2016;**10**: 767-73.
139. Greenberg D. Platelet Structure, Function, and Disorders. In: Elzouki AY, Harfi HA, Nazer HM, et al., eds. Textbook of Clinical Pediatrics. Berlin, Heidelberg: Springer Berlin Heidelberg, 2012:3067-77.
140. Blair P, Flaumenhaft R. Platelet α-granules: basic biology and clinical correlates. Blood reviews 2009;**23**: 177-89.
141. Nurden AT. Platelets, inflammation and tissue regeneration. Thrombosis and haemostasis 2011;**105**: S13-S33.
142. Golebiewska EM, Poole AW. Platelet secretion: From haemostasis to wound healing and beyond. Blood reviews 2015;**29**: 153-62.
143. Barsotti MC, Losi P, Briganti E, Sanguinetti E, Magera A, Al Kayal T, Feriani R, Di Stefano R, Soldani G. Effect of platelet lysate on human cells involved in different phases of wound healing. PLoS One 2013;**8**: e84753.
144. Franco AT, Corken A, Ware J. Platelets at the interface of thrombosis, inflammation, and cancer. Blood 2015;**126**: 582-8.
145. Li JL, Zarbock A, Hidalgo A. Platelets as autonomous drones for hemostatic and immune surveillance. Journal of Experimental Medicine 2017;**214**: 2193-204.
146. Cognasse F, Nguyen KA, Damien P, McNicol A, Pozzetto B, Hamzeh-Cognasse H, Garraud O. The inflammatory role of platelets via their TLRs and Siglec receptors. Frontiers in immunology 2015;**6**: 83.
147. Schallmoser K, Henschler R, Gabriel C, Koh MB, Burnouf T. Production and quality requirements of human platelet lysate: a position statement from the working party on cellular therapies of the international society of blood transfusion. Trends in biotechnology 2020;**38**: 13-23.

148. Feys HB, Van Aelst B, Compernolle V. Biomolecular consequences of platelet pathogen inactivation methods. Transfusion medicine reviews 2019;**33**: 29-34.
149. Goodrich RP, Edrich RA, Li J, Seghatchian J. The Mirasol PRT system for pathogen reduction of platelets and plasma: an overview of current status and future trends. Transfus Apher Sci 2006;**35**: 5-17.
150. Burgstaller P, Famulok M. Flavin-Dependent Photocleavage of RNA at G·U Base Pairs. Journal of the American Chemical Society 1997;**119**: 1137-8.
151. Reikvam H, Marschner S, Apelseth TO, Goodrich R, Hervig T. The Mirasol Pathogen Reduction Technology system and quality of platelets stored in platelet additive solution. Blood transfusion = Trasfusione del sangue 2010;**8**: 186-92.
152. Seltsam A. Pathogen Inactivation of Cellular Blood Products-An Additional Safety Layer in Transfusion Medicine. Frontiers in medicine 2017;**4**: 219-.
153. Galli L, Bruschi F. New strategies for the control of infectious and parasitic diseases in blood donors: the impact of pathogen inactivation methods. The EuroBiotech Journal 2020;**4**: 53-66.
154. Abonnenc M, Sonego G, Kaiser-Guignard J, Crettaz D, Prudent M, Tissot J-D, Lion N. In vitro evaluation of pathogen-inactivated buffy coat-derived platelet concentrates during storage: psoralen-based photochemical treatment step-by-step. Blood transfusion = Trasfusione del sangue 2015;**13**: 255-64.
155. Feys HB, Van Aelst B, Compernolle V. Biomolecular Consequences of Platelet Pathogen Inactivation Methods. Transfus Med Rev 2019;**33**: 29-34.
156. Solheim BG. Pathogen reduction of blood components. Transfusion and Apheresis Science 2008;**39**: 75-82.
157. Hauser L, Roque-Afonso A-M, Beylouné A, Simonet M, Deau Fischer B, Burin des Roziers N, Mallet V, Tiberghien P, Bierling P. Hepatitis E transmission by transfusion of Intercept blood system-treated plasma. Blood 2014;**123**: 796-7.
158. Schallmoser K, Henschler R, Gabriel C, Koh MBC, Burnouf T. Production and Quality Requirements of Human Platelet Lysate: A Position Statement from the Working Party on Cellular Therapies of the International Society of Blood Transfusion. Trends in Biotechnology 2020;**38**: 13-23.

159. Bieback K. Platelet lysate as replacement for fetal bovine serum in mesenchymal stromal cell cultures. Transfusion medicine and hemotherapy : offizielles Organ der Deutschen Gesellschaft fur Transfusionsmedizin und Immunhamatologie 2013;**40**: 326-35.
160. Burnouf T, Strunk D, Koh MBC, Schallmoser K. Human platelet lysate: Replacing fetal bovine serum as a gold standard for human cell propagation? Biomaterials 2016;**76**: 371-87.
161. Strandberg G, Sellberg F, Sommar P, Ronaghi M, Lubenow N, Knutson F, Berglund D. Standardizing the freeze-thaw preparation of growth factors from platelet lysate. Transfusion 2017;**57**: 1058-65.
162. Wang T-J, Chen M-S, Chou M-L, Lin H-C, Seghatchian J, Burnouf T. Comparison of three human platelet lysates used as supplements for in vitro expansion of corneal endothelium cells. Transfusion and Apheresis Science 2017;**56**: 769-73.
163. Mojica-Henshaw MP, Morris J, Kelley L, Pierce J, Boyer M, Reems J-A. Serum-converted platelet lysate can substitute for fetal bovine serum in human mesenchymal stromal cell cultures. Cytotherapy 2013;**15**: 1458-68.
164. Bernardi M, Albiero E, Alghisi A, Chieregato K, Lievore C, Madeo D, Rodeghiero F, Astori G. Production of human platelet lysate by use of ultrasound for ex vivo expansion of human bone marrow–derived mesenchymal stromal cells. Cytotherapy 2013;**15**: 920-9.
165. Luttenberger T, Schmid-Kotsas A, Menke A, Siech M, Beger H, Adler G, Grünert A, Bachem MG. Platelet-Derived Growth Factors Stimulate Proliferation and Extracellular Matrix Synthesis of Pancreatic Stellate Cells: Implications in Pathogenesis of Pancreas Fibrosis. Laboratory Investigation 2000;**80**: 47-55.
166. Shih DT-B, Burnouf T. Preparation, quality criteria, and properties of human blood platelet lysate supplements for ex vivo stem cell expansion. New biotechnology 2015;**32**: 199-211.
167. Burnouf T, Strunk D, Koh MB, Schallmoser K. Human platelet lysate: replacing fetal bovine serum as a gold standard for human cell propagation? Biomaterials 2016;**76**: 371-87.
168. Burkhart JM, Vaudel M, Gambaryan S, Radau S, Walter U, Martens L, Geiger J, Sickmann A, Zahedi RP. The first comprehensive and quantitative analysis of human platelet protein composition allows the comparative analysis of structural and functional pathways. Blood, The Journal of the American Society of Hematology 2012;**120**: e73-e82.

169. Klockenbusch C, Walsh GM, Brown LM, Hoffman MD, Ignatchenko V, Kislinger T, Kast J. Global proteome analysis identifies active immunoproteasome subunits in human platelets. Molecular & Cellular Proteomics 2014;**13**: 3308-19.
170. Leiter O, Walker TL. Platelets: The missing link between the blood and brain? Progress in Neurobiology 2019;**183**: 101695.
171. Espinosa-Parrilla Y, Gonzalez-Billault C, Fuentes E, Palomo I, Alarcón M. Decoding the Role of Platelets and Related MicroRNAs in Aging and Neurodegenerative Disorders. Frontiers in Aging Neuroscience 2019;**11**.
172. Italiano JE, Jr., Richardson JL, Patel-Hett S, Battinelli E, Zaslavsky A, Short S, Ryeom S, Folkman J, Klement GL. Angiogenesis is regulated by a novel mechanism: pro- and antiangiogenic proteins are organized into separate platelet α granules and differentially released. Blood 2008;**111**: 1227-33.
173. Milioli M, Ibáñez-Vea M, Sidoli S, Palmisano G, Careri M, Larsen MR. Quantitative proteomics analysis of platelet-derived microparticles reveals distinct protein signatures when stimulated by different physiological agonists. Journal of Proteomics 2015;**121**: 56-66.
174. Cananzi A, Ferro-Milone F, Grigoletto F, Toldo M, Meneghini F, Bortolon F, D'Andrea G. Relevance of platelet factor four (PF4) plasma levels in multiple sclerosis. Acta neurologica scandinavica 1987;**76**: 79-85.
175. Behari M, Shrivastava M. Role of platelets in neurodegenerative diseases: a universal pathophysiology. International Journal of Neuroscience 2013;**123**: 287-99.
176. Sheremata WA, Jy W, Horstman LL, Ahn YS, Alexander JS, Minagar A. Evidence of platelet activation in multiple sclerosis. Journal of neuroinflammation 2008;**5**: 27.
177. Elzey BD, Tian J, Jensen RJ, Swanson AK, Lees JR, Lentz SR, Stein CS, Nieswandt B, Wang Y, Davidson BL. Platelet-mediated modulation of adaptive immunity: a communication link between innate and adaptive immune compartments. Immunity 2003;**19**: 9-19.
178. Shiraki R, Inoue N, Kawasaki S, Takei A, Kadotani M, Ohnishi Y, Ejiri J, Kobayashi S, Hirata K, Kawashima S, Yokoyama M. Expression of Toll-like receptors on human platelets. Thromb Res 2004;**113**: 379-85.

179. Semple JW, Freedman J. Platelets and innate immunity. Cellular and Molecular Life Sciences 2010;**67**: 499-511.
180. Carvalho-Tavares J, Hickey MJ, Hutchison J, Michaud J, Sutcliffe IT, Kubes P. A role for platelets and endothelial selectins in tumor necrosis factor-α–induced leukocyte recruitment in the brain microvasculature. Circulation research 2000;**87**: 1141-8.
181. Kniewallner KM, Foidl BM, Humpel C. Platelets isolated from an Alzheimer mouse damage healthy cortical vessels and cause inflammation in an organotypic ex vivo brain slice model. Scientific reports 2018;**8**: 1-16.
182. Donner L, Fälker K, Gremer L, Klinker S, Pagani G, Ljungberg LU, Lothmann K, Rizzi F, Schaller M, Gohlke H. Platelets contribute to amyloid-β aggregation in cerebral vessels through integrin αIIbβ3–induced outside-in signaling and clusterin release. Science Signaling 2016;**9**: ra52-ra.
183. Kandasamy M, Lehner B, Kraus S, Sander PR, Marschallinger J, Rivera FJ, Trümbach D, Ueberham U, Reitsamer HA, Strauss O. TGF-beta signalling in the adult neurogenic niche promotes stem cell quiescence as well as generation of new neurons. Journal of cellular and molecular medicine 2014;**18**: 1444-59.
184. Smith LK, He Y, Park J-S, Bieri G, Snethlage CE, Lin K, Gontier G, Wabl R, Plambeck KE, Udeochu J, Wheatley EG, Bouchard J, Eggel A, Narasimha R, Grant JL, Luo J, Wyss-Coray T, Villeda SA. β2-microglobulin is a systemic pro-aging factor that impairs cognitive function and neurogenesis. Nature Medicine 2015;**21**: 932-7.
185. Kronenberg G, Gertz K, Baldinger T, Kirste I, Eckart S, Yildirim F, Ji S, Heuser I, Schröck H, Hörtnagl H, Sohr R, Djoufack PC, Jüttner R, Glass R, Przesdzing I, Kumar J, Freyer D, Hellweg R, Kettenmann H, Fink KB, Endres M. Impact of Actin Filament Stabilization on Adult Hippocampal and Olfactory Bulb Neurogenesis. The Journal of Neuroscience 2010;**30**: 3419.
186. Stellos K, Kopf S, Paul A, Marquardt JU, Gawaz M, Huard J, Langer HF. Platelets in regeneration. Semin Thromb Hemost 2010;**36**: 175-84.
187. Rivera FJ, Kazanis I, Ghevaert C, Aigner L. Beyond Clotting: A Role of Platelets in CNS Repair? Frontiers in Cellular Neuroscience 2016;**9**.

188. Boldrini M, Fulmore CA, Tartt AN, Simeon LR, Pavlova I, Poposka V, Rosoklija GB, Stankov A, Arango V, Dwork AJ. Human hippocampal neurogenesis persists throughout aging. Cell stem cell 2018;**22**: 589-99. e5.
189. Eriksson PS, Perfilieva E, Björk-Eriksson T, Alborn A-M, Nordborg C, Peterson DA, Gage FH. Neurogenesis in the adult human hippocampus. Nature medicine 1998;**4**: 1313-7.
190. Moreno-Jiménez EP, Flor-García M, Terreros-Roncal J, Rábano A, Cafini F, Pallas-Bazarra N, Ávila J, Llorens-Martín M. Adult hippocampal neurogenesis is abundant in neurologically healthy subjects and drops sharply in patients with Alzheimer's disease. Nature medicine 2019;**25**: 554-60.
191. Spalding KL, Bergmann O, Alkass K, Bernard S, Salehpour M, Huttner HB, Boström E, Westerlund I, Vial C, Buchholz BA. Dynamics of hippocampal neurogenesis in adult humans. Cell 2013;**153**: 1219-27.
192. Tobin MK, Musaraca K, Disouky A, Shetti A, Bheri A, Honer WG, Kim N, Dawe RJ, Bennett DA, Arfanakis K. Human hippocampal neurogenesis persists in aged adults and Alzheimer's disease patients. Cell Stem Cell 2019;**24**: 974-82. e3.
193. Castellano JM, Mosher KI, Abbey RJ, McBride AA, James ML, Berdnik D, Shen JC, Zou B, Xie XS, Tingle M. Human umbilical cord plasma proteins revitalize hippocampal function in aged mice. Nature 2017;**544**: 488-92.
194. Villeda SA, Plambeck KE, Middeldorp J, Castellano JM, Mosher KI, Luo J, Smith LK, Bieri G, Lin K, Berdnik D. Young blood reverses age-related impairments in cognitive function and synaptic plasticity in mice. Nature medicine 2014;**20**: 659-63.
195. Villeda SA, Luo J, Mosher KI, Zou B, Britschgi M, Bieri G, Stan TM, Fainberg N, Ding Z, Eggel A. The ageing systemic milieu negatively regulates neurogenesis and cognitive function. Nature 2011;**477**: 90-4.
196. Dukhinova M, Kuznetsova I, Kopeikina E, Veniaminova E, Yung AW, Veremeyko T, Levchuk K, Barteneva NS, Wing-Ho KK, Yung W-H. Platelets mediate protective neuroinflammation and promote neuronal plasticity at the site of neuronal injury. Brain, Behavior, and Immunity 2018;**74**: 7-27.
197. Wieraszko A, Li G, Kornecki E, Hogan MV, Ehrlich YH. Long-term potentiation in the hippocampus induced by platelet-activating factor. Neuron 1993;**10**: 553-7.

198. Langer HF, Stellos K, Steingen C, Froihofer A, Schönberger T, Krämer B, Bigalke B, May AE, Seizer P, Müller I. Platelet derived bFGF mediates vascular integrative mechanisms of mesenchymal stem cells in vitro. Journal of molecular and cellular cardiology 2009;**47**: 315-25.

199. Yoshimura S, Teramoto T, Whalen MJ, Irizarry MC, Takagi Y, Qiu J, Harada J, Waeber C, Breakefield XO, Moskowitz MA. FGF-2 regulates neurogenesis and degeneration in the dentate gyrus after traumatic brain injury in mice. The Journal of clinical investigation 2003;**112**: 1202-10.

200. Massberg S, Konrad I, Schürzinger K, Lorenz M, Schneider S, Zohlnhoefer D, Hoppe K, Schiemann M, Kennerknecht E, Sauer S. Platelets secrete stromal cell–derived factor 1α and recruit bone marrow–derived progenitor cells to arterial thrombi in vivo. The Journal of experimental medicine 2006;**203**: 1221-33.

201. Teng YD, Frenkel D, Nieto M, Mueller F-J, Park KI, Raddassi K, Imitola J, Li J, Sidman RL, Walsh CA. Directed migration of neural stem cells to sites of CNS injury by the stromal cell-derived factor 1 alpha/CXC chemokine receptor 4 pathway 2004.

202. Lee H, Chae S, Park J, Bae J, Go E-B, Kim S-J, Kim H, Hwang D, Lee S-W, Lee S-Y. Comprehensive Proteome Profiling of Platelet Identified a Protein Profile Predictive of Responses to An Antiplatelet Agent Sarpogrelate. Molecular & Cellular Proteomics 2016;**15**: 3461.

203. Zufferey A, Schvartz D, Nolli S, Reny J-L, Sanchez J-C, Fontana P. Characterization of the platelet granule proteome: Evidence of the presence of MHC1 in alpha-granules. Journal of Proteomics 2014;**101**: 130-40.

204. D'Mello C, Almishri W, Liu H, Swain MG. Interactions between platelets and inflammatory monocytes affect sickness behavior in mice with liver inflammation. Gastroenterology 2017;**153**: 1416-28. e2.

205. Bhat SA, Goel R, Shukla R, Hanif K. Platelet CD40L induces activation of astrocytes and microglia in hypertension. Brain, Behavior, and Immunity 2017;**59**: 173-89.

206. Rahpeymai Y, Hietala MA, Wilhelmsson U, Fotheringham A, Davies I, Nilsson A-K, Zwirner J, Wetsel RA, Gerard C, Pekny M, Pekna M. Complement: a novel factor in basal and ischemia-induced neurogenesis. The EMBO Journal 2006;**25**: 1364-74.

207. Miron VE, Franklin RJM. Macrophages and CNS remyelination. Journal of Neurochemistry 2014;**130**: 165-71.
208. Jaerve A, Müller HW. Chemokines in CNS injury and repair. Cell and Tissue Research 2012;**349**: 229-48.
209. Patel JR, McCandless EE, Dorsey D, Klein RS. CXCR4 promotes differentiation of oligodendrocyte progenitors and remyelination. Proceedings of the National Academy of Sciences 2010;**107**: 11062.
210. Brisson AR, Tan S, Linares R, Gounou C, Arraud N. Extracellular vesicles from activated platelets: a semiquantitative cryo-electron microscopy and immuno-gold labeling study. Platelets 2017;**28**: 263-71.
211. Han C, Sun X, Liu L, Jiang H, Shen Y, Xu X, Li J, Zhang G, Huang J, Lin Z, Xiong N, Wang T. Exosomes and Their Therapeutic Potentials of Stem Cells. Stem Cells International 2016;**2016**: 7653489.
212. Cauwenberghs S, Feijge MAH, Harper AGS, Sage SO, Curvers J, Heemskerk JWM. Shedding of procoagulant microparticles from unstimulated platelets by integrin-mediated destabilization of actin cytoskeleton. FEBS Letters 2006;**580**: 5313-20.
213. Aatonen MT, Öhman T, Nyman TA, Laitinen S, Grönholm M, Siljander PRM. Isolation and characterization of platelet-derived extracellular vesicles. Journal of Extracellular Vesicles 2014;**3**: 24692.
214. Bátiz LF, Castro MA, Burgos PV, Velásquez ZD, Muñoz RI, Lafourcade CA, Troncoso-Escudero P, Wyneken U. Exosomes as Novel Regulators of Adult Neurogenic Niches. Frontiers in Cellular Neuroscience 2016;**9**.
215. Nabiuni M, Shokohi R, Moghaddam P. CSF protein contents and their roles in brain development. Zahedan J Res Med Sci (ZJRMS) 2015;**17**: e1042.
216. Larpthaveesarp A, Ferriero DM, Gonzalez FF. Growth factors for the treatment of ischemic brain injury (growth factor treatment). Brain sciences 2015;**5**: 165-77.
217. Ramer MS, Priestley JV, McMahon SB. Functional regeneration of sensory axons into the adult spinal cord. Nature 2000;**403**: 312-6.
218. Kazanis I, Feichtner M, Lange S, Rotheneichner P, Hainzl S, Öller M, Schallmoser K, Rohde E, Reitsamer HA, Couillard-Despres S, Bauer H-C, Franklin RJM, Aigner L, Rivera

FJ. Lesion-Induced Accumulation of Platelets Promotes Survival of Adult Neural Stem / Progenitor Cells. Experimental Neurology 2015;**269**: 75-89.

219. Houlton J, Abumaria N, Hinkley SF, Clarkson AN. Therapeutic potential of neurotrophins for repair after brain injury: A helping hand from Biomaterials. Frontiers in neuroscience 2019;**13**: 790.
220. Lindsay RM, Altar CA, Cedarbaum JM, Hyman C, Wiegand SJ. The therapeutic potential of neurotrophic factors in the treatment of Parkinson's disease. Experimental neurology 1993;**124**: 103-18.
221. Thorne RG, Frey WH. Delivery of neurotrophic factors to the central nervous system. Clinical pharmacokinetics 2001;**40**: 907-46.
222. Hegarty SV, O'Keeffe GW, Sullivan AM. Neurotrophic factors: from neurodevelopmental regulators to novel therapies for Parkinson's disease. Neural regeneration research 2014;**9**: 1708.
223. Mahmood A, Lu D, Wang L, Chopp M. Intracerebral transplantation of marrow stromal cells cultured with neurotrophic factors promotes functional recovery in adult rats subjected to traumatic brain injury. Journal of neurotrauma 2002;**19**: 1609-17.
224. Ekestern E. Neurotrophic factors and amyotrophic lateral sclerosis. Neurodegenerative Diseases 2004;**1**: 88-100.
225. Funakoshi H, Ohya W, Kadoyama K, Nakamura T. ALS and neurotrophic factors--HGF as a novel neurotrophic and neuroregenerative factor. Brain and nerve= Shinkei kenkyu no shinpo 2007;**59**: 1195-202.
226. Terenghi G. Peripheral nerve regeneration and neurotrophic factors. Journal of anatomy 1999;**194**: 1-14.
227. Alcalá-Barraza SR, Lee MS, Hanson LR, McDonald AA, Frey WH, McLoon LK. Intranasal delivery of neurotrophic factors BDNF, CNTF, EPO, and NT-4 to the CNS. Journal of drug targeting 2010;**18**: 179-90.
228. Clarkson AN, Overman JJ, Zhong S, Mueller R, Lynch G, Carmichael ST. AMPA receptor-induced local brain-derived neurotrophic factor signaling mediates motor recovery after stroke. Journal of Neuroscience 2011;**31**: 3766-75.

229. Schabitz W-R, Berger C, Kollmar R, Seitz M, Tanay E, Kiessling M, Schwab S, Sommer C. Effect of brain-derived neurotrophic factor treatment and forced arm use on functional motor recovery after small cortical ischemia. Stroke 2004;**35**: 992-7.

230. Gonzalez-Perez O, Romero-Rodriguez R, Soriano-Navarro M, Garcia-Verdugo JM, Alvarez-Buylla A. Epidermal growth factor induces the progeny of subventricular zone type B cells to migrate and differentiate into oligodendrocytes. Stem cells 2009;**27**: 2032-43.

231. Berretta A, Tzeng Y-C, Clarkson AN. Post-stroke recovery: the role of activity-dependent release of brain-derived neurotrophic factor. Expert Review of Neurotherapeutics 2014;**14**: 1335-44.

232. Gouel F, Do Van B, Chou ML, Jonneaux A, Moreau C, Bordet R, Burnouf T, Devedjian JC, Devos D. The protective effect of human platelet lysate in models of neurodegenerative disease: involvement of the Akt and MEK pathways. Journal of tissue engineering and regenerative medicine 2017;**11**: 3236-40.

233. Chou ML, Wu JW, Gouel F, Jonneaux A, Timmerman K, Renn TY, Laloux C, Chang HM, Lin LT, Devedjian JC, Devos D, Burnouf T. Tailor-made purified human platelet lysate concentrated in neurotrophins for treatment of Parkinson's disease. Biomaterials 2017;**142**: 77-89.

234. Hayon Y, Dashevsky O, Shai E, Varon D, Leker RR. Platelet lysates stimulate angiogenesis, neurogenesis and neuroprotection after stroke. Thrombosis and haemostasis 2013;**110**: 323-30.

235. Anitua E, Pascual C, Antequera D, Bolos M, Padilla S, Orive G, Carro E. Plasma rich in growth factors (PRGF-Endoret) reduces neuropathologic hallmarks and improves cognitive functions in an Alzheimer's disease mouse model. Neurobiology of aging 2014;**35**: 1582-95.

236. Kazanis I, Feichtner M, Lange S, Rotheneichner P, Hainzl S, Öller M, Schallmoser K, Rohde E, Reitsamer HA, Couillard-Despres S, Bauer HC, Franklin RJ, Aigner L, Rivera FJ. Lesion-induced accumulation of platelets promotes survival of adult neural stem / progenitor cells. Exp Neurol 2015;**269**: 75-89.

237. Irsch J, Lin L. Pathogen Inactivation of Platelet and Plasma Blood Components for Transfusion Using the INTERCEPT Blood System^{TM}. Transfusion Medicine and Hemotherapy 2011;**38**: 19-31.
238. Chou M-L, Wu J-W, Gouel F, Jonneaux A, Timmerman K, Renn T-Y, Laloux C, Chang H-M, Lin L-T, Devedjian J-C, Devos D, Burnouf T. Tailor-made purified human platelet lysate concentrated in neurotrophins for treatment of Parkinson's disease. Biomaterials 2017;**142**: 77-89.
239. Do Van B, Gouel F, Jonneaux A, Timmerman K, Gelé P, Pétrault M, Bastide M, Laloux C, Moreau C, Bordet R. Ferroptosis, a newly characterized form of cell death in Parkinson's disease that is regulated by PKC. Neurobiology of disease 2016;**94**: 169-78.
240. Scholz D, Pöltl D, Genewsky A, Weng M, Waldmann T, Schildknecht S, Leist M. Rapid, complete and large-scale generation of post-mitotic neurons from the human LUHMES cell line. Journal of Neurochemistry 2011;**119**: 957-71.
241. Ganjam GK, Bolte K, Matschke LA, Neitemeier S, Dolga AM, Höllerhage M, Höglinger GU, Adamczyk A, Decher N, Oertel WH, Culmsee C. Mitochondrial damage by α-synuclein causes cell death in human dopaminergic neurons. Cell Death & Disease 2019;**10**: 865.
242. Vingtdeux V, Giliberto L, Zhao H, Chandakkar P, Wu Q, Simon JE, Janle EM, Lobo J, Ferruzzi MG, Davies P, Marambaud P. AMP-activated Protein Kinase Signaling Activation by Resveratrol Modulates Amyloid-β Peptide Metabolism. Journal of Biological Chemistry 2010;**285**: 9100-13.
243. Liang C-C, Park AY, Guan J-L. In vitro scratch assay: a convenient and inexpensive method for analysis of cell migration in vitro. Nature Protocols 2007;**2**: 329-33.
244. Miglio G, Rattazzi L, Rosa AC, Fantozzi R. PPARγ stimulation promotes neurite outgrowth in SH-SY5Y human neuroblastoma cells. Neuroscience Letters 2009;**454**: 134-8.
245. Környei Z, Czirók A, Vicsek T, Madarász E. Proliferative and migratory responses of astrocytes to in vitro injury. Journal of Neuroscience Research 2000;**61**: 421-9.
246. Liu X-F, Fawcett JR, Thorne RG, DeFor TA, Frey II WH. Intranasal administration of insulin-like growth factor-I bypasses the blood–brain barrier and protects against focal cerebral ischemic damage. Journal of the neurological sciences 2001;**187**: 91-7.

247. Lv Q, Fan X, Xu G, Liu Q, Tian L, Cai X, Sun W, Wang X, Cai Q, Bao Y, Zhou L, Zhang Y, Ge L, Guo R, Liu X. Intranasal delivery of nerve growth factor attenuates aquaporins-4-induced edema following traumatic brain injury in rats. Brain Research 2013;**1493**: 80-9.

248. Deacon RMJ. Measuring motor coordination in mice. Journal of visualized experiments : JoVE 2013: e2609-e.

249. Zhang Y, Fan B-Y, Pang Y-L, Shen W-Y, Wang X, Zhao C-X, Li W-X, Liu C, Kong X-H, Ning G-Z, Feng S-Q, Yao X. Neuroprotective effect of deferoxamine on erastininduced ferroptosis in primary cortical neurons. Neural Regeneration Research 2020;**15**: 1539-45.

250. Nguyen R, Fiest KM, McChesney J, Kwon C-S, Jette N, Frolkis AD, Atta C, Mah S, Dhaliwal H, Reid A. The international incidence of traumatic brain injury: a systematic review and meta-analysis. Canadian journal of neurological sciences 2016;**43**: 774-85.

251. Peeters W, van den Brande R, Polinder S, Brazinova A, Steyerberg EW, Lingsma HF, Maas AIR. Epidemiology of traumatic brain injury in Europe. Acta Neurochirurgica 2015;**157**: 1683-96.

252. Pavlovic D, Pekic S, Stojanovic M, Popovic V. Traumatic brain injury: neuropathological, neurocognitive and neurobehavioral sequelae. Pituitary 2019;**22**: 270-82.

253. Bramlett HM, Dietrich WD. Long-Term Consequences of Traumatic Brain Injury: Current Status of Potential Mechanisms of Injury and Neurological Outcomes. Journal of Neurotrauma 2014;**32**: 1834-48.

254. Mouzon BC, Bachmeier C, Ferro A, Ojo JO, Crynen G, Acker CM, Davies P, Mullan M, Stewart W, Crawford F. Chronic neuropathological and neurobehavioral changes in a repetitive mild traumatic brain injury model. Annals of neurology 2014;**75**: 241-54.

255. NONAKA M, CHEN X-H, PIERCE JE, LEONI MJ, McINTOSH TK, WOLF JA, SMITH DH. Prolonged activation of NF-κB following traumatic brain injury in rats. Journal of neurotrauma 1999;**16**: 1023-34.

256. Mayer CL, Huber BR, Peskind E. Traumatic Brain Injury, Neuroinflammation, and Post-Traumatic Headaches. Headache: The Journal of Head and Face Pain 2013;**53**: 1523-30.

257. Pre-Clinical Testing of Therapies for Traumatic Brain Injury. Journal of Neurotrauma 2018;**35**: 2737-54.

258. Peters ME, Gardner RC. Traumatic brain injury in older adults: do we need a different approach? Concussion (London, England) 2018;**3**: CNC56-CNC.
259. Xiong Y, Zhang Y, Mahmood A, Chopp M. Investigational agents for treatment of traumatic brain injury. Expert Opin Investig Drugs 2015;**24**: 743-60.
260. Nurden AT. The biology of the platelet with special reference to inflammation, wound healing and immunity. Front Biosci (Landmark Ed) 2018;**23**: 726-51.
261. Gouel F, Do Van B, Chou ML, Jonneaux A, Moreau C, Bordet R, Burnouf T, Devedjian JC, Devos D. The protective effect of human platelet lysate in models of neurodegenerative disease: involvement of the Akt and MEK pathways. J Tissue Eng Regen Med 2017;**11**: 3236-40.
262. Anitua E, Pascual C, Pérez-Gonzalez R, Orive G, Carro E. Intranasal PRGF-Endoret enhances neuronal survival and attenuates NF-κB-dependent inflammation process in a mouse model of Parkinson's disease. Journal of Controlled Release 2015;**203**: 170-80.
263. Anitua E, Pascual C, Pérez-Gonzalez R, Antequera D, Padilla S, Orive G, Carro E. Intranasal delivery of plasma and platelet growth factors using PRGF-Endoret system enhances neurogenesis in a mouse model of Alzheimer's disease. PLoS One 2013;**8**: e73118.
264. Hayon Y, Dashevsky O, Shai E, Varon D, Leker RR. Platelet lysates stimulate angiogenesis, neurogenesis and neuroprotection after stroke. Thromb Haemost 2013;**110**: 323-30.
265. Chen NF, Sung CS, Wen ZH, Chen CH, Feng CW, Hung HC, Yang SN, Tsui KH, Chen WF. Therapeutic Effect of Platelet-Rich Plasma in Rat Spinal Cord Injuries. Front Neurosci 2018;**12**: 252.
266. Burkhart JM, Gambaryan S, Watson SP, Jurk K, Walter U, Sickmann A, Heemskerk JWM, Zahedi RP. What Can Proteomics Tell Us About Platelets? Circulation Research 2014;**114**: 1204-19.
267. Renn TY, Kao YH, Wang CC, Burnouf T. Anti-inflammatory effects of platelet biomaterials in a macrophage cellular model. Vox Sang 2015;**109**: 138-47.
268. Woodcock T, Morganti-Kossmann C. The Role of Markers of Inflammation in Traumatic Brain Injury. Frontiers in Neurology 2013;**4**.

269. Henschler R, Gabriel C, Schallmoser K, Burnouf T, Koh MBC. Human platelet lysate current standards and future developments. Transfusion 2019.
270. Ciaravino V, McCullough T, Cimino G. The role of toxicology assessment in transfusion medicine. Transfusion 2003;**43**: 1481-92.
271. Kaiser-Guignard J, Canellini G, Lion N, Abonnenc M, Osselaer J-C, Tissot J-D. The clinical and biological impact of new pathogen inactivation technologies on platelet concentrates. Blood Reviews 2014;**28**: 235-41.
272. Sandgren P. Preserved in vitro metabolic and functional characteristics of double-dose apheresis platelet concentrates photochemically treated with amotosalen and ultraviolet A light. Blood transfusion = Trasfusione del sangue 2018;**16**: 118-20.
273. Habtemariam S. The brain-derived neurotrophic factor in neuronal plasticity and neuroregeneration: new pharmacological concepts for old and new drugs. Neural regeneration research 2018;**13**: 983-4.
274. Phipps MC, Xu Y, Bellis SL. Delivery of platelet-derived growth factor as a chemotactic factor for mesenchymal stem cells by bone-mimetic electrospun scaffolds. PLoS One 2012;**7**: e40831.
275. Zhao H, Alam A, San CY, Eguchi S, Chen Q, Lian Q, Ma D. Molecular mechanisms of brain-derived neurotrophic factor in neuro-protection: Recent developments. Brain Res 2017;**1665**: 1-21.
276. Agostini F, Polesel J, Battiston M, Lombardi E, Zanolin S, Da Ponte A, Astori G, Durante C, Mazzucato M. Standardization of platelet releasate products for clinical applications in cell therapy: a mathematical approach. Journal of Translational Medicine 2017;**15**: 107.
277. Cho HS, Song IH, Park S-Y, Sung MC, Ahn M-W, Song KE. Individual variation in growth factor concentrations in platelet-rich plasma and its influence on human mesenchymal stem cells. The Korean journal of laboratory medicine 2011;**31**: 212-8.
278. Nurden AT. Platelets, inflammation and tissue regeneration. Thromb Haemost 2011;**105 Suppl 1**: S13-33.
279. Barsotti MC, Losi P, Briganti E, Sanguinetti E, Magera A, Al Kayal T, Feriani R, Di Stefano R, Soldani G. Effect of platelet lysate on human cells involved in different phases of wound healing. PloS one 2013;**8**: e84753-e.

280. Baez-Jurado E, Hidalgo-Lanussa O, Guio-Vega G, Ashraf GM, Echeverria V, Aliev G, Barreto GE. Conditioned Medium of Human Adipose Mesenchymal Stem Cells Increases Wound Closure and Protects Human Astrocytes Following Scratch Assay In Vitro. Molecular Neurobiology 2018;**55**: 5377-92.
281. Torrente D, Avila MF, Cabezas R, Morales L, Gonzalez J, Samudio I, Barreto GE. Paracrine factors of human mesenchymal stem cells increase wound closure and reduce reactive oxygen species production in a traumatic brain injury in vitro model. Human & Experimental Toxicology 2013;**33**: 673-84.
282. Anitua E, Andia I, Ardanza B, Nurden P, Nurden AT. Autologous platelets as a source of proteins for healing and tissue regeneration. Thrombosis and haemostasis 2004;**91**: 4-15.
283. Pola S, Cattaneo MG, Vicentini LM. Anti-migratory and anti-invasive effect of somatostatin in human neuroblastoma cells: involvement of Rac and MAP kinase activity. J Biol Chem 2003;**278**: 40601-6.
284. Barrientos S, Stojadinovic O, Golinko MS, Brem H, Tomic-Canic M. Growth factors and cytokines in wound healing. Wound Repair Regen 2008;**16**: 585-601.
285. Graham S, Leonidou A, Lester M, Heliotis M, Mantalaris A, Tsiridis E. Investigating the role of PDGF as a potential drug therapy in bone formation and fracture healing. Expert Opinion on Investigational Drugs 2009;**18**: 1633-54.
286. Xie HR, Hu LS, Li GY. SH-SY5Y human neuroblastoma cell line: in vitro cell model of dopaminergic neurons in Parkinson's disease. Chin Med J (Engl) 2010;**123**: 1086-92.
287. Jamsa A, Hasslund K, Cowburn RF, Backstrom A, Vasange M. The retinoic acid and brain-derived neurotrophic factor differentiated SH-SY5Y cell line as a model for Alzheimer's disease-like tau phosphorylation. Biochem Biophys Res Commun 2004;**319**: 993-1000.
288. Dwane S, Durack E, Kiely PA. Optimising parameters for the differentiation of SH-SY5Y cells to study cell adhesion and cell migration. BMC Res Notes 2013;**6**: 6-366.
289. Ivankovic-Dikic I, Gronroos E, Blaukat A, Barth BU, Dikic I. Pyk2 and FAK regulate neurite outgrowth induced by growth factors and integrins. Nat Cell Biol 2000;**2**: 574-81.
290. Smith JM, Lunga P, Story D, Harris N, Le Belle J, James MF, Pickard JD, Fawcett JW. Inosine promotes recovery of skilled motor function in a model of focal brain injury. Brain 2007;**130**: 915-25.

291. Dixon SJ, Lemberg KM, Lamprecht MR, Skouta R, Zaitsev EM, Gleason CE, Patel DN, Bauer AJ, Cantley AM, Yang WS, Morrison B, 3rd, Stockwell BR. Ferroptosis: an iron-dependent form of nonapoptotic cell death. Cell 2012;**149**: 1060-72.
292. Doll S, Proneth B, Tyurina YY, Panzilius E, Kobayashi S, Ingold I, Irmler M, Beckers J, Aichler M, Walch A, Prokisch H, Trümbach D, Mao G, Qu F, Bayir H, Füllekrug J, Scheel CH, Wurst W, Schick JA, Kagan VE, Angeli JPF, Conrad M. ACSL4 dictates ferroptosis sensitivity by shaping cellular lipid composition. Nature Chemical Biology 2016;**13**: 91.
293. Yang WS, SriRamaratnam R, Welsch ME, Shimada K, Skouta R, Viswanathan VS, Cheah JH, Clemons PA, Shamji AF, Clish CB. Regulation of ferroptotic cancer cell death by GPX4. Cell 2014;**156**: 317-31.
294. Brigelius-Flohé R, Maiorino M. Glutathione peroxidases. Biochimica et Biophysica Acta (BBA)-General Subjects 2013;**1830**: 3289-303.
295. Lotharius J, Falsig J, van Beek J, Payne S, Dringen R, Brundin P, Leist M. Progressive degeneration of human mesencephalic neuron-derived cells triggered by dopamine-dependent oxidative stress is dependent on the mixed-lineage kinase pathway. J Neurosci 2005;**25**: 6329-42.
296. Dixon SJ, Winter GE, Musavi LS, Lee ED, Snijder B, Rebsamen M, Superti-Furga G, Stockwell BR. Human Haploid Cell Genetics Reveals Roles for Lipid Metabolism Genes in Nonapoptotic Cell Death. ACS Chemical Biology 2015;**10**: 1604-9.
297. Guiney SJ, Adlard PA, Bush AI, Finkelstein DI, Ayton S. Ferroptosis and cell death mechanisms in Parkinson's disease. Neurochem Int 2017;**104**: 34-48.
298. Do Van B, Gouel F, Jonneaux A, Timmerman K, Gele P, Petrault M, Bastide M, Laloux C, Moreau C, Bordet R, Devos D, Devedjian JC. Ferroptosis, a newly characterized form of cell death in Parkinson's disease that is regulated by PKC. Neurobiol Dis 2016;**94**: 169-78.
299. Gouel F, Do Van B, Chou M-L, Jonneaux A, Moreau C, Bordet R, Burnouf T, Devedjian J-C, Devos D. The protective effect of human platelet lysate in models of neurodegenerative disease: involvement of the Akt and MEK pathways. Journal of Tissue Engineering and Regenerative Medicine 2017;**11**: 3236-40.
300. Gawaz M, Vogel S. Platelets in tissue repair: control of apoptosis and interactions with regenerative cells. Blood 2013;**122**: 2550-4.

301. Jonsdottir-Buch SM, Lieder R, Sigurjonsson OE. Platelet lysates produced from expired platelet concentrates support growth and osteogenic differentiation of mesenchymal stem cells. PLoS One 2013;**8**: e68984.
302. Barro L, Su Y, Nebie O, Wu YW, Huang YH, Koh MBC, Knutson F, Burnouf T. A double virally-inactivated (Intercept-solvent/detergent) human platelet lysate for in vitro expansion of human mesenchymal stromal cells Transfusion 2019;**in press**.
303. Bieback K, Hecker A, Kocaomer A, Lannert H, Schallmoser K, Strunk D, Kluter H. Human alternatives to fetal bovine serum for the expansion of mesenchymal stromal cells from bone marrow. Stem Cells 2009;**27**: 2331-41.
304. Xiong G, Lingampalli N, Koltsov JCB, Leung LL, Bhutani N, Robinson WH, Chu CR. Men and Women Differ in the Biochemical Composition of Platelet-Rich Plasma. Am J Sports Med 2018;**46**: 409-19.
305. Evanson JR, Guyton MK, Oliver DL, Hire JM, Topolski RL, Zumbrun SD, McPherson JC, Bojescul JA. Gender and age differences in growth factor concentrations from platelet-rich plasma in adults. Mil Med 2014;**179**: 799-805.
306. Lommatzsch M, Zingler D, Schuhbaeck K, Schloetcke K, Zingler C, Schuff-Werner P, Virchow JC. The impact of age, weight and gender on BDNF levels in human platelets and plasma. Neurobiol Aging 2005;**26**: 115-23.
307. Keil SD, Bengrine A, Bowen R, Marschner S, Hovenga N, Rouse L, Gilmour D, Duverlie G, Goodrich RP. Inactivation of viruses in platelet and plasma products using a riboflavin-and-UV-based photochemical treatment. Transfusion 2015;**55**: 1736-44.
308. Gravemann U, Handke W, Lambrecht B, Schmidt JP, Muller TH, Seltsam A. Ultraviolet C light efficiently inactivates nonenveloped hepatitis A virus and feline calicivirus in platelet concentrates. Transfusion 2018;**58**: 2669-74.
309. Sharma B, Changoor A, Monteiro L, Colella B, Green R. Prognostic-factors for neurodegeneration in chronic moderate-to-severe traumatic brain injury: a systematic review protocol. Syst Rev 2020;**9**: 23.
310. Faden AI, Loane DJ. Chronic neurodegeneration after traumatic brain injury: Alzheimer disease, chronic traumatic encephalopathy, or persistent neuroinflammation? Neurotherapeutics 2015;**12**: 143-50.

311. Carvalho K, Faivre E, Pietrowski MJ, Marques X, Gomez-Murcia V, Deleau A, Huin V, Hansen JN, Kozlov S, Danis C, Temido-Ferreira M, Coelho JE, Mériaux C, Eddarkaoui S, Gras SL, Dumoulin M, Cellai L, Bank NB, Landrieu I, Chern Y, Hamdane M, Buée L, Boutillier A-L, Levi S, Halle A, Lopes LV, Blum D. Exacerbation of C1q dysregulation, synaptic loss and memory deficits in tau pathology linked to neuronal adenosine A2A receptor. Brain 2019;**142**: 3636-54.
312. Krukowski K, Chou A, Feng X, Tiret B, Paladini M-S, Riparip L-K, Chaumeil MM, Lemere C, Rosi S. Traumatic Brain Injury in Aged Mice Induces Chronic Microglia Activation, Synapse Loss, and Complement-Dependent Memory Deficits. International journal of molecular sciences 2018;**19**: 3753.
313. Wang Y, Liu Y, Lopez D, Lee M, Dayal S, Hurtado A, Bi X, Baudry M. Protection against TBI-Induced Neuronal Death with Post-Treatment with a Selective Calpain-2 Inhibitor in Mice. Journal of neurotrauma 2018;**35**: 105-17.
314. Kontos HA, Povlishock JT. Oxygen radicals in brain injury. Cent Nerv Syst Trauma 1986;**3**: 257-63.
315. Sulhan S, Lyon KA, Shapiro LA, Huang JH. Neuroinflammation and blood-brain barrier disruption following traumatic brain injury: Pathophysiology and potential therapeutic targets. J Neurosci Res 2020;**98**: 19-28.
316. Leiter O, Walker TL. Platelets in Neurodegenerative Conditions-Friend or Foe? Front Immunol 2020;**11**: 747.
317. Nurden AT, Nurden P, Sanchez M, Andia I, Anitua E. Platelets and wound healing. Front Biosci 2008;**13**: 3532-48.
318. Gouel F, Do Van B, Chou ML, Jonneaux A, Moreau C, Bordet R, Burnouf T, Devedjian J-C, Devos D. The protective effect of human platelet lysate in models of neurodegenerative disease: involvement of the Akt and MEK pathways. Journal of Tissue Engineering and Regenerative Medicine 2016 (accepted).
319. Nebie O, Barro L, Wu YW, Knutson F, Buee L, Devos D, Peng CW, Blum D, Burnouf T. Heat-treated human platelet pellet lysate modulates microglia activation, favors wound healing and promotes neuronal differentiation in vitro. Platelets 2020: 1-12.
320. Nebie O, Devos D, Vingtdeux V, Barro L, Devedjian JC, Jonneaux A, Chou ML, Bordet R, Buee L, Knutson F, Blum D, Burnouf T. The neuroprotective activity of heat-treated

human platelet lysate biomaterials manufactured from outdated pathogen-reduced (amotosalen/UVA) platelet concentrates. J Biomed Sci 2019;**26**: 89.

321. Leiter O, Walker TL. Platelets: The missing link between the blood and brain? Prog Neurobiol 2019;**183**: 101695.
322. Romero Rivera H, Cabeza-Morales M, Soto-Zarate E, Satyarthee GD, Padilla-Zambrano H, Joaquim A, Rubiano Escobar A, Pacheco-Hernández A, Agrawal A, Moscote-Salazar L. Antioxidant therapies in traumatic brain injury: a review. Romanian Neurosurgery 2017;**XXXI**: 319-34.
323. Anitua E, Pascual C, Pérez-Gonzalez R, Antequera D, Padilla S, Orive G, Carro E. Intranasal Delivery of Plasma and Platelet Growth Factors Using PRGF-Endoret System Enhances Neurogenesis in a Mouse Model of Alzheimer's Disease. PLOS ONE 2013;**8**: e73118.
324. Cox CS, Jr. Cellular therapy for traumatic neurological injury. Pediatr Res 2018;**83**: 325-32.
325. Kazanis I, Feichtner M, Lange S, Rotheneichner P, Hainzl S, Oller M, Schallmoser K, Rohde E, Reitsamer HA, Couillard-Despres S, Bauer HC, Franklin RJ, Aigner L, Rivera FJ. Lesion-induced accumulation of platelets promotes survival of adult neural stem / progenitor cells. Exp Neurol 2015;**269**: 75-89.

Annex 1: HPPL proteome identified by LC-MS/MS

Accession	Description
P04075	Fructose-bisphosphate aldolase A OS=Homo sapiens OX=9606 GN=ALDOA PE=1 SV=2
O43617	Trafficking protein particle complex subunit 3 OS=Homo sapiens OX=9606 GN=TRAPPC3 PE=1 SV=1
P04632	Calpain small subunit 1 OS=Homo sapiens OX=9606 GN=CAPNS1 PE=1 SV=1
P63104	14-3-3 protein zeta/delta OS=Homo sapiens OX=9606 GN=YWHAZ PE=1 SV=1
P58546	Myotrophin OS=Homo sapiens OX=9606 GN=MTPN PE=1 SV=2
A0A0B4J2D5	Glutamine amidotransferase-like class 1 domain-containing protein 3B, mitochondrial OS=Homo sapiens OX=9606 GN=GATD3B PE=1 SV=1
P26641	Elongation factor 1-gamma OS=Homo sapiens OX=9606 GN=EEF1G PE=1 SV=3
Q4G0F5	Vacuolar protein sorting-associated protein 26B OS=Homo sapiens OX=9606 GN=VPS26B PE=1 SV=2
P11586	C-1-tetrahydrofolate synthase, cytoplasmic OS=Homo sapiens OX=9606 GN=MTHFD1 PE=1 SV=3
O60234	Glia maturation factor gamma OS=Homo sapiens OX=9606 GN=GMFG PE=1 SV=1
P10644	cAMP-dependent protein kinase type I-alpha regulatory subunit OS=Homo sapiens OX=9606 GN=PRKAR1A PE=1 SV=1
Q9Y4G6	Talin-2 OS=Homo sapiens OX=9606 GN=TLN2 PE=1 SV=4
O15498	Synaptobrevin homolog YKT6 OS=Homo sapiens OX=9606 GN=YKT6 PE=1 SV=1
Q9UBS4	DnaJ homolog subfamily B member 11 OS=Homo sapiens OX=9606 GN=DNAJB11 PE=1 SV=1
P61026	Ras-related protein Rab-10 OS=Homo sapiens OX=9606 GN=RAB10 PE=1 SV=1
P61758	Prefoldin subunit 3 OS=Homo sapiens OX=9606 GN=VBP1 PE=1 SV=4
Q9UHL4	Dipeptidyl peptidase 2 OS=Homo sapiens OX=9606 GN=DPP7 PE=1 SV=3
Q9P1F3	Costars family protein ABRACL OS=Homo sapiens OX=9606 GN=ABRACL PE=1 SV=1
Q9BUH6	Protein PAXX OS=Homo sapiens OX=9606 GN=PAXX PE=1 SV=2
P40306	Proteasome subunit beta type-10 OS=Homo sapiens OX=9606 GN=PSMB10 PE=1 SV=1
P69905	Hemoglobin subunit alpha OS=Homo sapiens OX=9606 GN=HBA1 PE=1 SV=2
Q96EQ0	Small glutamine-rich tetratricopeptide repeat-containing protein beta OS=Homo sapiens OX=9606 GN=SGTB PE=1 SV=1
P13473	Lysosome-associated membrane glycoprotein 2 OS=Homo sapiens OX=9606 GN=LAMP2 PE=1 SV=2
Q15642	Cdc42-interacting protein 4 OS=Homo sapiens OX=9606 GN=TRIP10 PE=1 SV=3
P29692	Elongation factor 1-delta OS=Homo sapiens OX=9606 GN=EEF1D PE=1 SV=5
P05106	Integrin beta-3 OS=Homo sapiens OX=9606 GN=ITGB3 PE=1 SV=2
Q2TAA2	Isoamyl acetate-hydrolyzing esterase 1 homolog OS=Homo sapiens OX=9606 GN=IAH1 PE=1 SV=1
P28838	Cytosol aminopeptidase OS=Homo sapiens OX=9606 GN=LAP3 PE=1 SV=3
Q06124	Tyrosine-protein phosphatase non-receptor type 11 OS=Homo sapiens OX=9606 GN=PTPN11 PE=1 SV=3
P38606	V-type proton ATPase catalytic subunit A OS=Homo sapiens OX=9606 GN=ATP6V1A PE=1 SV=2
P23219	Prostaglandin G/H synthase 1 OS=Homo sapiens OX=9606 GN=PTGS1 PE=1 SV=2
P19823	Inter-alpha-trypsin inhibitor heavy chain H2 OS=Homo sapiens OX=9606 GN=ITIH2 PE=1 SV=2

Q8WW12	PEST proteolytic signal-containing nuclear protein OS=Homo sapiens OX=9606 GN=PCNP PE=1 SV=2
Q15631	Translin OS=Homo sapiens OX=9606 GN=TSN PE=1 SV=1
Q96PD5	N-acetylmuramoyl-L-alanine amidase OS=Homo sapiens OX=9606 GN=PGLYRP2 PE=1 SV=1
P48426	Phosphatidylinositol 5-phosphate 4-kinase type-2 alpha OS=Homo sapiens OX=9606 GN=PIP4K2A PE=1 SV=2
P78417	Glutathione S-transferase omega-1 OS=Homo sapiens OX=9606 GN=GSTO1 PE=1 SV=2
Q03013	Glutathione S-transferase Mu 4 OS=Homo sapiens OX=9606 GN=GSTM4 PE=1 SV=3
P54578	Ubiquitin carboxyl-terminal hydrolase 14 OS=Homo sapiens OX=9606 GN=USP14 PE=1 SV=3
Q99961	Endophilin-A2 OS=Homo sapiens OX=9606 GN=SH3GL1 PE=1 SV=1
A0A075B6S5	Immunoglobulin kappa variable 1-27 OS=Homo sapiens OX=9606 GN=IGKV1-27 PE=3 SV=1
Q9UIB8	SLAM family member 5 OS=Homo sapiens OX=9606 GN=CD84 PE=1 SV=1
Q06481	Amyloid-like protein 2 OS=Homo sapiens OX=9606 GN=APLP2 PE=1 SV=2
P0DPH7	Tubulin alpha-3C chain OS=Homo sapiens OX=9606 GN=TUBA3C PE=1 SV=1
P05156	Complement factor I OS=Homo sapiens OX=9606 GN=CFI PE=1 SV=2
Q86VP6	Cullin-associated NEDD8-dissociated protein 1 OS=Homo sapiens OX=9606 GN=CAND1 PE=1 SV=2
Q13561	Dynactin subunit 2 OS=Homo sapiens OX=9606 GN=DCTN2 PE=1 SV=4
P24844	Myosin regulatory light polypeptide 9 OS=Homo sapiens OX=9606 GN=MYL9 PE=1 SV=4
P62820	Ras-related protein Rab-1A OS=Homo sapiens OX=9606 GN=RAB1A PE=1 SV=3
P48059	LIM and senescent cell antigen-like-containing domain protein 1 OS=Homo sapiens OX=9606 GN=LIMS1 PE=1 SV=4
Q86UX7	Fermitin family homolog 3 OS=Homo sapiens OX=9606 GN=FERMT3 PE=1 SV=1
P21283	V-type proton ATPase subunit C 1 OS=Homo sapiens OX=9606 GN=ATP6V1C1 PE=1 SV=4
Q9H444	Charged multivesicular body protein 4b OS=Homo sapiens OX=9606 GN=CHMP4B PE=1 SV=1
P05121	Plasminogen activator inhibitor 1 OS=Homo sapiens OX=9606 GN=SERPINE1 PE=1 SV=1
O95810	Caveolae-associated protein 2 OS=Homo sapiens OX=9606 GN=CAVIN2 PE=1 SV=3
P15531	Nucleoside diphosphate kinase A OS=Homo sapiens OX=9606 GN=NME1 PE=1 SV=1
O75695	Protein XRP2 OS=Homo sapiens OX=9606 GN=RP2 PE=1 SV=4
O00629	Importin subunit alpha-3 OS=Homo sapiens OX=9606 GN=KPNA4 PE=1 SV=1
P22792	Carboxypeptidase N subunit 2 OS=Homo sapiens OX=9606 GN=CPN2 PE=1 SV=3
P02760	Protein AMBP OS=Homo sapiens OX=9606 GN=AMBP PE=1 SV=1
P01031	Complement C5 OS=Homo sapiens OX=9606 GN=C5 PE=1 SV=4
Q9Y333	U6 snRNA-associated Sm-like protein LSm2 OS=Homo sapiens OX=9606 GN=LSM2 PE=1 SV=1
O75347	Tubulin-specific chaperone A OS=Homo sapiens OX=9606 GN=TBCA PE=1 SV=3
P14625	Endoplasmin OS=Homo sapiens OX=9606 GN=HSP90B1 PE=1 SV=1
Q14203	Dynactin subunit 1 OS=Homo sapiens OX=9606 GN=DCTN1 PE=1 SV=3
Q08495	Dematin OS=Homo sapiens OX=9606 GN=DMTN PE=1 SV=3
P40763	Signal transducer and activator of transcription 3 OS=Homo sapiens OX=9606 GN=STAT3 PE=1 SV=2

Q9H3U1	Protein unc-45 homolog A OS=Homo sapiens OX=9606 GN=UNC45A PE=1 SV=1
P11216	Glycogen phosphorylase, brain form OS=Homo sapiens OX=9606 GN=PYGB PE=1 SV=5
P02655	Apolipoprotein C-II OS=Homo sapiens OX=9606 GN=APOC2 PE=1 SV=1
Q13126	S-methyl-5'-thioadenosine phosphorylase OS=Homo sapiens OX=9606 GN=MTAP PE=1 SV=2
Q14554	Protein disulfide-isomerase A5 OS=Homo sapiens OX=9606 GN=PDIA5 PE=1 SV=1
P28074	Proteasome subunit beta type-5 OS=Homo sapiens OX=9606 GN=PSMB5 PE=1 SV=3
Q9ULH1	Arf-GAP with SH3 domain, ANK repeat and PH domain-containing protein 1 OS=Homo sapiens OX=9606 GN=ASAP1 PE=1 SV=4
P01889	HLA class I histocompatibility antigen, B alpha chain OS=Homo sapiens OX=9606 GN=HLA-B PE=1 SV=3
Q70IA8	MOB kinase activator 3C OS=Homo sapiens OX=9606 GN=MOB3C PE=1 SV=1
P02042	Hemoglobin subunit delta OS=Homo sapiens OX=9606 GN=HBD PE=1 SV=2
Q99832	T-complex protein 1 subunit eta OS=Homo sapiens OX=9606 GN=CCT7 PE=1 SV=2
P16298	Serine/threonine-protein phosphatase 2B catalytic subunit beta isoform OS=Homo sapiens OX=9606 GN=PPP3CB PE=1 SV=2
Q6ZU35	Capping protein inhibiting regulator of actin dynamics OS=Homo sapiens OX=9606 GN=CRACD PE=1 SV=3
P61201	COP9 signalosome complex subunit 2 OS=Homo sapiens OX=9606 GN=COPS2 PE=1 SV=1
O14974	Protein phosphatase 1 regulatory subunit 12A OS=Homo sapiens OX=9606 GN=PPP1R12A PE=1 SV=1
Q15067	Peroxisomal acyl-coenzyme A oxidase 1 OS=Homo sapiens OX=9606 GN=ACOX1 PE=1 SV=3
Q9H223	EH domain-containing protein 4 OS=Homo sapiens OX=9606 GN=EHD4 PE=1 SV=1
O00534	von Willebrand factor A domain-containing protein 5A OS=Homo sapiens OX=9606 GN=VWA5A PE=2 SV=2
Q13347	Eukaryotic translation initiation factor 3 subunit I OS=Homo sapiens OX=9606 GN=EIF3I PE=1 SV=1
Q9BX10	GTP-binding protein 2 OS=Homo sapiens OX=9606 GN=GTPBP2 PE=1 SV=1
A6NHL2	Tubulin alpha chain-like 3 OS=Homo sapiens OX=9606 GN=TUBAL3 PE=1 SV=2
Q9HAB8	Phosphopantothenate--cysteine ligase OS=Homo sapiens OX=9606 GN=PPCS PE=1 SV=2
P27169	Serum paraoxonase/arylesterase 1 OS=Homo sapiens OX=9606 GN=PON1 PE=1 SV=3
Q16775	Hydroxyacylglutathione hydrolase, mitochondrial OS=Homo sapiens OX=9606 GN=HAGH PE=1 SV=2
Q86YW5	Trem-like transcript 1 protein OS=Homo sapiens OX=9606 GN=TREML1 PE=1 SV=2
Q9NVG8	TBC1 domain family member 13 OS=Homo sapiens OX=9606 GN=TBC1D13 PE=1 SV=3
O43182	Rho GTPase-activating protein 6 OS=Homo sapiens OX=9606 GN=ARHGAP6 PE=1 SV=3
Q9HCN6	Platelet glycoprotein VI OS=Homo sapiens OX=9606 GN=GP6 PE=1 SV=4
P17980	26S proteasome regulatory subunit 6A OS=Homo sapiens OX=9606 GN=PSMC3 PE=1 SV=3
A0A075B6I0	Immunoglobulin lambda variable 8-61 OS=Homo sapiens OX=9606 GN=IGLV8-61 PE=3 SV=7
O95292	Vesicle-associated membrane protein-associated protein B/C OS=Homo sapiens OX=9606 GN=VAPB PE=1 SV=3
P02765	Alpha-2-HS-glycoprotein OS=Homo sapiens OX=9606 GN=AHSG PE=1 SV=2
Q6XQN6	Nicotinate phosphoribosyltransferase OS=Homo sapiens OX=9606 GN=NAPRT PE=1 SV=2
P18031	Tyrosine-protein phosphatase non-receptor type 1 OS=Homo sapiens OX=9606 GN=PTPN1 PE=1 SV=1
P30085	UMP-CMP kinase OS=Homo sapiens OX=9606 GN=CMPK1 PE=1 SV=3

Q92734	Protein TFG OS=Homo sapiens OX=9606 GN=TFG PE=1 SV=2
Q8IZ83	Aldehyde dehydrogenase family 16 member A1 OS=Homo sapiens OX=9606 GN=ALDH16A1 PE=1 SV=2
P07996	Thrombospondin-1 OS=Homo sapiens OX=9606 GN=THBS1 PE=1 SV=2
Q13043	Serine/threonine-protein kinase 4 OS=Homo sapiens OX=9606 GN=STK4 PE=1 SV=2
Q3LXA3	Triokinase/FMN cyclase OS=Homo sapiens OX=9606 GN=TKFC PE=1 SV=2
P13667	Protein disulfide-isomerase A4 OS=Homo sapiens OX=9606 GN=PDIA4 PE=1 SV=2
P18669	Phosphoglycerate mutase 1 OS=Homo sapiens OX=9606 GN=PGAM1 PE=1 SV=2
P41208	Centrin-2 OS=Homo sapiens OX=9606 GN=CETN2 PE=1 SV=1
P13798	Acylamino-acid-releasing enzyme OS=Homo sapiens OX=9606 GN=APEH PE=1 SV=4
P08697	Alpha-2-antiplasmin OS=Homo sapiens OX=9606 GN=SERPINF2 PE=1 SV=3
P61204	ADP-ribosylation factor 3 OS=Homo sapiens OX=9606 GN=ARF3 PE=1 SV=2
P14174	Macrophage migration inhibitory factor OS=Homo sapiens OX=9606 GN=MIF PE=1 SV=4
P43487	Ran-specific GTPase-activating protein OS=Homo sapiens OX=9606 GN=RANBP1 PE=1 SV=1
O60784	Target of Myb protein 1 OS=Homo sapiens OX=9606 GN=TOM1 PE=1 SV=2
Q9BV40	Vesicle-associated membrane protein 8 OS=Homo sapiens OX=9606 GN=VAMP8 PE=1 SV=1
P09486	SPARC OS=Homo sapiens OX=9606 GN=SPARC PE=1 SV=1
P32019	Type II inositol 1,4,5-trisphosphate 5-phosphatase OS=Homo sapiens OX=9606 GN=INPP5B PE=1 SV=4
Q7L5N1	COP9 signalosome complex subunit 6 OS=Homo sapiens OX=9606 GN=COPS6 PE=1 SV=1
P00390	Glutathione reductase, mitochondrial OS=Homo sapiens OX=9606 GN=GSR PE=1 SV=2
Q9H4X1	Regulator of cell cycle RGCC OS=Homo sapiens OX=9606 GN=RGCC PE=1 SV=1
P0DMN0	Sulfotransferase 1A4 OS=Homo sapiens OX=9606 GN=SULT1A4 PE=1 SV=1
L0R6Q1	SLC35A4 upstream open reading frame protein OS=Homo sapiens OX=9606 GN=SLC35A4 PE=3 SV=1
P01861	Immunoglobulin heavy constant gamma 4 OS=Homo sapiens OX=9606 GN=IGHG4 PE=1 SV=1
Q9Y624	Junctional adhesion molecule A OS=Homo sapiens OX=9606 GN=F11R PE=1 SV=1
P29350	Tyrosine-protein phosphatase non-receptor type 6 OS=Homo sapiens OX=9606 GN=PTPN6 PE=1 SV=1
Q15836	Vesicle-associated membrane protein 3 OS=Homo sapiens OX=9606 GN=VAMP3 PE=1 SV=3
Q14974	Importin subunit beta-1 OS=Homo sapiens OX=9606 GN=KPNB1 PE=1 SV=2
P19367	Hexokinase-1 OS=Homo sapiens OX=9606 GN=HK1 PE=1 SV=3
P50991	T-complex protein 1 subunit delta OS=Homo sapiens OX=9606 GN=CCT4 PE=1 SV=4
Q8IZP0	Abl interactor 1 OS=Homo sapiens OX=9606 GN=ABI1 PE=1 SV=4
P35998	26S proteasome regulatory subunit 7 OS=Homo sapiens OX=9606 GN=PSMC2 PE=1 SV=3
O95747	Serine/threonine-protein kinase OSR1 OS=Homo sapiens OX=9606 GN=OXSR1 PE=1 SV=1
O75882	Attractin OS=Homo sapiens OX=9606 GN=ATRN PE=1 SV=2
Q96T51	RUN and FYVE domain-containing protein 1 OS=Homo sapiens OX=9606 GN=RUFY1 PE=1 SV=2
P39687	Acidic leucine-rich nuclear phosphoprotein 32 family member A OS=Homo sapiens OX=9606 GN=ANP32A PE=1 SV=1

A0A0C4DH29	Immunoglobulin heavy variable 1-3 OS=Homo sapiens OX=9606 GN=IGHV1-3 PE=3 SV=1
P09382	Galectin-1 OS=Homo sapiens OX=9606 GN=LGALS1 PE=1 SV=2
P08670	Vimentin OS=Homo sapiens OX=9606 GN=VIM PE=1 SV=4
Q9Y3Q8	TSC22 domain family protein 4 OS=Homo sapiens OX=9606 GN=TSC22D4 PE=1 SV=2
Q9UJW0	Dynactin subunit 4 OS=Homo sapiens OX=9606 GN=DCTN4 PE=1 SV=1
P07900	Heat shock protein HSP 90-alpha OS=Homo sapiens OX=9606 GN=HSP90AA1 PE=1 SV=5
P02768	Serum albumin OS=Homo sapiens OX=9606 GN=ALB PE=1 SV=2
P18206	Vinculin OS=Homo sapiens OX=9606 GN=VCL PE=1 SV=4
Q16531	DNA damage-binding protein 1 OS=Homo sapiens OX=9606 GN=DDB1 PE=1 SV=1
Q5JSH3	WD repeat-containing protein 44 OS=Homo sapiens OX=9606 GN=WDR44 PE=1 SV=1
P62714	Serine/threonine-protein phosphatase 2A catalytic subunit beta isoform OS=Homo sapiens OX=9606 GN=PPP2CB PE=1 SV=1
P31946	14-3-3 protein beta/alpha OS=Homo sapiens OX=9606 GN=YWHAB PE=1 SV=3
Q969T9	WW domain-binding protein 2 OS=Homo sapiens OX=9606 GN=WBP2 PE=1 SV=1
Q9H3N1	Thioredoxin-related transmembrane protein 1 OS=Homo sapiens OX=9606 GN=TMX1 PE=1 SV=1
P52565	Rho GDP-dissociation inhibitor 1 OS=Homo sapiens OX=9606 GN=ARHGDIA PE=1 SV=3
P11908	Ribose-phosphate pyrophosphokinase 2 OS=Homo sapiens OX=9606 GN=PRPS2 PE=1 SV=2
Q9UJU6	Drebrin-like protein OS=Homo sapiens OX=9606 GN=DBNL PE=1 SV=1
P04004	Vitronectin OS=Homo sapiens OX=9606 GN=VTN PE=1 SV=1
A0A0B4J1U7	Immunoglobulin heavy variable 6-1 OS=Homo sapiens OX=9606 GN=IGHV6-1 PE=3 SV=1
P55072	Transitional endoplasmic reticulum ATPase OS=Homo sapiens OX=9606 GN=VCP PE=1 SV=4
Q14165	Malectin OS=Homo sapiens OX=9606 GN=MLEC PE=1 SV=1
P23381	Tryptophan--tRNA ligase, cytoplasmic OS=Homo sapiens OX=9606 GN=WARS1 PE=1 SV=2
Q9UMX0	Ubiquilin-1 OS=Homo sapiens OX=9606 GN=UBQLN1 PE=1 SV=2
P10155	60 kDa SS-A/Ro ribonucleoprotein OS=Homo sapiens OX=9606 GN=RO60 PE=1 SV=2
Q96G03	Phosphoglucomutase-2 OS=Homo sapiens OX=9606 GN=PGM2 PE=1 SV=4
Q9P126	C-type lectin domain family 1 member B OS=Homo sapiens OX=9606 GN=CLEC1B PE=1 SV=2
Q9UNF0	Protein kinase C and casein kinase substrate in neurons protein 2 OS=Homo sapiens OX=9606 GN=PACSIN2 PE=1 SV=2
P49720	Proteasome subunit beta type-3 OS=Homo sapiens OX=9606 GN=PSMB3 PE=1 SV=2
Q96SB3	Neurabin-2 OS=Homo sapiens OX=9606 GN=PPP1R9B PE=1 SV=3
Q9C0I1	Myotubularin-related protein 12 OS=Homo sapiens OX=9606 GN=MTMR12 PE=1 SV=2
P21399	Cytoplasmic aconitate hydratase OS=Homo sapiens OX=9606 GN=ACO1 PE=1 SV=3
Q13617	Cullin-2 OS=Homo sapiens OX=9606 GN=CUL2 PE=1 SV=2
P08567	Pleckstrin OS=Homo sapiens OX=9606 GN=PLEK PE=1 SV=3
P21281	V-type proton ATPase subunit B, brain isoform OS=Homo sapiens OX=9606 GN=ATP6V1B2 PE=1 SV=3
Q9H9Q2	COP9 signalosome complex subunit 7b OS=Homo sapiens OX=9606 GN=COPS7B PE=1 SV=1

P13224	Platelet glycoprotein Ib beta chain OS=Homo sapiens OX=9606 GN=GP1BB PE=1 SV=1
Q6P3W7	SCY1-like protein 2 OS=Homo sapiens OX=9606 GN=SCYL2 PE=1 SV=1
Q92820	Gamma-glutamyl hydrolase OS=Homo sapiens OX=9606 GN=GGH PE=1 SV=2
Q96MW1	Coiled-coil domain-containing protein 43 OS=Homo sapiens OX=9606 GN=CCDC43 PE=1 SV=2
Q86V88	Magnesium-dependent phosphatase 1 OS=Homo sapiens OX=9606 GN=MDP1 PE=1 SV=1
Q08209	Serine/threonine-protein phosphatase 2B catalytic subunit alpha isoform OS=Homo sapiens OX=9606 GN=PPP3CA PE=1 SV=1
O95342	Bile salt export pump OS=Homo sapiens OX=9606 GN=ABCB11 PE=1 SV=2
P42768	Wiskott-Aldrich syndrome protein OS=Homo sapiens OX=9606 GN=WAS PE=1 SV=4
P33176	Kinesin-1 heavy chain OS=Homo sapiens OX=9606 GN=KIF5B PE=1 SV=1
Q93084	Sarcoplasmic/endoplasmic reticulum calcium ATPase 3 OS=Homo sapiens OX=9606 GN=ATP2A3 PE=1 SV=2
P80303	Nucleobindin-2 OS=Homo sapiens OX=9606 GN=NUCB2 PE=1 SV=3
P35908	Keratin, type II cytoskeletal 2 epidermal OS=Homo sapiens OX=9606 GN=KRT2 PE=1 SV=2
Q9UDY2	Tight junction protein ZO-2 OS=Homo sapiens OX=9606 GN=TJP2 PE=1 SV=2
Q9NTK5	Obg-like ATPase 1 OS=Homo sapiens OX=9606 GN=OLA1 PE=1 SV=2
P80748	Immunoglobulin lambda variable 3-21 OS=Homo sapiens OX=9606 GN=IGLV3-21 PE=1 SV=2
Q01433	AMP deaminase 2 OS=Homo sapiens OX=9606 GN=AMPD2 PE=1 SV=2
Q9Y3A3	MOB-like protein phocein OS=Homo sapiens OX=9606 GN=MOB4 PE=1 SV=1
Q96C24	Synaptotagmin-like protein 4 OS=Homo sapiens OX=9606 GN=SYTL4 PE=1 SV=2
P49767	Vascular endothelial growth factor C OS=Homo sapiens OX=9606 GN=VEGFC PE=1 SV=1
Q9UBC2	Epidermal growth factor receptor substrate 15-like 1 OS=Homo sapiens OX=9606 GN=EPS15L1 PE=1 SV=1
O15145	Actin-related protein 2/3 complex subunit 3 OS=Homo sapiens OX=9606 GN=ARPC3 PE=1 SV=3
Q13283	Ras GTPase-activating protein-binding protein 1 OS=Homo sapiens OX=9606 GN=G3BP1 PE=1 SV=1
Q99523	Sortilin OS=Homo sapiens OX=9606 GN=SORT1 PE=1 SV=3
Q5VY43	Platelet endothelial aggregation receptor 1 OS=Homo sapiens OX=9606 GN=PEAR1 PE=1 SV=1
P01876	Immunoglobulin heavy constant alpha 1 OS=Homo sapiens OX=9606 GN=IGHA1 PE=1 SV=2
Q03154	Aminoacylase-1 OS=Homo sapiens OX=9606 GN=ACY1 PE=1 SV=1
P04792	Heat shock protein beta-1 OS=Homo sapiens OX=9606 GN=HSPB1 PE=1 SV=2
P98172	Ephrin-B1 OS=Homo sapiens OX=9606 GN=EFNB1 PE=1 SV=1
P17301	Integrin alpha-2 OS=Homo sapiens OX=9606 GN=ITGA2 PE=1 SV=1
P67775	Serine/threonine-protein phosphatase 2A catalytic subunit alpha isoform OS=Homo sapiens OX=9606 GN=PPP2CA PE=1 SV=1
P01602	Immunoglobulin kappa variable 1-5 OS=Homo sapiens OX=9606 GN=IGKV1-5 PE=1 SV=2
P06132	Uroporphyrinogen decarboxylase OS=Homo sapiens OX=9606 GN=UROD PE=1 SV=2
Q9NR31	GTP-binding protein SAR1a OS=Homo sapiens OX=9606 GN=SAR1A PE=1 SV=1
P49327	Fatty acid synthase OS=Homo sapiens OX=9606 GN=FASN PE=1 SV=3
Q5T013	Putative hydroxypyruvate isomerase OS=Homo sapiens OX=9606 GN=HYI PE=1 SV=2

P30043	Flavin reductase (NADPH) OS=Homo sapiens OX=9606 GN=BLVRB PE=1 SV=3
Q96HC4	PDZ and LIM domain protein 5 OS=Homo sapiens OX=9606 GN=PDLIM5 PE=1 SV=5
P30405	Peptidyl-prolyl cis-trans isomerase F, mitochondrial OS=Homo sapiens OX=9606 GN=PPIF PE=1 SV=1
P55145	Mesencephalic astrocyte-derived neurotrophic factor OS=Homo sapiens OX=9606 GN=MANF PE=1 SV=3
P01033	Metalloproteinase inhibitor 1 OS=Homo sapiens OX=9606 GN=TIMP1 PE=1 SV=1
P01706	Immunoglobulin lambda variable 2-11 OS=Homo sapiens OX=9606 GN=IGLV2-11 PE=1 SV=2
P36959	GMP reductase 1 OS=Homo sapiens OX=9606 GN=GMPR PE=1 SV=1
P07225	Vitamin K-dependent protein S OS=Homo sapiens OX=9606 GN=PROS1 PE=1 SV=1
O00429	Dynamin-1-like protein OS=Homo sapiens OX=9606 GN=DNM1L PE=1 SV=2
P50225	Sulfotransferase 1A1 OS=Homo sapiens OX=9606 GN=SULT1A1 PE=1 SV=3
O75116	Rho-associated protein kinase 2 OS=Homo sapiens OX=9606 GN=ROCK2 PE=1 SV=4
P25787	Proteasome subunit alpha type-2 OS=Homo sapiens OX=9606 GN=PSMA2 PE=1 SV=2
P01782	Immunoglobulin heavy variable 3-9 OS=Homo sapiens OX=9606 GN=IGHV3-9 PE=1 SV=2
Q13637	Ras-related protein Rab-32 OS=Homo sapiens OX=9606 GN=RAB32 PE=1 SV=3
Q13200	26S proteasome non-ATPase regulatory subunit 2 OS=Homo sapiens OX=9606 GN=PSMD2 PE=1 SV=3
P19971	Thymidine phosphorylase OS=Homo sapiens OX=9606 GN=TYMP PE=1 SV=2
Q14247	Src substrate cortactin OS=Homo sapiens OX=9606 GN=CTTN PE=1 SV=2
P49591	Serine--tRNA ligase, cytoplasmic OS=Homo sapiens OX=9606 GN=SARS1 PE=1 SV=3
P17936	Insulin-like growth factor-binding protein 3 OS=Homo sapiens OX=9606 GN=IGFBP3 PE=1 SV=2
P11277	Spectrin beta chain, erythrocytic OS=Homo sapiens OX=9606 GN=SPTB PE=1 SV=5
O43399	Tumor protein D54 OS=Homo sapiens OX=9606 GN=TPD52L2 PE=1 SV=2
P46939	Utrophin OS=Homo sapiens OX=9606 GN=UTRN PE=1 SV=2
Q9HC35	Echinoderm microtubule-associated protein-like 4 OS=Homo sapiens OX=9606 GN=EML4 PE=1 SV=3
O43665	Regulator of G-protein signaling 10 OS=Homo sapiens OX=9606 GN=RGS10 PE=1 SV=3
Q969X0	RILP-like protein 2 OS=Homo sapiens OX=9606 GN=RILPL2 PE=1 SV=1
Q9NY33	Dipeptidyl peptidase 3 OS=Homo sapiens OX=9606 GN=DPP3 PE=1 SV=2
Q14764	Major vault protein OS=Homo sapiens OX=9606 GN=MVP PE=1 SV=4
P62328	Thymosin beta-4 OS=Homo sapiens OX=9606 GN=TMSB4X PE=1 SV=2
P46109	Crk-like protein OS=Homo sapiens OX=9606 GN=CRKL PE=1 SV=1
Q96A00	Protein phosphatase 1 regulatory subunit 14A OS=Homo sapiens OX=9606 GN=PPP1R14A PE=1 SV=1
Q99436	Proteasome subunit beta type-7 OS=Homo sapiens OX=9606 GN=PSMB7 PE=1 SV=1
Q15746	Myosin light chain kinase, smooth muscle OS=Homo sapiens OX=9606 GN=MYLK PE=1 SV=4
Q6WCQ1	Myosin phosphatase Rho-interacting protein OS=Homo sapiens OX=9606 GN=MPRIP PE=1 SV=3
Q16555	Dihydropyrimidinase-related protein 2 OS=Homo sapiens OX=9606 GN=DPYSL2 PE=1 SV=1
Q9UL18	Protein argonaute-1 OS=Homo sapiens OX=9606 GN=AGO1 PE=1 SV=3

P22061	Protein-L-isoaspartate(D-aspartate) O-methyltransferase OS=Homo sapiens OX=9606 GN=PCMT1 PE=1 SV=4
O43294	Transforming growth factor beta-1-induced transcript 1 protein OS=Homo sapiens OX=9606 GN=TGFB1I1 PE=1 SV=2
P11279	Lysosome-associated membrane glycoprotein 1 OS=Homo sapiens OX=9606 GN=LAMP1 PE=1 SV=3
O00161	Synaptosomal-associated protein 23 OS=Homo sapiens OX=9606 GN=SNAP23 PE=1 SV=1
P01871	Immunoglobulin heavy constant mu OS=Homo sapiens OX=9606 GN=IGHM PE=1 SV=4
Q99685	Monoglyceride lipase OS=Homo sapiens OX=9606 GN=MGLL PE=1 SV=2
Q96CV9	Optineurin OS=Homo sapiens OX=9606 GN=OPTN PE=1 SV=3
Q9H0P0	Cytosolic 5'-nucleotidase 3A OS=Homo sapiens OX=9606 GN=NT5C3A PE=1 SV=3
O14617	AP-3 complex subunit delta-1 OS=Homo sapiens OX=9606 GN=AP3D1 PE=1 SV=1
A0A075B6H7	Probable non-functional immunoglobulin kappa variable 3-7 OS=Homo sapiens OX=9606 GN=IGKV3-7 PE=5 SV=1
Q3V6T2	Girdin OS=Homo sapiens OX=9606 GN=CCDC88A PE=1 SV=2
P25786	Proteasome subunit alpha type-1 OS=Homo sapiens OX=9606 GN=PSMA1 PE=1 SV=1
Q9H4B7	Tubulin beta-1 chain OS=Homo sapiens OX=9606 GN=TUBB1 PE=1 SV=1
Q9BPX5	Actin-related protein 2/3 complex subunit 5-like protein OS=Homo sapiens OX=9606 GN=ARPC5L PE=1 SV=1
O75791	GRB2-related adapter protein 2 OS=Homo sapiens OX=9606 GN=GRAP2 PE=1 SV=1
P11233	Ras-related protein Ral-A OS=Homo sapiens OX=9606 GN=RALA PE=1 SV=1
P59998	Actin-related protein 2/3 complex subunit 4 OS=Homo sapiens OX=9606 GN=ARPC4 PE=1 SV=3
Q04637	Eukaryotic translation initiation factor 4 gamma 1 OS=Homo sapiens OX=9606 GN=EIF4G1 PE=1 SV=4
P61086	Ubiquitin-conjugating enzyme E2 K OS=Homo sapiens OX=9606 GN=UBE2K PE=1 SV=3
Q05397	Focal adhesion kinase 1 OS=Homo sapiens OX=9606 GN=PTK2 PE=1 SV=2
Q8WZA0	Protein LZIC OS=Homo sapiens OX=9606 GN=LZIC PE=1 SV=1
O75390	Citrate synthase, mitochondrial OS=Homo sapiens OX=9606 GN=CS PE=1 SV=2
Q99536	Synaptic vesicle membrane protein VAT-1 homolog OS=Homo sapiens OX=9606 GN=VAT1 PE=1 SV=2
P02656	Apolipoprotein C-III OS=Homo sapiens OX=9606 GN=APOC3 PE=1 SV=1
P01834	Immunoglobulin kappa constant OS=Homo sapiens OX=9606 GN=IGKC PE=1 SV=2
P54819	Adenylate kinase 2, mitochondrial OS=Homo sapiens OX=9606 GN=AK2 PE=1 SV=2
P31150	Rab GDP dissociation inhibitor alpha OS=Homo sapiens OX=9606 GN=GDI1 PE=1 SV=2
Q14012	Calcium/calmodulin-dependent protein kinase type 1 OS=Homo sapiens OX=9606 GN=CAMK1 PE=1 SV=1
P55212	Caspase-6 OS=Homo sapiens OX=9606 GN=CASP6 PE=1 SV=2
O95831	Apoptosis-inducing factor 1, mitochondrial OS=Homo sapiens OX=9606 GN=AIFM1 PE=1 SV=1
P47755	F-actin-capping protein subunit alpha-2 OS=Homo sapiens OX=9606 GN=CAPZA2 PE=1 SV=3
Q96K76	Ubiquitin carboxyl-terminal hydrolase 47 OS=Homo sapiens OX=9606 GN=USP47 PE=1 SV=3
Q8N3F0	Maturin OS=Homo sapiens OX=9606 GN=MTURN PE=1 SV=2
P30040	Endoplasmic reticulum resident protein 29 OS=Homo sapiens OX=9606 GN=ERP29 PE=1 SV=4
Q13201	Multimerin-1 OS=Homo sapiens OX=9606 GN=MMRN1 PE=1 SV=3

O43598	2'-deoxynucleoside 5'-phosphate N-hydrolase 1 OS=Homo sapiens OX=9606 GN=DNPH1 PE=1 SV=1
P48507	Glutamate--cysteine ligase regulatory subunit OS=Homo sapiens OX=9606 GN=GCLM PE=1 SV=1
Q9HBI1	Beta-parvin OS=Homo sapiens OX=9606 GN=PARVB PE=1 SV=1
O60610	Protein diaphanous homolog 1 OS=Homo sapiens OX=9606 GN=DIAPH1 PE=1 SV=2
Q13576	Ras GTPase-activating-like protein IQGAP2 OS=Homo sapiens OX=9606 GN=IQGAP2 PE=1 SV=4
P04899	Guanine nucleotide-binding protein G(i) subunit alpha-2 OS=Homo sapiens OX=9606 GN=GNAI2 PE=1 SV=3
P09972	Fructose-bisphosphate aldolase C OS=Homo sapiens OX=9606 GN=ALDOC PE=1 SV=2
P62491	Ras-related protein Rab-11A OS=Homo sapiens OX=9606 GN=RAB11A PE=1 SV=3
Q9P0L0	Vesicle-associated membrane protein-associated protein A OS=Homo sapiens OX=9606 GN=VAPA PE=1 SV=3
Q7Z434	Mitochondrial antiviral-signaling protein OS=Homo sapiens OX=9606 GN=MAVS PE=1 SV=2
P13796	Plastin-2 OS=Homo sapiens OX=9606 GN=LCP1 PE=1 SV=6
O14618	Copper chaperone for superoxide dismutase OS=Homo sapiens OX=9606 GN=CCS PE=1 SV=1
Q13098	COP9 signalosome complex subunit 1 OS=Homo sapiens OX=9606 GN=GPS1 PE=1 SV=4
P55036	26S proteasome non-ATPase regulatory subunit 4 OS=Homo sapiens OX=9606 GN=PSMD4 PE=1 SV=1
Q9Y4L1	Hypoxia up-regulated protein 1 OS=Homo sapiens OX=9606 GN=HYOU1 PE=1 SV=1
P01859	Immunoglobulin heavy constant gamma 2 OS=Homo sapiens OX=9606 GN=IGHG2 PE=1 SV=2
O95861	3'(2'),5'-bisphosphate nucleotidase 1 OS=Homo sapiens OX=9606 GN=BPNT1 PE=1 SV=1
P00739	Haptoglobin-related protein OS=Homo sapiens OX=9606 GN=HPR PE=2 SV=2
Q8NBM8	Prenylcysteine oxidase-like OS=Homo sapiens OX=9606 GN=PCYOX1L PE=1 SV=2
P28072	Proteasome subunit beta type-6 OS=Homo sapiens OX=9606 GN=PSMB6 PE=1 SV=4
O75822	Eukaryotic translation initiation factor 3 subunit J OS=Homo sapiens OX=9606 GN=EIF3J PE=1 SV=2
Q16881	Thioredoxin reductase 1, cytoplasmic OS=Homo sapiens OX=9606 GN=TXNRD1 PE=1 SV=3
Q04760	Lactoylglutathione lyase OS=Homo sapiens OX=9606 GN=GLO1 PE=1 SV=4
O00233	26S proteasome non-ATPase regulatory subunit 9 OS=Homo sapiens OX=9606 GN=PSMD9 PE=1 SV=3
P48147	Prolyl endopeptidase OS=Homo sapiens OX=9606 GN=PREP PE=1 SV=2
O75874	Isocitrate dehydrogenase NADP cytoplasmic OS=Homo sapiens OX=9606 GN=IDH1 PE=1 SV=2
P11169	Solute carrier family 2, facilitated glucose transporter member 3 OS=Homo sapiens OX=9606 GN=SLC2A3 PE=1 SV=1
Q9NT62	Ubiquitin-like-conjugating enzyme ATG3 OS=Homo sapiens OX=9606 GN=ATG3 PE=1 SV=1
P02743	Serum amyloid P-component OS=Homo sapiens OX=9606 GN=APCS PE=1 SV=2
P07947	Tyrosine-protein kinase Yes OS=Homo sapiens OX=9606 GN=YES1 PE=1 SV=3
P01594	Immunoglobulin kappa variable 1-33 OS=Homo sapiens OX=9606 GN=IGKV1-33 PE=1 SV=2
P20618	Proteasome subunit beta type-1 OS=Homo sapiens OX=9606 GN=PSMB1 PE=1 SV=2
O43583	Density-regulated protein OS=Homo sapiens OX=9606 GN=DENR PE=1 SV=2
Q9BSJ8	Extended synaptotagmin-1 OS=Homo sapiens OX=9606 GN=ESYT1 PE=1 SV=1
Q9HD15	Steroid receptor RNA activator 1 OS=Homo sapiens OX=9606 GN=SRA1 PE=1 SV=1

Q86Y82	Syntaxin-12 OS=Homo sapiens OX=9606 GN=STX12 PE=1 SV=1
P00738	Haptoglobin OS=Homo sapiens OX=9606 GN=HP PE=1 SV=1
P07948	Tyrosine-protein kinase Lyn OS=Homo sapiens OX=9606 GN=LYN PE=1 SV=3
P18085	ADP-ribosylation factor 4 OS=Homo sapiens OX=9606 GN=ARF4 PE=1 SV=3
Q9Y490	Talin-1 OS=Homo sapiens OX=9606 GN=TLN1 PE=1 SV=3
P61106	Ras-related protein Rab-14 OS=Homo sapiens OX=9606 GN=RAB14 PE=1 SV=4
P21333	Filamin-A OS=Homo sapiens OX=9606 GN=FLNA PE=1 SV=4
P50402	Emerin OS=Homo sapiens OX=9606 GN=EMD PE=1 SV=1
P51148	Ras-related protein Rab-5C OS=Homo sapiens OX=9606 GN=RAB5C PE=1 SV=2
Q8TAT6	Nuclear protein localization protein 4 homolog OS=Homo sapiens OX=9606 GN=NPLOC4 PE=1 SV=3
P30046	D-dopachrome decarboxylase OS=Homo sapiens OX=9606 GN=DDT PE=1 SV=3
Q9Y5P6	Mannose-1-phosphate guanyltransferase beta OS=Homo sapiens OX=9606 GN=GMPPB PE=1 SV=2
O60361	Putative nucleoside diphosphate kinase OS=Homo sapiens OX=9606 GN=NME2P1 PE=5 SV=1
O60763	General vesicular transport factor p115 OS=Homo sapiens OX=9606 GN=USO1 PE=1 SV=2
Q9UHY1	Nuclear receptor-binding protein OS=Homo sapiens OX=9606 GN=NRBP1 PE=1 SV=1
Q15121	Astrocytic phosphoprotein PEA-15 OS=Homo sapiens OX=9606 GN=PEA15 PE=1 SV=2
P15529	Membrane cofactor protein OS=Homo sapiens OX=9606 GN=CD46 PE=1 SV=3
Q96CW1	AP-2 complex subunit mu OS=Homo sapiens OX=9606 GN=AP2M1 PE=1 SV=2
O43488	Aflatoxin B1 aldehyde reductase member 2 OS=Homo sapiens OX=9606 GN=AKR7A2 PE=1 SV=3
P43034	Platelet-activating factor acetylhydrolase IB subunit alpha OS=Homo sapiens OX=9606 GN=PAFAH1B1 PE=1 SV=2
P05546	Heparin cofactor 2 OS=Homo sapiens OX=9606 GN=SERPIND1 PE=1 SV=3
Q9GZP4	PITH domain-containing protein 1 OS=Homo sapiens OX=9606 GN=PITHD1 PE=1 SV=1
P69891	Hemoglobin subunit gamma-1 OS=Homo sapiens OX=9606 GN=HBG1 PE=1 SV=2
P55209	Nucleosome assembly protein 1-like 1 OS=Homo sapiens OX=9606 GN=NAP1L1 PE=1 SV=1
P43405	Tyrosine-protein kinase SYK OS=Homo sapiens OX=9606 GN=SYK PE=1 SV=1
P11766	Alcohol dehydrogenase class-3 OS=Homo sapiens OX=9606 GN=ADH5 PE=1 SV=4
P06744	Glucose-6-phosphate isomerase OS=Homo sapiens OX=9606 GN=GPI PE=1 SV=4
P32321	Deoxycytidylate deaminase OS=Homo sapiens OX=9606 GN=DCTD PE=1 SV=2
P16949	Stathmin OS=Homo sapiens OX=9606 GN=STMN1 PE=1 SV=3
Q15370	Elongin-B OS=Homo sapiens OX=9606 GN=ELOB PE=1 SV=1
P16278	Beta-galactosidase OS=Homo sapiens OX=9606 GN=GLB1 PE=1 SV=2
P35442	Thrombospondin-2 OS=Homo sapiens OX=9606 GN=THBS2 PE=1 SV=2
P51452	Dual specificity protein phosphatase 3 OS=Homo sapiens OX=9606 GN=DUSP3 PE=1 SV=1
P13645	Keratin, type I cytoskeletal 10 OS=Homo sapiens OX=9606 GN=KRT10 PE=1 SV=6
P42566	Epidermal growth factor receptor substrate 15 OS=Homo sapiens OX=9606 GN=EPS15 PE=1 SV=2

P61006	Ras-related protein Rab-8A OS=Homo sapiens OX=9606 GN=RAB8A PE=1 SV=1
Q9Y6E0	Serine/threonine-protein kinase 24 OS=Homo sapiens OX=9606 GN=STK24 PE=1 SV=1
P51665	26S proteasome non-ATPase regulatory subunit 7 OS=Homo sapiens OX=9606 GN=PSMD7 PE=1 SV=2
P62979	Ubiquitin-40S ribosomal protein S27a OS=Homo sapiens OX=9606 GN=RPS27A PE=1 SV=2
P04264	Keratin, type II cytoskeletal 1 OS=Homo sapiens OX=9606 GN=KRT1 PE=1 SV=6
P17987	T-complex protein 1 subunit alpha OS=Homo sapiens OX=9606 GN=TCP1 PE=1 SV=1
Q9Y6K9	NF-kappa-B essential modulator OS=Homo sapiens OX=9606 GN=IKBKG PE=1 SV=2
P16157	Ankyrin-1 OS=Homo sapiens OX=9606 GN=ANK1 PE=1 SV=3
Q14116	Interleukin-18 OS=Homo sapiens OX=9606 GN=IL18 PE=1 SV=1
Q9UBQ5	Eukaryotic translation initiation factor 3 subunit K OS=Homo sapiens OX=9606 GN=EIF3K PE=1 SV=1
Q9BY32	Inosine triphosphate pyrophosphatase OS=Homo sapiens OX=9606 GN=ITPA PE=1 SV=2
Q86UE4	Protein LYRIC OS=Homo sapiens OX=9606 GN=MTDH PE=1 SV=2
P21291	Cysteine and glycine-rich protein 1 OS=Homo sapiens OX=9606 GN=CSRP1 PE=1 SV=3
Q7L9L4	MOB kinase activator 1B OS=Homo sapiens OX=9606 GN=MOB1B PE=1 SV=3
O95834	Echinoderm microtubule-associated protein-like 2 OS=Homo sapiens OX=9606 GN=EML2 PE=1 SV=1
P00450	Ceruloplasmin OS=Homo sapiens OX=9606 GN=CP PE=1 SV=1
A0A0C4DH72	Immunoglobulin kappa variable 1-6 OS=Homo sapiens OX=9606 GN=IGKV1-6 PE=3 SV=1
P10768	S-formylglutathione hydrolase OS=Homo sapiens OX=9606 GN=ESD PE=1 SV=2
P01024	Complement C3 OS=Homo sapiens OX=9606 GN=C3 PE=1 SV=2
P11413	Glucose-6-phosphate 1-dehydrogenase OS=Homo sapiens OX=9606 GN=G6PD PE=1 SV=4
P37235	Hippocalcin-like protein 1 OS=Homo sapiens OX=9606 GN=HPCAL1 PE=1 SV=3
O00505	Importin subunit alpha-4 OS=Homo sapiens OX=9606 GN=KPNA3 PE=1 SV=2
P49755	Transmembrane emp24 domain-containing protein 10 OS=Homo sapiens OX=9606 GN=TMED10 PE=1 SV=2
P01619	Immunoglobulin kappa variable 3-20 OS=Homo sapiens OX=9606 GN=IGKV3-20 PE=1 SV=2
P51884	Lumican OS=Homo sapiens OX=9606 GN=LUM PE=1 SV=2
Q96AG4	Leucine-rich repeat-containing protein 59 OS=Homo sapiens OX=9606 GN=LRRC59 PE=1 SV=1
P53582	Methionine aminopeptidase 1 OS=Homo sapiens OX=9606 GN=METAP1 PE=1 SV=2
Q99471	Prefoldin subunit 5 OS=Homo sapiens OX=9606 GN=PFDN5 PE=1 SV=2
Q9Y266	Nuclear migration protein nudC OS=Homo sapiens OX=9606 GN=NUDC PE=1 SV=1
Q9UBQ7	Glyoxylate reductase/hydroxypyruvate reductase OS=Homo sapiens OX=9606 GN=GRHPR PE=1 SV=1
Q9Y2X7	ARF GTPase-activating protein GIT1 OS=Homo sapiens OX=9606 GN=GIT1 PE=1 SV=2
Q96M27	Protein PRRC1 OS=Homo sapiens OX=9606 GN=PRRC1 PE=1 SV=1
P36543	V-type proton ATPase subunit E 1 OS=Homo sapiens OX=9606 GN=ATP6V1E1 PE=1 SV=1
Q15369	Elongin-C OS=Homo sapiens OX=9606 GN=ELOC PE=1 SV=1
Q04917	14-3-3 protein eta OS=Homo sapiens OX=9606 GN=YWHAH PE=1 SV=4

P53634	Dipeptidyl peptidase 1 OS=Homo sapiens OX=9606 GN=CTSC PE=1 SV=2
Q13033	Striatin-3 OS=Homo sapiens OX=9606 GN=STRN3 PE=1 SV=3
P02750	Leucine-rich alpha-2-glycoprotein OS=Homo sapiens OX=9606 GN=LRG1 PE=1 SV=2
Q9UHA4	Ragulator complex protein LAMTOR3 OS=Homo sapiens OX=9606 GN=LAMTOR3 PE=1 SV=1
O14745	Na(+)/H(+) exchange regulatory cofactor NHE-RF1 OS=Homo sapiens OX=9606 GN=SLC9A3R1 PE=1 SV=4
P40197	Platelet glycoprotein V OS=Homo sapiens OX=9606 GN=GP5 PE=1 SV=1
P00441	Superoxide dismutase Cu-Zn OS=Homo sapiens OX=9606 GN=SOD1 PE=1 SV=2
Q96AJ9	Vesicle transport through interaction with t-SNAREs homolog 1A OS=Homo sapiens OX=9606 GN=VTI1A PE=1 SV=2
P04430	Immunoglobulin kappa variable 1-16 OS=Homo sapiens OX=9606 GN=IGKV1-16 PE=1 SV=2
O14737	Programmed cell death protein 5 OS=Homo sapiens OX=9606 GN=PDCD5 PE=1 SV=3
Q9H098	Protein FAM107B OS=Homo sapiens OX=9606 GN=FAM107B PE=1 SV=1
P10124	Serglycin OS=Homo sapiens OX=9606 GN=SRGN PE=1 SV=3
Q9P270	SLAIN motif-containing protein 2 OS=Homo sapiens OX=9606 GN=SLAIN2 PE=1 SV=2
P30041	Peroxiredoxin-6 OS=Homo sapiens OX=9606 GN=PRDX6 PE=1 SV=3
Q15149	Plectin OS=Homo sapiens OX=9606 GN=PLEC PE=1 SV=3
P53004	Biliverdin reductase A OS=Homo sapiens OX=9606 GN=BLVRA PE=1 SV=2
Q9HA64	Ketosamine-3-kinase OS=Homo sapiens OX=9606 GN=FN3KRP PE=1 SV=2
P68402	Platelet-activating factor acetylhydrolase IB subunit beta OS=Homo sapiens OX=9606 GN=PAFAH1B2 PE=1 SV=1
Q9Y6W5	Wiskott-Aldrich syndrome protein family member 2 OS=Homo sapiens OX=9606 GN=WASF2 PE=1 SV=3
Q01970	1-phosphatidylinositol 4,5-bisphosphate phosphodiesterase beta-3 OS=Homo sapiens OX=9606 GN=PLCB3 PE=1 SV=2
Q7L266	Isoaspartyl peptidase/L-asparaginase OS=Homo sapiens OX=9606 GN=ASRGL1 PE=1 SV=2
Q96EP5	DAZ-associated protein 1 OS=Homo sapiens OX=9606 GN=DAZAP1 PE=1 SV=1
Q9UKY7	Protein CDV3 homolog OS=Homo sapiens OX=9606 GN=CDV3 PE=1 SV=1
P23919	Thymidylate kinase OS=Homo sapiens OX=9606 GN=DTYMK PE=1 SV=4
O14773	Tripeptidyl-peptidase 1 OS=Homo sapiens OX=9606 GN=TPP1 PE=1 SV=2
Q6PJW8	Consortin OS=Homo sapiens OX=9606 GN=CNST PE=1 SV=3
Q9H0W9	Ester hydrolase C11orf54 OS=Homo sapiens OX=9606 GN=C11orf54 PE=1 SV=1
Q7L591	Docking protein 3 OS=Homo sapiens OX=9606 GN=DOK3 PE=1 SV=2
P61163	Alpha-centractin OS=Homo sapiens OX=9606 GN=ACTR1A PE=1 SV=1
O75351	Vacuolar protein sorting-associated protein 4B OS=Homo sapiens OX=9606 GN=VPS4B PE=1 SV=2
Q14697	Neutral alpha-glucosidase AB OS=Homo sapiens OX=9606 GN=GANAB PE=1 SV=3
Q9Y696	Chloride intracellular channel protein 4 OS=Homo sapiens OX=9606 GN=CLIC4 PE=1 SV=4
B5ME19	Eukaryotic translation initiation factor 3 subunit C-like protein OS=Homo sapiens OX=9606 GN=EIF3CL PE=1 SV=1
P02671	Fibrinogen alpha chain OS=Homo sapiens OX=9606 GN=FGA PE=1 SV=2
P28066	Proteasome subunit alpha type-5 OS=Homo sapiens OX=9606 GN=PSMA5 PE=1 SV=3

Q6VY07	Phosphofurin acidic cluster sorting protein 1 OS=Homo sapiens OX=9606 GN=PACS1 PE=1 SV=2
O15305	Phosphomannomutase 2 OS=Homo sapiens OX=9606 GN=PMM2 PE=1 SV=1
Q8TCD5	5'(3')-deoxyribonucleotidase, cytosolic type OS=Homo sapiens OX=9606 GN=NT5C PE=1 SV=2
Q99757	Thioredoxin, mitochondrial OS=Homo sapiens OX=9606 GN=TXN2 PE=1 SV=2
Q9Y315	Deoxyribose-phosphate aldolase OS=Homo sapiens OX=9606 GN=DERA PE=1 SV=2
O14579	Coatomer subunit epsilon OS=Homo sapiens OX=9606 GN=COPE PE=1 SV=3
P62136	Serine/threonine-protein phosphatase PP1-alpha catalytic subunit OS=Homo sapiens OX=9606 GN=PPP1CA PE=1 SV=1
Q9Y678	Coatomer subunit gamma-1 OS=Homo sapiens OX=9606 GN=COPG1 PE=1 SV=1
O75190	DnaJ homolog subfamily B member 6 OS=Homo sapiens OX=9606 GN=DNAJB6 PE=1 SV=2
A0A0B4J1X5	Immunoglobulin heavy variable 3-74 OS=Homo sapiens OX=9606 GN=IGHV3-74 PE=3 SV=1
P68871	Hemoglobin subunit beta OS=Homo sapiens OX=9606 GN=HBB PE=1 SV=2
P61769	Beta-2-microglobulin OS=Homo sapiens OX=9606 GN=B2M PE=1 SV=1
O00232	26S proteasome non-ATPase regulatory subunit 12 OS=Homo sapiens OX=9606 GN=PSMD12 PE=1 SV=3
O75608	Acyl-protein thioesterase 1 OS=Homo sapiens OX=9606 GN=LYPLA1 PE=1 SV=1
Q14677	Clathrin interactor 1 OS=Homo sapiens OX=9606 GN=CLINT1 PE=1 SV=1
P07237	Protein disulfide-isomerase OS=Homo sapiens OX=9606 GN=P4HB PE=1 SV=3
P05090	Apolipoprotein D OS=Homo sapiens OX=9606 GN=APOD PE=1 SV=1
P14550	Aldo-keto reductase family 1 member A1 OS=Homo sapiens OX=9606 GN=AKR1A1 PE=1 SV=3
Q9UHV9	Prefoldin subunit 2 OS=Homo sapiens OX=9606 GN=PFDN2 PE=1 SV=1
P54920	Alpha-soluble NSF attachment protein OS=Homo sapiens OX=9606 GN=NAPA PE=1 SV=3
P05771	Protein kinase C beta type OS=Homo sapiens OX=9606 GN=PRKCB PE=1 SV=4
Q3ZCW2	Galectin-related protein OS=Homo sapiens OX=9606 GN=LGALSL PE=1 SV=2
P25686	DnaJ homolog subfamily B member 2 OS=Homo sapiens OX=9606 GN=DNAJB2 PE=1 SV=3
Q9Y3B8	Oligoribonuclease, mitochondrial OS=Homo sapiens OX=9606 GN=REXO2 PE=1 SV=3
P30044	Peroxiredoxin-5, mitochondrial OS=Homo sapiens OX=9606 GN=PRDX5 PE=1 SV=4
P05543	Thyroxine-binding globulin OS=Homo sapiens OX=9606 GN=SERPINA7 PE=1 SV=2
P40926	Malate dehydrogenase, mitochondrial OS=Homo sapiens OX=9606 GN=MDH2 PE=1 SV=3
Q13045	Protein flightless-1 homolog OS=Homo sapiens OX=9606 GN=FLII PE=1 SV=2
P57721	Poly(rC)-binding protein 3 OS=Homo sapiens OX=9606 GN=PCBP3 PE=2 SV=2
P01780	Immunoglobulin heavy variable 3-7 OS=Homo sapiens OX=9606 GN=IGHV3-7 PE=1 SV=2
P08238	Heat shock protein HSP 90-beta OS=Homo sapiens OX=9606 GN=HSP90AB1 PE=1 SV=4
Q04759	Protein kinase C theta type OS=Homo sapiens OX=9606 GN=PRKCQ PE=1 SV=3
Q92882	Osteoclast-stimulating factor 1 OS=Homo sapiens OX=9606 GN=OSTF1 PE=1 SV=2
P0DOX2	Immunoglobulin alpha-2 heavy chain OS=Homo sapiens OX=9606 PE=1 SV=2
A0A087WSY4	Immunoglobulin heavy variable 4-30-2 OS=Homo sapiens OX=9606 GN=IGHV4-30-2 PE=3 SV=1

O14964	Hepatocyte growth factor-regulated tyrosine kinase substrate OS=Homo sapiens OX=9606 GN=HGS PE=1 SV=1
P29401	Transketolase OS=Homo sapiens OX=9606 GN=TKT PE=1 SV=3
Q13642	Four and a half LIM domains protein 1 OS=Homo sapiens OX=9606 GN=FHL1 PE=1 SV=4
P02753	Retinol-binding protein 4 OS=Homo sapiens OX=9606 GN=RBP4 PE=1 SV=3
P41226	Ubiquitin-like modifier-activating enzyme 7 OS=Homo sapiens OX=9606 GN=UBA7 PE=1 SV=2
Q8WVM8	Sec1 family domain-containing protein 1 OS=Homo sapiens OX=9606 GN=SCFD1 PE=1 SV=4
P13489	Ribonuclease inhibitor OS=Homo sapiens OX=9606 GN=RNH1 PE=1 SV=2
P26599	Polypyrimidine tract-binding protein 1 OS=Homo sapiens OX=9606 GN=PTBP1 PE=1 SV=1
P01009	Alpha-1-antitrypsin OS=Homo sapiens OX=9606 GN=SERPINA1 PE=1 SV=3
Q9Y570	Protein phosphatase methylesterase 1 OS=Homo sapiens OX=9606 GN=PPME1 PE=1 SV=3
Q96QK1	Vacuolar protein sorting-associated protein 35 OS=Homo sapiens OX=9606 GN=VPS35 PE=1 SV=2
Q684P5	Rap1 GTPase-activating protein 2 OS=Homo sapiens OX=9606 GN=RAP1GAP2 PE=1 SV=2
Q01813	ATP-dependent 6-phosphofructokinase, platelet type OS=Homo sapiens OX=9606 GN=PFKP PE=1 SV=2
P12955	Xaa-Pro dipeptidase OS=Homo sapiens OX=9606 GN=PEPD PE=1 SV=3
P12259	Coagulation factor V OS=Homo sapiens OX=9606 GN=F5 PE=1 SV=4
P62333	26S proteasome regulatory subunit 10B OS=Homo sapiens OX=9606 GN=PSMC6 PE=1 SV=1
P00568	Adenylate kinase isoenzyme 1 OS=Homo sapiens OX=9606 GN=AK1 PE=1 SV=3
Q99969	Retinoic acid receptor responder protein 2 OS=Homo sapiens OX=9606 GN=RARRES2 PE=1 SV=1
O43504	Ragulator complex protein LAMTOR5 OS=Homo sapiens OX=9606 GN=LAMTOR5 PE=1 SV=1
P61952	Guanine nucleotide-binding protein G(I)/G(S)/G(O) subunit gamma-11 OS=Homo sapiens OX=9606 GN=GNG11 PE=1 SV=1
Q9ULV4	Coronin-1C OS=Homo sapiens OX=9606 GN=CORO1C PE=1 SV=1
E9PAV3	Nascent polypeptide-associated complex subunit alpha, muscle-specific form OS=Homo sapiens OX=9606 GN=NACA PE=1 SV=1
P61160	Actin-related protein 2 OS=Homo sapiens OX=9606 GN=ACTR2 PE=1 SV=1
Q9Y2A7	Nck-associated protein 1 OS=Homo sapiens OX=9606 GN=NCKAP1 PE=1 SV=1
P35813	Protein phosphatase 1A OS=Homo sapiens OX=9606 GN=PPM1A PE=1 SV=1
P11047	Laminin subunit gamma-1 OS=Homo sapiens OX=9606 GN=LAMC1 PE=1 SV=3
P31153	S-adenosylmethionine synthase isoform type-2 OS=Homo sapiens OX=9606 GN=MAT2A PE=1 SV=1
O43150	Arf-GAP with SH3 domain, ANK repeat and PH domain-containing protein 2 OS=Homo sapiens OX=9606 GN=ASAP2 PE=1 SV=3
Q15404	Ras suppressor protein 1 OS=Homo sapiens OX=9606 GN=RSU1 PE=1 SV=3
O15511	Actin-related protein 2/3 complex subunit 5 OS=Homo sapiens OX=9606 GN=ARPC5 PE=1 SV=3
P04217	Alpha-1B-glycoprotein OS=Homo sapiens OX=9606 GN=A1BG PE=1 SV=4
Q00013	55 kDa erythrocyte membrane protein OS=Homo sapiens OX=9606 GN=MPP1 PE=1 SV=2
P46976	Glycogenin-1 OS=Homo sapiens OX=9606 GN=GYG1 PE=1 SV=4
P61224	Ras-related protein Rap-1b OS=Homo sapiens OX=9606 GN=RAP1B PE=1 SV=1
Q9NRW1	Ras-related protein Rab-6B OS=Homo sapiens OX=9606 GN=RAB6B PE=1 SV=1

Q14011	Cold-inducible RNA-binding protein OS=Homo sapiens OX=9606 GN=CIRBP PE=1 SV=1
O14561	Acyl carrier protein, mitochondrial OS=Homo sapiens OX=9606 GN=NDUFAB1 PE=1 SV=3
Q14112	Nidogen-2 OS=Homo sapiens OX=9606 GN=NID2 PE=1 SV=3
Q92973	Transportin-1 OS=Homo sapiens OX=9606 GN=TNPO1 PE=1 SV=2
P35237	Serpin B6 OS=Homo sapiens OX=9606 GN=SERPINB6 PE=1 SV=3
P50502	Hsc70-interacting protein OS=Homo sapiens OX=9606 GN=ST13 PE=1 SV=2
P62873	Guanine nucleotide-binding protein G(I)/G(S)/G(T) subunit beta-1 OS=Homo sapiens OX=9606 GN=GNB1 PE=1 SV=3
P14770	Platelet glycoprotein IX OS=Homo sapiens OX=9606 GN=GP9 PE=1 SV=3
Q7LDG7	RAS guanyl-releasing protein 2 OS=Homo sapiens OX=9606 GN=RASGRP2 PE=1 SV=1
P35241	Radixin OS=Homo sapiens OX=9606 GN=RDX PE=1 SV=1
P01008	Antithrombin-III OS=Homo sapiens OX=9606 GN=SERPINC1 PE=1 SV=1
P60842	Eukaryotic initiation factor 4A-I OS=Homo sapiens OX=9606 GN=EIF4A1 PE=1 SV=1
Q9Y608	Leucine-rich repeat flightless-interacting protein 2 OS=Homo sapiens OX=9606 GN=LRRFIP2 PE=1 SV=1
Q8TF64	PDZ domain-containing protein GIPC3 OS=Homo sapiens OX=9606 GN=GIPC3 PE=1 SV=1
P23528	Cofilin-1 OS=Homo sapiens OX=9606 GN=CFL1 PE=1 SV=3
P12814	Alpha-actinin-1 OS=Homo sapiens OX=9606 GN=ACTN1 PE=1 SV=2
P10720	Platelet factor 4 variant OS=Homo sapiens OX=9606 GN=PF4V1 PE=1 SV=1
P61604	10 kDa heat shock protein, mitochondrial OS=Homo sapiens OX=9606 GN=HSPE1 PE=1 SV=2
O60664	Perilipin-3 OS=Homo sapiens OX=9606 GN=PLIN3 PE=1 SV=3
Q9Y251	Heparanase OS=Homo sapiens OX=9606 GN=HPSE PE=1 SV=2
Q99426	Tubulin-folding cofactor B OS=Homo sapiens OX=9606 GN=TBCB PE=1 SV=2
Q9H2U2	Inorganic pyrophosphatase 2, mitochondrial OS=Homo sapiens OX=9606 GN=PPA2 PE=1 SV=2
P24557	Thromboxane-A synthase OS=Homo sapiens OX=9606 GN=TBXAS1 PE=1 SV=3
P36873	Serine/threonine-protein phosphatase PP1-gamma catalytic subunit OS=Homo sapiens OX=9606 GN=PPP1CC PE=1 SV=1
Q9NQW7	Xaa-Pro aminopeptidase 1 OS=Homo sapiens OX=9606 GN=XPNPEP1 PE=1 SV=3
P22234	Multifunctional protein ADE2 OS=Homo sapiens OX=9606 GN=PAICS PE=1 SV=3
O76074	cGMP-specific 3',5'-cyclic phosphodiesterase OS=Homo sapiens OX=9606 GN=PDE5A PE=1 SV=2
P02675	Fibrinogen beta chain OS=Homo sapiens OX=9606 GN=FGB PE=1 SV=2
P43251	Biotinidase OS=Homo sapiens OX=9606 GN=BTD PE=1 SV=2
P01137	Transforming growth factor beta-1 proprotein OS=Homo sapiens OX=9606 GN=TGFB1 PE=1 SV=2
P21926	CD9 antigen OS=Homo sapiens OX=9606 GN=CD9 PE=1 SV=4
P26038	Moesin OS=Homo sapiens OX=9606 GN=MSN PE=1 SV=3
P11441	Ubiquitin-like protein 4A OS=Homo sapiens OX=9606 GN=UBL4A PE=1 SV=1
Q9H2G2	STE20-like serine/threonine-protein kinase OS=Homo sapiens OX=9606 GN=SLK PE=1 SV=1
P28482	Mitogen-activated protein kinase 1 OS=Homo sapiens OX=9606 GN=MAPK1 PE=1 SV=3

Q92890	Ubiquitin recognition factor in ER-associated degradation protein 1 OS=Homo sapiens OX=9606 GN=UFD1 PE=1 SV=3
Q16851	UTP--glucose-1-phosphate uridylyltransferase OS=Homo sapiens OX=9606 GN=UGP2 PE=1 SV=5
P00558	Phosphoglycerate kinase 1 OS=Homo sapiens OX=9606 GN=PGK1 PE=1 SV=3
P16284	Platelet endothelial cell adhesion molecule OS=Homo sapiens OX=9606 GN=PECAM1 PE=1 SV=2
P20073	Annexin A7 OS=Homo sapiens OX=9606 GN=ANXA7 PE=1 SV=3
A0A0J9YXX1	Immunoglobulin heavy variable 5-10-1 OS=Homo sapiens OX=9606 GN=IGHV5-10-1 PE=3 SV=1
P51659	Peroxisomal multifunctional enzyme type 2 OS=Homo sapiens OX=9606 GN=HSD17B4 PE=1 SV=3
P49721	Proteasome subunit beta type-2 OS=Homo sapiens OX=9606 GN=PSMB2 PE=1 SV=1
Q8TD19	Serine/threonine-protein kinase Nek9 OS=Homo sapiens OX=9606 GN=NEK9 PE=1 SV=2
P49189	4-trimethylaminobutyraldehyde dehydrogenase OS=Homo sapiens OX=9606 GN=ALDH9A1 PE=1 SV=3
P09104	Gamma-enolase OS=Homo sapiens OX=9606 GN=ENO2 PE=1 SV=3
P50990	T-complex protein 1 subunit theta OS=Homo sapiens OX=9606 GN=CCT8 PE=1 SV=4
Q14162	Scavenger receptor class F member 1 OS=Homo sapiens OX=9606 GN=SCARF1 PE=1 SV=3
O95782	AP-2 complex subunit alpha-1 OS=Homo sapiens OX=9606 GN=AP2A1 PE=1 SV=3
Q9NYL9	Tropomodulin-3 OS=Homo sapiens OX=9606 GN=TMOD3 PE=1 SV=1
O00299	Chloride intracellular channel protein 1 OS=Homo sapiens OX=9606 GN=CLIC1 PE=1 SV=4
P10619	Lysosomal protective protein OS=Homo sapiens OX=9606 GN=CTSA PE=1 SV=2
Q5T5C0	Syntaxin-binding protein 5 OS=Homo sapiens OX=9606 GN=STXBP5 PE=1 SV=1
Q53H82	Endoribonuclease LACTB2 OS=Homo sapiens OX=9606 GN=LACTB2 PE=1 SV=2
P52566	Rho GDP-dissociation inhibitor 2 OS=Homo sapiens OX=9606 GN=ARHGDIB PE=1 SV=3
P02746	Complement C1q subcomponent subunit B OS=Homo sapiens OX=9606 GN=C1QB PE=1 SV=3
O14980	Exportin-1 OS=Homo sapiens OX=9606 GN=XPO1 PE=1 SV=1
Q9NZQ3	NCK-interacting protein with SH3 domain OS=Homo sapiens OX=9606 GN=NCKIPSD PE=1 SV=1
P26447	Protein S100-A4 OS=Homo sapiens OX=9606 GN=S100A4 PE=1 SV=1
Q05682	Caldesmon OS=Homo sapiens OX=9606 GN=CALD1 PE=1 SV=3
P47897	Glutamine--tRNA ligase OS=Homo sapiens OX=9606 GN=QARS1 PE=1 SV=1
Q15366	Poly(rC)-binding protein 2 OS=Homo sapiens OX=9606 GN=PCBP2 PE=1 SV=1
P25311	Zinc-alpha-2-glycoprotein OS=Homo sapiens OX=9606 GN=AZGP1 PE=1 SV=2
Q05193	Dynamin-1 OS=Homo sapiens OX=9606 GN=DNM1 PE=1 SV=2
Q96C90	Protein phosphatase 1 regulatory subunit 14B OS=Homo sapiens OX=9606 GN=PPP1R14B PE=1 SV=3
P15170	Eukaryotic peptide chain release factor GTP-binding subunit ERF3A OS=Homo sapiens OX=9606 GN=GSPT1 PE=1 SV=1
Q8IY22	C-Maf-inducing protein OS=Homo sapiens OX=9606 GN=CMIP PE=1 SV=3
P15814	Immunoglobulin lambda-like polypeptide 1 OS=Homo sapiens OX=9606 GN=IGLL1 PE=1 SV=1
P49908	Selenoprotein P OS=Homo sapiens OX=9606 GN=SELENOP PE=1 SV=3
P11142	Heat shock cognate 71 kDa protein OS=Homo sapiens OX=9606 GN=HSPA8 PE=1 SV=1

P06396	Gelsolin OS=Homo sapiens OX=9606 GN=GSN PE=1 SV=1
Q14789	Golgin subfamily B member 1 OS=Homo sapiens OX=9606 GN=GOLGB1 PE=1 SV=2
O60749	Sorting nexin-2 OS=Homo sapiens OX=9606 GN=SNX2 PE=1 SV=2
O00139	Kinesin-like protein KIF2A OS=Homo sapiens OX=9606 GN=KIF2A PE=1 SV=3
O60229	Kalirin OS=Homo sapiens OX=9606 GN=KALRN PE=1 SV=3
Q9UNS2	COP9 signalosome complex subunit 3 OS=Homo sapiens OX=9606 GN=COPS3 PE=1 SV=3
O14791	Apolipoprotein L1 OS=Homo sapiens OX=9606 GN=APOL1 PE=1 SV=5
P01023	Alpha-2-macroglobulin OS=Homo sapiens OX=9606 GN=A2M PE=1 SV=3
P55957	BH3-interacting domain death agonist OS=Homo sapiens OX=9606 GN=BID PE=1 SV=1
P34932	Heat shock 70 kDa protein 4 OS=Homo sapiens OX=9606 GN=HSPA4 PE=1 SV=4
Q13496	Myotubularin OS=Homo sapiens OX=9606 GN=MTM1 PE=1 SV=2
P46736	Lys-63-specific deubiquitinase BRCC36 OS=Homo sapiens OX=9606 GN=BRCC3 PE=1 SV=2
Q9BY43	Charged multivesicular body protein 4a OS=Homo sapiens OX=9606 GN=CHMP4A PE=1 SV=3
P06702	Protein S100-A9 OS=Homo sapiens OX=9606 GN=S100A9 PE=1 SV=1
P13598	Intercellular adhesion molecule 2 OS=Homo sapiens OX=9606 GN=ICAM2 PE=1 SV=2
Q15762	CD226 antigen OS=Homo sapiens OX=9606 GN=CD226 PE=1 SV=2
P30153	Serine/threonine-protein phosphatase 2A 65 kDa regulatory subunit A alpha isoform OS=Homo sapiens OX=9606 GN=PPP2R1A PE=1 SV=4
Q99719	Septin-5 OS=Homo sapiens OX=9606 GN=SEPTIN5 PE=1 SV=1
P0CG39	POTE ankyrin domain family member J OS=Homo sapiens OX=9606 GN=POTEJ PE=3 SV=1
P60953	Cell division control protein 42 homolog OS=Homo sapiens OX=9606 GN=CDC42 PE=1 SV=2
O60506	Heterogeneous nuclear ribonucleoprotein Q OS=Homo sapiens OX=9606 GN=SYNCRIP PE=1 SV=2
P17174	Aspartate aminotransferase, cytoplasmic OS=Homo sapiens OX=9606 GN=GOT1 PE=1 SV=3
Q8WUW1	Protein BRICK1 OS=Homo sapiens OX=9606 GN=BRK1 PE=1 SV=1
P53618	Coatomer subunit beta OS=Homo sapiens OX=9606 GN=COPB1 PE=1 SV=3
O43639	Cytoplasmic protein NCK2 OS=Homo sapiens OX=9606 GN=NCK2 PE=1 SV=2
P30086	Phosphatidylethanolamine-binding protein 1 OS=Homo sapiens OX=9606 GN=PEBP1 PE=1 SV=3
A0A0C4DH38	Immunoglobulin heavy variable 5-51 OS=Homo sapiens OX=9606 GN=IGHV5-51 PE=3 SV=1
Q8IZD0	Sterile alpha motif domain-containing protein 14 OS=Homo sapiens OX=9606 GN=SAMD14 PE=2 SV=2
P68104	Elongation factor 1-alpha 1 OS=Homo sapiens OX=9606 GN=EEF1A1 PE=1 SV=1
P51809	Vesicle-associated membrane protein 7 OS=Homo sapiens OX=9606 GN=VAMP7 PE=1 SV=3
P07311	Acylphosphatase-1 OS=Homo sapiens OX=9606 GN=ACYP1 PE=1 SV=2
Q15257	Serine/threonine-protein phosphatase 2A activator OS=Homo sapiens OX=9606 GN=PTPA PE=1 SV=3
Q9BWD1	Acetyl-CoA acetyltransferase, cytosolic OS=Homo sapiens OX=9606 GN=ACAT2 PE=1 SV=2
P26885	Peptidyl-prolyl cis-trans isomerase FKBP2 OS=Homo sapiens OX=9606 GN=FKBP2 PE=1 SV=2
Q32MZ4	Leucine-rich repeat flightless-interacting protein 1 OS=Homo sapiens OX=9606 GN=LRRFIP1 PE=1 SV=2

Q96HY6	DDRGK domain-containing protein 1 OS=Homo sapiens OX=9606 GN=DDRGK1 PE=1 SV=2
Q27J81	Inverted formin-2 OS=Homo sapiens OX=9606 GN=INF2 PE=1 SV=2
P25788	Proteasome subunit alpha type-3 OS=Homo sapiens OX=9606 GN=PSMA3 PE=1 SV=2
P60709	Actin, cytoplasmic 1 OS=Homo sapiens OX=9606 GN=ACTB PE=1 SV=1
P07195	L-lactate dehydrogenase B chain OS=Homo sapiens OX=9606 GN=LDHB PE=1 SV=2
P20810	Calpastatin OS=Homo sapiens OX=9606 GN=CAST PE=1 SV=4
Q12805	EGF-containing fibulin-like extracellular matrix protein 1 OS=Homo sapiens OX=9606 GN=EFEMP1 PE=1 SV=2
P16671	Platelet glycoprotein 4 OS=Homo sapiens OX=9606 GN=CD36 PE=1 SV=2
P07358	Complement component C8 beta chain OS=Homo sapiens OX=9606 GN=C8B PE=1 SV=3
P20338	Ras-related protein Rab-4A OS=Homo sapiens OX=9606 GN=RAB4A PE=1 SV=3
P35754	Glutaredoxin-1 OS=Homo sapiens OX=9606 GN=GLRX PE=1 SV=2
P00492	Hypoxanthine-guanine phosphoribosyltransferase OS=Homo sapiens OX=9606 GN=HPRT1 PE=1 SV=2
P22352	Glutathione peroxidase 3 OS=Homo sapiens OX=9606 GN=GPX3 PE=1 SV=2
Q13813	Spectrin alpha chain, non-erythrocytic 1 OS=Homo sapiens OX=9606 GN=SPTAN1 PE=1 SV=3
Q9BXS5	AP-1 complex subunit mu-1 OS=Homo sapiens OX=9606 GN=AP1M1 PE=1 SV=3
P51878	Caspase-5 OS=Homo sapiens OX=9606 GN=CASP5 PE=1 SV=3
P51149	Ras-related protein Rab-7a OS=Homo sapiens OX=9606 GN=RAB7A PE=1 SV=1
Q8NCW5	NAD(P)H-hydrate epimerase OS=Homo sapiens OX=9606 GN=NAXE PE=1 SV=2
Q14008	Cytoskeleton-associated protein 5 OS=Homo sapiens OX=9606 GN=CKAP5 PE=1 SV=3
O15083	ERC protein 2 OS=Homo sapiens OX=9606 GN=ERC2 PE=1 SV=3
Q969H8	Myeloid-derived growth factor OS=Homo sapiens OX=9606 GN=MYDGF PE=1 SV=1
Q14141	Septin-6 OS=Homo sapiens OX=9606 GN=SEPTIN6 PE=1 SV=4
Q9H0R4	Haloacid dehalogenase-like hydrolase domain-containing protein 2 OS=Homo sapiens OX=9606 GN=HDHD2 PE=1 SV=1
P67936	Tropomyosin alpha-4 chain OS=Homo sapiens OX=9606 GN=TPM4 PE=1 SV=3
P11597	Cholesteryl ester transfer protein OS=Homo sapiens OX=9606 GN=CETP PE=1 SV=2
P52306	Rap1 GTPase-GDP dissociation stimulator 1 OS=Homo sapiens OX=9606 GN=RAP1GDS1 PE=1 SV=3
P78356	Phosphatidylinositol 5-phosphate 4-kinase type-2 beta OS=Homo sapiens OX=9606 GN=PIP4K2B PE=1 SV=1
O75410	Transforming acidic coiled-coil-containing protein 1 OS=Homo sapiens OX=9606 GN=TACC1 PE=1 SV=2
O00244	Copper transport protein ATOX1 OS=Homo sapiens OX=9606 GN=ATOX1 PE=1 SV=1
Q13188	Serine/threonine-protein kinase 3 OS=Homo sapiens OX=9606 GN=STK3 PE=1 SV=2
Q14696	LRP chaperone MESD OS=Homo sapiens OX=9606 GN=MESD PE=1 SV=2
P02776	Platelet factor 4 OS=Homo sapiens OX=9606 GN=PF4 PE=1 SV=2
Q14644	Ras GTPase-activating protein 3 OS=Homo sapiens OX=9606 GN=RASA3 PE=1 SV=3
O43633	Charged multivesicular body protein 2a OS=Homo sapiens OX=9606 GN=CHMP2A PE=1 SV=1
Q12841	Follistatin-related protein 1 OS=Homo sapiens OX=9606 GN=FSTL1 PE=1 SV=1

P49247	Ribose-5-phosphate isomerase OS=Homo sapiens OX=9606 GN=RPIA PE=1 SV=3
Q9BRF8	Serine/threonine-protein phosphatase CPPED1 OS=Homo sapiens OX=9606 GN=CPPED1 PE=1 SV=3
P34913	Bifunctional epoxide hydrolase 2 OS=Homo sapiens OX=9606 GN=EPHX2 PE=1 SV=2
Q9UJY5	ADP-ribosylation factor-binding protein GGA1 OS=Homo sapiens OX=9606 GN=GGA1 PE=1 SV=1
P61018	Ras-related protein Rab-4B OS=Homo sapiens OX=9606 GN=RAB4B PE=1 SV=1
Q13094	Lymphocyte cytosolic protein 2 OS=Homo sapiens OX=9606 GN=LCP2 PE=1 SV=1
O95866	Megakaryocyte and platelet inhibitory receptor G6b OS=Homo sapiens OX=9606 GN=MPIG6B PE=1 SV=1
Q15365	Poly(rC)-binding protein 1 OS=Homo sapiens OX=9606 GN=PCBP1 PE=1 SV=2
P00915	Carbonic anhydrase 1 OS=Homo sapiens OX=9606 GN=CA1 PE=1 SV=2
A0A0J9YX35	Immunoglobulin heavy variable 3-64D OS=Homo sapiens OX=9606 GN=IGHV3-64D PE=3 SV=1
P42229	Signal transducer and activator of transcription 5A OS=Homo sapiens OX=9606 GN=STAT5A PE=1 SV=1
P60900	Proteasome subunit alpha type-6 OS=Homo sapiens OX=9606 GN=PSMA6 PE=1 SV=1
P08962	CD63 antigen OS=Homo sapiens OX=9606 GN=CD63 PE=1 SV=2
O00194	Ras-related protein Rab-27B OS=Homo sapiens OX=9606 GN=RAB27B PE=1 SV=4
Q70J99	Protein unc-13 homolog D OS=Homo sapiens OX=9606 GN=UNC13D PE=1 SV=1
P04406	Glyceraldehyde-3-phosphate dehydrogenase OS=Homo sapiens OX=9606 GN=GAPDH PE=1 SV=3
P09488	Glutathione S-transferase Mu 1 OS=Homo sapiens OX=9606 GN=GSTM1 PE=1 SV=3
P26639	Threonine--tRNA ligase 1, cytoplasmic OS=Homo sapiens OX=9606 GN=TARS1 PE=1 SV=3
P61981	14-3-3 protein gamma OS=Homo sapiens OX=9606 GN=YWHAG PE=1 SV=2
Q92835	Phosphatidylinositol 3,4,5-trisphosphate 5-phosphatase 1 OS=Homo sapiens OX=9606 GN=INPP5D PE=1 SV=2
P54725	UV excision repair protein RAD23 homolog A OS=Homo sapiens OX=9606 GN=RAD23A PE=1 SV=1
Q16643	Drebrin OS=Homo sapiens OX=9606 GN=DBN1 PE=1 SV=4
Q14766	Latent-transforming growth factor beta-binding protein 1 OS=Homo sapiens OX=9606 GN=LTBP1 PE=1 SV=4
Q99733	Nucleosome assembly protein 1-like 4 OS=Homo sapiens OX=9606 GN=NAP1L4 PE=1 SV=1
P11021	Endoplasmic reticulum chaperone BiP OS=Homo sapiens OX=9606 GN=HSPA5 PE=1 SV=2
Q15436	Protein transport protein Sec23A OS=Homo sapiens OX=9606 GN=SEC23A PE=1 SV=2
Q5T0N5	Formin-binding protein 1-like OS=Homo sapiens OX=9606 GN=FNBP1L PE=1 SV=3
Q96RL7	Vacuolar protein sorting-associated protein 13A OS=Homo sapiens OX=9606 GN=VPS13A PE=1 SV=2
Q9BVK6	Transmembrane emp24 domain-containing protein 9 OS=Homo sapiens OX=9606 GN=TMED9 PE=1 SV=2
P00352	Retinal dehydrogenase 1 OS=Homo sapiens OX=9606 GN=ALDH1A1 PE=1 SV=2
Q6ICL3	Transport and Golgi organization protein 2 homolog OS=Homo sapiens OX=9606 GN=TANGO2 PE=1 SV=1
Q15843	NEDD8 OS=Homo sapiens OX=9606 GN=NEDD8 PE=1 SV=1
O43464	Serine protease HTRA2, mitochondrial OS=Homo sapiens OX=9606 GN=HTRA2 PE=1 SV=2
P15153	Ras-related C3 botulinum toxin substrate 2 OS=Homo sapiens OX=9606 GN=RAC2 PE=1 SV=1
Q86WR7	Proline and serine-rich protein 2 OS=Homo sapiens OX=9606 GN=PROSER2 PE=1 SV=2

P48444	Coatomer subunit delta OS=Homo sapiens OX=9606 GN=ARCN1 PE=1 SV=1
Q9NZ08	Endoplasmic reticulum aminopeptidase 1 OS=Homo sapiens OX=9606 GN=ERAP1 PE=1 SV=3
Q8NBS9	Thioredoxin domain-containing protein 5 OS=Homo sapiens OX=9606 GN=TXNDC5 PE=1 SV=2
Q9UHD1	Cysteine and histidine-rich domain-containing protein 1 OS=Homo sapiens OX=9606 GN=CHORDC1 PE=1 SV=2
O00264	Membrane-associated progesterone receptor component 1 OS=Homo sapiens OX=9606 GN=PGRMC1 PE=1 SV=3
Q4KMP7	TBC1 domain family member 10B OS=Homo sapiens OX=9606 GN=TBC1D10B PE=1 SV=3
P41091	Eukaryotic translation initiation factor 2 subunit 3 OS=Homo sapiens OX=9606 GN=EIF2S3 PE=1 SV=3
P56377	AP-1 complex subunit sigma-2 OS=Homo sapiens OX=9606 GN=AP1S2 PE=1 SV=1
P01701	Immunoglobulin lambda variable 1-51 OS=Homo sapiens OX=9606 GN=IGLV1-51 PE=1 SV=2
P23588	Eukaryotic translation initiation factor 4B OS=Homo sapiens OX=9606 GN=EIF4B PE=1 SV=2
P28065	Proteasome subunit beta type-9 OS=Homo sapiens OX=9606 GN=PSMB9 PE=1 SV=2
Q8WXC6	COP9 signalosome complex subunit 9 OS=Homo sapiens OX=9606 GN=COPS9 PE=1 SV=3
P0DOX5	Immunoglobulin gamma-1 heavy chain OS=Homo sapiens OX=9606 PE=1 SV=2
Q15185	Prostaglandin E synthase 3 OS=Homo sapiens OX=9606 GN=PTGES3 PE=1 SV=1
P00747	Plasminogen OS=Homo sapiens OX=9606 GN=PLG PE=1 SV=2
Q13404	Ubiquitin-conjugating enzyme E2 variant 1 OS=Homo sapiens OX=9606 GN=UBE2V1 PE=1 SV=2
P08185	Corticosteroid-binding globulin OS=Homo sapiens OX=9606 GN=SERPINA6 PE=1 SV=1
Q15691	Microtubule-associated protein RP/EB family member 1 OS=Homo sapiens OX=9606 GN=MAPRE1 PE=1 SV=3
Q6UWL2	Sushi domain-containing protein 1 OS=Homo sapiens OX=9606 GN=SUSD1 PE=1 SV=1
P04196	Histidine-rich glycoprotein OS=Homo sapiens OX=9606 GN=HRG PE=1 SV=1
P00734	Prothrombin OS=Homo sapiens OX=9606 GN=F2 PE=1 SV=2
Q9Y4D1	Disheveled-associated activator of morphogenesis 1 OS=Homo sapiens OX=9606 GN=DAAM1 PE=1 SV=2
O94973	AP-2 complex subunit alpha-2 OS=Homo sapiens OX=9606 GN=AP2A2 PE=1 SV=2
P02654	Apolipoprotein C-I OS=Homo sapiens OX=9606 GN=APOC1 PE=1 SV=1
O75154	Rab11 family-interacting protein 3 OS=Homo sapiens OX=9606 GN=RAB11FIP3 PE=1 SV=1
A6NDG6	Glycerol-3-phosphate phosphatase OS=Homo sapiens OX=9606 GN=PGP PE=1 SV=1
Q9NRG1	Phosphoribosyltransferase domain-containing protein 1 OS=Homo sapiens OX=9606 GN=PRTFDC1 PE=1 SV=1
P62495	Eukaryotic peptide chain release factor subunit 1 OS=Homo sapiens OX=9606 GN=ETF1 PE=1 SV=3
Q9BR76	Coronin-1B OS=Homo sapiens OX=9606 GN=CORO1B PE=1 SV=1
Q9Y2I8	WD repeat-containing protein 37 OS=Homo sapiens OX=9606 GN=WDR37 PE=1 SV=2
Q9NZM3	Intersectin-2 OS=Homo sapiens OX=9606 GN=ITSN2 PE=1 SV=3
P31323	cAMP-dependent protein kinase type II-beta regulatory subunit OS=Homo sapiens OX=9606 GN=PRKAR2B PE=1 SV=3
Q8TF42	Ubiquitin-associated and SH3 domain-containing protein B OS=Homo sapiens OX=9606 GN=UBASH3B PE=1 SV=2
Q9H0E2	Toll-interacting protein OS=Homo sapiens OX=9606 GN=TOLLIP PE=1 SV=1
Q9BUL8	Programmed cell death protein 10 OS=Homo sapiens OX=9606 GN=PDCD10 PE=1 SV=1

P16615	Sarcoplasmic/endoplasmic reticulum calcium ATPase 2 OS=Homo sapiens OX=9606 GN=ATP2A2 PE=1 SV=1
P13716	Delta-aminolevulinic acid dehydratase OS=Homo sapiens OX=9606 GN=ALAD PE=1 SV=1
P51606	N-acylglucosamine 2-epimerase OS=Homo sapiens OX=9606 GN=RENBP PE=1 SV=2
P07737	Profilin-1 OS=Homo sapiens OX=9606 GN=PFN1 PE=1 SV=2
P05198	Eukaryotic translation initiation factor 2 subunit 1 OS=Homo sapiens OX=9606 GN=EIF2S1 PE=1 SV=3
Q9UL25	Ras-related protein Rab-21 OS=Homo sapiens OX=9606 GN=RAB21 PE=1 SV=3
Q15019	Septin-2 OS=Homo sapiens OX=9606 GN=SEPTIN2 PE=1 SV=1
P30101	Protein disulfide-isomerase A3 OS=Homo sapiens OX=9606 GN=PDIA3 PE=1 SV=4
Q9NY65	Tubulin alpha-8 chain OS=Homo sapiens OX=9606 GN=TUBA8 PE=1 SV=1
P31942	Heterogeneous nuclear ribonucleoprotein H3 OS=Homo sapiens OX=9606 GN=HNRNPH3 PE=1 SV=2
Q8N4Q1	Mitochondrial intermembrane space import and assembly protein 40 OS=Homo sapiens OX=9606 GN=CHCHD4 PE=1 SV=1
P55854	Small ubiquitin-related modifier 3 OS=Homo sapiens OX=9606 GN=SUMO3 PE=1 SV=2
P01019	Angiotensinogen OS=Homo sapiens OX=9606 GN=AGT PE=1 SV=1
P61978	Heterogeneous nuclear ribonucleoprotein K OS=Homo sapiens OX=9606 GN=HNRNPK PE=1 SV=1
P24534	Elongation factor 1-beta OS=Homo sapiens OX=9606 GN=EEF1B2 PE=1 SV=3
Q99598	Translin-associated protein X OS=Homo sapiens OX=9606 GN=TSNAX PE=1 SV=1
P12429	Annexin A3 OS=Homo sapiens OX=9606 GN=ANXA3 PE=1 SV=3
Q9BT78	COP9 signalosome complex subunit 4 OS=Homo sapiens OX=9606 GN=COPS4 PE=1 SV=1
Q96FW1	Ubiquitin thioesterase OTUB1 OS=Homo sapiens OX=9606 GN=OTUB1 PE=1 SV=2
Q6IAA8	Ragulator complex protein LAMTOR1 OS=Homo sapiens OX=9606 GN=LAMTOR1 PE=1 SV=2
Q15018	BRISC complex subunit Abraxas 2 OS=Homo sapiens OX=9606 GN=ABRAXAS2 PE=1 SV=2
Q6IA69	Glutamine-dependent NAD(+) synthetase OS=Homo sapiens OX=9606 GN=NADSYN1 PE=1 SV=3
A0A0C4DH36	Probable non-functional immunoglobulin heavy variable 3-38 OS=Homo sapiens OX=9606 GN=IGHV3-38 PE=5 SV=1
P54136	Arginine--tRNA ligase, cytoplasmic OS=Homo sapiens OX=9606 GN=RARS1 PE=1 SV=2
Q5T1M5	FK506-binding protein 15 OS=Homo sapiens OX=9606 GN=FKBP15 PE=1 SV=2
O15117	FYN-binding protein 1 OS=Homo sapiens OX=9606 GN=FYB1 PE=1 SV=2
Q9Y6A5	Transforming acidic coiled-coil-containing protein 3 OS=Homo sapiens OX=9606 GN=TACC3 PE=1 SV=1
P06730	Eukaryotic translation initiation factor 4E OS=Homo sapiens OX=9606 GN=EIF4E PE=1 SV=2
P07919	Cytochrome b-c1 complex subunit 6, mitochondrial OS=Homo sapiens OX=9606 GN=UQCRH PE=1 SV=2
P28070	Proteasome subunit beta type-4 OS=Homo sapiens OX=9606 GN=PSMB4 PE=1 SV=4
P17858	ATP-dependent 6-phosphofructokinase, liver type OS=Homo sapiens OX=9606 GN=PFKL PE=1 SV=6
Q14353	Guanidinoacetate N-methyltransferase OS=Homo sapiens OX=9606 GN=GAMT PE=1 SV=1
P55735	Protein SEC13 homolog OS=Homo sapiens OX=9606 GN=SEC13 PE=1 SV=3
Q709C8	Vacuolar protein sorting-associated protein 13C OS=Homo sapiens OX=9606 GN=VPS13C PE=1 SV=1
Q96CD2	Phosphopantothenoylcysteine decarboxylase OS=Homo sapiens OX=9606 GN=PPCDC PE=1 SV=2

Q9UNK0	Syntaxin-8 OS=Homo sapiens OX=9606 GN=STX8 PE=1 SV=2
Q9NZZ3	Charged multivesicular body protein 5 OS=Homo sapiens OX=9606 GN=CHMP5 PE=1 SV=1
P01344	Insulin-like growth factor II OS=Homo sapiens OX=9606 GN=IGF2 PE=1 SV=1
O43776	Asparagine--tRNA ligase, cytoplasmic OS=Homo sapiens OX=9606 GN=NARS1 PE=1 SV=1
Q9H479	Fructosamine-3-kinase OS=Homo sapiens OX=9606 GN=FN3K PE=1 SV=1
Q01518	Adenylyl cyclase-associated protein 1 OS=Homo sapiens OX=9606 GN=CAP1 PE=1 SV=5
P0DOY2	Immunoglobulin lambda constant 2 OS=Homo sapiens OX=9606 GN=IGLC2 PE=1 SV=1
Q9BRA2	Thioredoxin domain-containing protein 17 OS=Homo sapiens OX=9606 GN=TXNDC17 PE=1 SV=1
P63208	S-phase kinase-associated protein 1 OS=Homo sapiens OX=9606 GN=SKP1 PE=1 SV=2
Q15907	Ras-related protein Rab-11B OS=Homo sapiens OX=9606 GN=RAB11B PE=1 SV=4
Q9NPH2	Inositol-3-phosphate synthase 1 OS=Homo sapiens OX=9606 GN=ISYNA1 PE=1 SV=1
P53396	ATP-citrate synthase OS=Homo sapiens OX=9606 GN=ACLY PE=1 SV=3
P07741	Adenine phosphoribosyltransferase OS=Homo sapiens OX=9606 GN=APRT PE=1 SV=2
P06241	Tyrosine-protein kinase Fyn OS=Homo sapiens OX=9606 GN=FYN PE=1 SV=3
O00151	PDZ and LIM domain protein 1 OS=Homo sapiens OX=9606 GN=PDLIM1 PE=1 SV=4
P61626	Lysozyme C OS=Homo sapiens OX=9606 GN=LYZ PE=1 SV=1
Q8IVB4	Sodium/hydrogen exchanger 9 OS=Homo sapiens OX=9606 GN=SLC9A9 PE=1 SV=1
Q9NTJ4	Alpha-mannosidase 2C1 OS=Homo sapiens OX=9606 GN=MAN2C1 PE=1 SV=1
P36871	Phosphoglucomutase-1 OS=Homo sapiens OX=9606 GN=PGM1 PE=1 SV=3
Q8IW45	ATP-dependent (S)-NAD(P)H-hydrate dehydratase OS=Homo sapiens OX=9606 GN=NAXD PE=1 SV=1
P01743	Immunoglobulin heavy variable 1-46 OS=Homo sapiens OX=9606 GN=IGHV1-46 PE=1 SV=2
P08519	Apolipoprotein(a) OS=Homo sapiens OX=9606 GN=LPA PE=1 SV=1
Q02153	Guanylate cyclase soluble subunit beta-1 OS=Homo sapiens OX=9606 GN=GUCY1B1 PE=1 SV=1
Q13162	Peroxiredoxin-4 OS=Homo sapiens OX=9606 GN=PRDX4 PE=1 SV=1
O75396	Vesicle-trafficking protein SEC22b OS=Homo sapiens OX=9606 GN=SEC22B PE=1 SV=4
Q92619	Rho GTPase-activating protein 45 OS=Homo sapiens OX=9606 GN=ARHGAP45 PE=1 SV=2
P63241	Eukaryotic translation initiation factor 5A-1 OS=Homo sapiens OX=9606 GN=EIF5A PE=1 SV=2
P09493	Tropomyosin alpha-1 chain OS=Homo sapiens OX=9606 GN=TPM1 PE=1 SV=2
P52597	Heterogeneous nuclear ribonucleoprotein F OS=Homo sapiens OX=9606 GN=HNRNPF PE=1 SV=3
Q86VS8	Protein Hook homolog 3 OS=Homo sapiens OX=9606 GN=HOOK3 PE=1 SV=2
P62937	Peptidyl-prolyl cis-trans isomerase A OS=Homo sapiens OX=9606 GN=PPIA PE=1 SV=2
O00743	Serine/threonine-protein phosphatase 6 catalytic subunit OS=Homo sapiens OX=9606 GN=PPP6C PE=1 SV=1
P41240	Tyrosine-protein kinase CSK OS=Homo sapiens OX=9606 GN=CSK PE=1 SV=1
Q9H074	Polyadenylate-binding protein-interacting protein 1 OS=Homo sapiens OX=9606 GN=PAIP1 PE=1 SV=1
Q9Y262	Eukaryotic translation initiation factor 3 subunit L OS=Homo sapiens OX=9606 GN=EIF3L PE=1 SV=1

Q96AP7	Endothelial cell-selective adhesion molecule OS=Homo sapiens OX=9606 GN=ESAM PE=1 SV=1
P08134	Rho-related GTP-binding protein RhoC OS=Homo sapiens OX=9606 GN=RHOC PE=1 SV=1
Q93052	Lipoma-preferred partner OS=Homo sapiens OX=9606 GN=LPP PE=1 SV=1
P13693	Translationally-controlled tumor protein OS=Homo sapiens OX=9606 GN=TPT1 PE=1 SV=1
P30622	CAP-Gly domain-containing linker protein 1 OS=Homo sapiens OX=9606 GN=CLIP1 PE=1 SV=2
P22314	Ubiquitin-like modifier-activating enzyme 1 OS=Homo sapiens OX=9606 GN=UBA1 PE=1 SV=3
P10643	Complement component C7 OS=Homo sapiens OX=9606 GN=C7 PE=1 SV=2
P27824	Calnexin OS=Homo sapiens OX=9606 GN=CANX PE=1 SV=2
Q9NUQ9	Protein FAM49B OS=Homo sapiens OX=9606 GN=FAM49B PE=1 SV=1
Q9GZT8	NIF3-like protein 1 OS=Homo sapiens OX=9606 GN=NIF3L1 PE=1 SV=2
Q96P48	Arf-GAP with Rho-GAP domain, ANK repeat and PH domain-containing protein 1 OS=Homo sapiens OX=9606 GN=ARAP1 PE=1 SV=3
P62256	Ubiquitin-conjugating enzyme E2 H OS=Homo sapiens OX=9606 GN=UBE2H PE=1 SV=1
P98082	Disabled homolog 2 OS=Homo sapiens OX=9606 GN=DAB2 PE=1 SV=3
P04433	Immunoglobulin kappa variable 3-11 OS=Homo sapiens OX=9606 GN=IGKV3-11 PE=1 SV=1
Q9UKK9	ADP-sugar pyrophosphatase OS=Homo sapiens OX=9606 GN=NUDT5 PE=1 SV=1
P12931	Proto-oncogene tyrosine-protein kinase Src OS=Homo sapiens OX=9606 GN=SRC PE=1 SV=3
Q9C0C9	(E3-independent) E2 ubiquitin-conjugating enzyme OS=Homo sapiens OX=9606 GN=UBE2O PE=1 SV=3
P00338	L-lactate dehydrogenase A chain OS=Homo sapiens OX=9606 GN=LDHA PE=1 SV=2
O60268	Uncharacterized protein KIAA0513 OS=Homo sapiens OX=9606 GN=KIAA0513 PE=1 SV=1
P13861	cAMP-dependent protein kinase type II-alpha regulatory subunit OS=Homo sapiens OX=9606 GN=PRKAR2A PE=1 SV=2
Q5M775	Cytospin-B OS=Homo sapiens OX=9606 GN=SPECC1 PE=1 SV=1
Q13976	cGMP-dependent protein kinase 1 OS=Homo sapiens OX=9606 GN=PRKG1 PE=1 SV=3
P0DMV8	Heat shock 70 kDa protein 1A OS=Homo sapiens OX=9606 GN=HSPA1A PE=1 SV=1
P04275	von Willebrand factor OS=Homo sapiens OX=9606 GN=VWF PE=1 SV=4
P18054	Arachidonate 12-lipoxygenase, 12S-type OS=Homo sapiens OX=9606 GN=ALOX12 PE=1 SV=4
P30626	Sorcin OS=Homo sapiens OX=9606 GN=SRI PE=1 SV=1
Q96EK6	Glucosamine 6-phosphate N-acetyltransferase OS=Homo sapiens OX=9606 GN=GNPNAT1 PE=1 SV=1
P02679	Fibrinogen gamma chain OS=Homo sapiens OX=9606 GN=FGG PE=1 SV=3
Q5VW32	BRO1 domain-containing protein BROX OS=Homo sapiens OX=9606 GN=BROX PE=1 SV=1
P35579	Myosin-9 OS=Homo sapiens OX=9606 GN=MYH9 PE=1 SV=4
P78371	T-complex protein 1 subunit beta OS=Homo sapiens OX=9606 GN=CCT2 PE=1 SV=4
P0DOX3	Immunoglobulin delta heavy chain OS=Homo sapiens OX=9606 PE=1 SV=1
Q8WUD1	Ras-related protein Rab-2B OS=Homo sapiens OX=9606 GN=RAB2B PE=1 SV=1
P0DP25	Calmodulin-3 OS=Homo sapiens OX=9606 GN=CALM3 PE=1 SV=1
Q12974	Protein tyrosine phosphatase type IVA 2 OS=Homo sapiens OX=9606 GN=PTP4A2 PE=1 SV=1

P08514	Integrin alpha-IIb OS=Homo sapiens OX=9606 GN=ITGA2B PE=1 SV=3
Q9NTJ5	Phosphatidylinositide phosphatase SAC1 OS=Homo sapiens OX=9606 GN=SACM1L PE=1 SV=2
Q00796	Sorbitol dehydrogenase OS=Homo sapiens OX=9606 GN=SORD PE=1 SV=4
P02774	Vitamin D-binding protein OS=Homo sapiens OX=9606 GN=GC PE=1 SV=2
Q3YEC7	Rab-like protein 6 OS=Homo sapiens OX=9606 GN=RABL6 PE=1 SV=2
Q8WXH0	Nesprin-2 OS=Homo sapiens OX=9606 GN=SYNE2 PE=1 SV=3
P01042	Kininogen-1 OS=Homo sapiens OX=9606 GN=KNG1 PE=1 SV=2
Q15942	Zyxin OS=Homo sapiens OX=9606 GN=ZYX PE=1 SV=1
P20936	Ras GTPase-activating protein 1 OS=Homo sapiens OX=9606 GN=RASA1 PE=1 SV=1
Q6IBS0	Twinfilin-2 OS=Homo sapiens OX=9606 GN=TWF2 PE=1 SV=2
Q96IU4	Protein ABHD14B OS=Homo sapiens OX=9606 GN=ABHD14B PE=1 SV=1
P02787	Serotransferrin OS=Homo sapiens OX=9606 GN=TF PE=1 SV=3
Q15833	Syntaxin-binding protein 2 OS=Homo sapiens OX=9606 GN=STXBP2 PE=1 SV=2
Q16181	Septin-7 OS=Homo sapiens OX=9606 GN=SEPTIN7 PE=1 SV=2
P40227	T-complex protein 1 subunit zeta OS=Homo sapiens OX=9606 GN=CCT6A PE=1 SV=3
P02751	Fibronectin OS=Homo sapiens OX=9606 GN=FN1 PE=1 SV=5
Q9NR56	Muscleblind-like protein 1 OS=Homo sapiens OX=9606 GN=MBNL1 PE=1 SV=2
Q9UFN0	Protein NipSnap homolog 3A OS=Homo sapiens OX=9606 GN=NIPSNAP3A PE=1 SV=2
Q9UEW8	STE20/SPS1-related proline-alanine-rich protein kinase OS=Homo sapiens OX=9606 GN=STK39 PE=1 SV=3
P50851	Lipopolysaccharide-responsive and beige-like anchor protein OS=Homo sapiens OX=9606 GN=LRBA PE=1 SV=4
Q9Y6C2	EMILIN-1 OS=Homo sapiens OX=9606 GN=EMILIN1 PE=1 SV=3
O43242	26S proteasome non-ATPase regulatory subunit 3 OS=Homo sapiens OX=9606 GN=PSMD3 PE=1 SV=2
Q0ZGT2	Nexilin OS=Homo sapiens OX=9606 GN=NEXN PE=1 SV=1
P55884	Eukaryotic translation initiation factor 3 subunit B OS=Homo sapiens OX=9606 GN=EIF3B PE=1 SV=3
P06703	Protein S100-A6 OS=Homo sapiens OX=9606 GN=S100A6 PE=1 SV=1
P48735	Isocitrate dehydrogenase (NADP) mitochondrial OS=Homo sapiens OX=9606 GN=IDH2 PE=1 SV=2
P29144	Tripeptidyl-peptidase 2 OS=Homo sapiens OX=9606 GN=TPP2 PE=1 SV=4
P19105	Myosin regulatory light chain 12A OS=Homo sapiens OX=9606 GN=MYL12A PE=1 SV=2
O95197	Reticulon-3 OS=Homo sapiens OX=9606 GN=RTN3 PE=1 SV=2
Q8WUM4	Programmed cell death 6-interacting protein OS=Homo sapiens OX=9606 GN=PDCD6IP PE=1 SV=1
O43707	Alpha-actinin-4 OS=Homo sapiens OX=9606 GN=ACTN4 PE=1 SV=2
Q9NS28	Regulator of G-protein signaling 18 OS=Homo sapiens OX=9606 GN=RGS18 PE=1 SV=1
P49588	Alanine--tRNA ligase, cytoplasmic OS=Homo sapiens OX=9606 GN=AARS1 PE=1 SV=2
Q9UNM6	26S proteasome non-ATPase regulatory subunit 13 OS=Homo sapiens OX=9606 GN=PSMD13 PE=1 SV=2

P16152	Carbonyl reductase (NADPH) 1 OS=Homo sapiens OX=9606 GN=CBR1 PE=1 SV=3
O95630	STAM-binding protein OS=Homo sapiens OX=9606 GN=STAMBP PE=1 SV=1
Q86TP1	Exopolyphosphatase PRUNE1 OS=Homo sapiens OX=9606 GN=PRUNE1 PE=1 SV=2
Q8TEA8	D-aminoacyl-tRNA deacylase 1 OS=Homo sapiens OX=9606 GN=DTD1 PE=1 SV=2
Q9UDT6	CAP-Gly domain-containing linker protein 2 OS=Homo sapiens OX=9606 GN=CLIP2 PE=1 SV=1
Q9NZN3	EH domain-containing protein 3 OS=Homo sapiens OX=9606 GN=EHD3 PE=1 SV=2
Q96M96	FYVE, RhoGEF and PH domain-containing protein 4 OS=Homo sapiens OX=9606 GN=FGD4 PE=1 SV=2
P62993	Growth factor receptor-bound protein 2 OS=Homo sapiens OX=9606 GN=GRB2 PE=1 SV=1
Q9NZ52	ADP-ribosylation factor-binding protein GGA3 OS=Homo sapiens OX=9606 GN=GGA3 PE=1 SV=1
Q9Y6F6	Protein MRVI1 OS=Homo sapiens OX=9606 GN=MRVI1 PE=1 SV=4
Q9NVA2	Septin-11 OS=Homo sapiens OX=9606 GN=SEPTIN11 PE=1 SV=3
P13639	Elongation factor 2 OS=Homo sapiens OX=9606 GN=EEF2 PE=1 SV=4
Q05655	Protein kinase C delta type OS=Homo sapiens OX=9606 GN=PRKCD PE=1 SV=2
P31939	Bifunctional purine biosynthesis protein PURH OS=Homo sapiens OX=9606 GN=ATIC PE=1 SV=3
P50570	Dynamin-2 OS=Homo sapiens OX=9606 GN=DNM2 PE=1 SV=2
Q9BSF0	Small membrane A-kinase anchor protein OS=Homo sapiens OX=9606 GN=C2orf88 PE=1 SV=2
P31948	Stress-induced-phosphoprotein 1 OS=Homo sapiens OX=9606 GN=STIP1 PE=1 SV=1
Q6ZNJ1	Neurobeachin-like protein 2 OS=Homo sapiens OX=9606 GN=NBEAL2 PE=1 SV=2
Q96FJ2	Dynein light chain 2, cytoplasmic OS=Homo sapiens OX=9606 GN=DYNLL2 PE=1 SV=1
P60660	Myosin light polypeptide 6 OS=Homo sapiens OX=9606 GN=MYL6 PE=1 SV=2
Q9P2E9	Ribosome-binding protein 1 OS=Homo sapiens OX=9606 GN=RRBP1 PE=1 SV=5
Q00688	Peptidyl-prolyl cis-trans isomerase FKBP3 OS=Homo sapiens OX=9606 GN=FKBP3 PE=1 SV=1
P11171	Protein 4.1 OS=Homo sapiens OX=9606 GN=EPB41 PE=1 SV=4
Q9UQ80	Proliferation-associated protein 2G4 OS=Homo sapiens OX=9606 GN=PA2G4 PE=1 SV=3
Q96AX2	Ras-related protein Rab-37 OS=Homo sapiens OX=9606 GN=RAB37 PE=1 SV=3
O43747	AP-1 complex subunit gamma-1 OS=Homo sapiens OX=9606 GN=AP1G1 PE=1 SV=5
P15374	Ubiquitin carboxyl-terminal hydrolase isozyme L3 OS=Homo sapiens OX=9606 GN=UCHL3 PE=1 SV=1
P55786	Puromycin-sensitive aminopeptidase OS=Homo sapiens OX=9606 GN=NPEPPS PE=1 SV=2
Q562R1	Beta-actin-like protein 2 OS=Homo sapiens OX=9606 GN=ACTBL2 PE=1 SV=2
Q9H1Z4	WD repeat-containing protein 13 OS=Homo sapiens OX=9606 GN=WDR13 PE=1 SV=2
O75563	Src kinase-associated phosphoprotein 2 OS=Homo sapiens OX=9606 GN=SKAP2 PE=1 SV=1
P04439	HLA class I histocompatibility antigen, A alpha chain OS=Homo sapiens OX=9606 GN=HLA-A PE=1 SV=2
P42025	Beta-centractin OS=Homo sapiens OX=9606 GN=ACTR1B PE=1 SV=1
Q14254	Flotillin-2 OS=Homo sapiens OX=9606 GN=FLOT2 PE=1 SV=2
Q06830	Peroxiredoxin-1 OS=Homo sapiens OX=9606 GN=PRDX1 PE=1 SV=1

Q15435	Protein phosphatase 1 regulatory subunit 7 OS=Homo sapiens OX=9606 GN=PPP1R7 PE=1 SV=1
P17612	cAMP-dependent protein kinase catalytic subunit alpha OS=Homo sapiens OX=9606 GN=PRKACA PE=1 SV=2
Q9NQ75	Cas scaffolding protein family member 4 OS=Homo sapiens OX=9606 GN=CASS4 PE=1 SV=2
P06727	Apolipoprotein A-IV OS=Homo sapiens OX=9606 GN=APOA4 PE=1 SV=3
P63010	AP-2 complex subunit beta OS=Homo sapiens OX=9606 GN=AP2B1 PE=1 SV=1
Q8IX18	Probable ATP-dependent RNA helicase DHX40 OS=Homo sapiens OX=9606 GN=DHX40 PE=1 SV=2
P49593	Protein phosphatase 1F OS=Homo sapiens OX=9606 GN=PPM1F PE=1 SV=3
O14979	Heterogeneous nuclear ribonucleoprotein D-like OS=Homo sapiens OX=9606 GN=HNRNPDL PE=1 SV=3
Q9Y3F4	Serine-threonine kinase receptor-associated protein OS=Homo sapiens OX=9606 GN=STRAP PE=1 SV=1
Q07960	Rho GTPase-activating protein 1 OS=Homo sapiens OX=9606 GN=ARHGAP1 PE=1 SV=1
P05155	Plasma protease C1 inhibitor OS=Homo sapiens OX=9606 GN=SERPING1 PE=1 SV=2
P27105	Erythrocyte band 7 integral membrane protein OS=Homo sapiens OX=9606 GN=STOM PE=1 SV=3
Q9H4A3	Serine/threonine-protein kinase WNK1 OS=Homo sapiens OX=9606 GN=WNK1 PE=1 SV=2
Q8NEZ2	Vacuolar protein sorting-associated protein 37A OS=Homo sapiens OX=9606 GN=VPS37A PE=1 SV=1
Q12913	Receptor-type tyrosine-protein phosphatase eta OS=Homo sapiens OX=9606 GN=PTPRJ PE=1 SV=3
P51858	Hepatoma-derived growth factor OS=Homo sapiens OX=9606 GN=HDGF PE=1 SV=1
P54577	Tyrosine--tRNA ligase, cytoplasmic OS=Homo sapiens OX=9606 GN=YARS1 PE=1 SV=4
O60493	Sorting nexin-3 OS=Homo sapiens OX=9606 GN=SNX3 PE=1 SV=3
P01599	Immunoglobulin kappa variable 1-17 OS=Homo sapiens OX=9606 GN=IGKV1-17 PE=1 SV=2
P19634	Sodium/hydrogen exchanger 1 OS=Homo sapiens OX=9606 GN=SLC9A1 PE=1 SV=2
Q9BS26	Endoplasmic reticulum resident protein 44 OS=Homo sapiens OX=9606 GN=ERP44 PE=1 SV=1
P01601	Immunoglobulin kappa variable 1D-16 OS=Homo sapiens OX=9606 GN=IGKV1D-16 PE=3 SV=2
P23526	Adenosylhomocysteinase OS=Homo sapiens OX=9606 GN=AHCY PE=1 SV=4
Q7L576	Cytoplasmic FMR1-interacting protein 1 OS=Homo sapiens OX=9606 GN=CYFIP1 PE=1 SV=1
P50148	Guanine nucleotide-binding protein G(q) subunit alpha OS=Homo sapiens OX=9606 GN=GNAQ PE=1 SV=4
P00491	Purine nucleoside phosphorylase OS=Homo sapiens OX=9606 GN=PNP PE=1 SV=2
P0DOX7	Immunoglobulin kappa light chain OS=Homo sapiens OX=9606 PE=1 SV=1
Q99627	COP9 signalosome complex subunit 8 OS=Homo sapiens OX=9606 GN=COPS8 PE=1 SV=1
P48637	Glutathione synthetase OS=Homo sapiens OX=9606 GN=GSS PE=1 SV=1
P08603	Complement factor H OS=Homo sapiens OX=9606 GN=CFH PE=1 SV=4
P24666	Low molecular weight phosphotyrosine protein phosphatase OS=Homo sapiens OX=9606 GN=ACP1 PE=1 SV=3
P14868	Aspartate--tRNA ligase, cytoplasmic OS=Homo sapiens OX=9606 GN=DARS1 PE=1 SV=2
Q9NVK5	FGFR1 oncogene partner 2 OS=Homo sapiens OX=9606 GN=FGFR1OP2 PE=1 SV=1
P63098	Calcineurin subunit B type 1 OS=Homo sapiens OX=9606 GN=PPP3R1 PE=1 SV=2
P02763	Alpha-1-acid glycoprotein 1 OS=Homo sapiens OX=9606 GN=ORM1 PE=1 SV=1

Q96AT9	Ribulose-phosphate 3-epimerase OS=Homo sapiens OX=9606 GN=RPE PE=1 SV=1
O60496	Docking protein 2 OS=Homo sapiens OX=9606 GN=DOK2 PE=1 SV=2
P0C0L4	Complement C4-A OS=Homo sapiens OX=9606 GN=C4A PE=1 SV=2
Q5H9R7	Serine/threonine-protein phosphatase 6 regulatory subunit 3 OS=Homo sapiens OX=9606 GN=PPP6R3 PE=1 SV=2
P61586	Transforming protein RhoA OS=Homo sapiens OX=9606 GN=RHOA PE=1 SV=1
Q00610	Clathrin heavy chain 1 OS=Homo sapiens OX=9606 GN=CLTC PE=1 SV=5
O94919	Endonuclease domain-containing 1 protein OS=Homo sapiens OX=9606 GN=ENDOD1 PE=1 SV=2
P30740	Leukocyte elastase inhibitor OS=Homo sapiens OX=9606 GN=SERPINB1 PE=1 SV=1
O95373	Importin-7 OS=Homo sapiens OX=9606 GN=IPO7 PE=1 SV=1
Q96CN7	Isochorismatase domain-containing protein 1 OS=Homo sapiens OX=9606 GN=ISOC1 PE=1 SV=3
Q96KP4	Cytosolic non-specific dipeptidase OS=Homo sapiens OX=9606 GN=CNDP2 PE=1 SV=2
P61020	Ras-related protein Rab-5B OS=Homo sapiens OX=9606 GN=RAB5B PE=1 SV=1
P02647	Apolipoprotein A-I OS=Homo sapiens OX=9606 GN=APOA1 PE=1 SV=1
Q6ZVM7	TOM1-like protein 2 OS=Homo sapiens OX=9606 GN=TOM1L2 PE=1 SV=1
Q86X76	Deaminated glutathione amidase OS=Homo sapiens OX=9606 GN=NIT1 PE=1 SV=2
P31146	Coronin-1A OS=Homo sapiens OX=9606 GN=CORO1A PE=1 SV=4
Q9UL46	Proteasome activator complex subunit 2 OS=Homo sapiens OX=9606 GN=PSME2 PE=1 SV=4
Q02108	Guanylate cyclase soluble subunit alpha-1 OS=Homo sapiens OX=9606 GN=GUCY1A1 PE=1 SV=2
Q7Z3D4	LysM and putative peptidoglycan-binding domain-containing protein 3 OS=Homo sapiens OX=9606 GN=LYSMD3 PE=1 SV=2
Q13867	Bleomycin hydrolase OS=Homo sapiens OX=9606 GN=BLMH PE=1 SV=1
O95721	Synaptosomal-associated protein 29 OS=Homo sapiens OX=9606 GN=SNAP29 PE=1 SV=1
Q9UJC5	SH3 domain-binding glutamic acid-rich-like protein 2 OS=Homo sapiens OX=9606 GN=SH3BGRL2 PE=1 SV=2
Q9C0H2	Protein tweety homolog 3 OS=Homo sapiens OX=9606 GN=TTYH3 PE=1 SV=3
P36955	Pigment epithelium-derived factor OS=Homo sapiens OX=9606 GN=SERPINF1 PE=1 SV=4
P07357	Complement component C8 alpha chain OS=Homo sapiens OX=9606 GN=C8A PE=1 SV=2
P55160	Nck-associated protein 1-like OS=Homo sapiens OX=9606 GN=NCKAP1L PE=1 SV=3
Q9HC38	Glyoxalase domain-containing protein 4 OS=Homo sapiens OX=9606 GN=GLOD4 PE=1 SV=1
Q99417	c-Myc-binding protein OS=Homo sapiens OX=9606 GN=MYCBP PE=1 SV=3
P43686	26S proteasome regulatory subunit 6B OS=Homo sapiens OX=9606 GN=PSMC4 PE=1 SV=2
Q9Y613	FH1/FH2 domain-containing protein 1 OS=Homo sapiens OX=9606 GN=FHOD1 PE=1 SV=3
Q9H939	Proline-serine-threonine phosphatase-interacting protein 2 OS=Homo sapiens OX=9606 GN=PSTPIP2 PE=1 SV=4
P19827	Inter-alpha-trypsin inhibitor heavy chain H1 OS=Homo sapiens OX=9606 GN=ITIH1 PE=1 SV=3
P50453	Serpin B9 OS=Homo sapiens OX=9606 GN=SERPINB9 PE=1 SV=1
P14317	Hematopoietic lineage cell-specific protein OS=Homo sapiens OX=9606 GN=HCLS1 PE=1 SV=3
P09211	Glutathione S-transferase P OS=Homo sapiens OX=9606 GN=GSTP1 PE=1 SV=2

Q6UXH1	Protein disulfide isomerase CRELD2 OS=Homo sapiens OX=9606 GN=CRELD2 PE=1 SV=1
P37840	Alpha-synuclein OS=Homo sapiens OX=9606 GN=SNCA PE=1 SV=1
Q14847	LIM and SH3 domain protein 1 OS=Homo sapiens OX=9606 GN=LASP1 PE=1 SV=2
Q9H2K8	Serine/threonine-protein kinase TAO3 OS=Homo sapiens OX=9606 GN=TAOK3 PE=1 SV=2
Q14240	Eukaryotic initiation factor 4A-II OS=Homo sapiens OX=9606 GN=EIF4A2 PE=1 SV=2
O43312	Protein MTSS 1 OS=Homo sapiens OX=9606 GN=MTSS1 PE=1 SV=2
P19652	Alpha-1-acid glycoprotein 2 OS=Homo sapiens OX=9606 GN=ORM2 PE=1 SV=2
P06737	Glycogen phosphorylase, liver form OS=Homo sapiens OX=9606 GN=PYGL PE=1 SV=4
P23229	Integrin alpha-6 OS=Homo sapiens OX=9606 GN=ITGA6 PE=1 SV=5
O75340	Programmed cell death protein 6 OS=Homo sapiens OX=9606 GN=PDCD6 PE=1 SV=1
Q07817	Bcl-2-like protein 1 OS=Homo sapiens OX=9606 GN=BCL2L1 PE=1 SV=1
P22307	Non-specific lipid-transfer protein OS=Homo sapiens OX=9606 GN=SCP2 PE=1 SV=2
Q9Y5K6	CD2-associated protein OS=Homo sapiens OX=9606 GN=CD2AP PE=1 SV=1
O75368	SH3 domain-binding glutamic acid-rich-like protein OS=Homo sapiens OX=9606 GN=SH3BGRL PE=1 SV=1
Q96GD0	Pyridoxal phosphate phosphatase OS=Homo sapiens OX=9606 GN=PDXP PE=1 SV=2
O15143	Actin-related protein 2/3 complex subunit 1B OS=Homo sapiens OX=9606 GN=ARPC1B PE=1 SV=3
Q16539	Mitogen-activated protein kinase 14 OS=Homo sapiens OX=9606 GN=MAPK14 PE=1 SV=3
P37837	Transaldolase OS=Homo sapiens OX=9606 GN=TALDO1 PE=1 SV=2
P10321	HLA class I histocompatibility antigen, C alpha chain OS=Homo sapiens OX=9606 GN=HLA-C PE=1 SV=3
P98171	Rho GTPase-activating protein 4 OS=Homo sapiens OX=9606 GN=ARHGAP4 PE=1 SV=2
Q99959	Plakophilin-2 OS=Homo sapiens OX=9606 GN=PKP2 PE=1 SV=2
P13797	Plastin-3 OS=Homo sapiens OX=9606 GN=PLS3 PE=1 SV=4
P61019	Ras-related protein Rab-2A OS=Homo sapiens OX=9606 GN=RAB2A PE=1 SV=1
Q15075	Early endosome antigen 1 OS=Homo sapiens OX=9606 GN=EEA1 PE=1 SV=2
P06733	Alpha-enolase OS=Homo sapiens OX=9606 GN=ENO1 PE=1 SV=2
P63000	Ras-related C3 botulinum toxin substrate 1 OS=Homo sapiens OX=9606 GN=RAC1 PE=1 SV=1
A0A0B4J1Y9	Immunoglobulin heavy variable 3-72 OS=Homo sapiens OX=9606 GN=IGHV3-72 PE=3 SV=1
P10809	60 kDa heat shock protein, mitochondrial OS=Homo sapiens OX=9606 GN=HSPD1 PE=1 SV=2
P04179	Superoxide dismutase Mn, mitochondrial OS=Homo sapiens OX=9606 GN=SOD2 PE=1 SV=3
P25325	3-mercaptopyruvate sulfurtransferase OS=Homo sapiens OX=9606 GN=MPST PE=1 SV=3
Q9UMX5	Neudesin OS=Homo sapiens OX=9606 GN=NENF PE=1 SV=1
P30566	Adenylosuccinate lyase OS=Homo sapiens OX=9606 GN=ADSL PE=1 SV=2
P01011	Alpha-1-antichymotrypsin OS=Homo sapiens OX=9606 GN=SERPINA3 PE=1 SV=2
P16109	P-selectin OS=Homo sapiens OX=9606 GN=SELP PE=1 SV=3
Q14155	Rho guanine nucleotide exchange factor 7 OS=Homo sapiens OX=9606 GN=ARHGEF7 PE=1 SV=2

Q9NXR7	BRISC and BRCA1-A complex member 2 OS=Homo sapiens OX=9606 GN=BABAM2 PE=1 SV=2
O43396	Thioredoxin-like protein 1 OS=Homo sapiens OX=9606 GN=TXNL1 PE=1 SV=3
P00387	NADH-cytochrome b5 reductase 3 OS=Homo sapiens OX=9606 GN=CYB5R3 PE=1 SV=3
Q16543	Hsp90 co-chaperone Cdc37 OS=Homo sapiens OX=9606 GN=CDC37 PE=1 SV=1
Q7Z406	Myosin-14 OS=Homo sapiens OX=9606 GN=MYH14 PE=1 SV=2
P22694	cAMP-dependent protein kinase catalytic subunit beta OS=Homo sapiens OX=9606 GN=PRKACB PE=1 SV=2
Q15084	Protein disulfide-isomerase A6 OS=Homo sapiens OX=9606 GN=PDIA6 PE=1 SV=1
P02649	Apolipoprotein E OS=Homo sapiens OX=9606 GN=APOE PE=1 SV=1
P14543	Nidogen-1 OS=Homo sapiens OX=9606 GN=NID1 PE=1 SV=3
Q9NP79	Vacuolar protein sorting-associated protein VTA1 homolog OS=Homo sapiens OX=9606 GN=VTA1 PE=1 SV=1
Q13418	Integrin-linked protein kinase OS=Homo sapiens OX=9606 GN=ILK PE=1 SV=2
Q92598	Heat shock protein 105 kDa OS=Homo sapiens OX=9606 GN=HSPH1 PE=1 SV=1
Q13464	Rho-associated protein kinase 1 OS=Homo sapiens OX=9606 GN=ROCK1 PE=1 SV=1
Q01082	Spectrin beta chain, non-erythrocytic 1 OS=Homo sapiens OX=9606 GN=SPTBN1 PE=1 SV=2
P28062	Proteasome subunit beta type-8 OS=Homo sapiens OX=9606 GN=PSMB8 PE=1 SV=3
P47756	F-actin-capping protein subunit beta OS=Homo sapiens OX=9606 GN=CAPZB PE=1 SV=4
P10599	Thioredoxin OS=Homo sapiens OX=9606 GN=TXN PE=1 SV=3
P35611	Alpha-adducin OS=Homo sapiens OX=9606 GN=ADD1 PE=1 SV=2
O60888	Protein CutA OS=Homo sapiens OX=9606 GN=CUTA PE=1 SV=2
O75083	WD repeat-containing protein 1 OS=Homo sapiens OX=9606 GN=WDR1 PE=1 SV=4
P61158	Actin-related protein 3 OS=Homo sapiens OX=9606 GN=ACTR3 PE=1 SV=3
P02766	Transthyretin OS=Homo sapiens OX=9606 GN=TTR PE=1 SV=1
P42574	Caspase-3 OS=Homo sapiens OX=9606 GN=CASP3 PE=1 SV=2
Q6YHK3	CD109 antigen OS=Homo sapiens OX=9606 GN=CD109 PE=1 SV=2
Q13442	28 kDa heat- and acid-stable phosphoprotein OS=Homo sapiens OX=9606 GN=PDAP1 PE=1 SV=1
O43852	Calumenin OS=Homo sapiens OX=9606 GN=CALU PE=1 SV=2
P52788	Spermine synthase OS=Homo sapiens OX=9606 GN=SMS PE=1 SV=2
P40925	Malate dehydrogenase, cytoplasmic OS=Homo sapiens OX=9606 GN=MDH1 PE=1 SV=4
P35606	Coatomer subunit beta' OS=Homo sapiens OX=9606 GN=COPB2 PE=1 SV=2
P00505	Aspartate aminotransferase, mitochondrial OS=Homo sapiens OX=9606 GN=GOT2 PE=1 SV=3
Q969R2	Oxysterol-binding protein 2 OS=Homo sapiens OX=9606 GN=OSBP2 PE=1 SV=2
P34896	Serine hydroxymethyltransferase, cytosolic OS=Homo sapiens OX=9606 GN=SHMT1 PE=1 SV=1
P23284	Peptidyl-prolyl cis-trans isomerase B OS=Homo sapiens OX=9606 GN=PPIB PE=1 SV=2
P00751	Complement factor B OS=Homo sapiens OX=9606 GN=CFB PE=1 SV=2
Q0VDG4	Secernin-3 OS=Homo sapiens OX=9606 GN=SCRN3 PE=1 SV=1

P07951	Tropomyosin beta chain OS=Homo sapiens OX=9606 GN=TPM2 PE=1 SV=1
Q9P289	Serine/threonine-protein kinase 26 OS=Homo sapiens OX=9606 GN=STK26 PE=1 SV=2
P07359	Platelet glycoprotein Ib alpha chain OS=Homo sapiens OX=9606 GN=GP1BA PE=1 SV=2
Q5T2E6	Armadillo-like helical domain-containing protein 3 OS=Homo sapiens OX=9606 GN=ARMH3 PE=1 SV=1
Q5SQ64	Lymphocyte antigen 6 complex locus protein G6f OS=Homo sapiens OX=9606 GN=LY6G6F PE=1 SV=2
Q8IUZ5	5-phosphohydroxy-L-lysine phospho-lyase OS=Homo sapiens OX=9606 GN=PHYKPL PE=1 SV=1
P07203	Glutathione peroxidase 1 OS=Homo sapiens OX=9606 GN=GPX1 PE=1 SV=4
Q9NYU2	UDP-glucose:glycoprotein glucosyltransferase 1 OS=Homo sapiens OX=9606 GN=UGGT1 PE=1 SV=3
Q53FA7	Quinone oxidoreductase PIG3 OS=Homo sapiens OX=9606 GN=TP53I3 PE=1 SV=2
Q14019	Coactosin-like protein OS=Homo sapiens OX=9606 GN=COTL1 PE=1 SV=3
P07437	Tubulin beta chain OS=Homo sapiens OX=9606 GN=TUBB PE=1 SV=2
P14618	Pyruvate kinase PKM OS=Homo sapiens OX=9606 GN=PKM PE=1 SV=4
Q9Y2B0	Protein canopy homolog 2 OS=Homo sapiens OX=9606 GN=CNPY2 PE=1 SV=1
P50552	Vasodilator-stimulated phosphoprotein OS=Homo sapiens OX=9606 GN=VASP PE=1 SV=3
P55010	Eukaryotic translation initiation factor 5 OS=Homo sapiens OX=9606 GN=EIF5 PE=1 SV=2
Q9BQE3	Tubulin alpha-1C chain OS=Homo sapiens OX=9606 GN=TUBA1C PE=1 SV=1
P84085	ADP-ribosylation factor 5 OS=Homo sapiens OX=9606 GN=ARF5 PE=1 SV=2
Q8TCF1	AN1-type zinc finger protein 1 OS=Homo sapiens OX=9606 GN=ZFAND1 PE=1 SV=1
P62826	GTP-binding nuclear protein Ran OS=Homo sapiens OX=9606 GN=RAN PE=1 SV=3
Q14157	Ubiquitin-associated protein 2-like OS=Homo sapiens OX=9606 GN=UBAP2L PE=1 SV=2
P01860	Immunoglobulin heavy constant gamma 3 OS=Homo sapiens OX=9606 GN=IGHG3 PE=1 SV=2
O00154	Cytosolic acyl coenzyme A thioester hydrolase OS=Homo sapiens OX=9606 GN=ACOT7 PE=1 SV=3
O15400	Syntaxin-7 OS=Homo sapiens OX=9606 GN=STX7 PE=1 SV=4
P02749	Beta-2-glycoprotein 1 OS=Homo sapiens OX=9606 GN=APOH PE=1 SV=3
P68371	Tubulin beta-4B chain OS=Homo sapiens OX=9606 GN=TUBB4B PE=1 SV=1
P50395	Rab GDP dissociation inhibitor beta OS=Homo sapiens OX=9606 GN=GDI2 PE=1 SV=2
P01591	Immunoglobulin J chain OS=Homo sapiens OX=9606 GN=JCHAIN PE=1 SV=4
Q6FI81	Anamorsin OS=Homo sapiens OX=9606 GN=CIAPIN1 PE=1 SV=2
Q9UNZ2	NSFL1 cofactor p47 OS=Homo sapiens OX=9606 GN=NSFL1C PE=1 SV=2
P68032	Actin, alpha cardiac muscle 1 OS=Homo sapiens OX=9606 GN=ACTC1 PE=1 SV=1
P61916	NPC intracellular cholesterol transporter 2 OS=Homo sapiens OX=9606 GN=NPC2 PE=1 SV=1
P07108	Acyl-CoA-binding protein OS=Homo sapiens OX=9606 GN=DBI PE=1 SV=2
Q15008	26S proteasome non-ATPase regulatory subunit 6 OS=Homo sapiens OX=9606 GN=PSMD6 PE=1 SV=1
Q9H7J1	Protein phosphatase 1 regulatory subunit 3E OS=Homo sapiens OX=9606 GN=PPP1R3E PE=1 SV=2
O60256	Phosphoribosyl pyrophosphate synthase-associated protein 2 OS=Homo sapiens OX=9606 GN=PRPSAP2 PE=1 SV=1

A0A0C4DH25	Immunoglobulin kappa variable 3D-20 OS=Homo sapiens OX=9606 GN=IGKV3D-20 PE=3 SV=1
P02790	Hemopexin OS=Homo sapiens OX=9606 GN=HPX PE=1 SV=2
P20042	Eukaryotic translation initiation factor 2 subunit 2 OS=Homo sapiens OX=9606 GN=EIF2S2 PE=1 SV=2
P16930	Fumarylacetoacetase OS=Homo sapiens OX=9606 GN=FAH PE=1 SV=2
P49368	T-complex protein 1 subunit gamma OS=Homo sapiens OX=9606 GN=CCT3 PE=1 SV=4
O43681	ATPase ASNA1 OS=Homo sapiens OX=9606 GN=ASNA1 PE=1 SV=2
Q9UHD8	Septin-9 OS=Homo sapiens OX=9606 GN=SEPTIN9 PE=1 SV=2
P11940	Polyadenylate-binding protein 1 OS=Homo sapiens OX=9606 GN=PABPC1 PE=1 SV=2
P22392	Nucleoside diphosphate kinase B OS=Homo sapiens OX=9606 GN=NME2 PE=1 SV=1
O00442	RNA 3'-terminal phosphate cyclase OS=Homo sapiens OX=9606 GN=RTCA PE=1 SV=1
Q13459	Unconventional myosin-IXb OS=Homo sapiens OX=9606 GN=MYO9B PE=1 SV=3
P01714	Immunoglobulin lambda variable 3-19 OS=Homo sapiens OX=9606 GN=IGLV3-19 PE=1 SV=2
Q4V328	GRIP1-associated protein 1 OS=Homo sapiens OX=9606 GN=GRIPAP1 PE=1 SV=2
Q9H0U4	Ras-related protein Rab-1B OS=Homo sapiens OX=9606 GN=RAB1B PE=1 SV=1
P08758	Annexin A5 OS=Homo sapiens OX=9606 GN=ANXA5 PE=1 SV=2
P63167	Dynein light chain 1, cytoplasmic OS=Homo sapiens OX=9606 GN=DYNLL1 PE=1 SV=1
Q9Y3C8	Ubiquitin-fold modifier-conjugating enzyme 1 OS=Homo sapiens OX=9606 GN=UFC1 PE=1 SV=3
Q14624	Inter-alpha-trypsin inhibitor heavy chain H4 OS=Homo sapiens OX=9606 GN=ITIH4 PE=1 SV=4
P52209	6-phosphogluconate dehydrogenase, decarboxylating OS=Homo sapiens OX=9606 GN=PGD PE=1 SV=3
Q9BT09	Protein canopy homolog 3 OS=Homo sapiens OX=9606 GN=CNPY3 PE=1 SV=1
P08174	Complement decay-accelerating factor OS=Homo sapiens OX=9606 GN=CD55 PE=1 SV=4
P0C0L5	Complement C4-B OS=Homo sapiens OX=9606 GN=C4B PE=1 SV=2
Q8TDQ7	Glucosamine-6-phosphate isomerase 2 OS=Homo sapiens OX=9606 GN=GNPDA2 PE=1 SV=1
P04424	Argininosuccinate lyase OS=Homo sapiens OX=9606 GN=ASL PE=1 SV=4
P61088	Ubiquitin-conjugating enzyme E2 N OS=Homo sapiens OX=9606 GN=UBE2N PE=1 SV=1
Q9P2T1	GMP reductase 2 OS=Homo sapiens OX=9606 GN=GMPR2 PE=1 SV=1
Q8NEU8	DCC-interacting protein 13-beta OS=Homo sapiens OX=9606 GN=APPL2 PE=1 SV=3
P52907	F-actin-capping protein subunit alpha-1 OS=Homo sapiens OX=9606 GN=CAPZA1 PE=1 SV=3
P49407	Beta-arrestin-1 OS=Homo sapiens OX=9606 GN=ARRB1 PE=1 SV=2
Q15382	GTP-binding protein Rheb OS=Homo sapiens OX=9606 GN=RHEB PE=1 SV=1
P62942	Peptidyl-prolyl cis-trans isomerase FKBP1A OS=Homo sapiens OX=9606 GN=FKBP1A PE=1 SV=2
Q14118	Dystroglycan OS=Homo sapiens OX=9606 GN=DAG1 PE=1 SV=2
Q8N392	Rho GTPase-activating protein 18 OS=Homo sapiens OX=9606 GN=ARHGAP18 PE=1 SV=3
Q8WWA1	Transmembrane protein 40 OS=Homo sapiens OX=9606 GN=TMEM40 PE=1 SV=2
O75915	PRA1 family protein 3 OS=Homo sapiens OX=9606 GN=ARL6IP5 PE=1 SV=1

Q99439	Calponin-2 OS=Homo sapiens OX=9606 GN=CNN2 PE=1 SV=4
P06312	Immunoglobulin kappa variable 4-1 OS=Homo sapiens OX=9606 GN=IGKV4-1 PE=1 SV=1
Q96IZ0	PRKC apoptosis WT1 regulator protein OS=Homo sapiens OX=9606 GN=PAWR PE=1 SV=1
Q8IUI8	Cytokine receptor-like factor 3 OS=Homo sapiens OX=9606 GN=CRLF3 PE=1 SV=2
Q9ULA0	Aspartyl aminopeptidase OS=Homo sapiens OX=9606 GN=DNPEP PE=1 SV=1
P48643	T-complex protein 1 subunit epsilon OS=Homo sapiens OX=9606 GN=CCT5 PE=1 SV=1
Q01469	Fatty acid-binding protein 5 OS=Homo sapiens OX=9606 GN=FABP5 PE=1 SV=3
P09960	Leukotriene A-4 hydrolase OS=Homo sapiens OX=9606 GN=LTA4H PE=1 SV=2
Q9H4M9	EH domain-containing protein 1 OS=Homo sapiens OX=9606 GN=EHD1 PE=1 SV=2
O14672	Disintegrin and metalloproteinase domain-containing protein 10 OS=Homo sapiens OX=9606 GN=ADAM10 PE=1 SV=1
Q9BPZ3	Polyadenylate-binding protein-interacting protein 2 OS=Homo sapiens OX=9606 GN=PAIP2 PE=1 SV=1
Q03591	Complement factor H-related protein 1 OS=Homo sapiens OX=9606 GN=CFHR1 PE=1 SV=2
P50579	Methionine aminopeptidase 2 OS=Homo sapiens OX=9606 GN=METAP2 PE=1 SV=1
O43149	Zinc finger ZZ-type and EF-hand domain-containing protein 1 OS=Homo sapiens OX=9606 GN=ZZEF1 PE=1 SV=6
Q13510	Acid ceramidase OS=Homo sapiens OX=9606 GN=ASAH1 PE=1 SV=5
P10909	Clusterin OS=Homo sapiens OX=9606 GN=CLU PE=1 SV=1
Q9UBW5	Bridging integrator 2 OS=Homo sapiens OX=9606 GN=BIN2 PE=1 SV=3
P07384	Calpain-1 catalytic subunit OS=Homo sapiens OX=9606 GN=CAPN1 PE=1 SV=1
P14314	Glucosidase 2 subunit beta OS=Homo sapiens OX=9606 GN=PRKCSH PE=1 SV=2
Q13177	Serine/threonine-protein kinase PAK 2 OS=Homo sapiens OX=9606 GN=PAK2 PE=1 SV=3
Q9Y376	Calcium-binding protein 39 OS=Homo sapiens OX=9606 GN=CAB39 PE=1 SV=1
Q14BN4	Sarcolemmal membrane-associated protein OS=Homo sapiens OX=9606 GN=SLMAP PE=1 SV=1
O14818	Proteasome subunit alpha type-7 OS=Homo sapiens OX=9606 GN=PSMA7 PE=1 SV=1
Q9P0R6	GSK3B-interacting protein OS=Homo sapiens OX=9606 GN=GSKIP PE=1 SV=2
O75886	Signal transducing adapter molecule 2 OS=Homo sapiens OX=9606 GN=STAM2 PE=1 SV=1
P02652	Apolipoprotein A-II OS=Homo sapiens OX=9606 GN=APOA2 PE=1 SV=1
P61970	Nuclear transport factor 2 OS=Homo sapiens OX=9606 GN=NUTF2 PE=1 SV=1
Q9NQC3	Reticulon-4 OS=Homo sapiens OX=9606 GN=RTN4 PE=1 SV=2
P13501	C-C motif chemokine 5 OS=Homo sapiens OX=9606 GN=CCL5 PE=1 SV=3
P41250	Glycine--tRNA ligase OS=Homo sapiens OX=9606 GN=GARS1 PE=1 SV=3
Q7KZF4	Staphylococcal nuclease domain-containing protein 1 OS=Homo sapiens OX=9606 GN=SND1 PE=1 SV=1
P00918	Carbonic anhydrase 2 OS=Homo sapiens OX=9606 GN=CA2 PE=1 SV=2
P05067	Amyloid-beta precursor protein OS=Homo sapiens OX=9606 GN=APP PE=1 SV=3
P14324	Farnesyl pyrophosphate synthase OS=Homo sapiens OX=9606 GN=FDPS PE=1 SV=4
P06753	Tropomyosin alpha-3 chain OS=Homo sapiens OX=9606 GN=TPM3 PE=1 SV=2

P20962	Parathymosin OS=Homo sapiens OX=9606 GN=PTMS PE=1 SV=2
O15212	Prefoldin subunit 6 OS=Homo sapiens OX=9606 GN=PFDN6 PE=1 SV=1
P05556	Integrin beta-1 OS=Homo sapiens OX=9606 GN=ITGB1 PE=1 SV=2
O94979	Protein transport protein Sec31A OS=Homo sapiens OX=9606 GN=SEC31A PE=1 SV=3
P35527	Keratin, type I cytoskeletal 9 OS=Homo sapiens OX=9606 GN=KRT9 PE=1 SV=3
Q9P260	RAB11-binding protein RELCH OS=Homo sapiens OX=9606 GN=RELCH PE=1 SV=2
P32119	Peroxiredoxin-2 OS=Homo sapiens OX=9606 GN=PRDX2 PE=1 SV=5
Q06323	Proteasome activator complex subunit 1 OS=Homo sapiens OX=9606 GN=PSME1 PE=1 SV=1
P53814	Smoothelin OS=Homo sapiens OX=9606 GN=SMTN PE=1 SV=7
P29218	Inositol monophosphatase 1 OS=Homo sapiens OX=9606 GN=IMPA1 PE=1 SV=1
P00488	Coagulation factor XIII A chain OS=Homo sapiens OX=9606 GN=F13A1 PE=1 SV=4
P27348	14-3-3 protein theta OS=Homo sapiens OX=9606 GN=YWHAQ PE=1 SV=1
O43866	CD5 antigen-like OS=Homo sapiens OX=9606 GN=CD5L PE=1 SV=1
Q16799	Reticulon-1 OS=Homo sapiens OX=9606 GN=RTN1 PE=1 SV=1
Q15293	Reticulocalbin-1 OS=Homo sapiens OX=9606 GN=RCN1 PE=1 SV=1
P54727	UV excision repair protein RAD23 homolog B OS=Homo sapiens OX=9606 GN=RAD23B PE=1 SV=1
P05387	60S acidic ribosomal protein P2 OS=Homo sapiens OX=9606 GN=RPLP2 PE=1 SV=1
P20645	Cation-dependent mannose-6-phosphate receptor OS=Homo sapiens OX=9606 GN=M6PR PE=1 SV=1
P01764	Immunoglobulin heavy variable 3-23 OS=Homo sapiens OX=9606 GN=IGHV3-23 PE=1 SV=2
P60981	Destrin OS=Homo sapiens OX=9606 GN=DSTN PE=1 SV=3
Q9H7C9	Mth938 domain-containing protein OS=Homo sapiens OX=9606 GN=AAMDC PE=1 SV=1
Q9H299	SH3 domain-binding glutamic acid-rich-like protein 3 OS=Homo sapiens OX=9606 GN=SH3BGRL3 PE=1 SV=1
O43768	Alpha-endosulfine OS=Homo sapiens OX=9606 GN=ENSA PE=1 SV=1
P68036	Ubiquitin-conjugating enzyme E2 L3 OS=Homo sapiens OX=9606 GN=UBE2L3 PE=1 SV=1
P53680	AP-2 complex subunit sigma OS=Homo sapiens OX=9606 GN=AP2S1 PE=1 SV=2
Q86WI1	Fibrocystin-L OS=Homo sapiens OX=9606 GN=PKHD1L1 PE=2 SV=2
P62258	14-3-3 protein epsilon OS=Homo sapiens OX=9606 GN=YWHAE PE=1 SV=1
P07339	Cathepsin D OS=Homo sapiens OX=9606 GN=CTSD PE=1 SV=1
Q13555	Calcium/calmodulin-dependent protein kinase type II subunit gamma OS=Homo sapiens OX=9606 GN=CAMK2G PE=1 SV=4
P04040	Catalase OS=Homo sapiens OX=9606 GN=CAT PE=1 SV=3
O95249	Golgi SNAP receptor complex member 1 OS=Homo sapiens OX=9606 GN=GOSR1 PE=1 SV=1
P07602	Prosaposin OS=Homo sapiens OX=9606 GN=PSAP PE=1 SV=2
O15116	U6 snRNA-associated Sm-like protein LSm1 OS=Homo sapiens OX=9606 GN=LSM1 PE=1 SV=1
Q9Y5S2	Serine/threonine-protein kinase MRCK beta OS=Homo sapiens OX=9606 GN=CDC42BPB PE=1 SV=2
P78344	Eukaryotic translation initiation factor 4 gamma 2 OS=Homo sapiens OX=9606 GN=EIF4G2 PE=1 SV=1

Q9NR12	PDZ and LIM domain protein 7 OS=Homo sapiens OX=9606 GN=PDLIM7 PE=1 SV=1
Q9NRY5	Protein FAM114A2 OS=Homo sapiens OX=9606 GN=FAM114A2 PE=1 SV=4
P20340	Ras-related protein Rab-6A OS=Homo sapiens OX=9606 GN=RAB6A PE=1 SV=3
Q92783	Signal transducing adapter molecule 1 OS=Homo sapiens OX=9606 GN=STAM PE=1 SV=3
Q9UEY8	Gamma-adducin OS=Homo sapiens OX=9606 GN=ADD3 PE=1 SV=1
P0DOX8	Immunoglobulin lambda-1 light chain OS=Homo sapiens OX=9606 PE=1 SV=1
P37802	Transgelin-2 OS=Homo sapiens OX=9606 GN=TAGLN2 PE=1 SV=3
Q9H8H3	Methyltransferase-like protein 7A OS=Homo sapiens OX=9606 GN=METTL7A PE=1 SV=1
Q99497	Protein/nucleic acid deglycase DJ-1 OS=Homo sapiens OX=9606 GN=PARK7 PE=1 SV=2
Q86YL5	Testis development-related protein OS=Homo sapiens OX=9606 GN=TDRP PE=1 SV=2
P14854	Cytochrome c oxidase subunit 6B1 OS=Homo sapiens OX=9606 GN=COX6B1 PE=1 SV=2
O15144	Actin-related protein 2/3 complex subunit 2 OS=Homo sapiens OX=9606 GN=ARPC2 PE=1 SV=1
Q9Y385	Ubiquitin-conjugating enzyme E2 J1 OS=Homo sapiens OX=9606 GN=UBE2J1 PE=1 SV=2
Q9P1Z2	Calcium-binding and coiled-coil domain-containing protein 1 OS=Homo sapiens OX=9606 GN=CALCOCO1 PE=1 SV=2
P46379	Large proline-rich protein BAG6 OS=Homo sapiens OX=9606 GN=BAG6 PE=1 SV=2
O75935	Dynactin subunit 3 OS=Homo sapiens OX=9606 GN=DCTN3 PE=1 SV=1
P27797	Calreticulin OS=Homo sapiens OX=9606 GN=CALR PE=1 SV=1
Q15555	Microtubule-associated protein RP/EB family member 2 OS=Homo sapiens OX=9606 GN=MAPRE2 PE=1 SV=1
P61960	Ubiquitin-fold modifier 1 OS=Homo sapiens OX=9606 GN=UFM1 PE=1 SV=1
Q93099	Homogentisate 1,2-dioxygenase OS=Homo sapiens OX=9606 GN=HGD PE=1 SV=2
Q9NQR4	Omega-amidase NIT2 OS=Homo sapiens OX=9606 GN=NIT2 PE=1 SV=1
P04114	Apolipoprotein B-100 OS=Homo sapiens OX=9606 GN=APOB PE=1 SV=2
P43652	Afamin OS=Homo sapiens OX=9606 GN=AFM PE=1 SV=1
Q86UP2	Kinectin OS=Homo sapiens OX=9606 GN=KTN1 PE=1 SV=1
P09496	Clathrin light chain A OS=Homo sapiens OX=9606 GN=CLTA PE=1 SV=1
Q13586	Stromal interaction molecule 1 OS=Homo sapiens OX=9606 GN=STIM1 PE=1 SV=3
Q08380	Galectin-3-binding protein OS=Homo sapiens OX=9606 GN=LGALS3BP PE=1 SV=1
O14933	Ubiquitin/ISG15-conjugating enzyme E2 L6 OS=Homo sapiens OX=9606 GN=UBE2L6 PE=1 SV=4
Q15056	Eukaryotic translation initiation factor 4H OS=Homo sapiens OX=9606 GN=EIF4H PE=1 SV=5
P09622	Dihydrolipoyl dehydrogenase, mitochondrial OS=Homo sapiens OX=9606 GN=DLD PE=1 SV=2
Q92930	Ras-related protein Rab-8B OS=Homo sapiens OX=9606 GN=RAB8B PE=1 SV=2
P60174	Triosephosphate isomerase OS=Homo sapiens OX=9606 GN=TPI1 PE=1 SV=3
Q9UN19	Dual adapter for phosphotyrosine and 3-phosphotyrosine and 3-phosphoinositide OS=Homo sapiens OX=9606 GN=DAPP1 PE=1 SV=1
Q9BZF9	Uveal autoantigen with coiled-coil domains and ankyrin repeats OS=Homo sapiens OX=9606 GN=UACA PE=1 SV=2
P68366	Tubulin alpha-4A chain OS=Homo sapiens OX=9606 GN=TUBA4A PE=1 SV=1

Q16891	MICOS complex subunit MIC60 OS=Homo sapiens OX=9606 GN=IMMT PE=1 SV=1
Q10567	AP-1 complex subunit beta-1 OS=Homo sapiens OX=9606 GN=AP1B1 PE=1 SV=2
O43516	WAS/WASL-interacting protein family member 1 OS=Homo sapiens OX=9606 GN=WIPF1 PE=1 SV=3
O75223	Gamma-glutamylcyclotransferase OS=Homo sapiens OX=9606 GN=GGCT PE=1 SV=1
Q05209	Tyrosine-protein phosphatase non-receptor type 12 OS=Homo sapiens OX=9606 GN=PTPN12 PE=1 SV=3
A0A0C4DH31	Immunoglobulin heavy variable 1-18 OS=Homo sapiens OX=9606 GN=IGHV1-18 PE=3 SV=1
P02775	Platelet basic protein OS=Homo sapiens OX=9606 GN=PPBP PE=1 SV=3
O75832	26S proteasome non-ATPase regulatory subunit 10 OS=Homo sapiens OX=9606 GN=PSMD10 PE=1 SV=1
Q9NQP4	Prefoldin subunit 4 OS=Homo sapiens OX=9606 GN=PFDN4 PE=1 SV=1
P99999	Cytochrome c OS=Homo sapiens OX=9606 GN=CYCS PE=1 SV=2
O00410	Importin-5 OS=Homo sapiens OX=9606 GN=IPO5 PE=1 SV=4
Q8NBF2	NHL repeat-containing protein 2 OS=Homo sapiens OX=9606 GN=NHLRC2 PE=1 SV=1
P60983	Glia maturation factor beta OS=Homo sapiens OX=9606 GN=GMFB PE=1 SV=2
O95336	6-phosphogluconolactonase OS=Homo sapiens OX=9606 GN=PGLS PE=1 SV=2
Q99816	Tumor susceptibility gene 101 protein OS=Homo sapiens OX=9606 GN=TSG101 PE=1 SV=2
Q9P0J7	E3 ubiquitin-protein ligase KCMF1 OS=Homo sapiens OX=9606 GN=KCMF1 PE=1 SV=2
P25685	DnaJ homolog subfamily B member 1 OS=Homo sapiens OX=9606 GN=DNAJB1 PE=1 SV=4
P31483	Nucleolysin TIA-1 isoform p40 OS=Homo sapiens OX=9606 GN=TIA1 PE=1 SV=3
P25789	Proteasome subunit alpha type-4 OS=Homo sapiens OX=9606 GN=PSMA4 PE=1 SV=1
A0A087WSY6	Immunoglobulin kappa variable 3D-15 OS=Homo sapiens OX=9606 GN=IGKV3D-15 PE=3 SV=6
Q641Q2	WASH complex subunit 2A OS=Homo sapiens OX=9606 GN=WASHC2A PE=1 SV=3
P04156	Major prion protein OS=Homo sapiens OX=9606 GN=PRNP PE=1 SV=1
Q96DZ9	CKLF-like MARVEL transmembrane domain-containing protein 5 OS=Homo sapiens OX=9606 GN=CMTM5 PE=1 SV=2
Q07812	Apoptosis regulator BAX OS=Homo sapiens OX=9606 GN=BAX PE=1 SV=1